THE BEHAVIOUR OF REINFORCED CONCRETE BEAM-COLUMN JOINTS UNDER CYCLIC LOADING.

A thesis submitted for the degree of
Master of Engineering in Civil Engineering
in the University of Canterbury,
Christchurch, New Zealand.

by

G.W. RENTON

1972.

ABSTRACT

This project investigates the behaviour of reinforced concrete beam-column joints under the application of high intensity cyclic loading.

The experiments, which were carried out on specimens with a beam framing in on only one side of the joint, were conducted to investigate the amount of transverse reinforcement required for confinement and shear resistance in the joint and column regions, in order to establish the ductility available in the column, when subjected to simulated seismic loading.

Four units were tested during the experimental program, the design parameters being:-

(i) the amount of transverse reinforcement in the joint.

(ii) the method of anchoring the beam flexural steel in the joint.

(iii) the amount of transverse reinforcement in the column.

The type of failure mechanism, and the cause of degradation in stiffness in the post-elastic range, is examined for each specimen leading to a critical appraisal of the joint detail.

From the results obtained during testing, recommendations have been suggested for the design of reinforced concrete joints, including ways in which detailing could be improved to enable the load resisting capacity to be sustained during post-elastic cycles.

ACKNOWLEDGEMENTS.

I gratefully acknowledge the assistance given by members of the academic and technical staff of the Civil Engineering Department, and extend my thanks to the following people:

Professor H.J. Hopkins, Head of the Civil Engineering Dept., under whose overall guidance this study was performed;

Professor R. Park, supervisor of this project, for his guidance and assistance during the experimental work and in the preparation of this thesis;

Dr. T. Paulay, supervisor of this project, for his constructive suggestions and encouragement throughout this study;

Messrs H .T. Watson and P.C. Dawson, Technical Officers, for co-ordination of the testing programme;

Mr N.W. Prebble, Senior Technician, for his technical advice and practical help throughout the preparation and testing of the specimens;

Messrs J.N. Byers, Senior Technician, J.M. Adams and S.R. Robinson, Technicians, for their valuable assistance during testing;

Mr H. Patterson for photographic work;

Mr R.W.G. Blakeley for the design of the test rig;

Mr S.J. Dawson for his tireless efforts tracing diagrams;

Mrs N.J. Robinson for typing the manuscript;

I also gratefully acknowledge the financial aid from my parents and the University of Canterbury.

TABLE OF CONTENTS.

Page

Page

Page

LIST OF FIGURES.

Page

Page

Page

Page

LIST OF TABLES.

NOTATION.

A_c = area of core of reinforced column, measured to the outside of the transverse reinforcement.

A_g = gross area of section.

A_n = $A_g + (n - 1) A_{st}$, the equivalent concrete area of a section.

A_s = area of tension reinforcement.

A'_s = area of compression reinforcement.

A_{sh} = area of transverse hoop bar (one leg).

A_{st} = area of structural steel in a composite section.

a = depth of equivalent rectangular stress block.

a_b = depth of equivalent rectangular stress block under balanced load conditions.

a_s = area of individual reinforcing bar.

a_v = area of transverse tie (one leg)

b = width of compression face of member.

C = concrete compressive force.

C_s = steel compressive force.

c = distance from extreme compression fibre to neutral axis.

c_b = distance from extreme compression fibre to neutral axis under balanced load conditions.

D = nominal diameter of reinforcing bar.

d = distance from extreme compression fibre to centroid of tension reinforcement.

d' = distance from extreme compression fibre to centroid of compression reinforcement.

E_c = modulus of elasticity of concrete.

E_s = modulus of elasticity of steel.

e_c = concrete strain.

e_{cu} = limiting concrete strain.

e_s = steel strain in tension reinforcement.

e'_s = steel strain in compression reinforcement.

e_y = yield strain in reinforcement.

e^* = difference in strain readings from DEMEC gauges and electric resistance gauges at same gauge locations.

f = compressive stress.

f_c = concrete compressive stress.

f'_c = concrete cylinder compressive strength.

f_h = tensile stress developed by a standard hook.

f_s = steel tensile stress.

f'_s = steel compressive stress.

f_t = tensile strength of concrete.

f_y = yield stress in reinforcement.

g = parameter in equation of parabola (Section A.5.4.1).

H = horizontal reaction at top and bottom of column.

h' = maximum unsupported length of rectangular hoop measured between perpendicular legs of the hoop or supplementary cross-ties.

I_b = moment of inertia of beam.

I_c = moment of inertia of column.

k = ratio of distance from extreme compression fibre to the neutral axis/d.

L = anchorage length of reinforcing bar.

L_d = computed development length.

L_e = equivalent embedment length.

M' = modified bending moment.

M_b = bending moment applied to beam.

M_c = bending moment applied to column.

M_{cr} = moment at first cracking.

M_{ub} = ultimate moment capacity of the beam.

M_{uc} = ultimate moment capacity of the column.

M_{uo} = theoretical moment strength of a section.

m = number of ties in the joint.

N = column axial load.

N_b = axial load on column to produce balanced load conditions.

N_u = column axial load at the ultimate strength of the column.

n = ratio of modulus of elasticity of steel to that of concrete.

P = load applied at the end of the beam.

$P_{cr.}$ = load on beam at first cracking.

$P_{max.}$ = the maximum load applied to the beam either during one load run or over the whole test.

P_u^* = the load on the beam at which theoretical ultimate capacity of the specimen is attained.

P_y^* = the load on the beam at which first yield of the flexural reinforcement should theoretically occur.

p = tension steel area ratio, A_s/bd.

p' = compression steel area ratio, A'_s/bd.

p_b = steel area ratio to produce balanced load conditions.

p'_s = ratio of volume of transverse reinforcement to total volume of core (out to out of ties) of a reinforced concrete column.

p_t = total steel area ratio, A_{st}/bd.

r = length of demec studs.

s = spacing of transverse reinforcement.

T = steel tensile force.

t = overall depth of section.

u = bond stress.

u_{max} = maximum bond stress developed.

u_u = ultimate bond stress.

V_c = shear force carried by concrete.

V_j = shear force applied to the joint.

V_s = shear force carried by reinforcement.

V_u = ultimate shear force.

v = shear stress.

v_c = shear stress carried by concrete.

w = density of concrete.

x,y = co-ordinates of parabolic equation (section A.5.4.1).

$\bar{y}$ = distance from centroid to extreme tension fibre.

α,β,θ = general angles defined in text.

Δ = deflection.

Δ_u = lateral displacement of centre of gravity of a building at ultimate.

Δ_{v1} = deflection at end of beam due to rotation of the column.

Δ_{v2} = deflection at end of beam due to bending of beam.

Δ_v = $\Delta_{v1} + \Delta_{v2}$

Δ_y = lateral displacement of centre of gravity of a building at first yield.

δ = movement at end of demec stud due to bending of reinforcing bar.

ϕ = rotation of column.

ϕ_u = ultimate curvature.

ϕ_y = curvature at first yield.

CHAPTER ONE.

INTRODUCTION

1.1 GENERAL:

The task of designing earthquake resistant structures has come under close scrutiny during the last decade as the effects of earthquake loading on structural behaviour becomes more apparent. Recent observations[1,2] have shown that many buildings, even though they have not been designed for the purpose, have the ability to resist earthquakes without undergoing any major structural damage due to the inherent safety incorporated in traditional design methods. However, the failure of many other buildings subjected to seismic excitation, and the increase in construction of high-rise buildings, has lead to a demand for increased knowledge of the earthquake behaviour of such structures in order to establish adequate seismic design criteria.

Prior to this, the design of structures insured that allowable stresses were not exceeded in the elastic range. However, modern earthquake - resistant structures are designed on the assumption that, although the large lateral forces induced by a major earthquake in the post-elastic range may cause local overstressing, adequate ductility is available to dissipate the energy of the earthquake motions. Thus it is the aim of the more recent design methods to ensure that sufficient post-elastic deformation can take place to enable the structure to survive without collapse.

The concept of ductility in reinforced concrete entails much revision of the traditional design procedures which basically depended on concrete for its strength. It does however, lead to more efficient and economical use of construction materials, and increased confidence by engineers in their ability to design structures able to resist the large post-elastic deformations imposed by a severe earthquake.

1.2 BEHAVIOUR OF REINFORCED CONCRETE FRAMES:

The recommendations pertaining to ductility in reinforced concrete structures were first proposed by Blume, Newmark, and Corning in 1961,[1] which eventually lead to a section in the S.E.A.O.C. 1968 Revision of "Recommended Lateral Force Requirements" which states[3] ".....buildings more than 160 ft. in height shall have ductile moment-resisting space frames..... The necessary ductility shall be provided by a frame of structural steel..... or by a reinforced concrete frame.....". Consequently the behaviour of reinforced concrete frames has been a topic of considerable interest.

Reinforced concrete frames designed as ductile moment-resisting space frames may, depending on the intensity of the earthquake, be subjected to several post-elastic cycles throughout its duration. With each cycle, the accumulation of damage in the failure region means a degradation in stiffness, and since ductility is determined by the ratio of deflection at ultimate to the deflection at first yield (Δ_u/Δ_y), this loss of stiffness tends to increase the apparent ductility of the structure. However the ability for energy absorption, as indicated by the area under the load-deflection curve, is generally not enhanced due to a loss in load-resisting capacity. Conventional theories based on maintaining the ultimate strength of the structure cannot, therefore, be forgotten in the need to satisfy ductility requirements.

Since energy absorption in reinforced concrete is best acheived by yielding of the flexural reinforcement, care must be taken to ensure that other stress requirements are not underestimated. If a "brittle" failure occurs - that is, one due primarily to bond, shear or compression - little or no ductility is available for post-elastic deformations and collapse of the structure is a likely outcome. The beam-column joint is a region where shear and bond stresses are critical, and since the strength and ductility

of the members cannot be achieved without an adequate connecting detail, the performance of this region can be a decisive factor in determining the overall behaviour of the structure.

When a reinforced concrete frame is subjected to earthquake motions it will deform as shown in Fig. 1.1. Considering the region surrounding an exterior beam-column joint (circled) as a free body, the forces required to establish equilibrium are shown in Fig. 1.2 (a). If the assembly is rotated through the angle θ, then the specimen is located conveniently for testing purposes, Fig. 1.2 (b).

1.3 SCOPE OF THIS PROJECT:

The original purpose of this series of tests was to determine the amount of transverse reinforcement necessary to provide sufficient ductility and energy absorption in the column region immediately adjacent to the joint, by subjecting different specimens to high intensity cyclic loading. For this reason it was necessary to absorb the energy by yielding of the column flexural steel, and therefore the ultimate flexural capacity of the beam was designed to be greater than that of the column, but other requirements for shear, bond and confinement as specified by the code were considered in the design.

The intention was to test specimens with differing amounts of transverse reinforcement in the column, increasing the steel content from nominal ties until the required ductility was acheived. As results obtained during the testing programme indicated that the joint was prone to fail before the ultimate moment of the column could be attained, it became increasingly obvious that little satisfactory information concerning column ductility could be derived from the tests until an adequate joint detail could be designed.

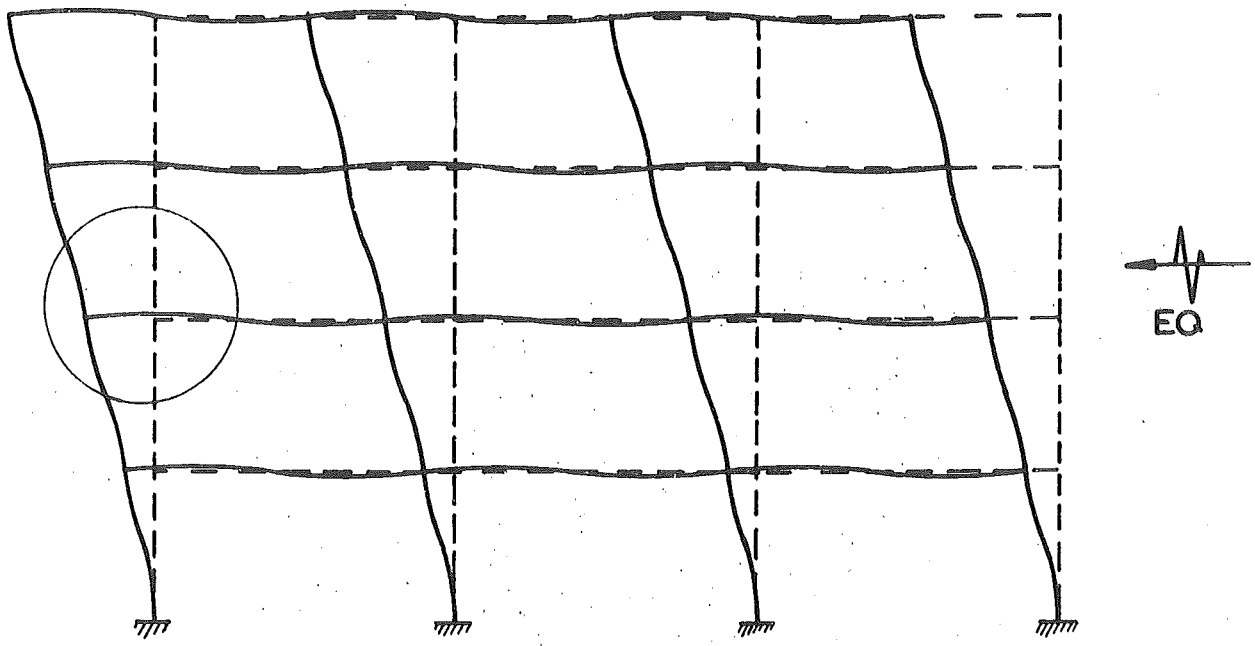

FIG. 1.1 RESPONSE OF FRAMED STRUCTURE TO LATERAL FORCE.

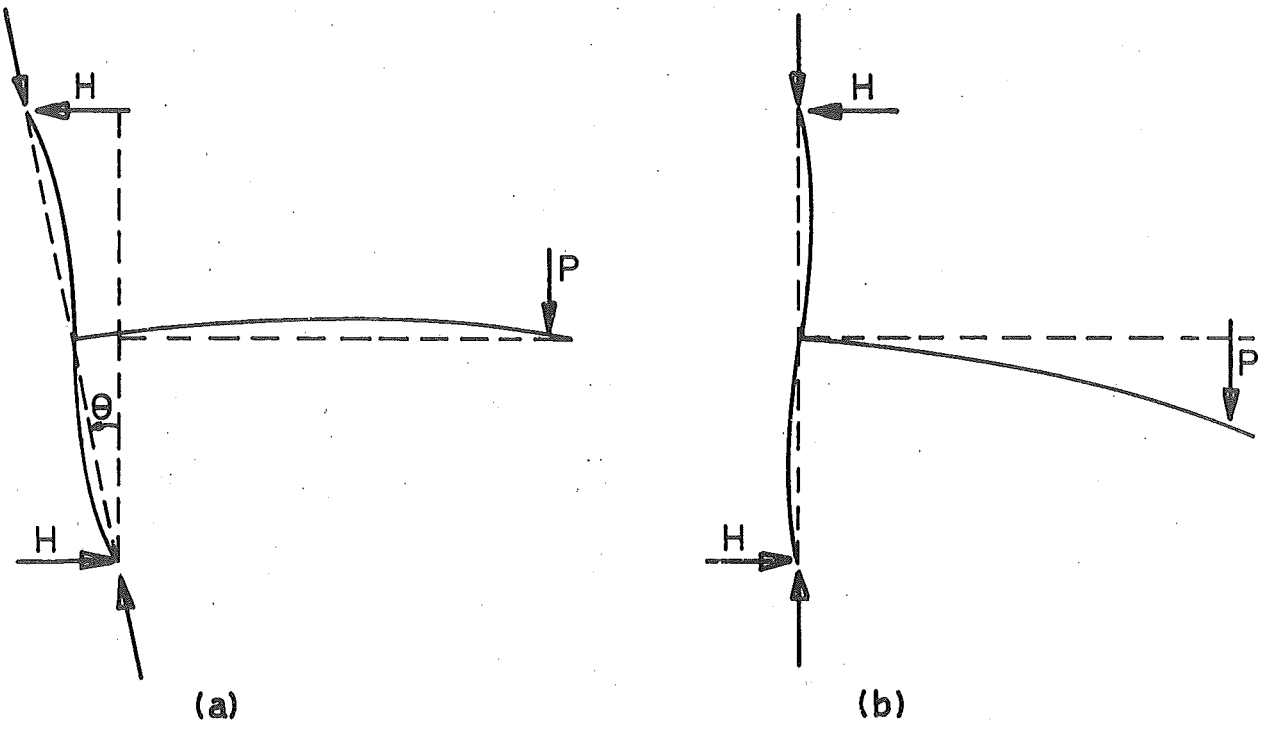

FIG. 1.2 TEST SPECIMEN

The emphasis of the test programme, therefore, shifted from investigating column ductility to endeavouring to detail a joint with the strength to enforce yielding of the flexural bars. Obviously much of the difficulty arose from testing specimens with joints unconfined by spandrel beams. However, although exterior joints such as these are not often used in actual construction, the tests revealed weaknesses in the detail and gave indications of stress distributions, which would not have been apparent had the specimens consisted of other than an isolated joint detail.

CHAPTER TWO

THE STATE OF THE ART

2.1 PRESENT DESIGN PROCEDURES:

The concept of designing for ductility in reinforced concrete structures was initiated by Blume, Newmark and Corning[1] and its acceptance was such that it is now a basic design procedure incorporated in the design codes of the majority of earthquake prone countries. It is well recognised[1,4] that, should failure occur, the flexural yielding should preferably be enforced in the horizontal rather than the vertical members. Therefore it is stipulated[5] that the ultimate moment capacity of the column must be greater than that of the beam, where they frame into the same joint.

However even though the column is designed to be stronger than the beam there are factors which in practice can greatly influence the relative strengths of the members. The most significant of these is when the direction of the earthquake is at 45° to the axes of the building. At any beam-column joint the column is subjected to the full earthquake effect while the beams need only resist the component of the earthquake along their longitudinal axes. This means that the column must be designed more than 40% stronger than the beams. If, in addition to this, the variability in material strengths of both concrete and steel in the members combine unfavourably, then it is obviously impractical to design the column stronger than the beam for every situation. Therefore it is specified that, although the column should not attain its ultimate flexural strength, it shall be provided with sufficient transverse reinforcement so that if it does so, it will have adequate ductility to survive the earthquake.

The importance of joint integrity during earthquake response is

basic. Should a joint fail, the capacity of all members framing into the joint is reduced or eliminated.

2.2 REVIEW OF PREVIOUS WORK.

The analysis and design of structures has become increasingly theoretical due presumably to the continued sophistication of the electronic computer, the speed and accuracy of which is unattainable by the usual design procedures. However, owing to the assumptions and simplifications which must be imposed to enable the program to be adaptable, the accuracy of the results obtainable are limited by the applicability of these restrictions. Because the properties of many structural materials, particularly reinforced concrete, are unpredictable to the required degree of accuracy, there is a need for experimental work to be performed whereby the structure, or a model thereof, is subjected to forces from a simulated earthquake in order to understand the behaviour of the actual structure. Since much of the information revealed by tests of this sort are obtained in the post-elastic range it is impractical to perform any experiments on existing structures.

The recommendations developed from the results of tests on small scale specimens are not in many cases applicable to large building members[6]. Therefore the need for tests on full scale component parts of structures becomes evident and may, in some circumstances, provide the only reliable source of information.

Much of the research which has been done on the ductility of columns has involved testing of members subjected to flexure and axial load[7]. When large shear forces are also present the problem becomes more acute. This is the situation at a beam-column joint where these three forces are all present. The work which has been done to determine the behaviour of interior beam column joints[8] cannot be extended to apply to exterior joints because of the special provisions required - in particular where no spandrel beams

frame into the joint to provide extra confinement.

The most significant work on exterior joints to be attempted was performed in the P.C.A. laboratories, a review of which is published by the A.S.C.E.[9]. Results from this paper indicate that for the identical specimens III and IV, which were designed with the column weaker than the beam, with different column axial loads, the greater column load was more favourable for attainment of the theoretical ultimate moment capacity. Even so the ability of the specimen to maintain its ultimate capacity was diminished significantly after the first post-elastic cycle. The fact that the results from these two specimens did not appear to affect the conclusions to any extent, even though specimen IV did not at any stage attain its theoretical ultimate capacity, indicates that the authors placed little emphasis on the performance of these specimens. The other test specimens and subsequent tests[10] showed that the code requirements for these beam-column joints are conservative with regard to transverse reinforcement. It is apparent that a joint, detailed according to accepted design practice, will provide sufficient ductility and energy absorption to survive a series of post-elastic load cycles.

Megget[11] developed the work on exterior joints further when he tested three specimens with different beam anchorage reinforcement in the joint. However the transverse joint reinforcement was insufficient to maintain the integrity of the joint and brittle failures occurred in all three specimens.

Therefore it is obvious that much work is yet to be done in this field to establish an adequate mechanism for resistance in exterior joints and it is with this purpose that the experiments reviewed herein have been undertaken.

CHAPTER THREE

TEST SPECIMENS.

3.1 INTRODUCTION:

The philosophy behind the design of the specimens is described in this chapter. Restrictions from code requirements are outlined in an attempt to show the reasons upon which many of the decisions are based.

Theoretical predictions of the behaviour of the specimens are also formulated so that, subsequently, a comparison can be made with the actual behaviour.

3.2 DESIGN OF SPECIMEN:

3.2.1 Overall Specifications:

The specimen represented an exterior beam column assembly with only one beam framing into the joint. Although the dimensions of the assembly were determined to some extent by the size and load capacity of the existing test rig[12], it was considered necessary to test a full scale specimen to avoid the possibility of scale effects[6]. Therefore the dimensions of the structural components were as large as possible within the limitations of the apparatus.

As well as designing a specimen in which the ultimate moments of resistance of the columns were less than that of the beam, as discussed in section 1.3, the detail reflected current trend in construction in an attempt to provide information directly applicable to practical conditions.

The strength properties of the materials used throughout the design were:-

concrete f'_c = 4,000 psi

steel f_y = 45,000 psi

3.2.2 Size and Flexural Reinforcement of Members:

3.2.2.1 Column:

The dimensions of the column were the most important criteria when selecting representative sizes and a 15" x 15" square column was considered to be the optimum size.

The restrictions on flexural reinforcement in columns[13] stipulates there must be at least four bars for tied columns so that

$$0.01 < p_t < 0.08$$

Taking this into account, the column was 15" x 15", with four $1\frac{1}{8}$ in. diameter bars symmetrically placed, giving p = 0.0206.

For this column

$$N_b = 370 \text{ kips.}$$

The earthquake provisions for lateral confining steel[5], apply only to columns where

$$N_u \geq 0.4N_b = 148 \text{ kips.}$$

Therefore the load N = 148 kips was the minimum load on the column throughout the test.

The test specimen with applied loads is shown in Fig. 3.1.

However, with the intended load arrangements, since the horizontal reactions, H, must be equal, only equal moments could be generated in the column. That is, from Appendix B,

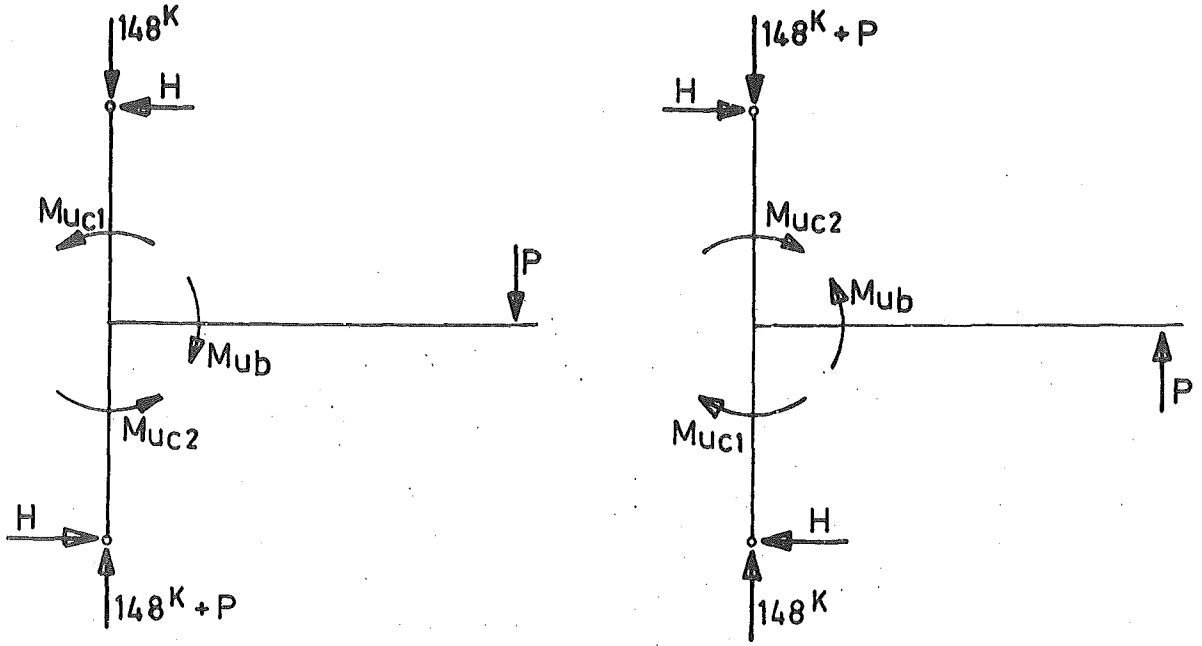

(a) downward load (b) upward load

FIG. 3.1 FORCES ON TEST SPECIMEN

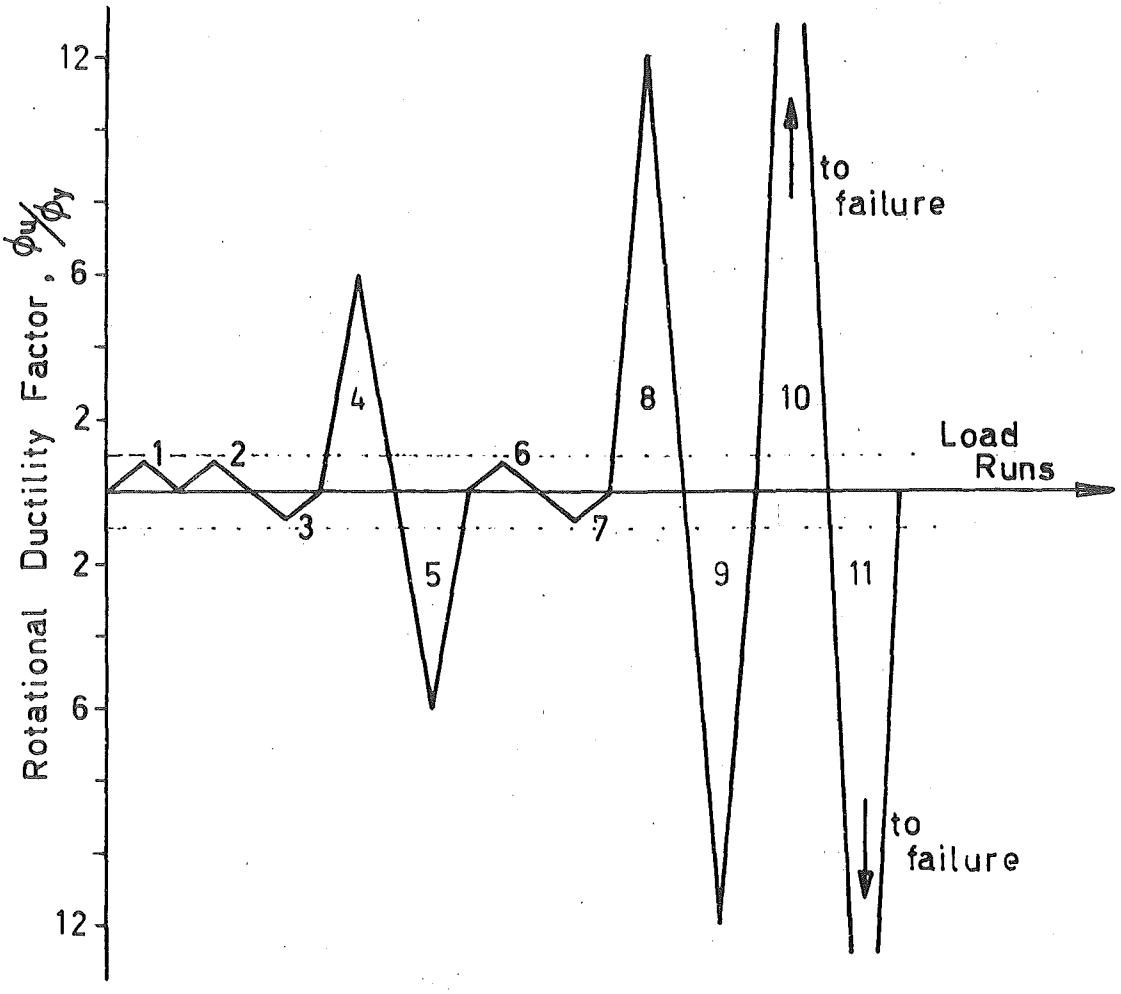

FIG. 3.2 LOADING SEQUENCE

$$M_{uc1} = M_{uc2} = M_{uc} = 1875 \text{ kip-in.}$$

3.2.2.2 Beam.

It was decided that the beam should have an ultimate moment of resistance 20% greater than that of the columns to allow for variations in material strengths.

$$\text{Required } M_{ub} = 1.20 \times 2 M_{uc}$$

$$= 4,500 \text{ kip-in.}$$

The reinforcing ratio, p, was restricted[13] by

$$\frac{200}{f_y} < p < 0.50\, pb$$

$$0.005 < p < 0.023$$

The beam width was 12 in. and the flexural reinforcement, both top and bottom, consisted of four $1\frac{1}{4}$ in. diameter bars in a single layer. The depth of the beam was determined by the required moment capacity. Assuming a steel couple to produce M_{ub} = 4500 kip-in

$$M_{ub} = A_s f_y (d-d')$$

$$d-d' = \frac{4500}{4.92 \times 45} = 20.35 \text{ in.}$$

$$t = 24.6 \text{ in.}$$

Dimensions of the beam were 12" x 25", with four $1\frac{1}{4}$ in. diameter bars, top and bottom, giving p = p' = 0.018.

Anchorage requirements[5] (calculated in Appendix B), indicate that an anchorage length of 32 in. is required of each bar measured from the face of the column. However, problems arise in the joint with separate anchorages for the top and bottom bars, with congestion in the joint and interlacing of the bars. Although these were by no means insurmountable problems, it was decided that running the top and bottom steel in a continuous U through the joint would provide the best solution and also test

the capability of a detail commonly used in N.Z. construction. The anchorage length of the bars must transfer to the concrete both the tensile and compressive forces from the top and bottom beam bars. In this specimen, from the details given in Appendix B, the maximum expected bond stress, u, is given by:

$$u = \frac{(f_s + f'_s)\, D}{4L}$$

$$= \frac{1.378 \times 41{,}800 \times 1.25}{4 \times 40}$$

$$= 450 \text{ psi.}$$

A bond stress of this magnitude should be easily attainable in a well confined joint. However, this anchorage detail was found to be one of the reasons for deterioration in the joint during testing, and for UNIT 4 separate anchorages for top and bottom bars were used.

3.2.3 Transverse Reinforcement:

3.2.3.1 Joint Ties:

The transverse reinforcement in the joint is provided to resist both bursting forces from the concrete and shear forces.

Using $\frac{5}{8}$ in. diameter hoops, five were required for confinement within the joint. (see calculations in Appendix B).

From standard design procedure for joint detailing[10,14], six $\frac{5}{8}$ in. diameter joint ties are required to resist the shear forces. However because of the conservative nature of joint shear requirements as evidenced by previous tests[9,10], UNIT 1 was provided with five $\frac{5}{8}$ in. diameter joint ties to determine the validity of these conclusions. These ties were insufficient to prevent deterioration of the joint of UNIT 1, and so for UNIT 2 seven $\frac{5}{8}$ in. diameter ties were provided, which represented 25% more transverse

reinforcement than was theoretically required. Because of the inadequacy, also, of these ties, UNITS 3 and 4 had nine $\frac{5}{8}$ in. diameter ties which more than satisfied the more conservative code requirements outlined in Section 8.1.

3.2.3.2 Column Ties:

The original intention of the research was to provide only sufficient column ties to resist the shear force, and to increase the number of ties in succeeding specimens until adequate ductility was obtained from the plastic hinges.

Since the concrete was capable of resisting the applied shear force only nominal ties were required in the column. These consisted of $\frac{1}{4}$ in. diameter ties at 12 in. spacing. This reinforcement was provided for both UNITS 1 and 2. For UNITS 3 and 4 additional confinement was provided by $\frac{3}{8}$ in. diameter ties at 2 in. spacing adjacent to the joint. The spacing increased to 4 in. and eventually 8 in., further away from the joint, as shown in Figs. 6.1 and 7.1.

3.2.3.3 Beam Stirrups:

The minimum shear reinforcement in flexural members means $\frac{3}{8}$ in. diameter stirrups must be provided at 6 in. spacing. In all specimens, stirrups were provided at 4 in. spacing close to the joint, to fit conveniently between the demec studs on the flexural bars. The spacing increased to the maximum spacing of 11 in. beyond the demec studs.

3.3 THEORETICAL BEHAVIOUR:

3.3.1 Elastic Range:

Much of the information concerning behaviour of the specimens in

the elastic range is determined from equilibrium and strain compatibility after the material properties have been established. The calculations are presented in Appendix B with the specific results for each specimen included in the relevant chapter.

3.3.1.1 Flexural Cracking:

Cracking first occurs in the beam then in the column. The loads at which cracking should theoretically occur are calculated and the effects are shown on the load-deflection relationships.

3.3.1.2 Yield Load:

Once f'_c had been established for each specimen, the load at which first yield should occur was determined. In fact, yield, which occurs in the column flexural bars, was observed only in UNIT 4. The theoretical yield load is tabulated for each specimen in Table 8.1 along with the actual loads obtained.

3.3.1.3 Rotations and Deflections:

The elastic rotation of the column is calculated for both the uncracked and cracked sections and compared in Table 8.3. Deflection at the end of the beam is considered to be contributed to by rotation of the column and bending of the beam. This is shown on the load-deflection relationships.

The theoretical deflected shapes at the peaks of the elastic load runs are shown diagrammatically in each chapter and compared with the actual shapes obtained. Joint distortion, which can have a considerable effect on the deflection of the structure was not considered in the theoretical predictions. Its effect then becomes apparent when theoretical and actual values of deflection are compared.

3.3.1.3 Steel Strains:

The strains in the flexural reinforcement are calculated by elastic theory for the first run of loading in each direction and compared with the recorded strains on the figures of strain distribution in each chapter.

3.3.2 Post-Elastic Range.

Although UNITS 1, 2, and 3 do not yield in flexure, the response to the applied load is similar to what would be expected and although not strictly correct it is convenient to refer to the "elastic" and "post-elastic" portion of each load run.

3.3.2.1 Ultimate Load:

The ultimate loads for each specimen are calculated in Appendix B, and tabulated in Table 8.2 for comparison with actual maximum loads obtained.

3.3.2.2 Rotational Ductility:

For the design specimen the ductility available can be determined from consideration of the rotations at ultimate and at first yield. It has been suggested[1] that although the ultimate concrete strain is generally taken as 0.003, for confined concrete a more realistic figure would be 0.01. This means that provided the concrete is well confined the theoretical maximum rotational ductility factor attainable is given, by Appendix B, as

$$\phi_u/\phi_y = 15.4$$

However the performance of the specimens, with the exception of UNIT 4, showed that this is not applicable if the concrete is not sufficiently

confined. The ductility factors for post-elastic load runs are computed using the method outlined by Bennett el al[15] and tabulated in each chapter.

3.4 EARTHQUAKE LOADING REPRESENTATION:

3.4.1 Rate of Load Application:

Static cyclic loading was applied to the end of the beam by means of screw jacks to simulate the high intensity reversals imposed by an earthquake. Although earthquake loadings are dynamic in character, it has been shown[16] that the strength and energy absorption characteriestics of reinforced concrete members are increased with increased speed of loading, and,[17] that static tests can satisfactorily predict the structural response of reinforced concrete structures to earthquakes. Consequently it appears conservative to use static loading as a basis for testing seismic specimens.

3.4.2 Loading Sequence:

The load sequence applied was adjusted slightly depending on the performance of the individual specimens. However the sequence took the general form as shown in Fig. 3.2. The initial runs 1,2, and 3 were to establish the stiffness of the structure in its uncracked and cracked states. Runs 4 and 5 subjected the specimen to deformations which would be expected during a major earthquake, which were followed by two elastic runs to determine the stiffness and general performance after the earthquake. The remaining cycles were to demonstrate the response and ductility of the structure during a second major earthquake.

CHAPTER FOUR

UNIT 1

4.1 INTRODUCTION:

The overall performance of the first specimen is described in this chapter and account is given of the behaviour and stress distribution of reinforcing components of the structure. The way in which the stiffness deteriorated under continued load application leading to eventual failure of the specimen is also described.

4.2 DETAIL OF REINFORCEMENT:

This specimen, designed as described in section 3.1, had reinforcement details as shown in Fig. 4.1.

The joint hoops were sufficient for confinement according to ACI 318 - 71 and were theoretically capable of resisting 83% of the joint shear force at theoretical ultimate. The column had only nominal ties outside the joint region.

4.3 GENERAL PERFORMANCE:

The cracks in the joint, which appeared early in the loading sequence, widened considerably, indicating large stresses in the joint ties, even during the initial elastic cycles. The width and number of cracks increased during subsequent cycles until eventually the cover concrete became ineffective.

Most of the joint ties reached yield stress during Run 2 and were obviously inadequate to resist both the shear forces in the joint and bursting forces from the column core. Failure subsequently occurred primarily

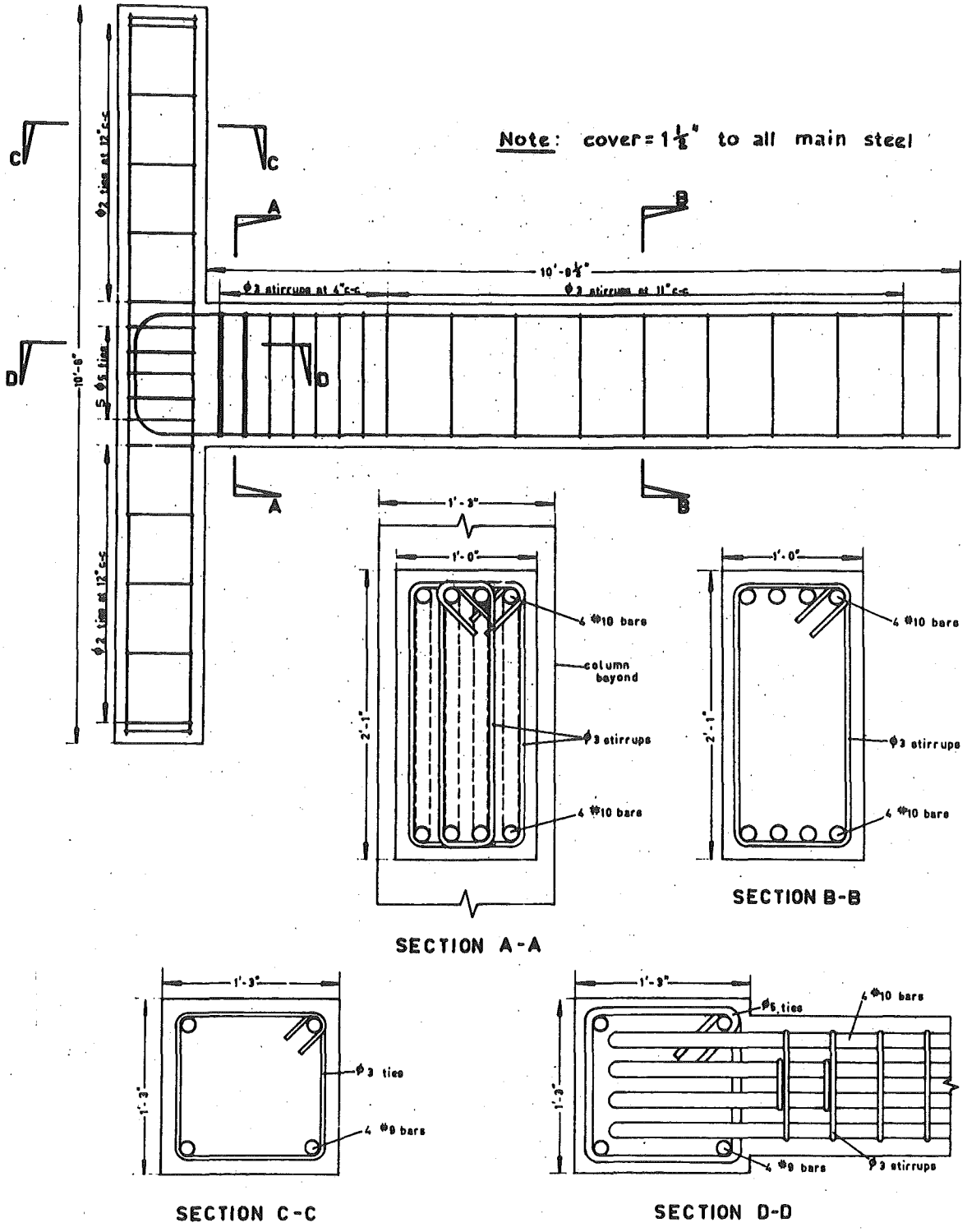

FIG. 4.1 REINFORCING DETAIL FOR UNIT 1

in the joint region. The inadequate joint shear reinforcement allowed the diagonal tension cracks to widen, leading to degradation in the joint stiffness and the moment resisting capacity. This premature failure meant that the flexural bars did not yield and the specimen attained only 71% of its computed theoretical ultimate flexural capacity.

The distressed nature of the joint after Run 5 indicated that little information would be provided from application of further elastic cycles and so, during Runs 6 and 7, the specimen was taken to its maximum deflection in each direction before the test was terminated.

4.4 BEHAVIOUR OF FLEXURAL REINFORCEMENT:

All strain measurements were taken by DEMEC gauges as explained in Appendix A.

4.4.1 Column Bars:

Apart from inconsistencies resulting from the effects described in section A.5.4, the recorded strains in the bars were generally consistent with theoretical predictions for cyclic loading (see Figs. 4.2 (a) and 4.2 (b)).

Strain readings on the more reliable outer column bars (the two furthest from the beam) indicated stresses of approximately 35 ksi in each bar at maximum load. This stress must be dissipated within the joint, by bond with the concrete, over a distance of about 12 in., representing a bond stress, u, given by

$$u = \frac{Df_s}{4L}$$

$$= \frac{1.125 \times 35000}{4 \times 12}$$

$$= 820 \text{ psi}$$

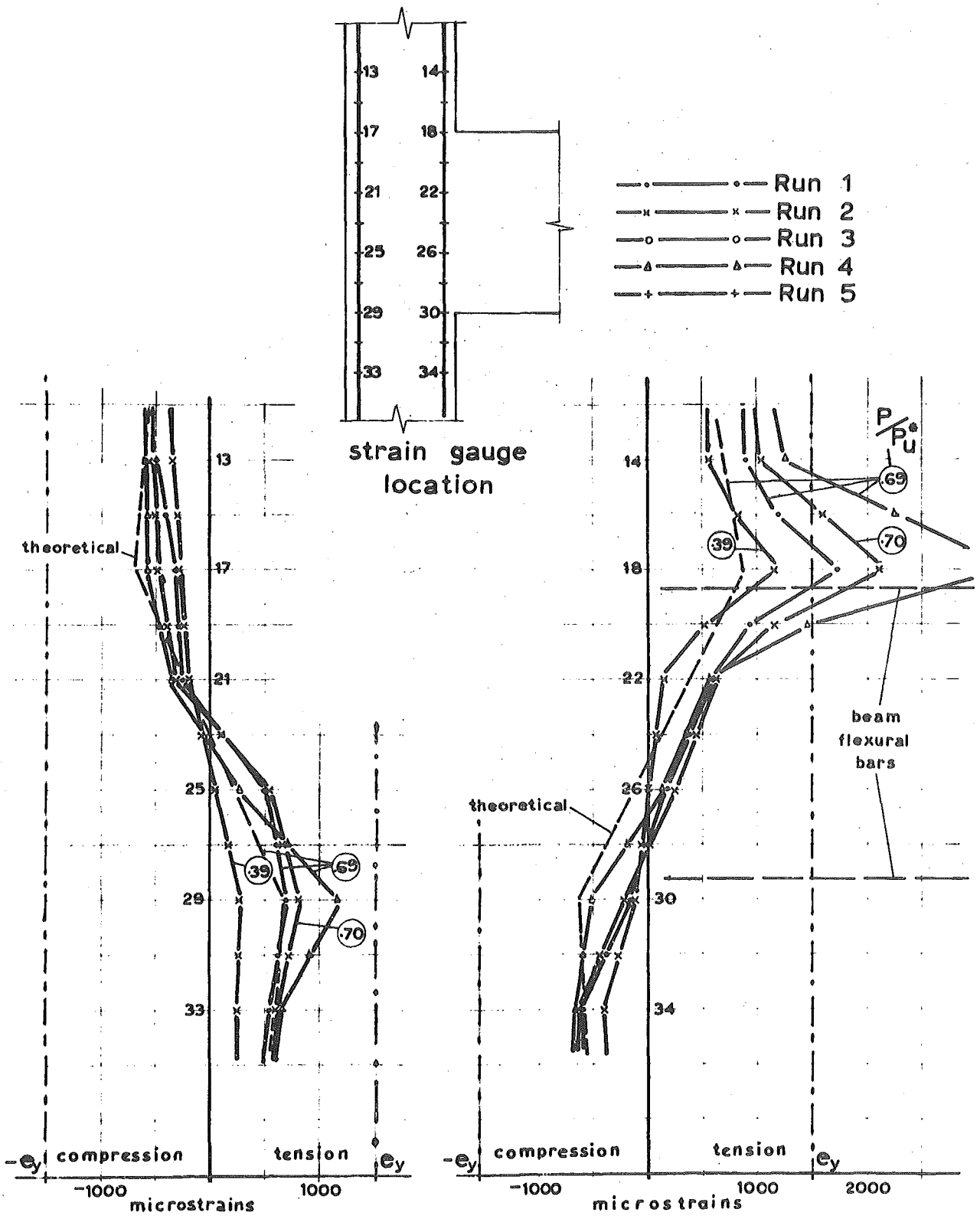

FIG. 4·2(a) THE DISTRIBUTION OF STEEL STRAINS IN COLUMN FLEXURAL BARS IN UNIT 1 [FOR DOWNWARD LOAD RUNS]

For strain gauge locations see Fig.4.2(a)

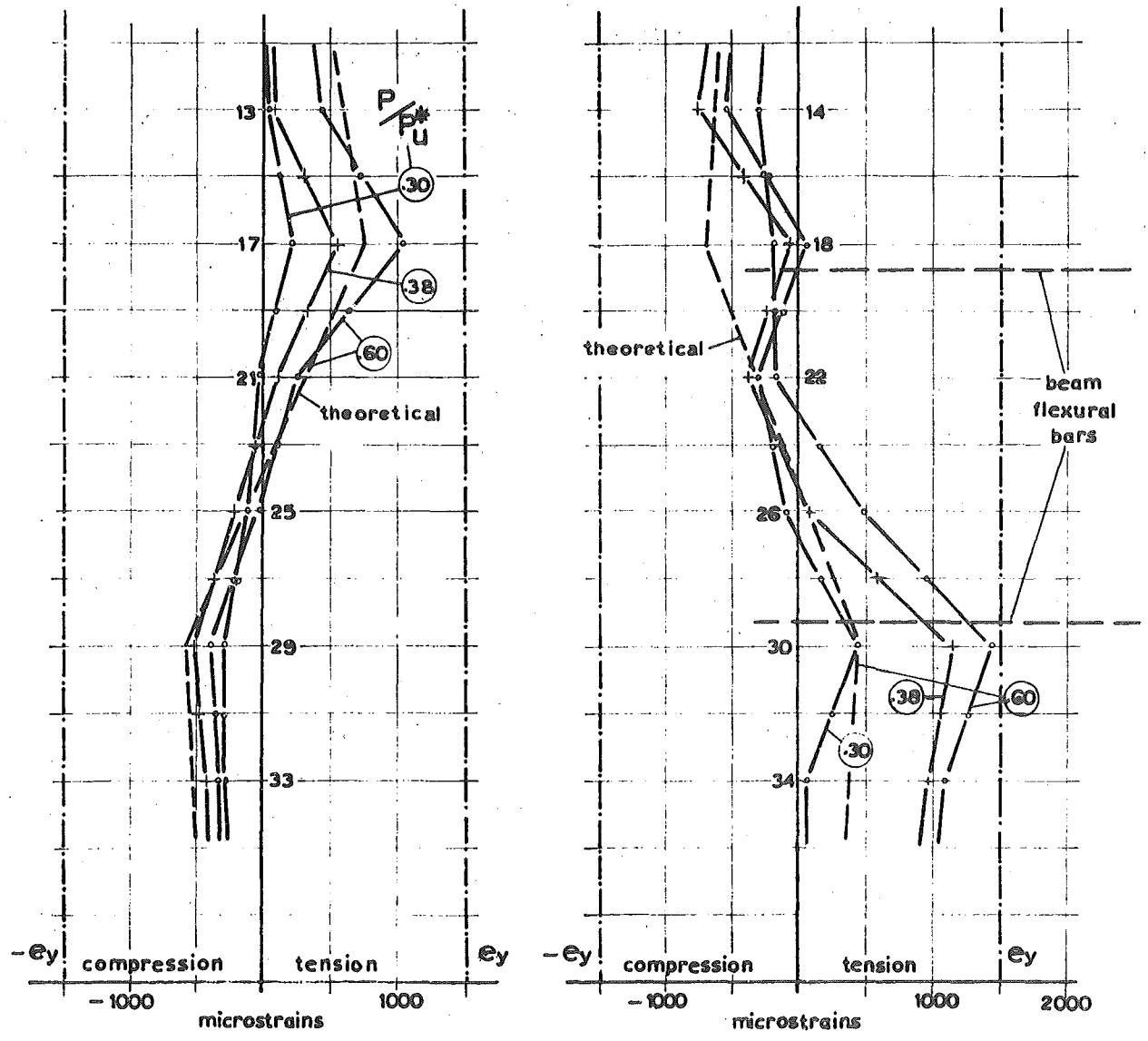

FIG.4.2(b) THE DISTRIBUTION OF STEEL STRAINS IN COLUMN FLEXURAL BARS IN UNIT 1 [FOR UPWARD LOAD RUNS]

The maximum bond stress specified by the ACI for ultimate strength design is 800 psi[13], which is not difficult to acheive in a region which is well confined. However, these bars were not adequately confined to withstand the splitting stresses induced by the cyclic loading, and vertical cracks down the back sides of the column during Run 4 gave evidence of partial bond failure.

4.4.2 Beam Bars:

The strain distributions for these bars, shown in Figs. 4.3 (a) and 4.3 (b) were as expected with the steel providing the tensile force and the majority of the compressive force being resisted by the concrete.

The readings of strain taken in the column at gauge locations 37 and 42 were obtained from $\frac{1}{4}$ in. diameter studs 3 in. long, which were too flexible to produce consistently accurate results as is evident from the distributions shown at these locations.

4.5 BEHAVIOUR OF TRANSVERSE REINFORCEMENT:

Strain measurements were again taken by DEMEC gauges on the ties, however only a general idea of the behaviour of the ties could be deduced since the accuracy of the strain readings was influenced by the bowing of the ties, as explained in section A.5.4.1.

4.5.1 Column Ties:

The $\frac{1}{4}$ in. diameter ties provided only minimal resistance in shear and confinement, however for the majority of the test when the failure was confined to the joint, they were not required since the concrete resisted all the shear. Once cracking extended outside the joint region, the inadequacy of these ties was clearly demonstrated. The level of strain mainly reflected the diversification of cracking in the column, since

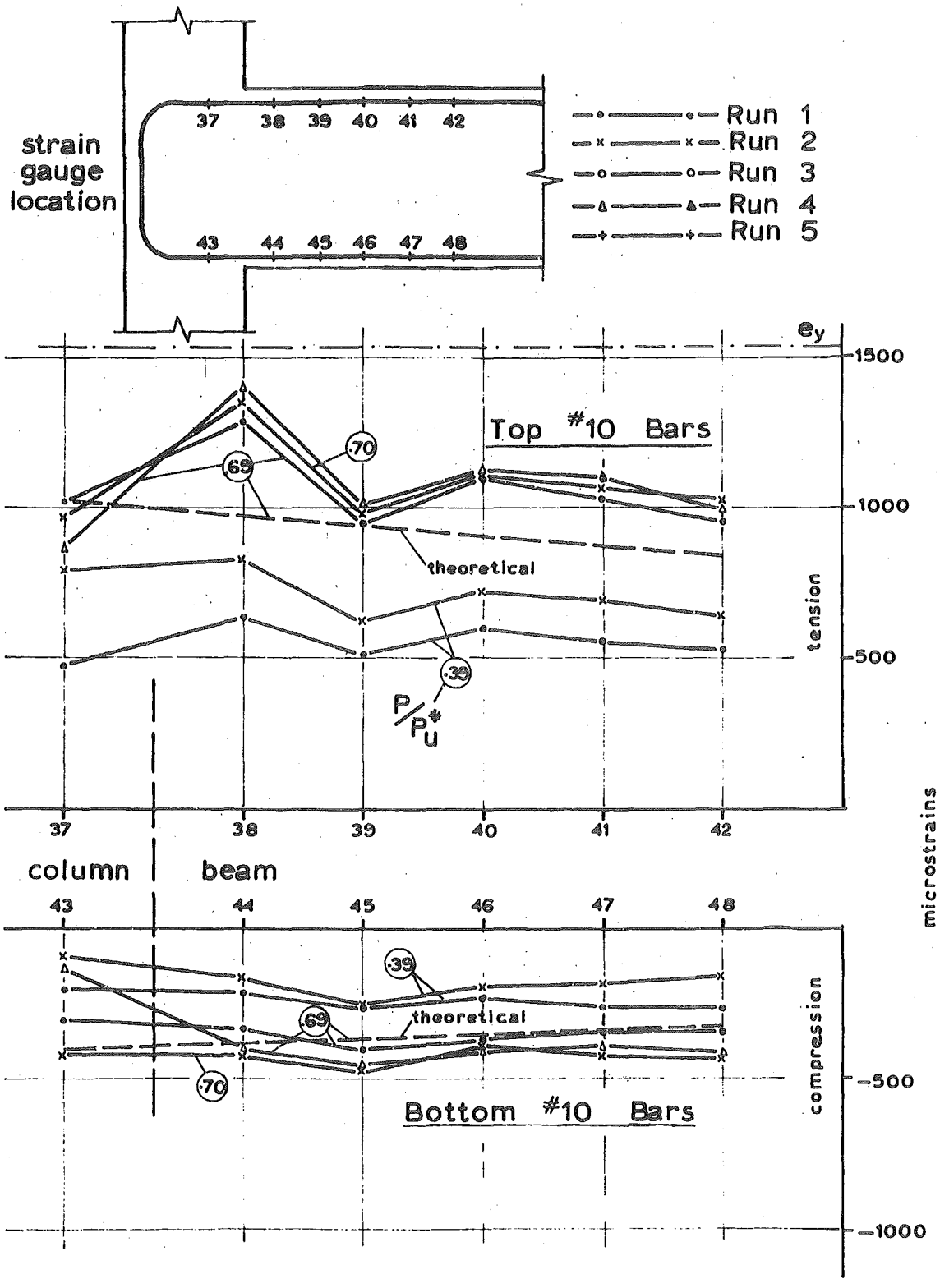

FIG. 4.3(a) THE DISTRIBUTION OF STEEL STRAINS IN BEAM FLEXURAL BARS IN UNIT 1 [FOR DOWNWARD LOAD RUNS]

For strain gauge locations see Fig . 4.3(a)

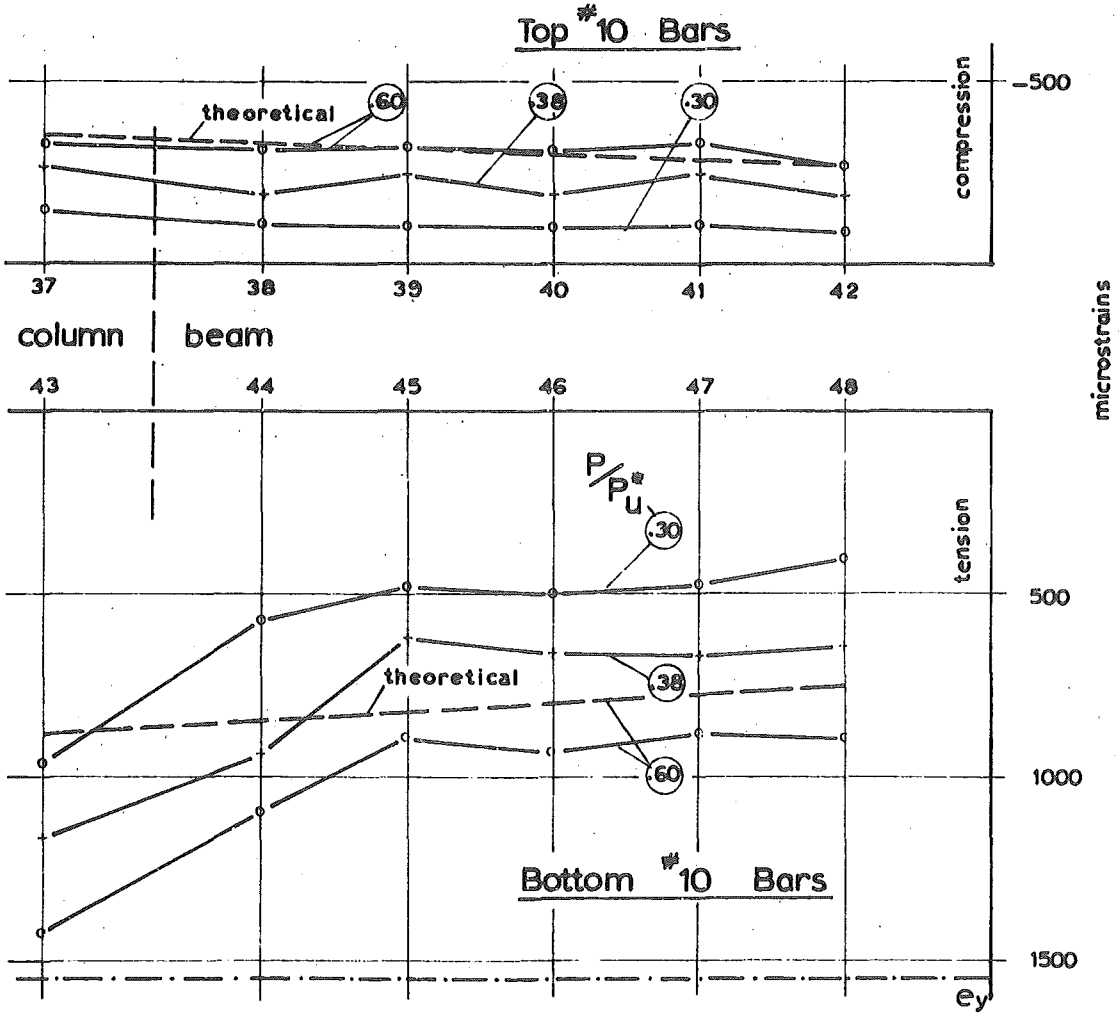

FIG . 4 . 3(b) THE DISTRIBUTION OF STEEL STRAINS IN BEAM FLEXURAL BARS IN UNIT 1 [FOR UPWARD LOAD RUNS]

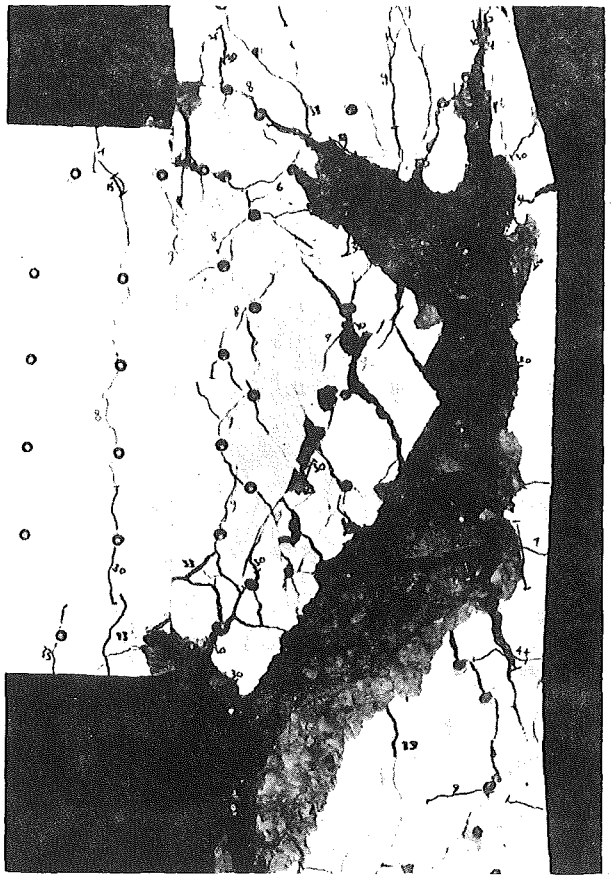

FIG. 4.4 UNIT 1 ON LOAD RUN 6

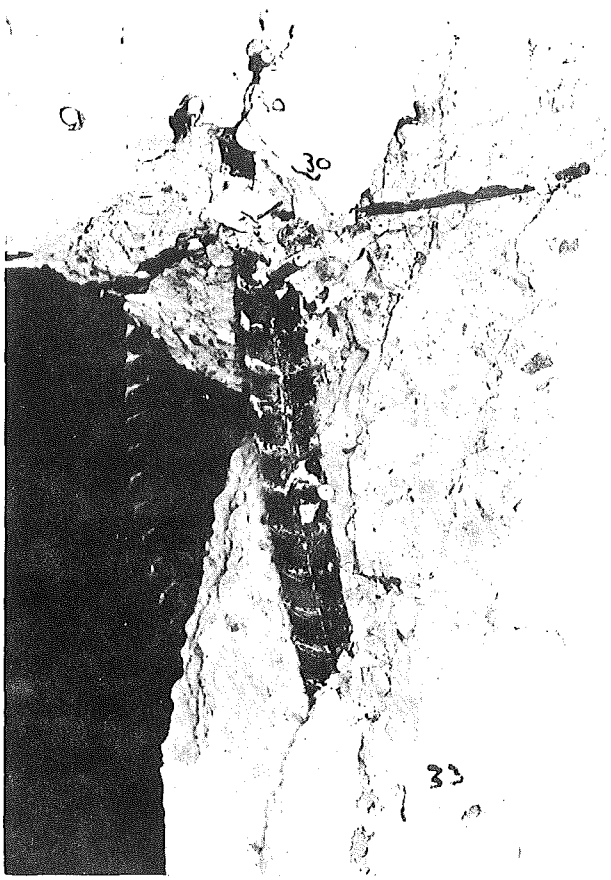

FIG. 4.5 BUCKLING OF COLUMN FLEXURAL BARS

the reading generally showed at least yield strain wherever a crack crossed the gauge location on a tie.

The inability of these ties to prevent buckling of the column flexural bars in the compression region, as shown by Figs. 4.4 and 4.5, indicated that they would be unsatisfactory if required as lateral confining steel in the column.

4.5.2 Joint Ties:

The strain readings on these ties did not reflect the situation for individual ties to any degree of accuracy because of bowing of the ties. The relative participation of each tie can be determined, however, from the measured strains shown in Figs. 4.6 (a) and 4.6 (b). The strain distributions indicate that the ties do not all resist the bursting and shear forces equally. The general trend of the upper ties being subjected to a

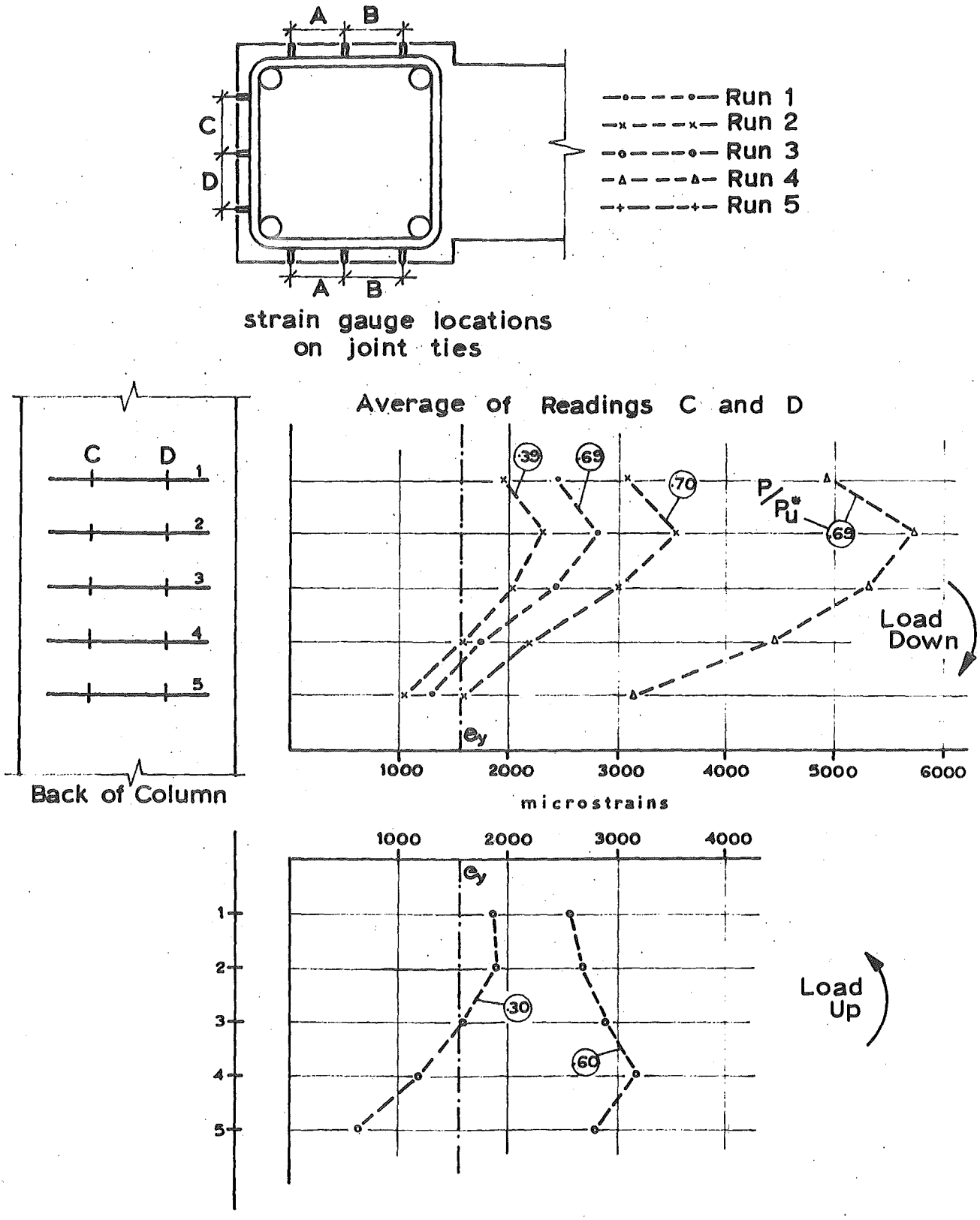

FIG. 4.6 (a) THE DISTRIBUTION OF JOINT TIE STRAINS AT BACK OF COLUMN IN UNIT 1

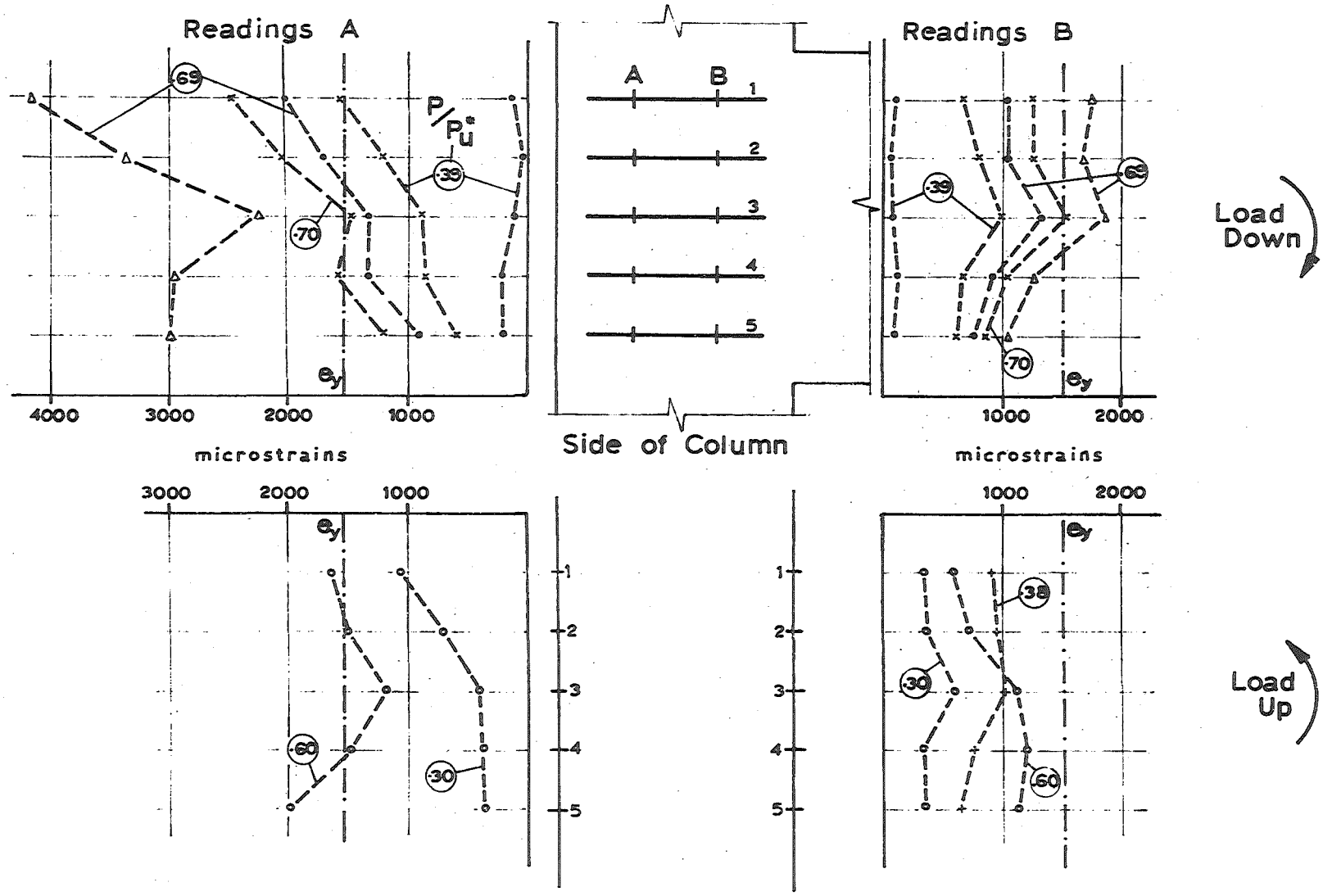

FIG. 4.6 (b) THE DISTRIBUTION OF JOINT TIE STRAINS AT SIDE OF COLUMN IN UNIT 1

greater amount of bending, for downward load, than the lower ties would be due to them either resisting a larger force or having less restraint for the imposed force. This is caused by the type of failure which occurred in this specimen, and results in the opposite distribution for upward load runs.

The actual strain readings at the back of the ties, as shown in Fig. 4.7 (a) demonstrate the symmetrical curvature of each tie caused by the internal forces in the column core. The strain along the sides of the ties, shown in Fig. 4.7 (b) indicate a difference in curvature, as explained in section A.5.4, rather than a non-uniform stress along the tie.

Figs. 4.8 (a) and 4.8 (b) show how the strain in the ties increases with increase in applied load for each load run. The effect that the bowing of the ties has on the readings is clearly shown in Run 1. At 40% of the theoretical ultimate load the bowing of the ties appeared to be negligible, the strain readings being caused by minor diagonal tension cracking in the joint. As the cracks opened, the ties picked up more strain until eventually, due to a combination of this, and internal cracking causing expansion of the column core, the strain readings increased considerably.

4.5.3 Beam Stirrups:

Although these were instrumented in this specimen, only minor flexural cracks formed in the beam resulting in the beam stirrups being virtually unstressed.

4.6 DEFORMATIONS:

Deflections and rotations were measured by means of dial gauges as described in Appendix A.

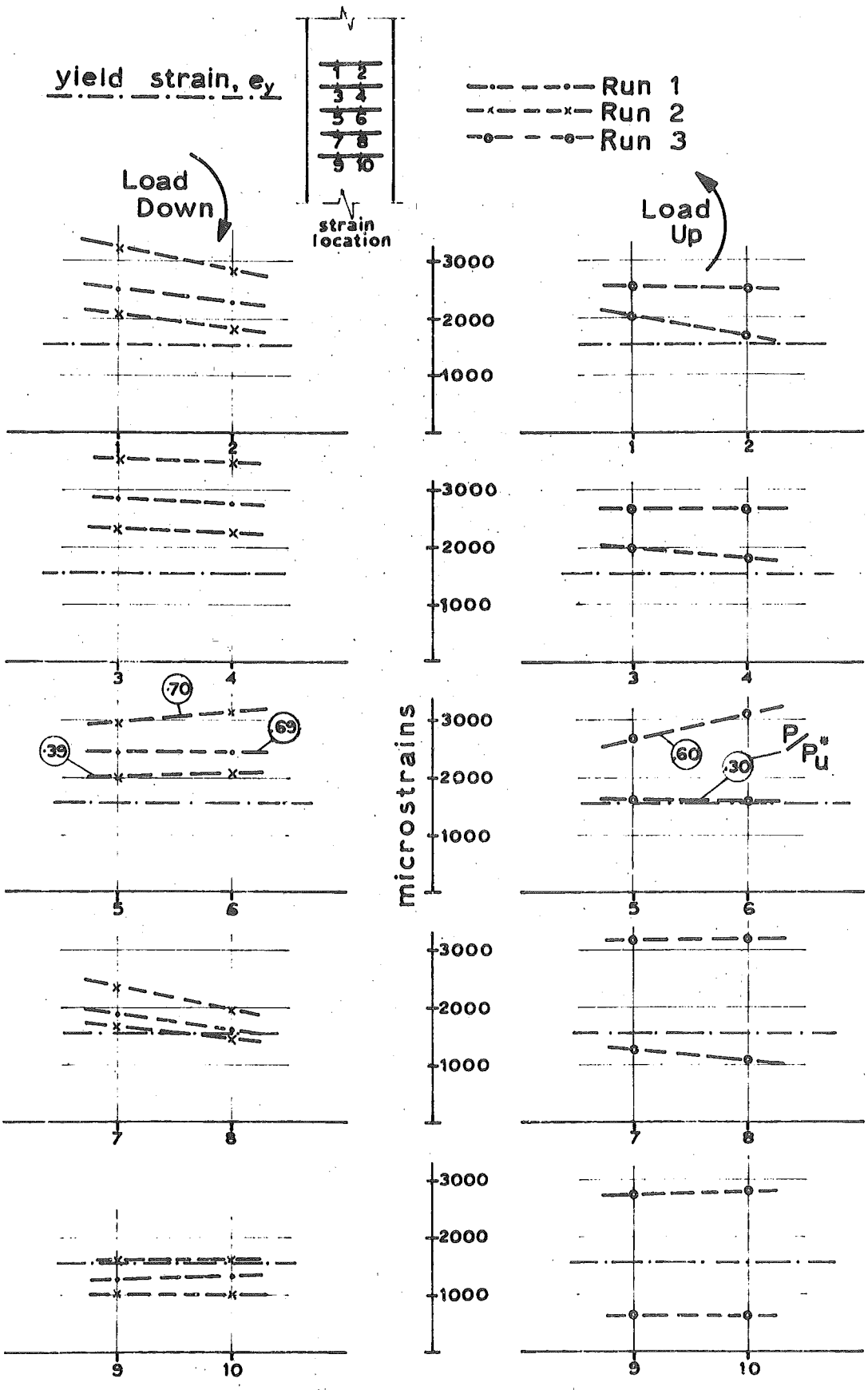

FIG. 4.7 (a) THE DISTRIBUTION OF STEEL STRAINS ON BACK OF JOINT TIES IN UNIT 1

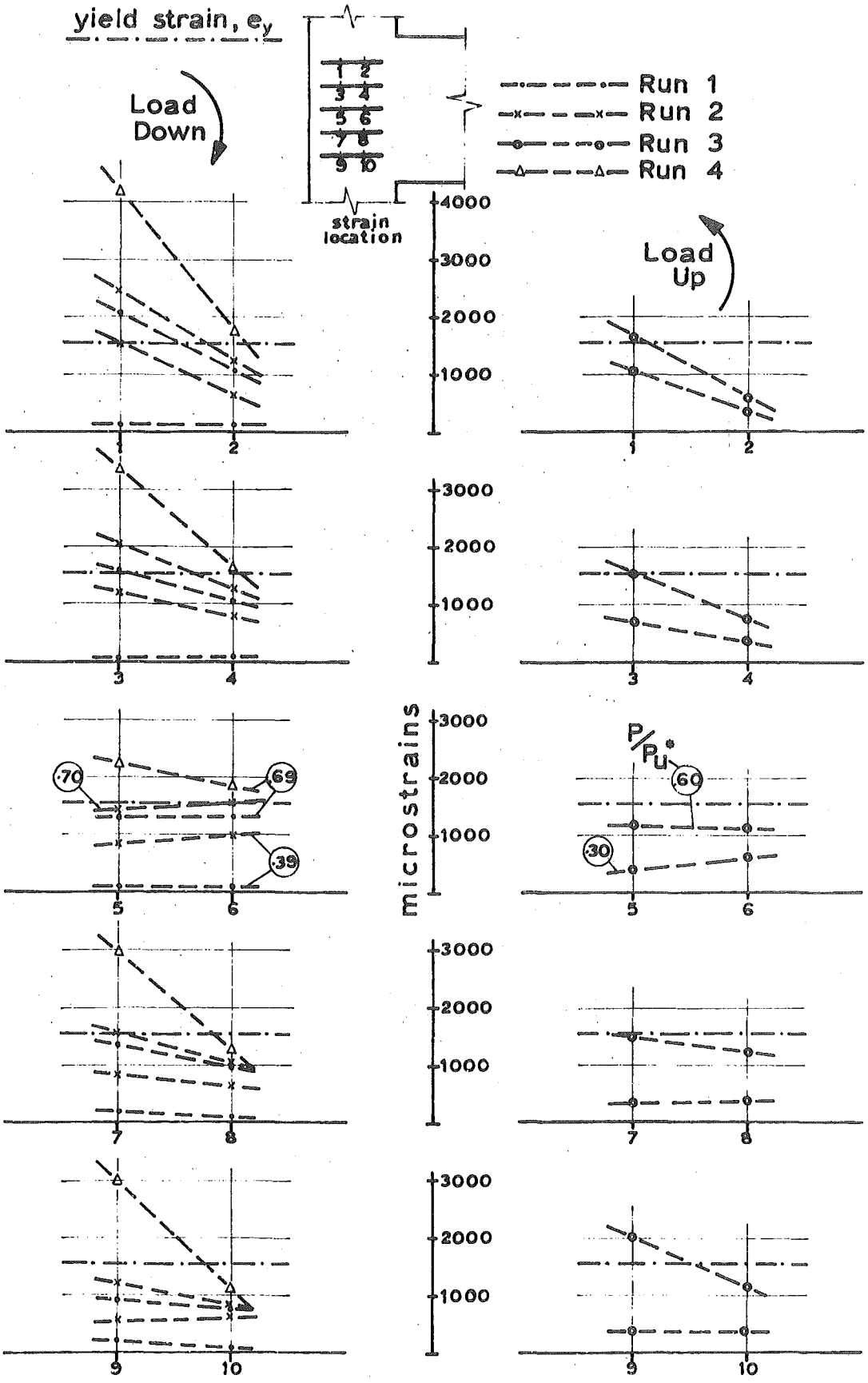

FIG. 4.7 (b) THE DISTRIBUTION OF STEEL STRAINS ON SIDE OF JOINT TIES IN UNIT 1

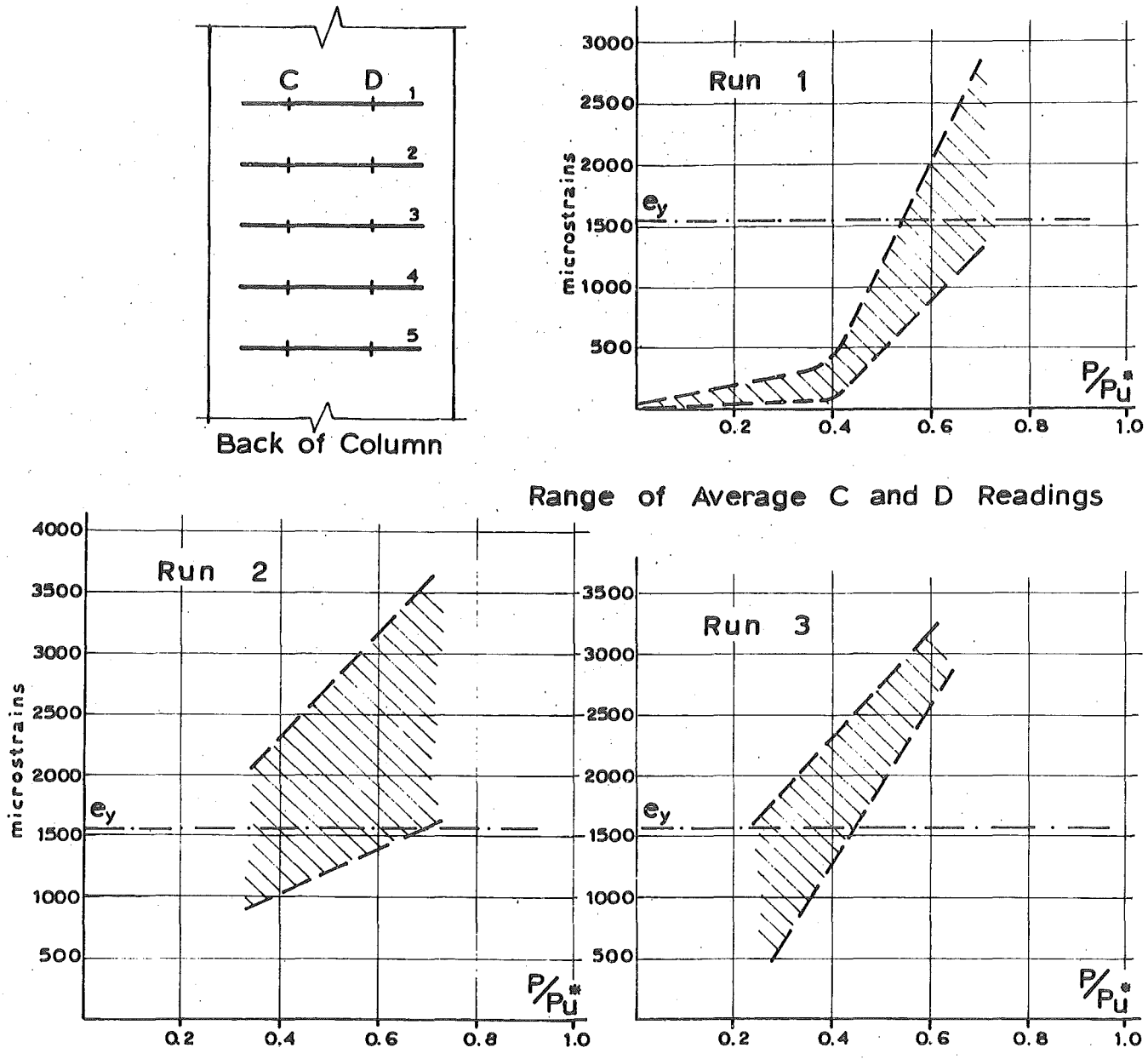

FIG. 4.8(a) THE LOAD-STRAIN RELATIONSHIP FOR JOINT TIES IN UNIT 1 AT BACK OF COLUMN

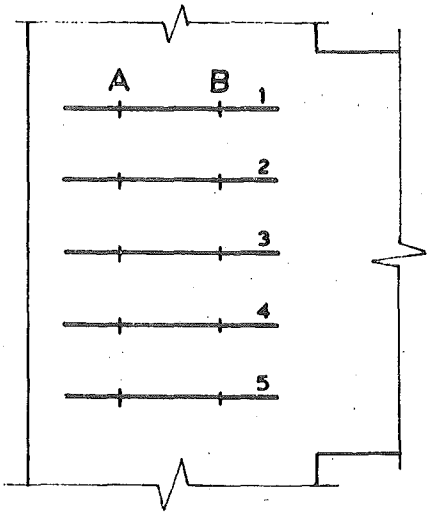

Side of Column

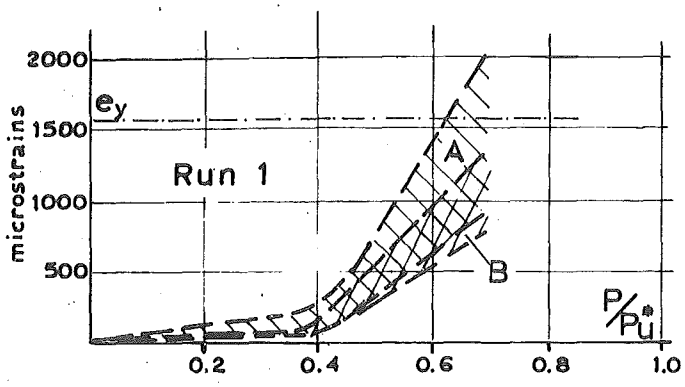

Range of Readings A and B

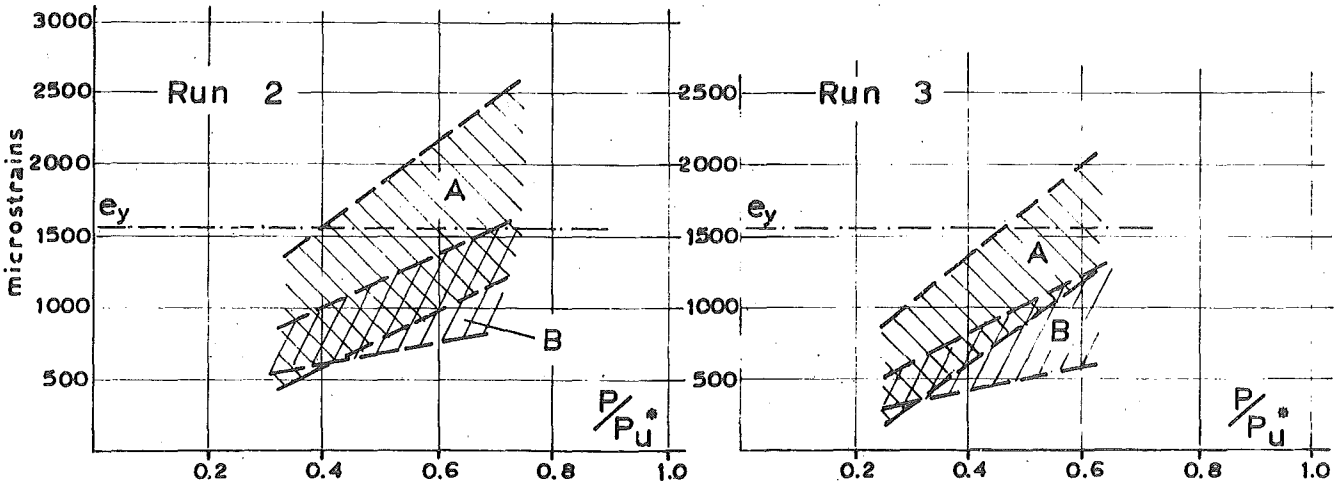

FIG. 4.8 (b) THE LOAD-STRAIN RELATIONSHIP FOR JOINT TIES IN UNIT 1 AT SIDE OF COLUMN

4.6.1 Deflections:

The deflected shapes of the specimen at the peaks of the elastic runs are shown in Fig. 4.9 and compared with the theoretical deflected shapes. The column does not deform symmetrically about its centre-line because of the difference in stiffness of the upper and lower columns caused by more cracks forming in the region of lower axial load.

4.6.2 Moment-Rotation Relationships:

The moment-rotation relationships for the column, both above and below the joint, are plotted in Figs. 4.10 (a) and 4.10 (b). The rotations were measured over a length of 15 in. from the face of the beam.

Fig. 4.10 shows the rotational ductility achieved during each cycle. However because other components of the structure, such as the joint and the beam, also contribute to the deformation of the specimen, this relationship cannot be used as a measure of overall ductility.

The rotation recording apparatus had to be removed after Run 5 due to excessive deformation of the frames around the column, and therefore the rotation could not be determined during Runs 6 and 7.

4.6.3 Load-Deflection Relationship:

The load-deflection relationship as shown in Fig. 4.11, gives a truer representation of the ductility and energy absorbing capacity of the structure. Since the deflection was measured at the end of the beam, deformations caused by beam and column rotations and joint distortion were all taken into account. The ductility factor obtained during each load run is shown in Table 4.1.

The loss of stiffness of the specimen due to cracking, and bond failure

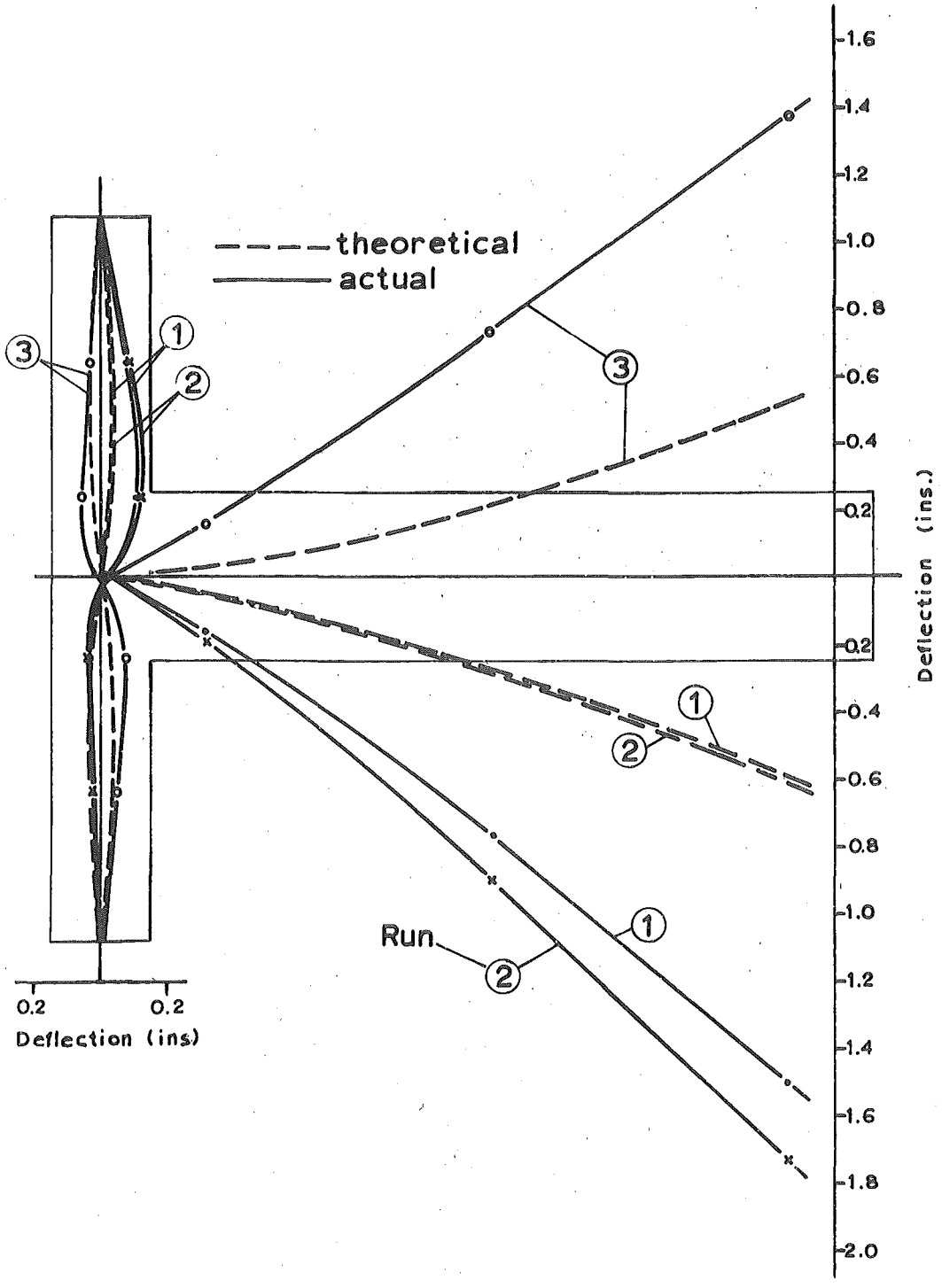

FIG. 4.9 DEFLECTED SHAPES OF UNIT 1 AT PEAKS OF ELASTIC LOAD RUNS

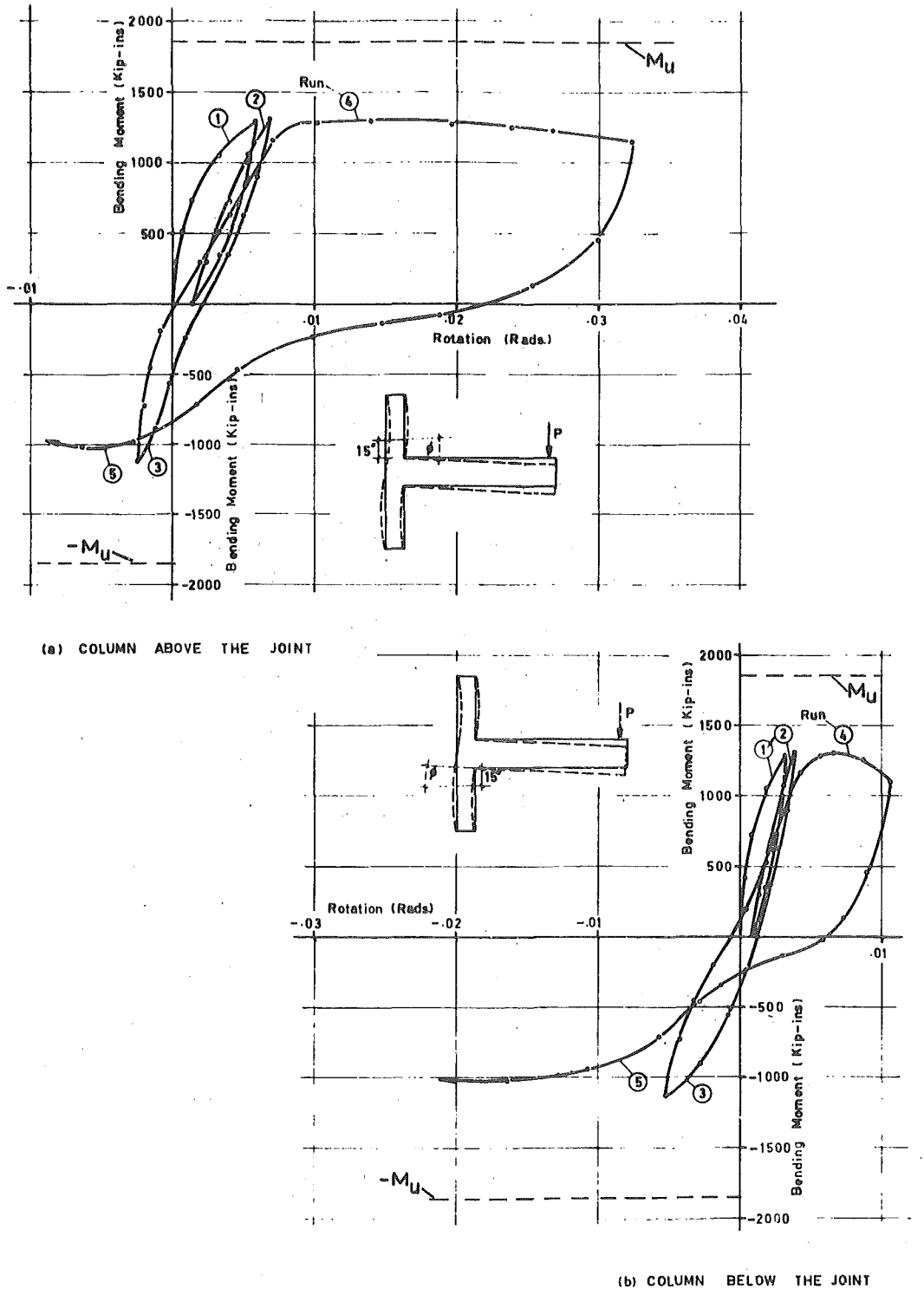

FIG. 4.10 THE MOMENT-ROTATION RELATIONSHIPS FOR UNIT 1

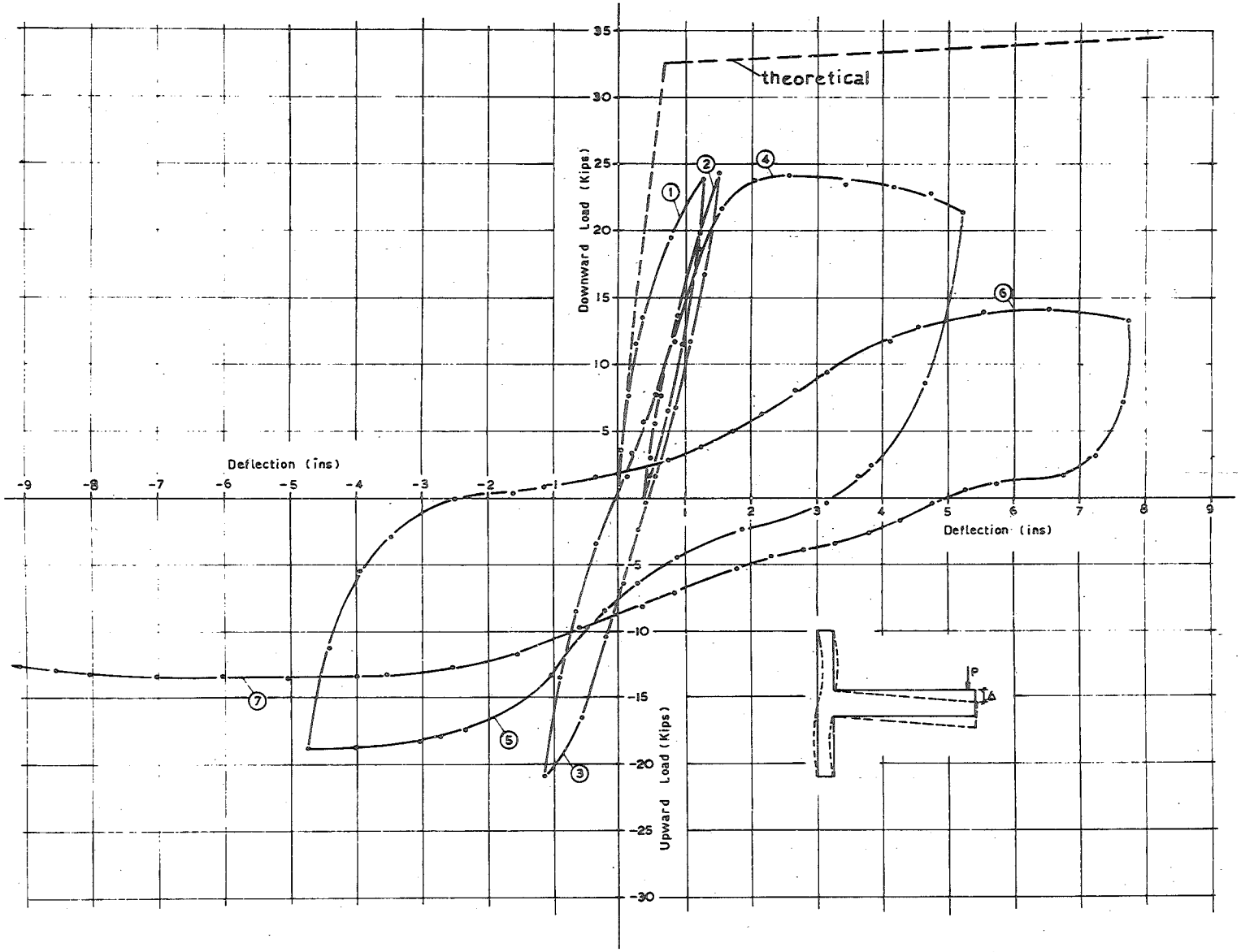

FIG. 4.11 THE LOAD DEFLECTION RELATIONSHIP FOR UNIT 1

of the flexural bars, is demonstrated in Fig. 4.11 after application of Run 4, the first run into the post-elastic range. The load resisted during Run 6 represents a loss of more than 40% of the load resisted during Run 4.

The theoretical bilinear load-deflection curve is shown for comparison in Fig. 4.11 and the effect of stiffness degradation is tabulated in Table 4.1.

TABLE 4.1 Performance of UNIT 1 During Load Cycling.

Run	Maximum Load $P_{max.}$ (kips)	$\frac{P_{max}}{P^*_u} \times 100$ (%)	Ductility Factor	Average % Stiffness †
1	23.9	69.7	-	47.8
2	24.3	70.8	-	54.9
3	20.9	61.0	-	35.9
4	24.0	70.0	7.0	36.1
5	18.8	54.8	9.0	7.9
6	14.0	40.8	13.7	4.6
7	13.6	39.7	15.5	4.3

† Expressed as % of the theoretical stiffness.

4.7 CRACKING:

Flexural cracks first appeared in the beam as predicted by theory at $P = 0.25\ P^*_u$. However, apart from the crack at the junction of the beam with the column, these remained minor cracks influenced only by the strain in the beam flexural bars, generally closing on reversal of loading. Cracks in the tension regions of the column above and below the joint became visible at $P = 0.40\ P^*_u$. More than 50% of the theoretical ultimate load had been applied before diagonal tension cracks formed in the joint region. To some extent the configuration of the cracks was influenced by the holes around the studs for gauge points on the reinforcement. However the general angle of diagonal tension cracks, as shown by Fig. 4.12, is steeper than 45° due to the presence of axial compression affecting the direction of principal tension.

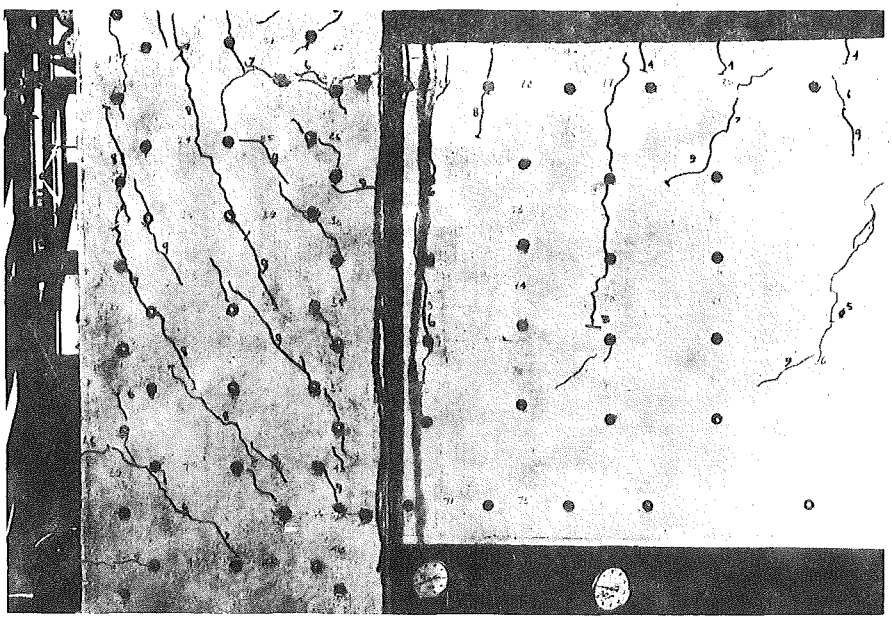

FIG. 4.12 UNIT 1 ON LOAD RUN 1

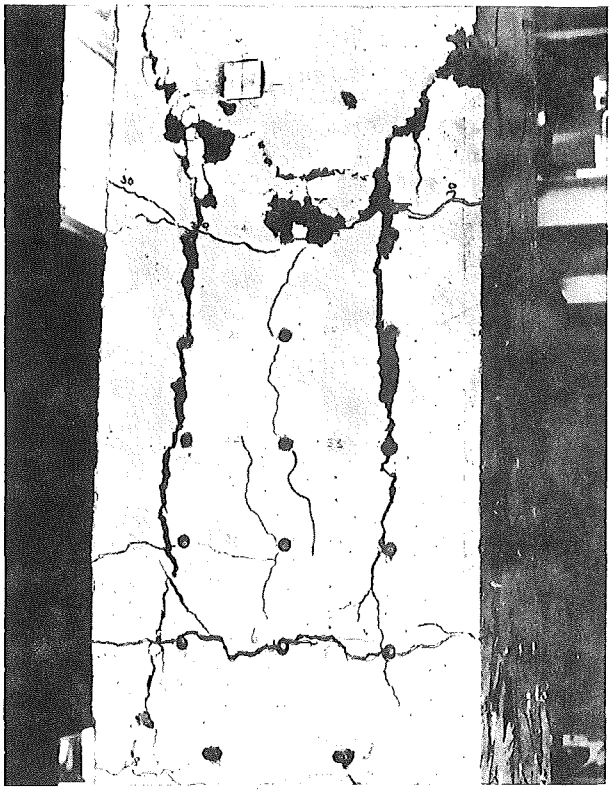

FIG. 4.13 BACK OF JOINT IN UNIT 1 ON LOAD RUN 6

FIG. 4.14 UNIT 1 ON LOAD RUN 4

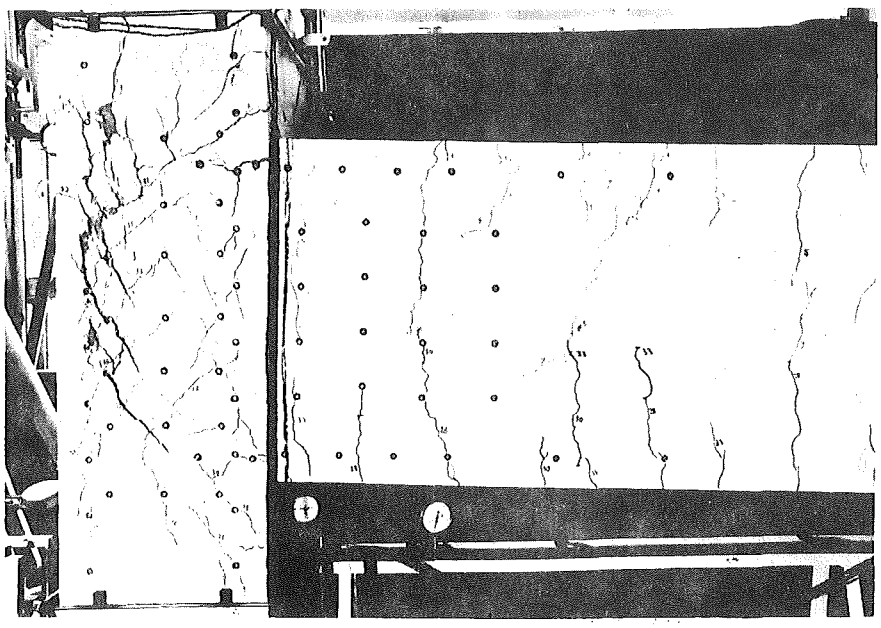

Vertical cracks down the line of the outer column bars both at the back, Fig. 4.13, and sides of the column indicated the high splitting stresses in this region. The cracks in the side of the column which followed the line of these bars eventually connected with the diagonal tension cracks to form the main failure cracks across the joint, as shown in Fig. 4.14.

4.8 THE FAILURE MECHANISM.

From the observations made during the load sequence and from the appearance of the specimen at failure, Fig. 4.15, it is apparent that the joint ties were insufficient to provide both adequate confinement and shear resistance.

The strain readings in the steel, and the crack pattern, indicated that the beam was attempting to rotate independently of the column, the joint ties being the connecting links. On downward cycles the beam appears to rotate about the base of the beam-column junction, pulling out at the top, therefore subjecting the upper ties to a greater strain than the lower ties. The reverse is the case for upward loading, thereby giving the strain distribution in the ties as shown in Fig. 4.6 (b).

Breaking up of the concrete in the joint lowered its ability to resist the applied shear force, which meant that the joint ties were then expected to take a larger proportion of the joint shear. However the distribution of strain in the joint ties shows that not all the ties work effectively during each load run. This led to yielding of the ties which allowed cracks to widen in the joint region. The diagonal tension cracks opened sufficiently to promote a shear failure across the joint as represented diagrammatically in Fig. 4.16.

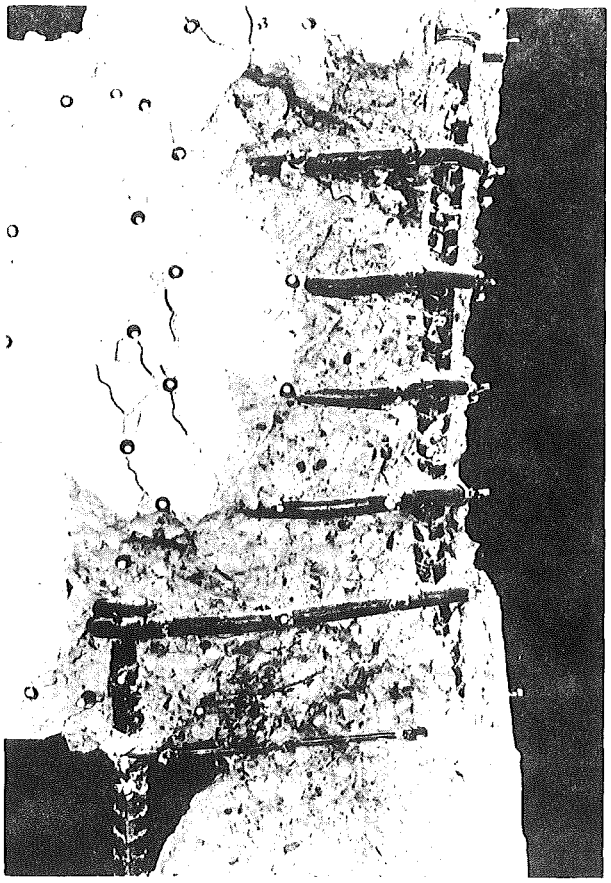

FIG. 4.15 UNIT 1 AT FAILURE ON LOAD RUN 7

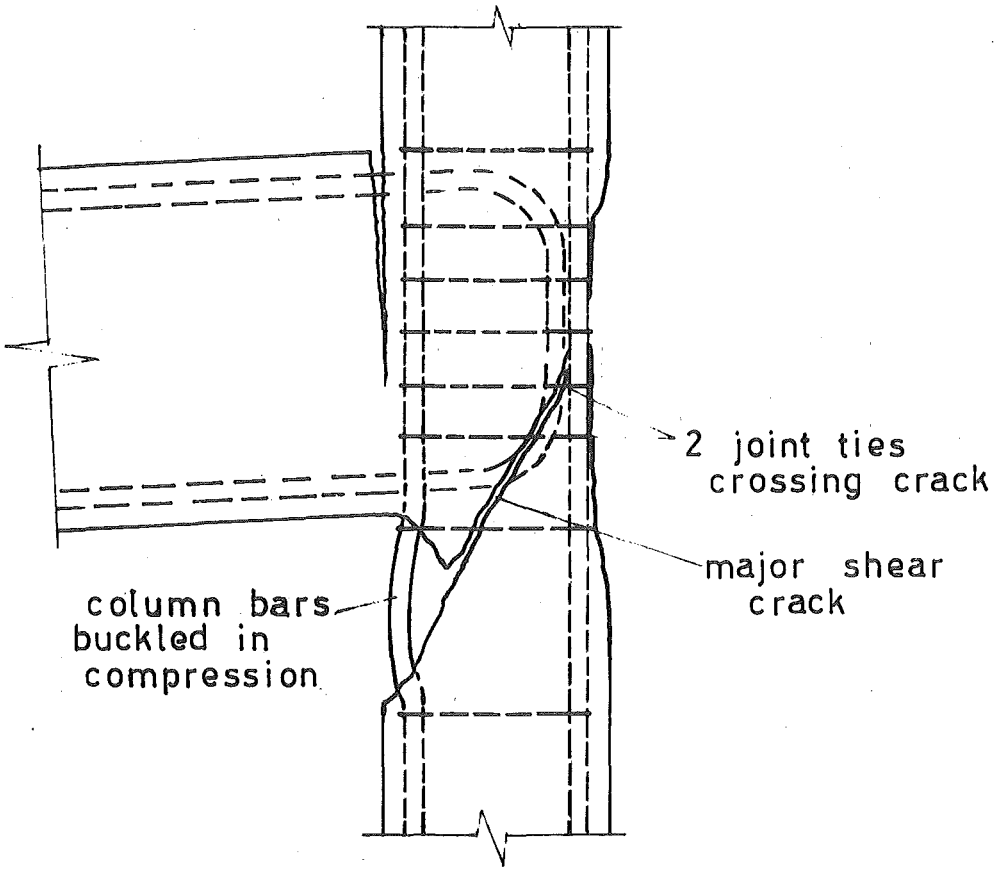

FIG. 4.16 FAILURE MECHANISM OF UNIT 1

CHAPTER FIVE

UNIT 2.

5.1 INTRODUCTION:

The behaviour of the second specimen is described in this chapter with particular reference to the strength of the joint itself, and the improvements shown over the strength of UNIT 1.

The majority of the results are presented in the form of graphs, to facilitate comparison of responses at different load levels.

5.2 DETAIL OF REINFORCEMENT:

To improve both the confining capability and the shear resistance of the joint, seven $\frac{5}{8}$ in. diameter ties were provided within this critical region, in an attempt to alleviate the stress in each tie, caused by the tendency for unequal stress distribution during different cycles. This represents 25% more transverse reinforcement than is theoretically required.

The other reinforcing details remained as specified in section 3.1, and are shown in Fig. 5.1.

5.3 GENERAL PERFORMANCE:

During the initial elastic cycles the behaviour of this specimen showed similar tendencies to UNIT 1, except that the less intense diagonal tension cracking in the joint, Fig. 5.2, indicated the effect of the increase in the amount of transverse reinforcement. Less strain in the joint ties supported the belief that the specimen was resisting the applied load more effectively than its predecessor, however the fact that the majority of the cracking was confined to the joint region indicated that this was again going to be the

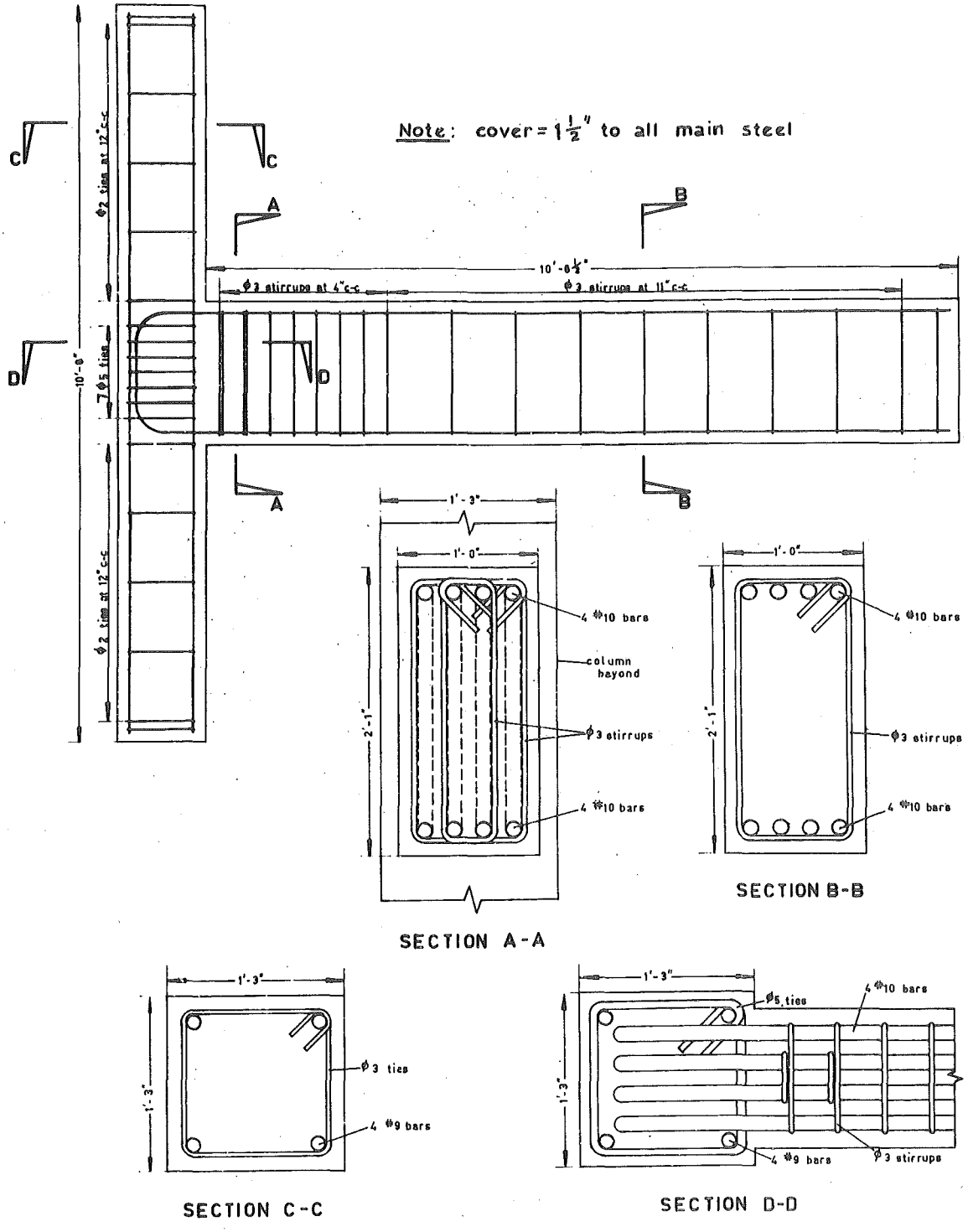

FIG. 5.1 REINFORCING DETAIL FOR UNIT 2

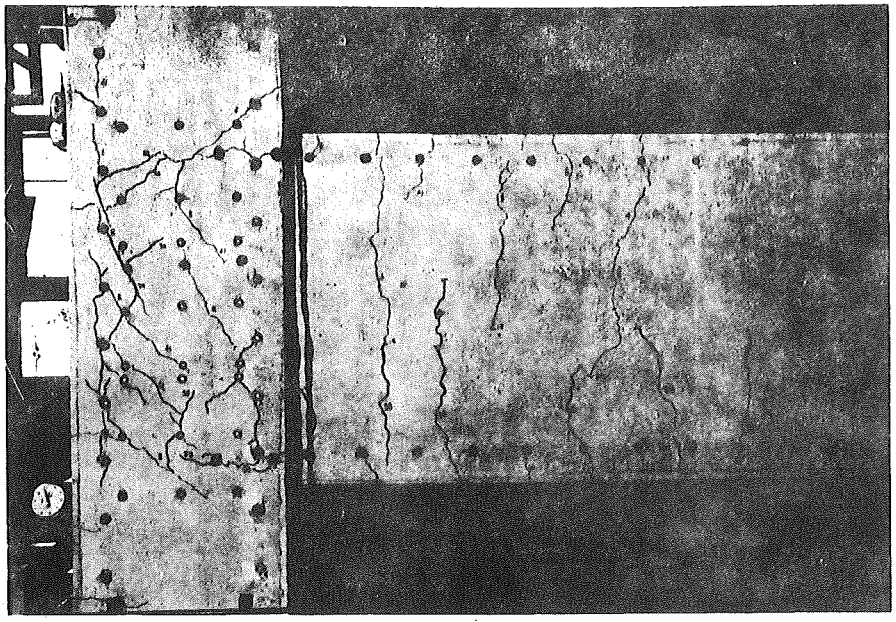

FIG. 5.2 UNIT 2 ON LOAD RUN 3

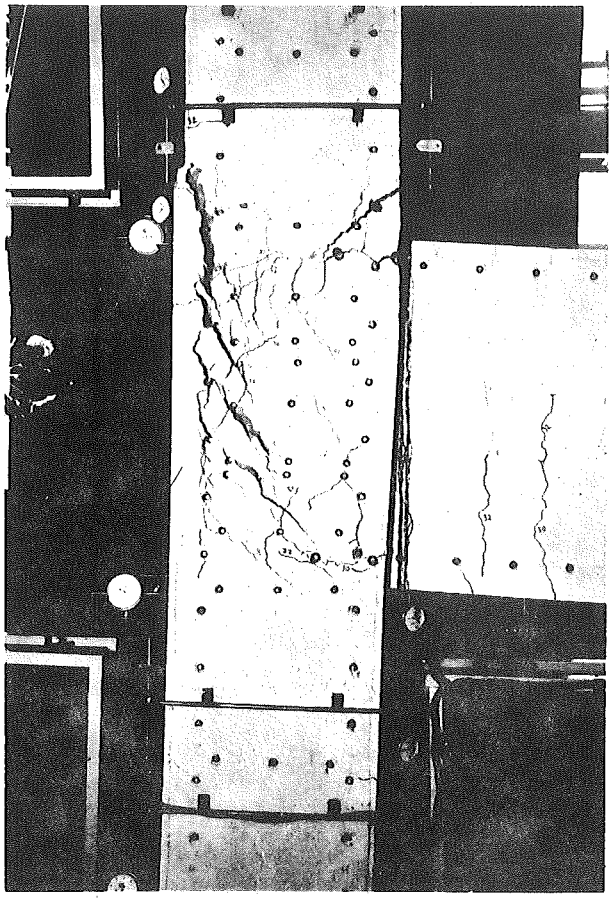

FIG. 5.3 UNIT 2 ON LOAD RUN 4

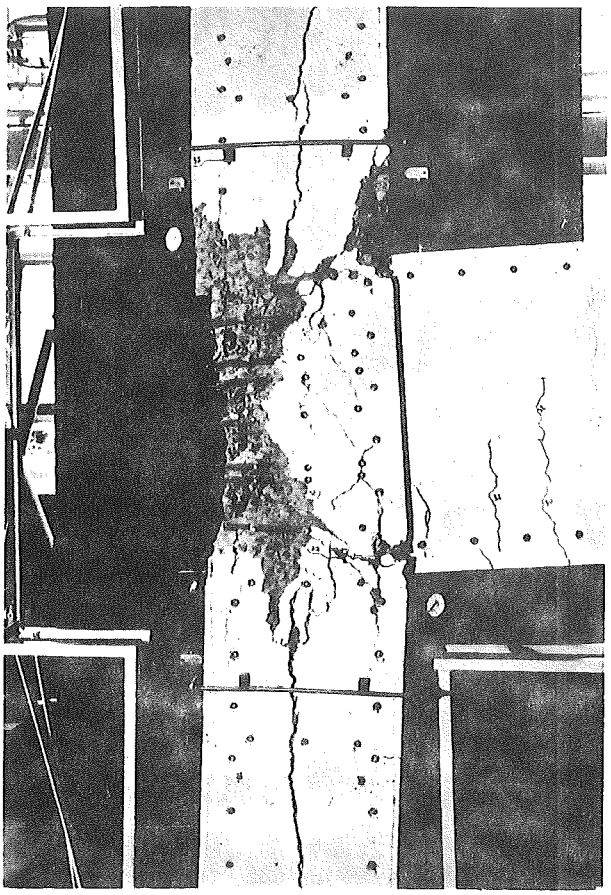

FIG. 5.4 UNIT 2 SHOWING SEC. VERTICAL CRACK AT FAILURE

weakest component of the structure.

Most of the deterioration of the joint, both visually and structurally, became apparent during Run 4, the first post-elastic run, following similar lines to UNIT 1. The vertical cracks connected with the diagonal tension cracks in the joint, to form the major failure cracks. Cover concrete was forced off, particularly around the joint, providing negligible load resistance after the elastic cycles.

Although the specimen exhibited better resilience than UNIT 1, by sustaining its load over a greater number of cycles, the maximum load resisted was still only 75% of the theoretical ultimate load - an insignificant improvement over UNIT 1. A bond failure of the beam flexural bars in the column appeared to be the main cause of the loss in load resisting capacity.

Runs 6 and 7 were imposed on this specimen in an attempt to attain $0.75\ P_u^*$, rather than a ductility factor of 0.75. It was soon realised that this could not be achieved. The test was terminated after Run 9 when the specimen could not resist a significant proportion of the theoretical ultimate load.

5.4 BEHAVIOUR OF FLEXURAL REINFORCEMENT:

5.4.1 Column Bars:

Apart from the occasional inaccurate reading, strains were generally consistent with theoretical predictions. The distribution of strain in the column bars is shown in Figs. 5.5 (a) and 5.5 (b). At low beam loads the bars in the column may be in compression over their whole length, indicating the effect of axial column load.

Vertical cracks down the side of the column on the line of the outer column bars again indicated the imminence of bond failure, which became

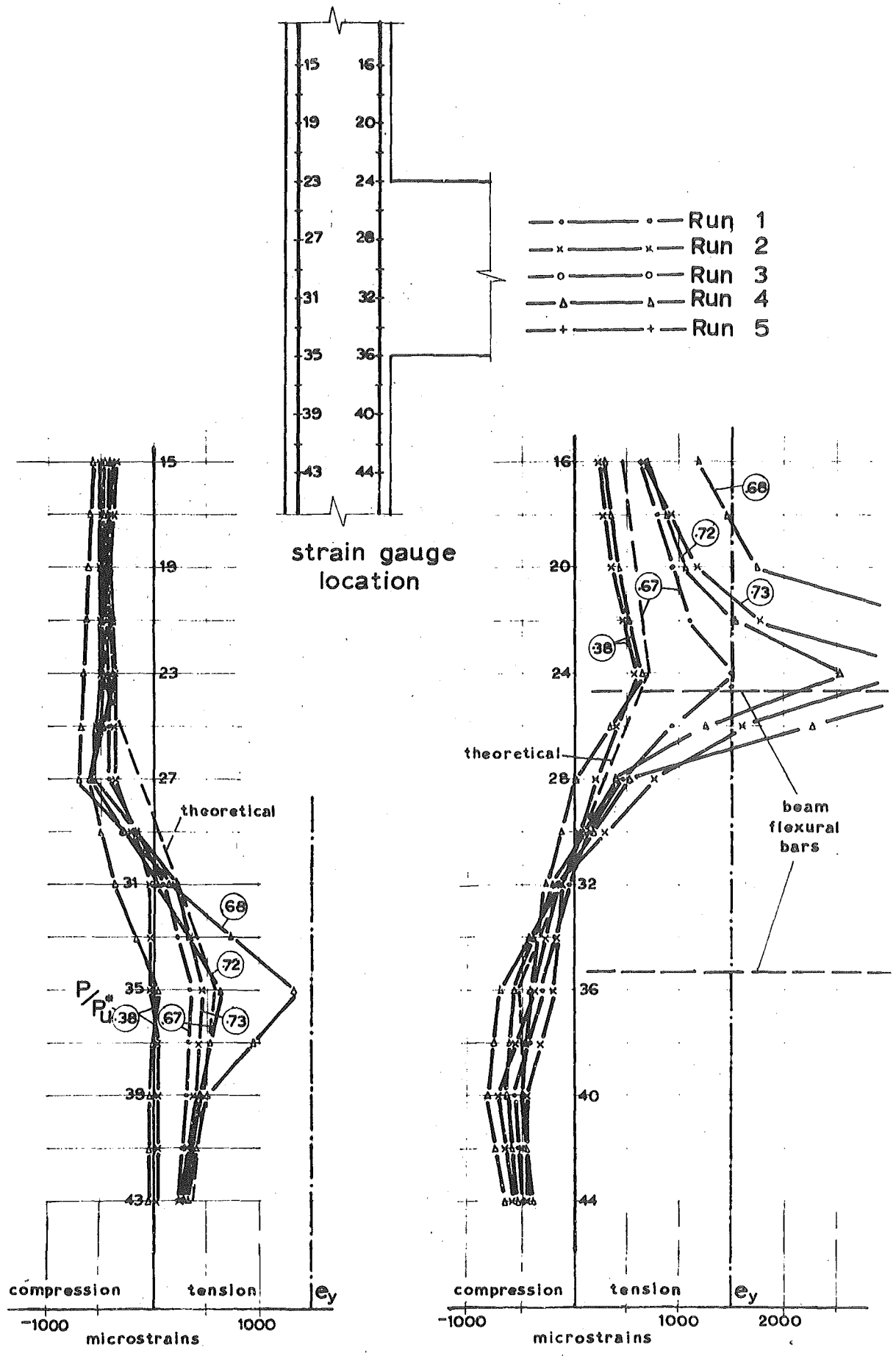

FIG. 5.5 (a) THE DISTRIBUTION OF STEEL STRAINS IN COLUMN FLEXURAL BARS IN UNIT 2 [FOR DOWNWARD LOAD RUNS]

For strain gauge locations see Fig. 5.5(a)

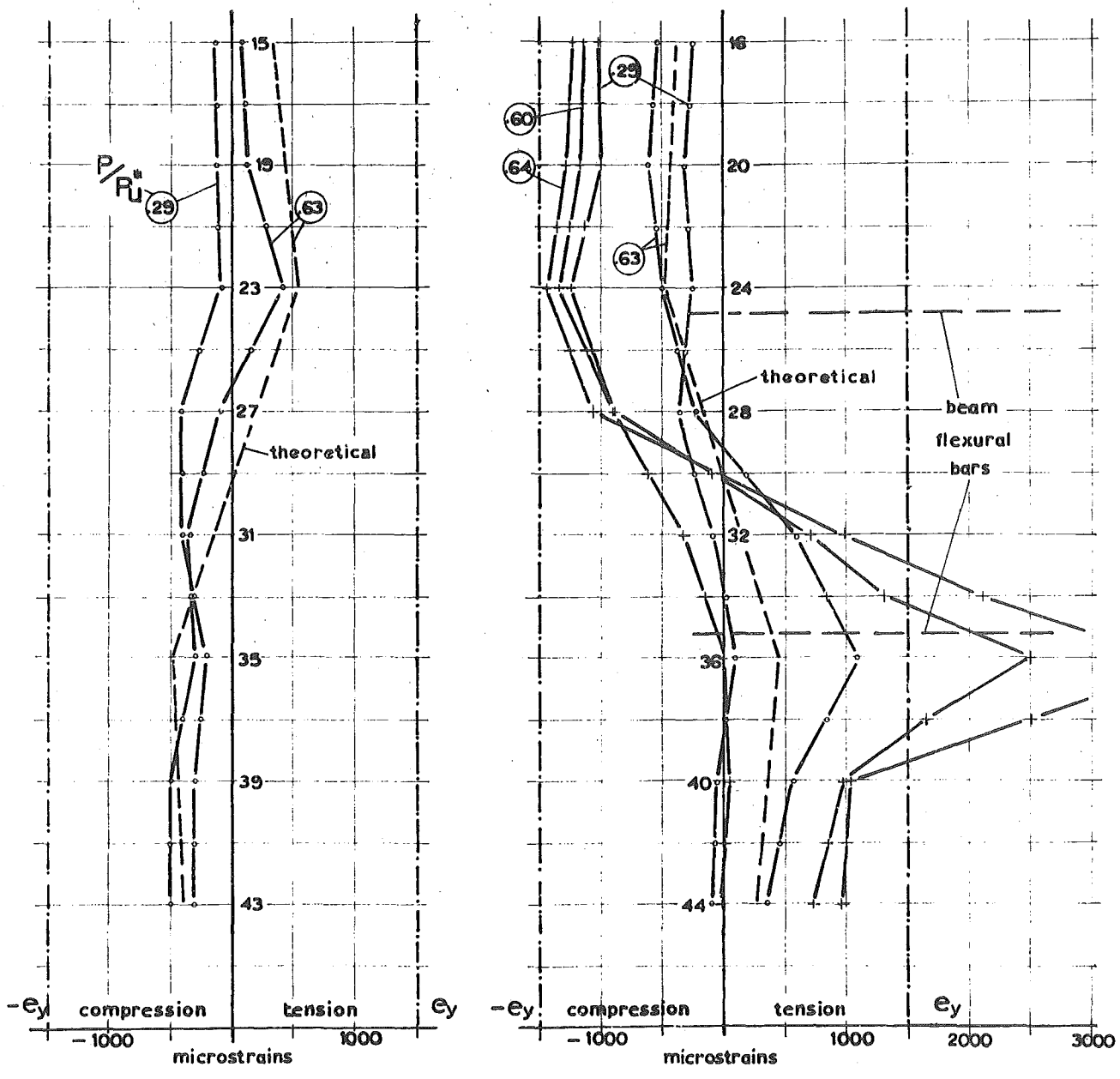

FIG. 5.5(b) THE DISTRIBUTION OF STEEL STRAINS IN COLUMN FLEXURAL BARS IN UNIT 2 [FOR UPWARD LOAD RUNS]

apparent as early as Runs 3 and 4 in the load sequence. From observation of the nature of the bond failure it was evident that although the bond stress was reasonably large, it was the application of reversed loading which was detrimental to bond performance. The slip between the concrete and steel during Run 5 was large enough for the concrete to be forced against the demec studs, so that readings of strain in the outer column bars were not meaningful.

Eventually, once the cover concrete had been dislodged, the column bars buckled in compression in the region above the joint due to inadequate restraint from the transverse reinforcement.

5.4.2 Beam Bars:

The strain in these bars showed a reasonably consistent trend at the various load levels for different cycles, as shown in Figs. 5.6 (a) and 5.6 (b), where variations in strain at different locations show the effect of cracking in the particular region. Although the readings from the demec studs in the column (locations 77 and 85) are obviously suspect, there appears to be a tendency for the stress to be dissipated from the point where the bar enters the column.

The increase in strain during the post-elastic range of Run 4 is presumably caused by the greater deflection applied at the end of the beam. The increased stress in the bars did not, however, produce a greater moment of resistance in the beam since the measured load is virtually unchanged in this range.

The anchorage of the beam bars in the column was inadequate for this specimen once the joint began to deteriorate, and at failure, when the cover concrete had been dislodged, it was obvious that bond failure had occurred around the outside of the bend of the beam flexural bars in the

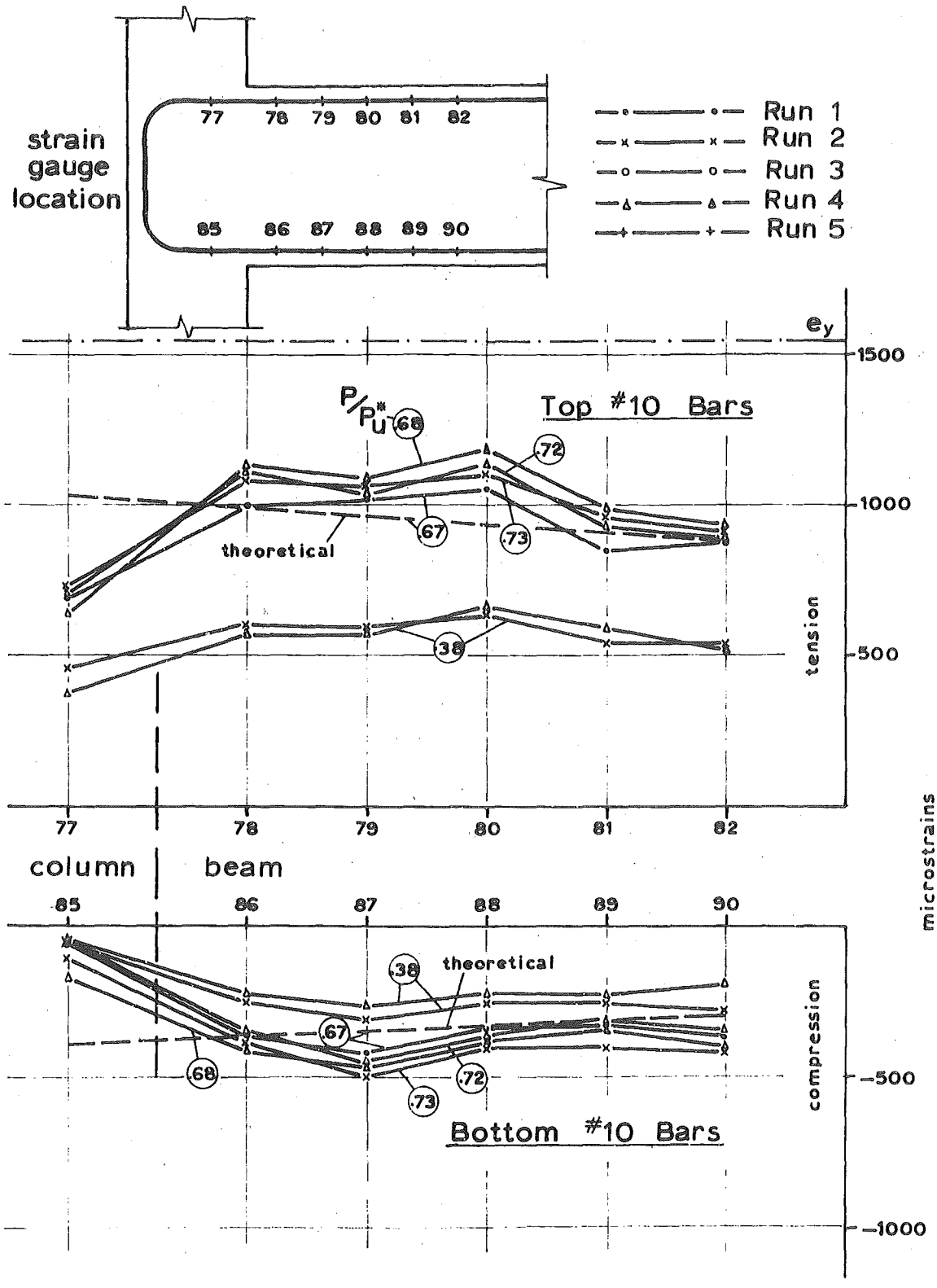

FIG. 5.6(a) THE DISTRIBUTION OF STEEL STRAINS IN BEAM FLEXURAL BARS IN UNIT 2 [FOR DOWNWARD LOAD RUNS].

For strain gauge locations see Fig. 5.4(a)

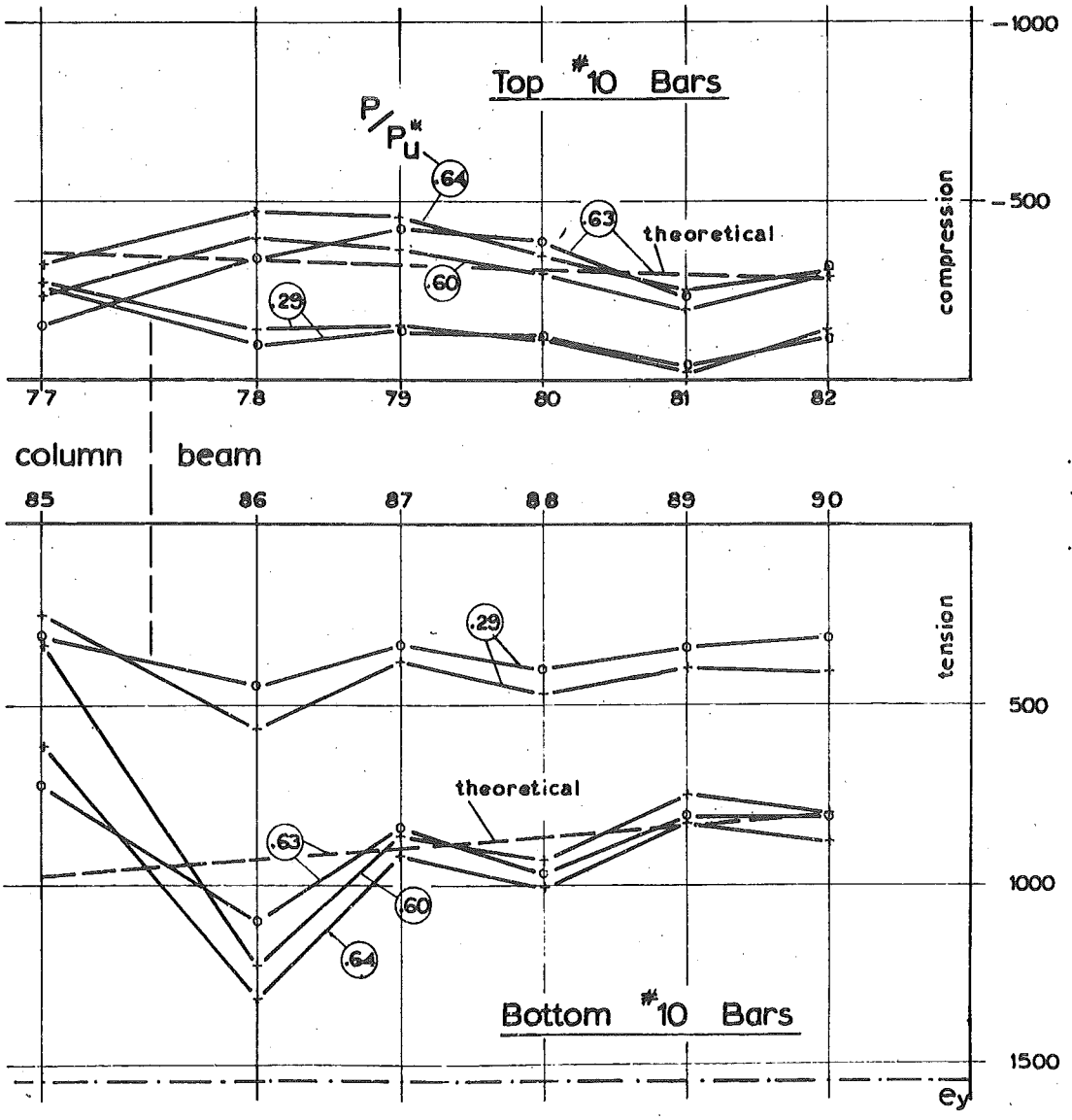

FIG. 5.6(b) THE DISTRIBUTION OF STEEL STRAINS IN BEAM FLEXURAL BARS IN UNIT 2 [FOR UPWARD LOAD RUNS]

joint (see Fig. 5.16).

5.5 BEHAVIOUR OF TRANSVERSE REINFORCEMENT:

5.5.1 Column Ties:

Again the column ties proved to be inadequate. During the elastic cycles when shear was the major consideration and the extent of cracking was as shown in Fig. 5.2, the strain readings indicated a maximum stress in the ties of 30,000 psi. However when Run 4 was applied the cracking propagated above the joint region (see Fig. 5.3) and the strain in the ties in this region increased by 500% into the yield range. The ties below the joint yielded on Run 5.

A vertical crack down the centre of the column, shown in Fig. 5.4, which opened during the post-elastic cycles gave further evidence of the inability of these ties to restrain lateral expansion of the column.

5.5.2 Joint Ties:

The effect that bowing of the ties had on the strain readings was not realised until after the testing of UNIT 2 and therefore the DEMEC strain gauge readings are subject to the same inaccuracies as UNIT 1.

Considering the strain distribution on the back of the ties, as shown in Fig. 5.7 (a), the vast difference between the strain readings in the elastic and post-elastic cycles suggests that the expansion of the joint concrete really takes effect after the elastic range, with very little expansion before then. The readings at the same load for successive cycles show consistently higher values, indicating some permanent strain in the hoops or, possibly, a small amount of permanent bending. The trend for the upper ties showing larger readings on downward load runs was again the case.

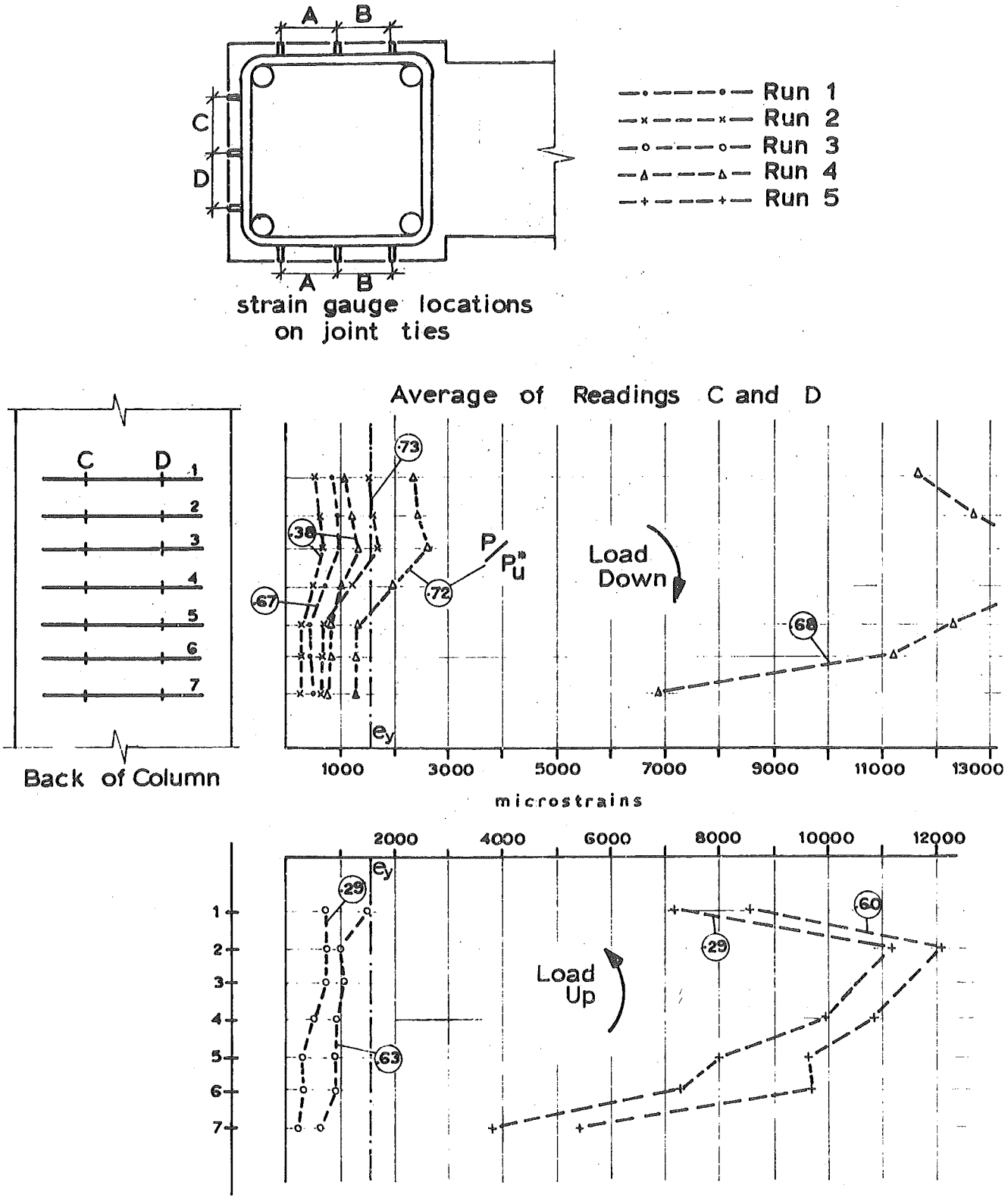

FIG. 5.7(a) THE DISTRIBUTION OF JOINT TIE STRAINS AT BACK OF COLUMN IN UNIT 2

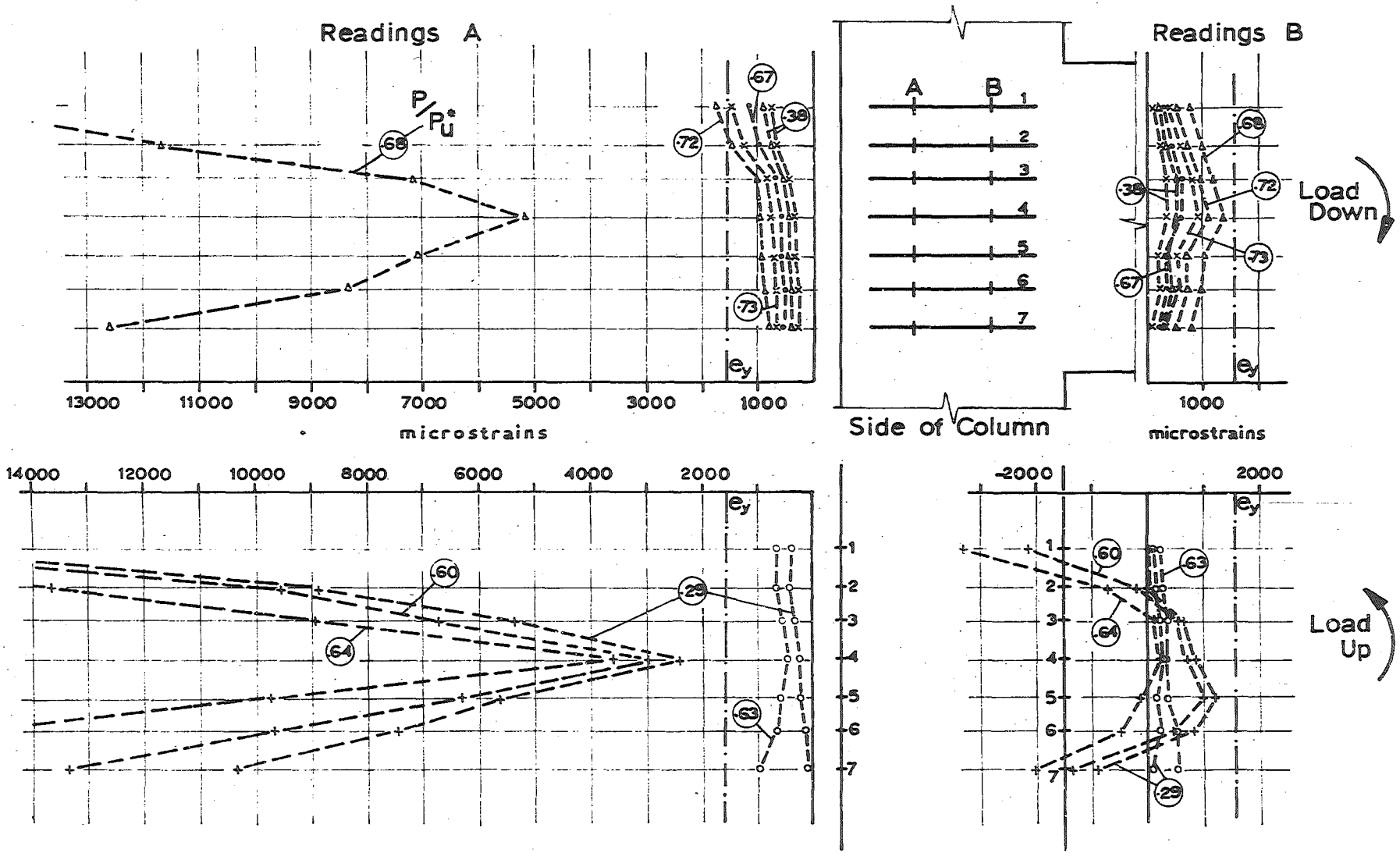

FIG. 5.7 (b) THE DISTRIBUTION OF JOINT TIE STRAINS AT SIDE OF COLUMN IN UNIT 2

The strain readings from the side of the ties, shown in Fig. 5.7 (b), demonstrated good performance in the elastic range, as expected, since the ties are here mainly concerned with shear resistance.

Vertical cracks down the back of the column became apparent during Run 3 and by the onset of the post-elastic range of Run 4 the cracks were fully developed down the joint which coincided with the dramatic strain increase shown in Fig. 5.7 (b). The distribution of strain during Run 5 is consistent with the theory explained in section 3.5.2.

Fig. 5.8 (a) shows the consistency and symmetry of the readings on the back of the joint ties. The increase in readings at the same load level for successive cycles can be easily seen, and in this case, is probably due to a permanent bend left in the ties from the previous cycle.

Fig. 5.8 (b), apart from the two upper ties, shows remarkably consistent readings along each tie, considering the unsymmetrical nature of the diagonal tension cracking. The top two ties may have been subjected to some bursting pressure before the lower ties, since the vertical crack at the back of the column extends from above the joint, Fig. 5.9, thereby affecting the readings on these ties.

The development of stress in the ties can be seen from Figs. 5.10 (a) and 5.10 (b) where the recovery of strain from a previous cycle can be easily extrapolated. The readings on the side of the ties show very little permanent strain, indicating that the higher readings for successive cycles may be due more to degradation in joint stiffness rather than a permanent strain from the previous cycle.

From the higher readings on the back of the ties, compared with the side readings, it appears that this region is subjected to considerably more bursting pressure than the side of the ties.

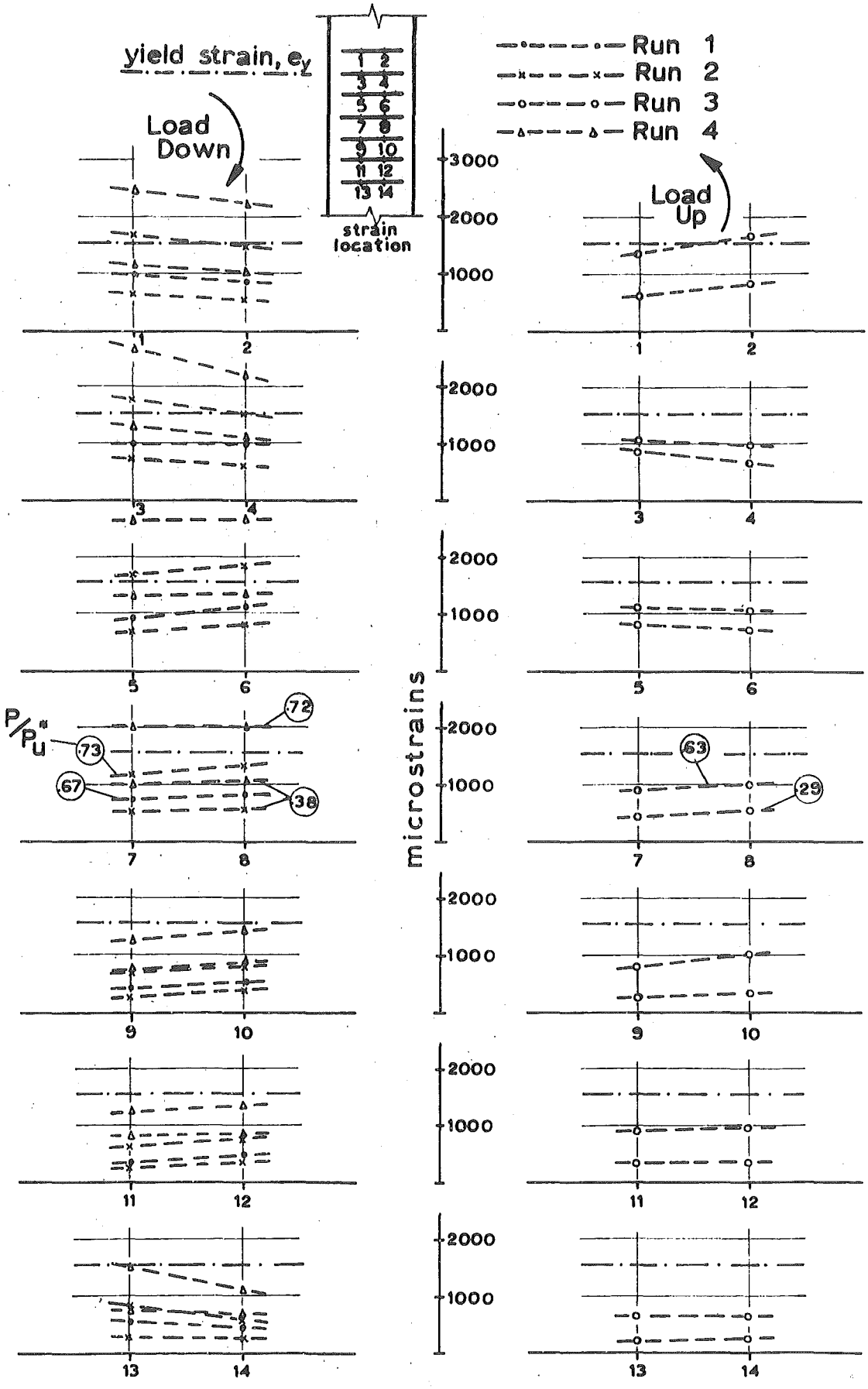

FIG. 5.8(a) THE DISTRIBUTION OF STEEL STRAINS ON BACK OF JOINT TIES IN UNIT 2

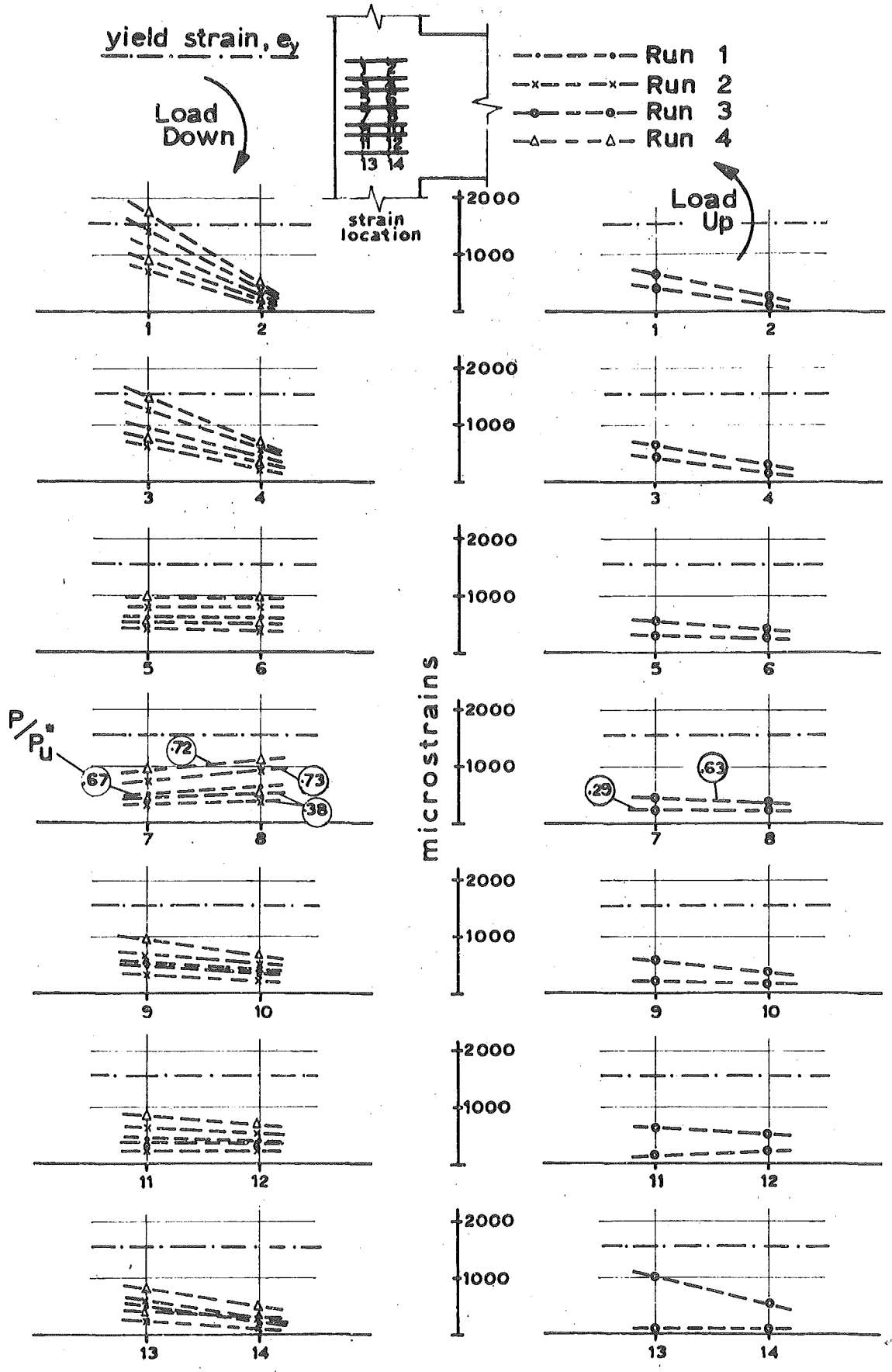

FIG. 5.8 (b) THE DISTRIBUTION OF STEEL STRAINS ON SIDE OF JOINT TIES IN UNIT 2

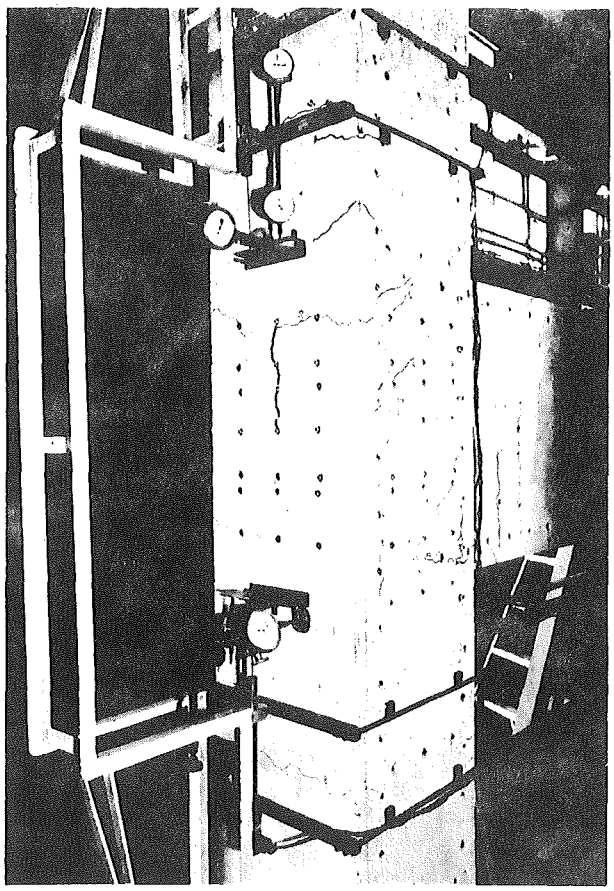

FIG. 5.9

BACK OF JOINT SHOWING VERTICAL SPLITTING CRACK IN UNIT 2

The overall performance of the ties appeared to be adequate in the elastic range, however, from the rapid deterioration of the joint during Run 4 it was obvious that the ties were insufficient for confinement of the joint under post-elastic cyclic loading conditions.

5.6 DEFORMATIONS:

5.6.1 Deflections:

The deflected shapes of the specimen at the peaks of the elastic runs are shown in Fig. 5.11 and compared with the theoretical shapes. It is apparent from the shape of the column that it did not rotate freely about the base hinge, thereby upsetting some of the theoretical assumptions of equilibrium of the specimen, although this did not affect the outcome of the test.

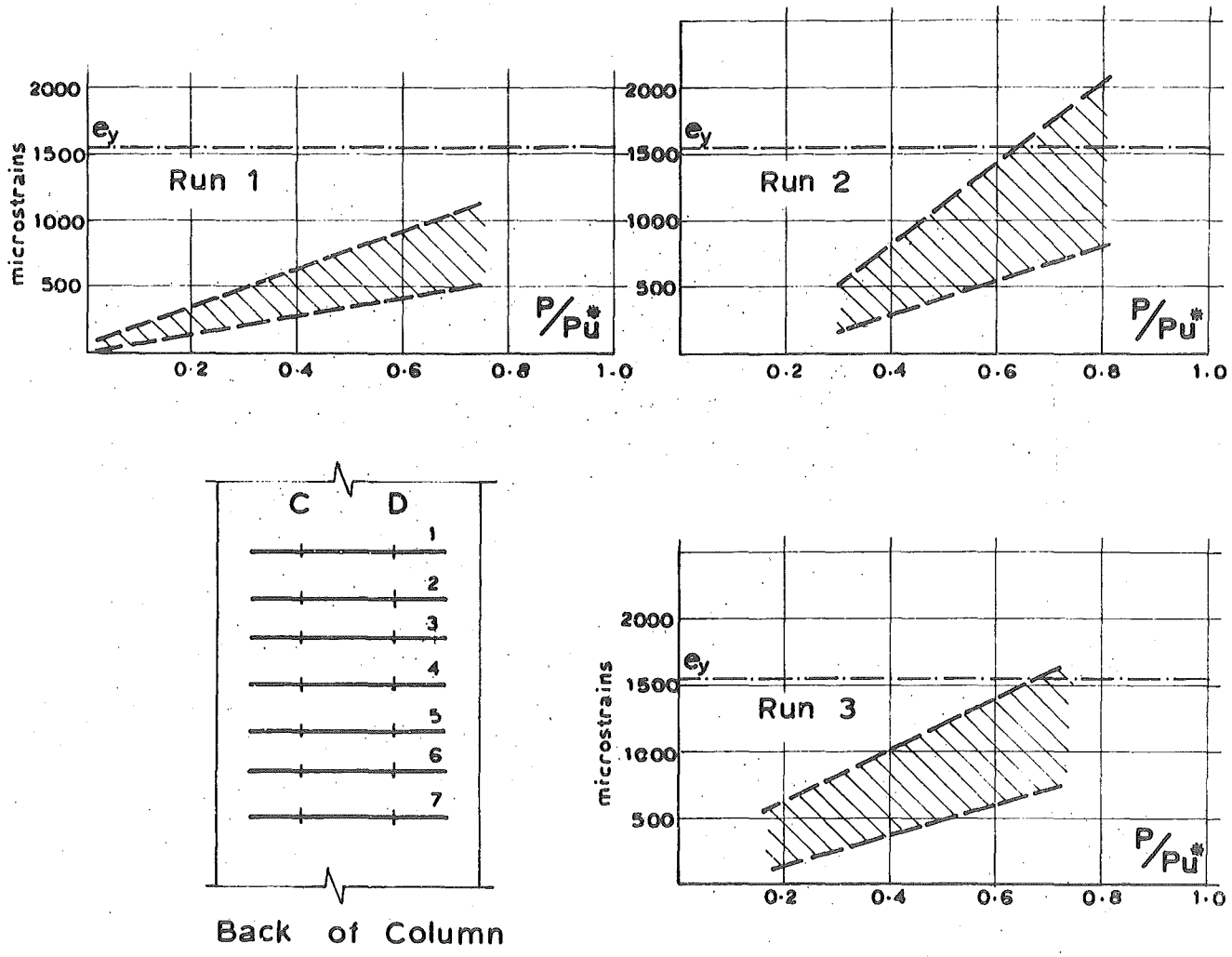

FIG. 5.10(a) THE LOAD–STRAIN RELATIONSHIP FOR JOINT TIES IN UNIT 2 AT BACK OF COLUMN

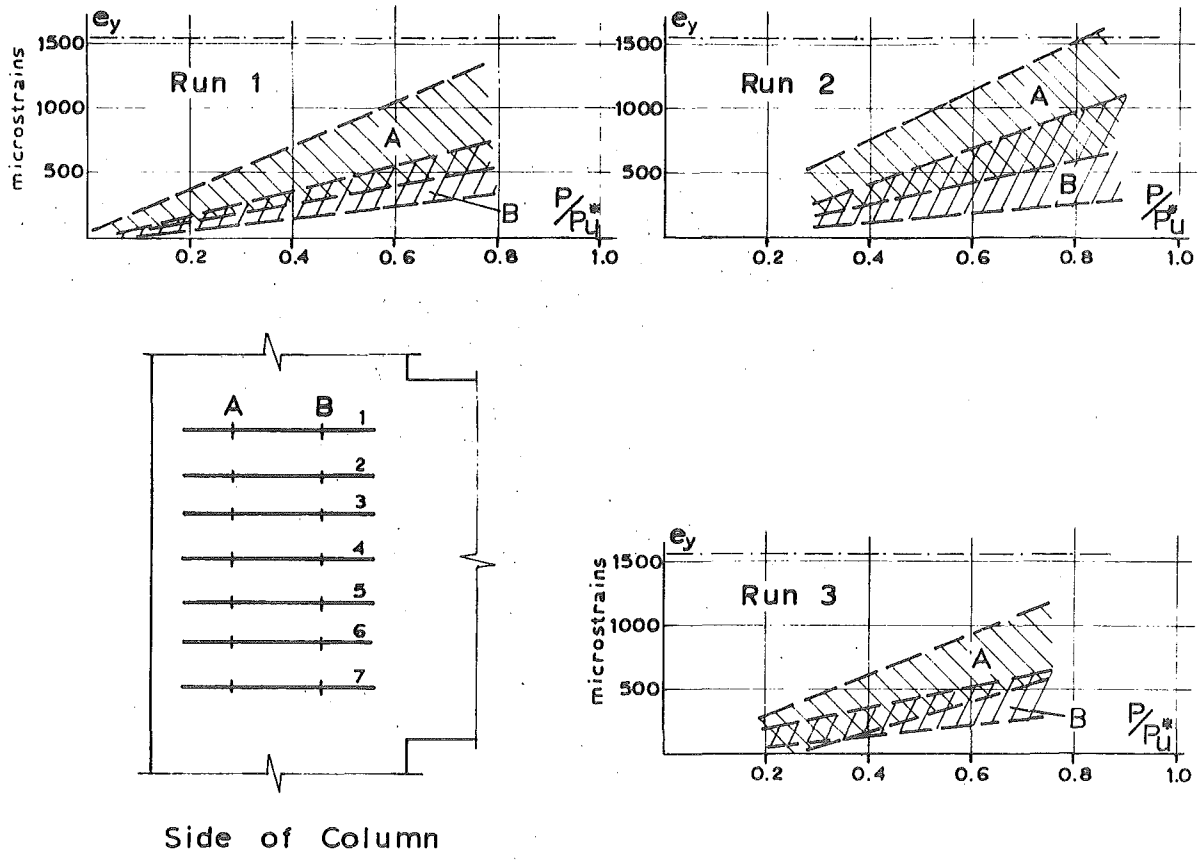

FIG. 5.10 (b) THE LOAD-STRAIN RELATIONSHIP FOR JOINT TIES IN UNIT 2 AT SIDE OF COLUMN

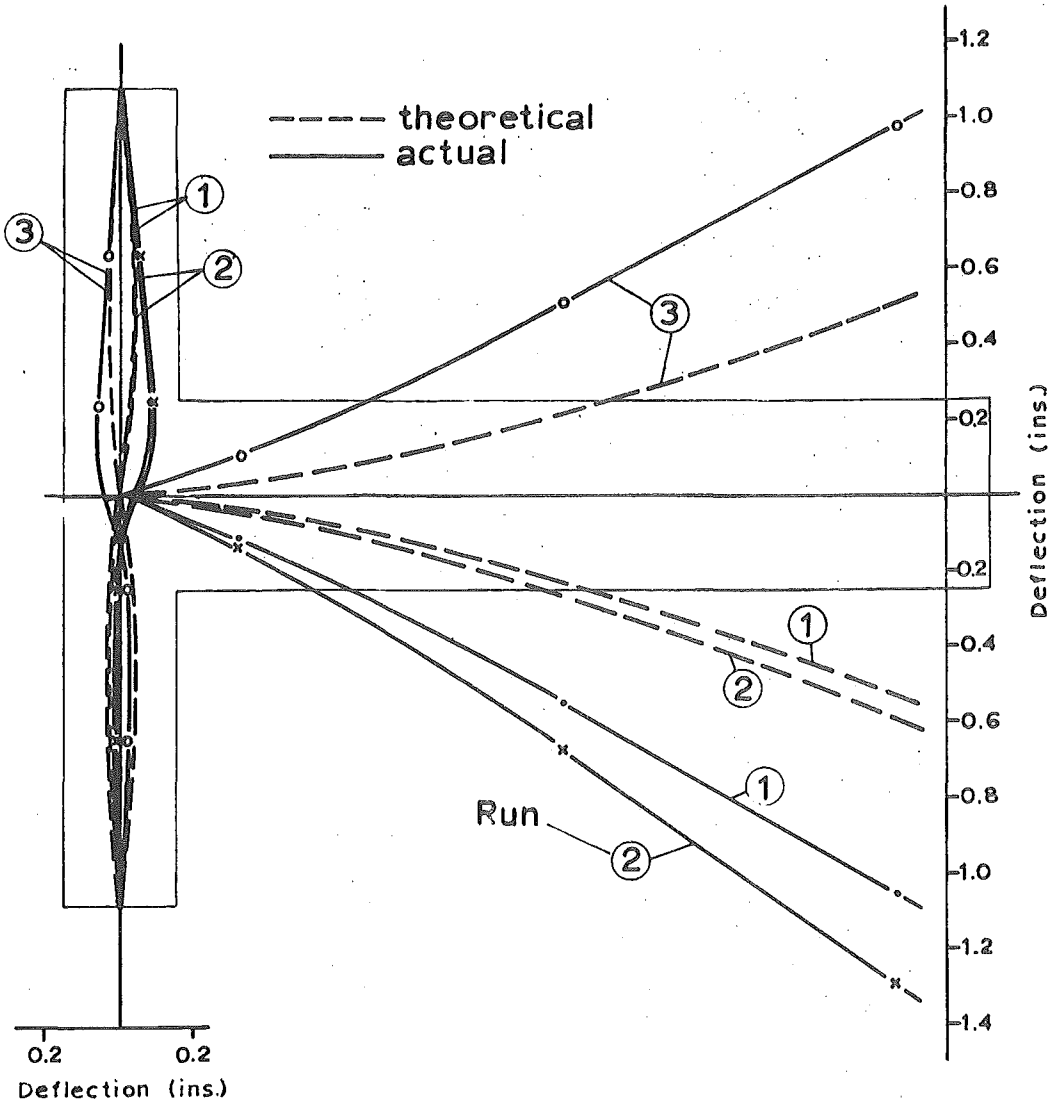

FIG. 5.11 DEFLECTED SHAPES OF UNIT 2 AT PEAKS OF ELASTIC LOAD RUNS

5.6.2 Moment-Rotation Relationships:

These are shown plotted in Fig. 5.12. The column exhibited a greater stiffness than did UNIT 1, presumably because of the reduction in the amount of cracking extending outside the joint region, during the initial elastic cycles. However the loss of stiffness of the column during subsequent cycles is clearly demonstrated.

5.6.3 Load-Deflection Relationship:

As shown in Fig. 5.13, the specimen exhibits a greater stiffness than UNIT 1 and also, although not providing sufficient ductility for the applied cyclic load sequence, does show a marked improvement in resilience under repeated load. The load capacity of Run 6 represents a 25% decrease in the maximum load resisted by Run 4.

The ductility factor and stiffness of the specimen during each load run can be obtained from Table 5.1.

TABLE 5.1. Performance of UNIT 2 During Load Cycling.

Run	Maximum Load P_{max} (kips)	$\frac{P_{max}}{P_u^*} \times 100$ (%)	Ductility Factor	Average % Stiffness †
1	24.0	66.9	-	69.1
2	26.3	73.3	-	72.2
3	22.7	63.2	-	50.8
4	27.1	75.5	7.2	48.6
5	22.9	63.8	9.3	9.8
6	20.3	56.6	9.7	7.9
7	18.7	52.1	8.0	6.5
8	18.8	52.4	12.3	7.0
9	17.7	49.3	14.4	4.5

† Expressed as % of the theoretical stiffness.

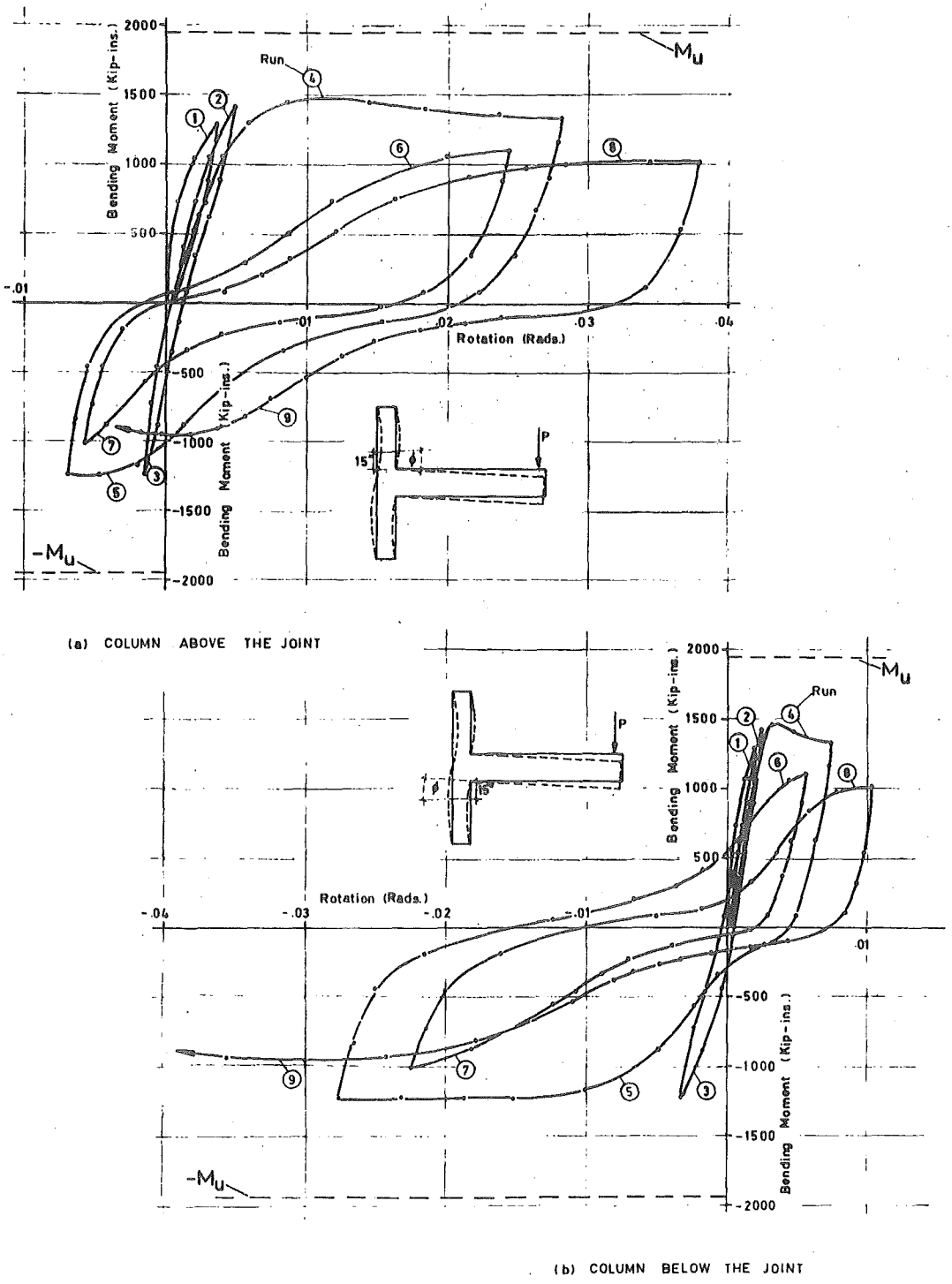

FIG. 5.12 THE MOMENT - ROTATION RELATIONSHIPS FOR UNIT 2

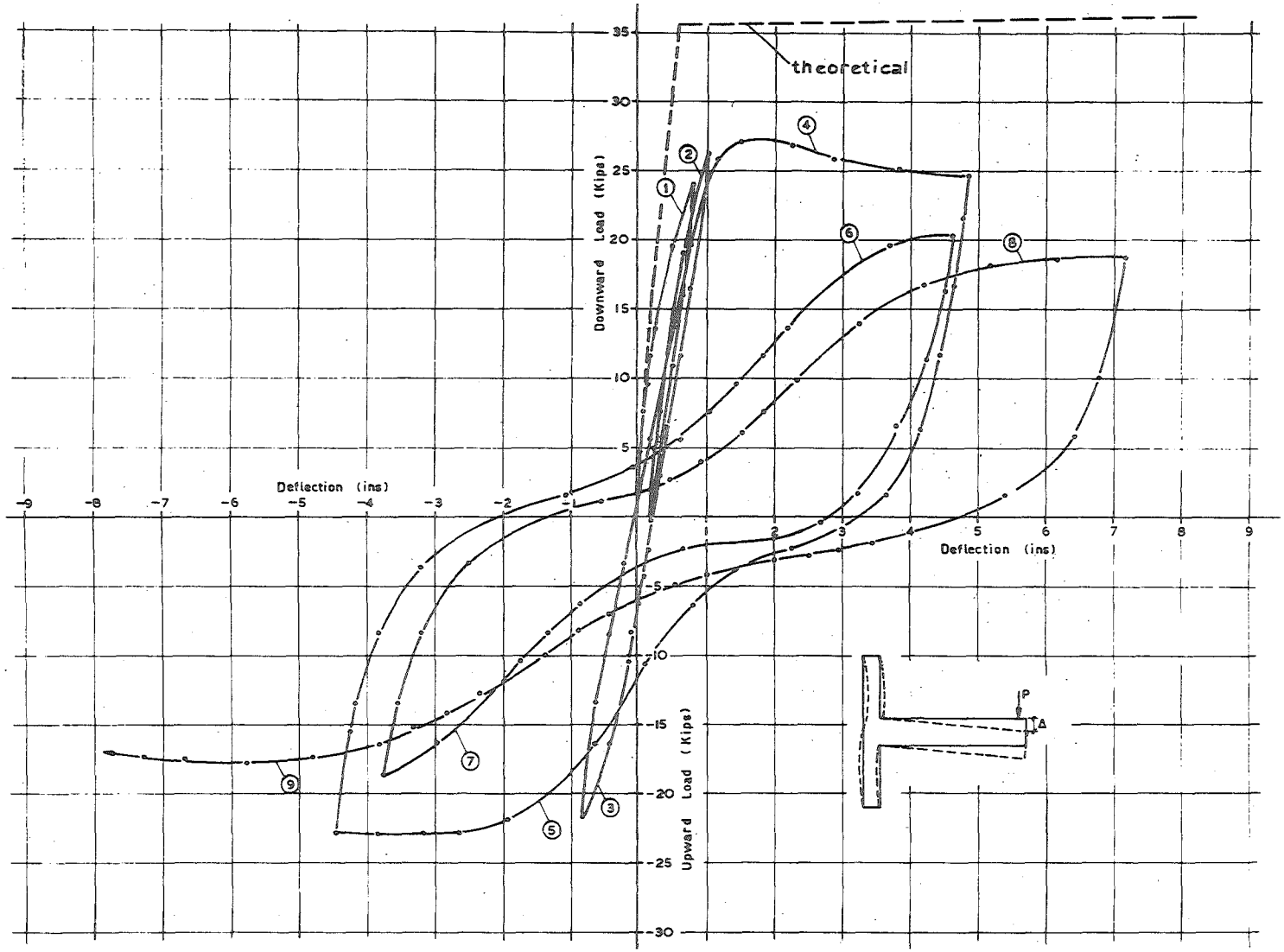

FIG. 5.13 THE LOAD DEFLECTION RELATIONSHIP FOR UNIT 2

5.7 CRACKING:

The pattern of cracking was similar to UNIT 1 initially but with fewer diagonal tension cracks in the joint. The major diagonal tension cracks and vertical cracks down the line of the outer column bars combined on reversal of load to form a semi-circular crack following the line of the beam flexural bars in the column (see Fig. 5.14). The subsequent deterioration followed similar lines to UNIT 1, with the cover concrete being dislodged and diagonal tension cracks widening and extending outside the joint region. There was local evidence of crushing and tension cracking both above and below the joint, see Fig. 5.15, however the tendency for the beam to pull out of the column caused a secondary vertical crack to form up the centre of the column necessitating the termination of the test. The crack can be seen clearly in Fig. 5.4.

5.8 THE FAILURE MECHANISM:

From observed behaviour of the specimen and strain readings taken during the test, it was apparent that the joint was sufficiently confined to withstand a number of reversed cycles in the elastic range. However the strength of the specimen was not appreciably increased over UNIT 1. From strain readings on the joint ties both at the side and back of the joint, the ties really began to bow as the maximum load was attained on Run 4. This suggests that the expansion which is then allowed to occur is directly responsible for the reduction in load resisting capacity, by facilitating bond failure of the flexural bars. This bond failure, shown in Fig. 5.16, results in the loss of stiffness of the specimen, since the beam tends to act independently of the column, as shown diagrammatically in Fig. 5.17. This mechanism causes the vertical crack to form up the centre of the column because of lack of resistance from the column ties.

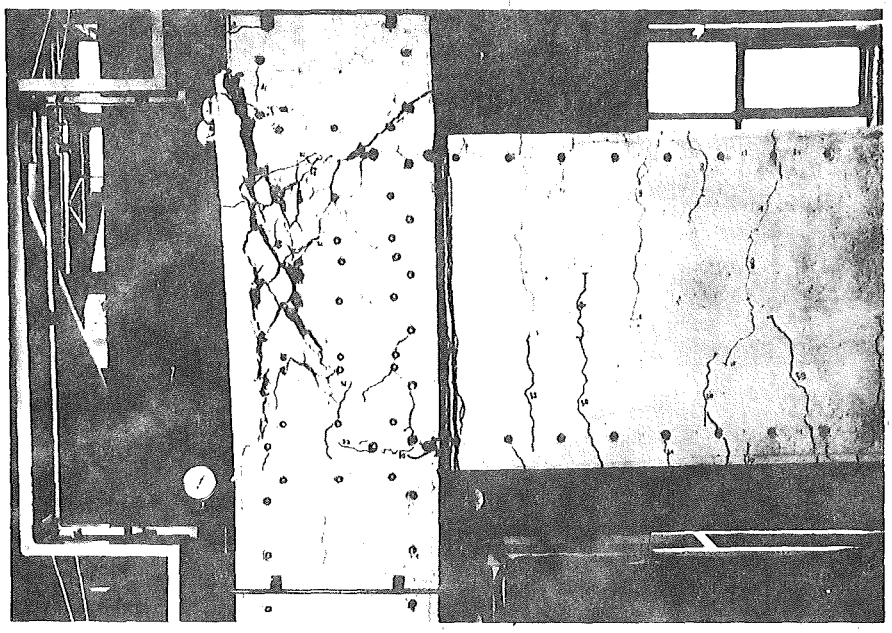

FIG. 5.14 UNIT 2 ON LOAD RUN 5

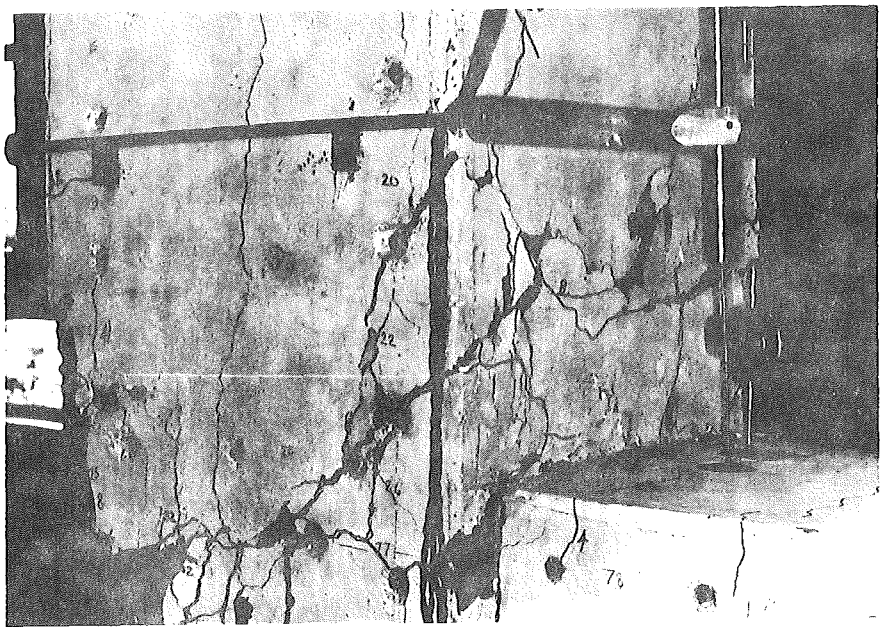

FIG. 5.15 CRUSHING OF CONCRETE IN COLUMN OF UNIT 2 IMMEDIATELY ABOVE BEAM-COLUMN JUNCTION

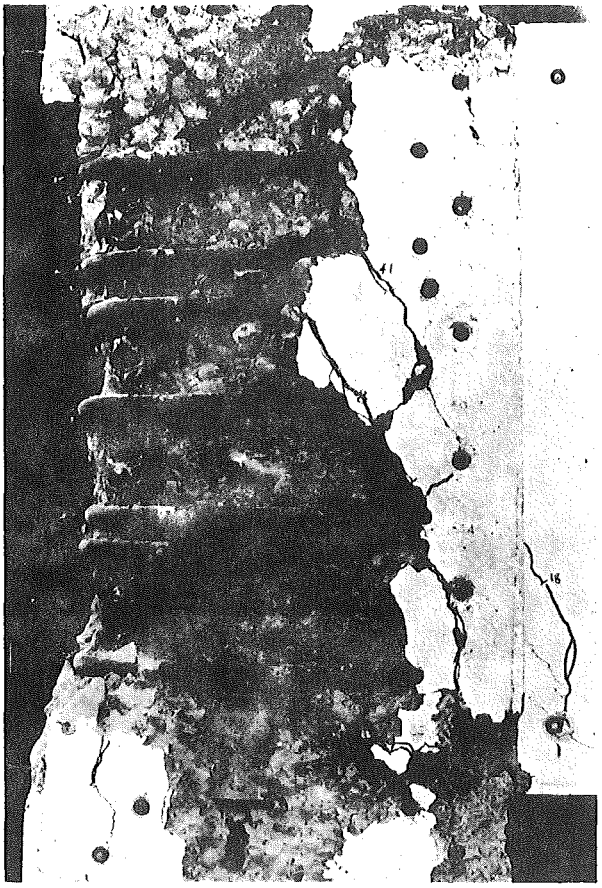

FIG. 5.16 UNIT 2 AT FAILURE

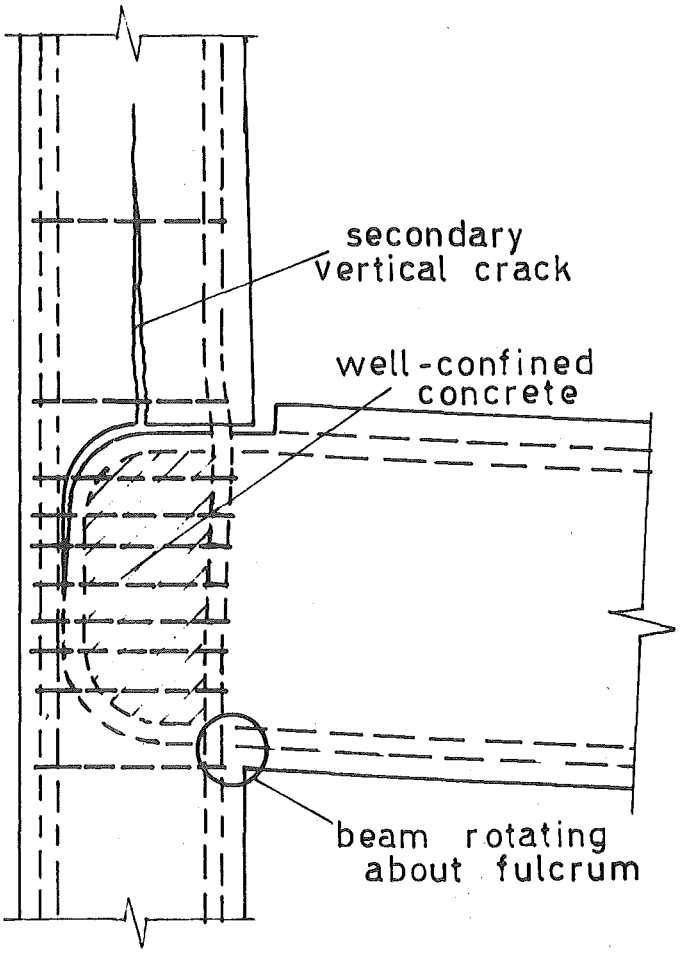

FIG. 5.17 FAILURE MECHANISM OF UNIT 2

CHAPTER SIX.

UNIT 3.

6.1 INTRODUCTION:

This chapter deals with the performance of the third specimen throughout the cyclic loading sequence, and the deterioration of the specimen as a load resisting structure leading to failure. The description is particularly concerned with the influence which the increase in the number of joint ties have on the behaviour of the specimen in comparison with UNITS 1 and 2.

6.2 DETAIL OF REINFORCEMENT:

From the results obtained from UNIT 2, further confinement is obviously required in the joint region. Although the performance of UNIT 2 indicated that the seven joint ties were adequate to resist the applied shear force during the elastic cycles, they did not impose the necessary confinement to prevent deterioration of the joint under the application of the post-elastic reversed cycles.

At this stage the emphasis was on providing a joint with the necessary strength to ensure that full flexural strength of the column can be attained. The natural progression for UNIT 3 was to provide further confinement reinforcement in the joint. However, from the results of UNITS 1 and 2, the column ties were obviously inadequate and little improvement had been observed from the increase in transverse reinforcement in the joint. Therefore it was decided the best solution would be to fully reinforce both regions of the column and joint, thereby hoping to show the need for, primarily, an improved anchorage detail.

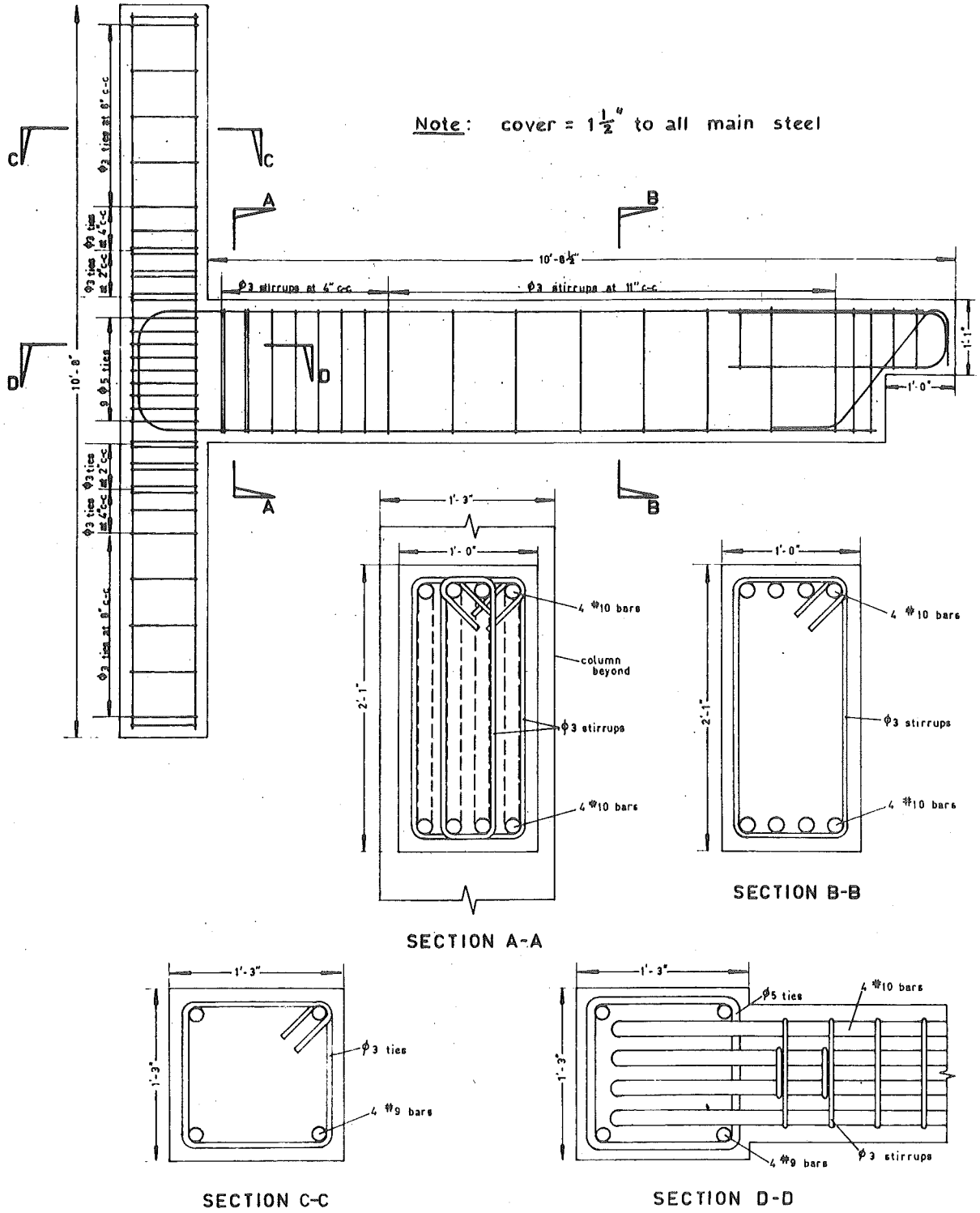

FIG. 6.1 REINFORCING DETAIL FOR UNIT 3

The outcome of this decision, as shown in Fig. 6.1, was nine $\frac{5}{8}$ in. diameter ties in the joint and $\frac{3}{8}$ in. diameter ties, at spacings varying from 2 in. to 8 in., in the column.

6.3 GENERAL PERFORMANCE:

As a load resisting structure, this specimen appeared to have very few advantages over UNIT 2. The performance of the specimen was similar to UNITS 1 and 2 with vertical cracks at the sides of the column connecting with the diagonal tension cracks in the joint (see Fig. 6.2) which widened under the application of the cyclic loading (see Fig. 6.3), indicating the commencement of joint failure. However on subsequent cycles, evidence of crushing of the concrete outside the joint region, Fig. 6.4, showed the tendency for the failure to be propagated in the column. The breakdown of the cover concrete on the back and sides of the joint is unavoidable once the cracks open, and the bond between the steel and the concrete is diminished. However it appears that, provided the confinement is adequate, this does not have a significant effect on the structural performance.

In terms of theoretical ultimate capacity based on the actual materials used, UNIT 3 resisted 72% of its ultimate load, which was less than the percentage for UNIT 2. It is expected that the crushing strength of the concrete had a greater effect on the strength of these specimens than would be accounted for by theory, since the failures are attributable to cracking in the joint resulting in bond failure, rather than flexural yielding of the steel. However, the increase in the number of ties meant that the load was resisted effectively over a greater number of reversed cycles.

The load sequence for this specimen included elastic cycles after the first post-elastic cycles 4 and 5, showing the loss of stiffness of the specimen, followed by two more post-elastic cycles in which the beam was taken to maximum deflection and the test terminated.

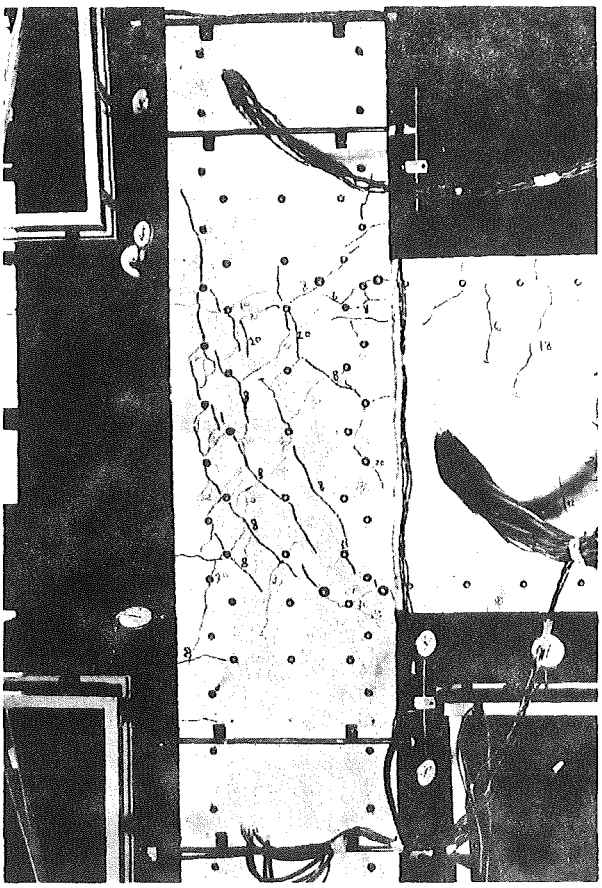

FIG. 6.2 UNIT 3 ON LOAD RUN 3

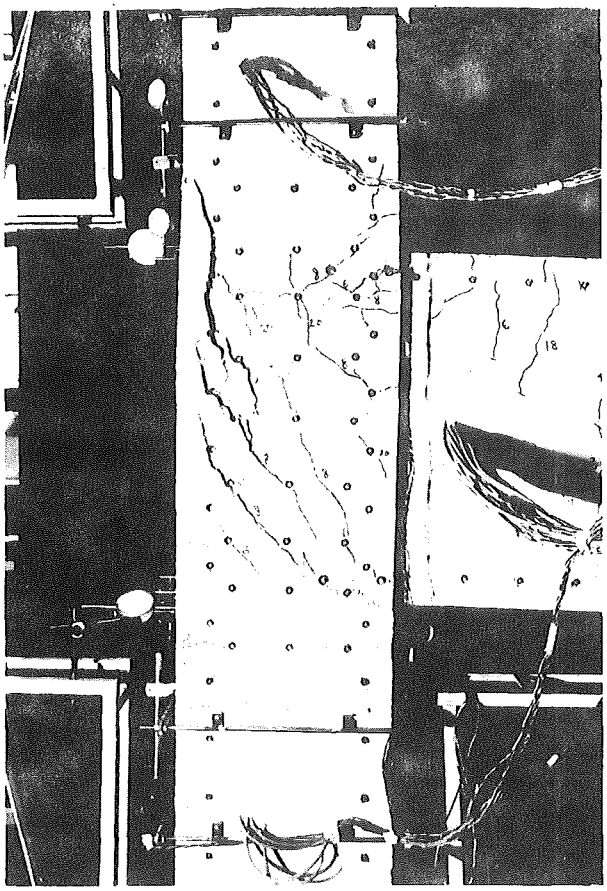

FIG. 6.3 UNIT 3 ON LOAD RUN 4

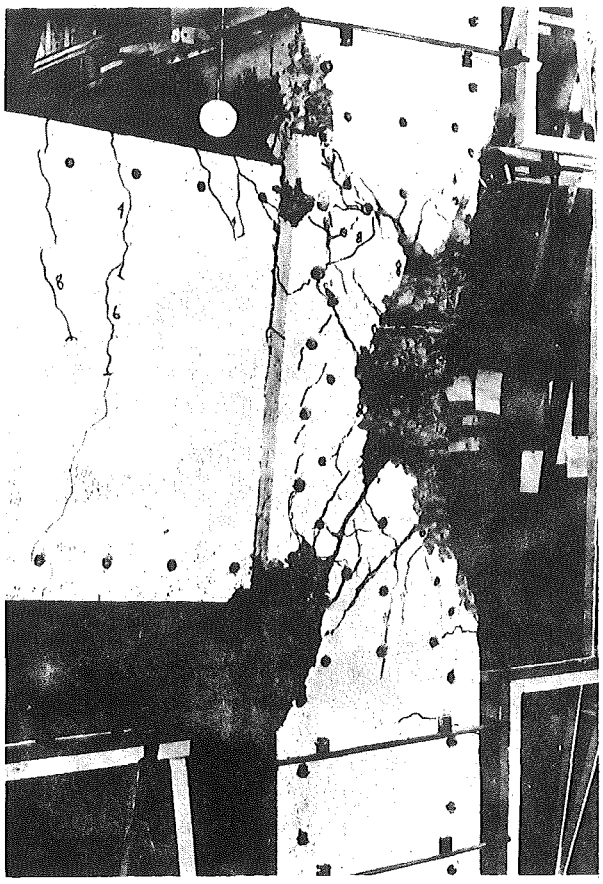

FIG. 6.4 UNIT 3 ON LOAD RUN 9

6.4 BEHAVIOUR OF FLEXURAL REINFORCEMENT:

6.4.1 Column Bars:

The difficulty in preventing the cover concrete from spalling means that it is difficult to obtain the required bond stress of the column flexural bars as long as the joint continues to be the failure region. Even though the confinement of the joint for this specimen was improved over UNIT 2, bond failure of flexural bars was still apparent. The breaking up of surface concrete round the outer column bars, Fig. 6.3, meant that the DEMEC readings were unreliable during Run 5 and could not be recorded. However, the strain distributions shown in Fig. 6.5 (a) and 6.5 (b) were consistent with the expected theoretical distribution. The critical readings on the inner column bars are affected to a larger extent where the tensile beam flexural bars enter the column, rather than where the compressive bars enter because of the larger bond forces which must be developed.

6.4.2 Beam Bars:

The strain gauge readings are shown in Figs. 6.6 (a) and 6.6 (b) and, as for UNITS 1 and 2, indicate the values of tensile strain greater than would be expected for the load which is resisted. Fig. 6.6 (a) shows a trend in the strain readings which makes it apparent that there is a local high reading of strain on the first gauge location in the beam (location 70). Since, from Fig. 6.2, there is no crack crossing the gauge length to provide the large strain, this indicates that there could be a slight bending of the bars at this section.

Fig. 6.7 indicates the influence of the position of the bar on its performance under cyclic loading. While the inner two bars show good recovery of strain, indicating efficient bond, the strain in the outer bars shows a deterioration in bond performance. This would be due to the

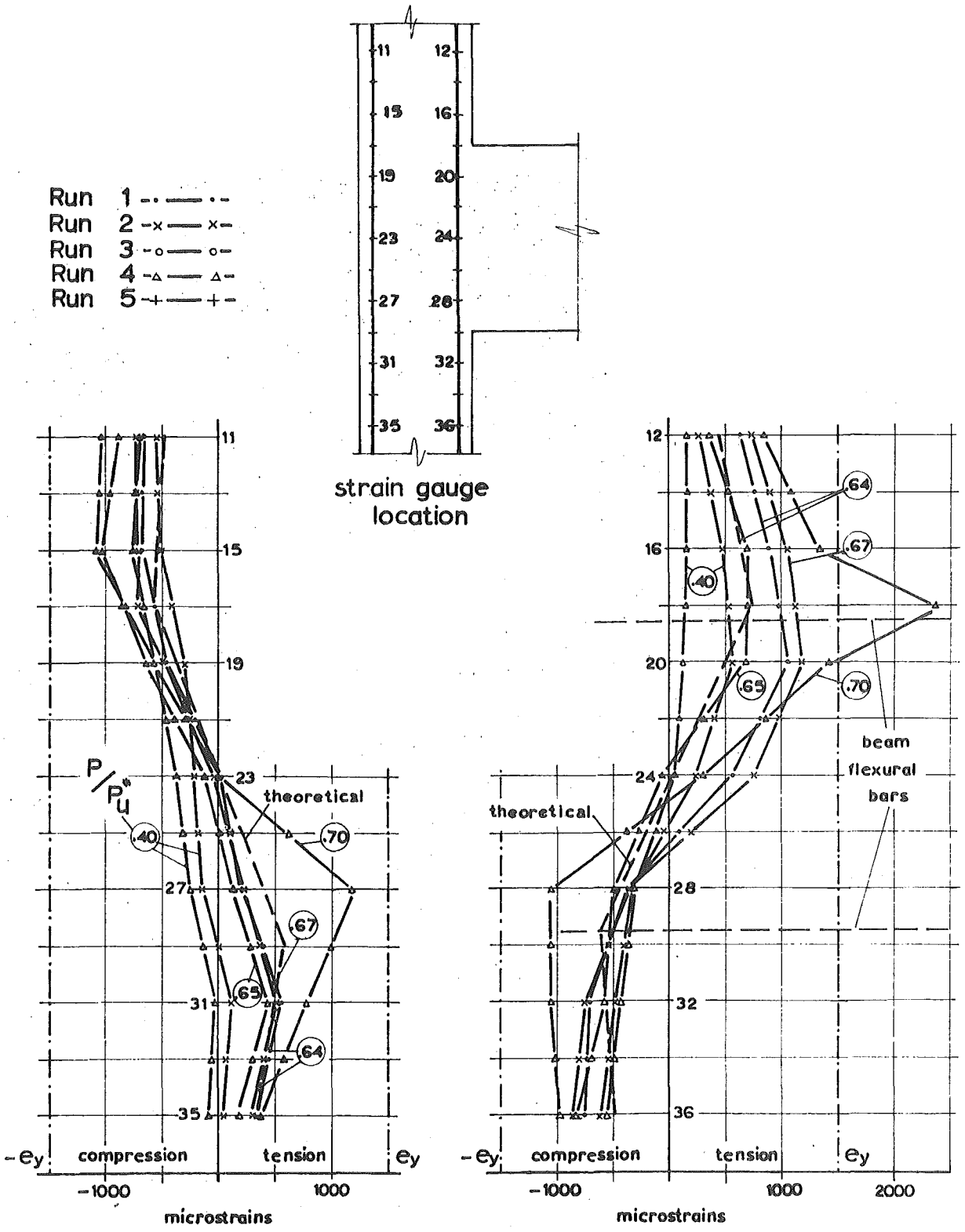

FIG. 6.5(a) THE DISTRIBUTION OF STEEL STRAINS IN COLUMN FLEXURAL BARS IN UNIT 3 [FOR DOWNWARD LOAD RUNS]

For strain gauge locations see Fig. 6.5(a)

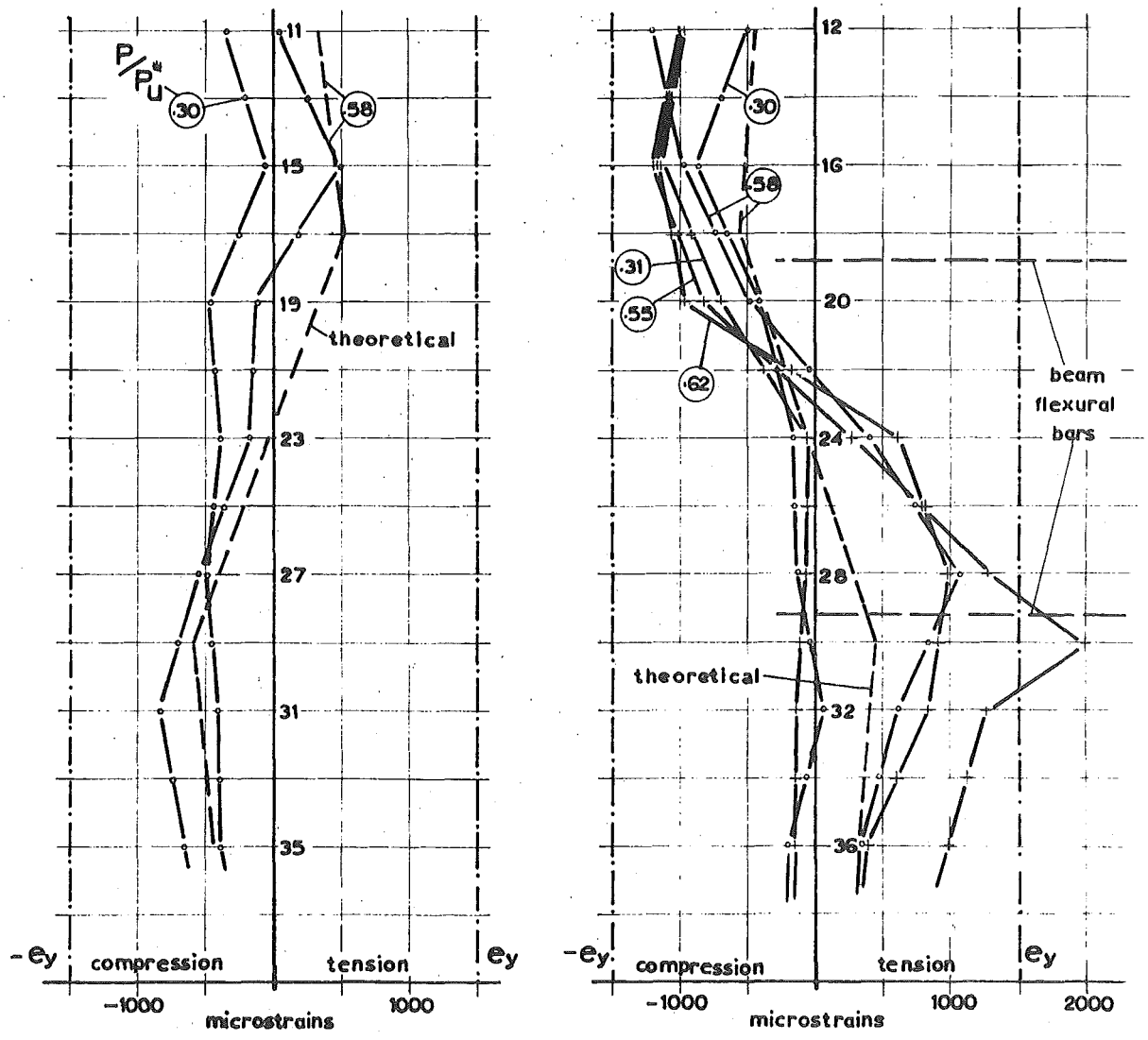

FIG. 6.5(b) THE DISTRIBUTION OF STEEL STRAINS IN COLUMN FLEXURAL BARS IN UNIT 3 [FOR UPWARD LOAD RUNS]

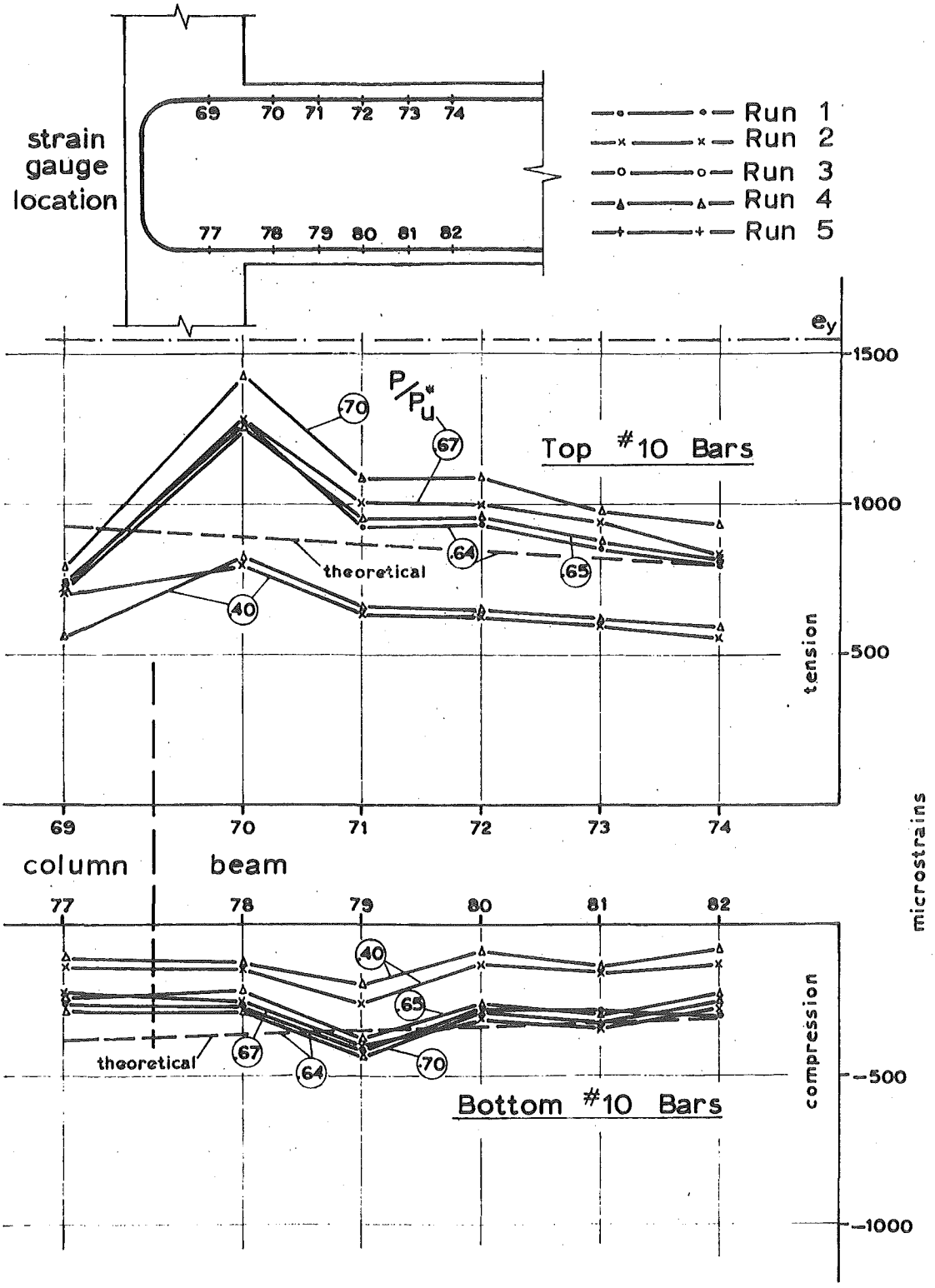

FIG. 6.6 (a) THE DISTRIBUTION OF STEEL STRAINS IN BEAM FLEXURAL BARS IN UNIT 3 [FOR DOWNWARD LOAD RUNS]

For strain gauge locations see Fig. 6.6(a)

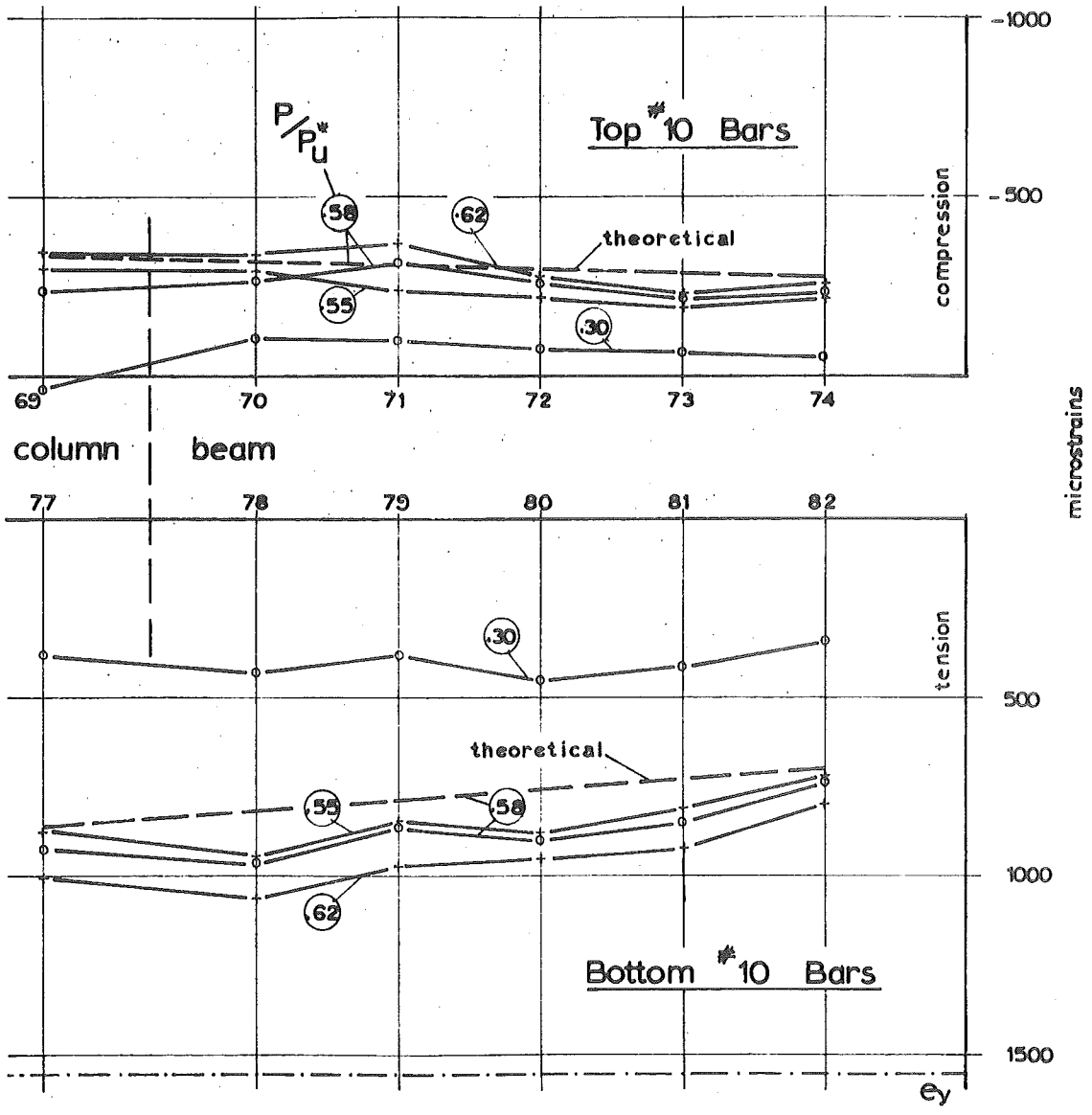

FIG. 6.6(b) THE DISTRIBUTION OF STEEL STRAINS IN BEAM FLEXURAL BARS IN UNIT 3 [FOR UPWARD LOAD RUNS]

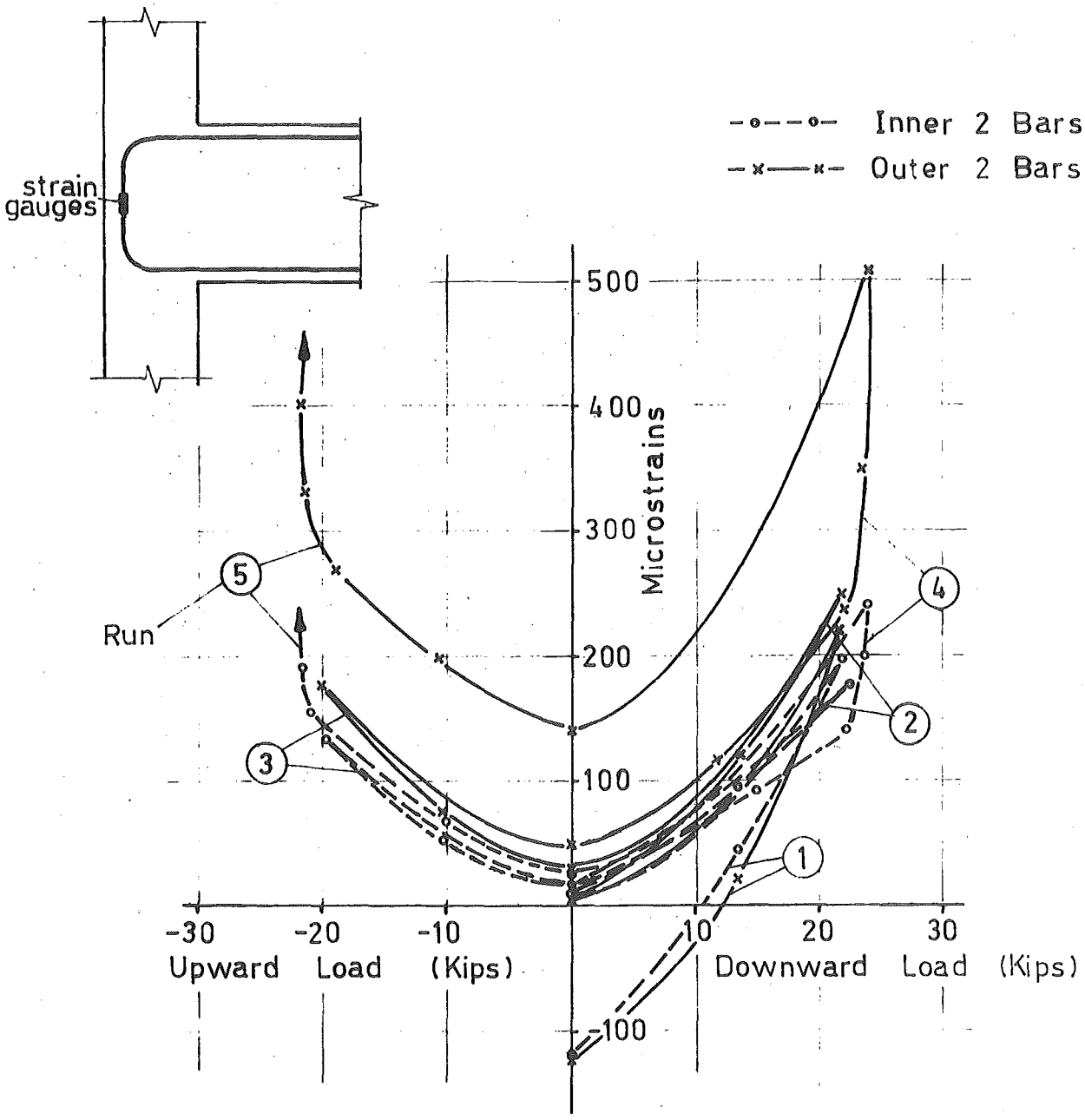

FIG. 6.7 THE HISTORY OF STRAIN FOR THE BEAM FLEXURAL BARS IN UNIT 3

different depth of cover to the bars from the sides of the column which has been shown[18] to influence the bond performance significantly. The strain developed in the bars at the mid point of the anchorage, shows that the anchorage length is insufficient for the tensile force in the bars to be dissipated.

6.5 BEHAVIOUR OF TRANSVERSE REINFORCEMENT:

6.5.1 Column Ties:

Again, due to the tendency for the cracking and breaking up to be confined to the joint region, little interest was generated in the performance of the column ties, except for their ability to prevent a secondary failure being prppagated outside the joint region once the joint had deteriorated sufficiently to allow it. The absence of a splitting crack up the column and the prevention from buckling of the column flexural bars testified to the adequacy of the column ties.

6.5.2 Joint Ties:

All the DEMEC readings on these ties were duplicated in this specimen by having electric resistance strain gauges placed on the ties between each pair of demec studs. The strain readings from both sources, as shown in Figs. 6.8 (a), 6.8 (b) and 6.8 (c), verified the effect that bowing of the ties had on the strain readings. For the strain readings on the back of the ties, no DEMEC readings were recorded during Run 1, but the comparison of DEMEC and electric resistance strain gauge readings for subsequent cycles shows the extent to which bowing of the ties affects the readings. It is obvious that even from the first cycle the DEMEC readings are unreliable, but the electric resistance strain gauge readings show that the use of nine ties in the joint is sufficient to prevent yielding at the back

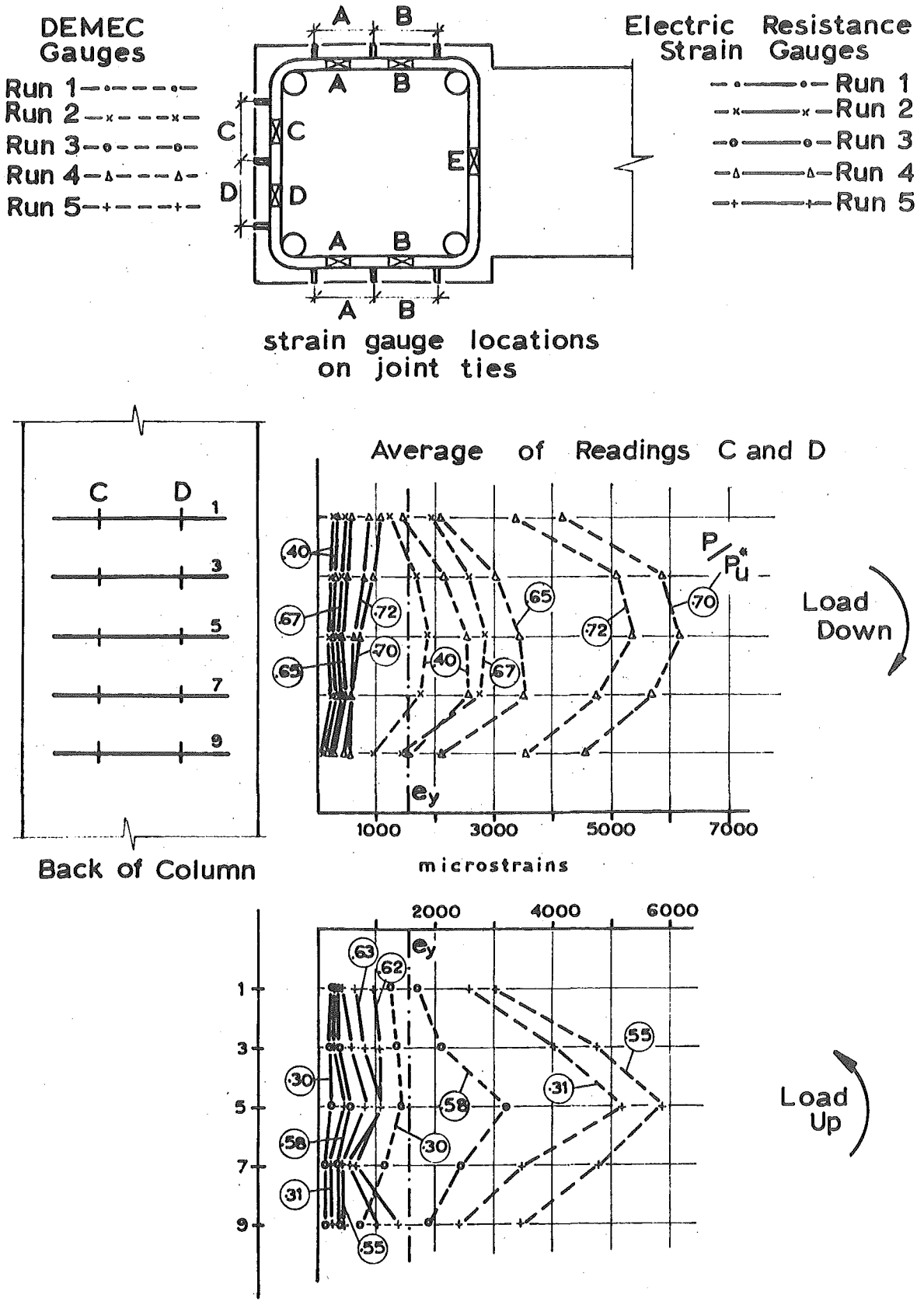

FIG. 6.8(a) THE DISTRIBUTION OF JOINT TIE STRAINS AT BACK OF COLUMN IN UNIT 3

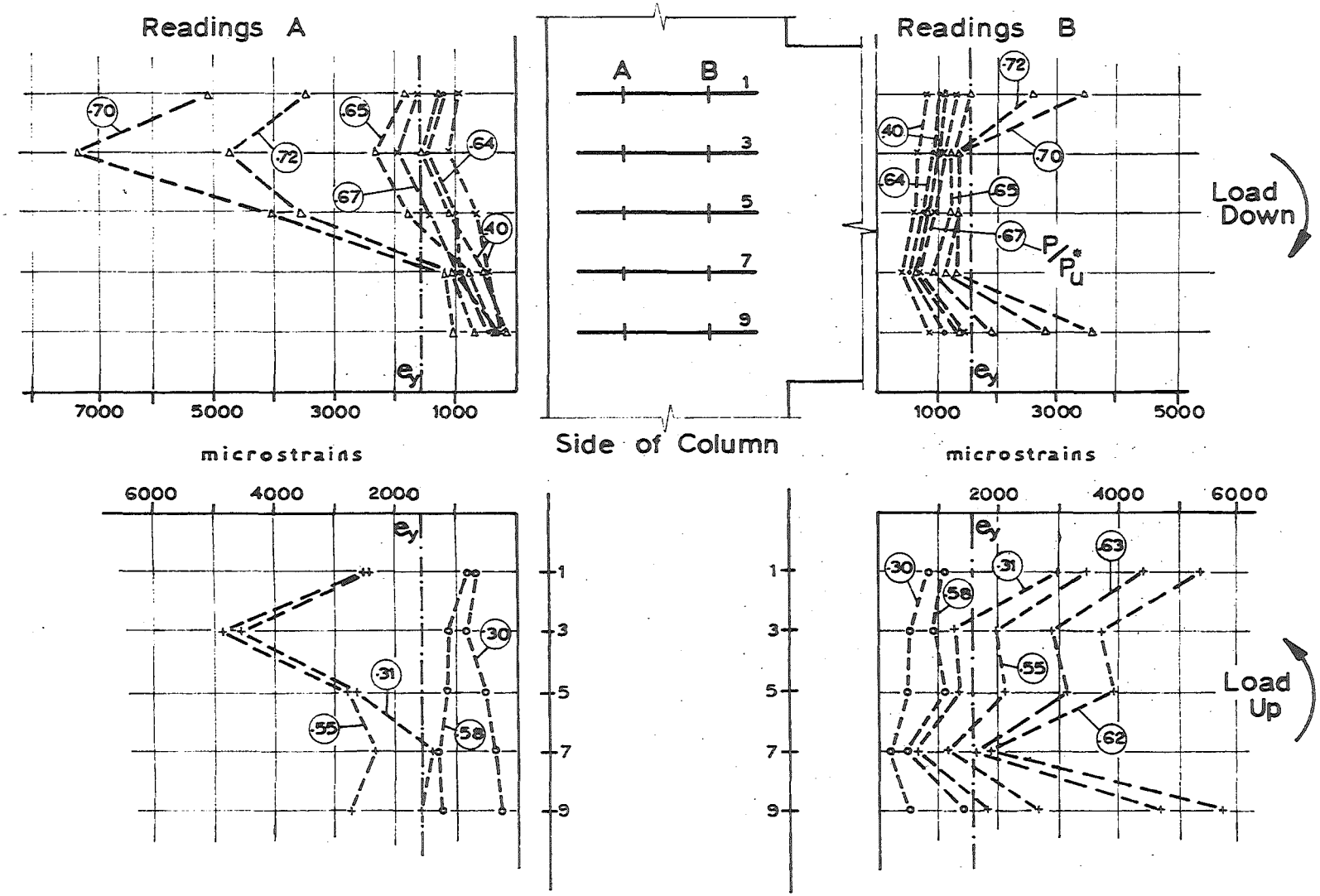

FIG. 6.8 (b) THE DISTRIBUTION OF JOINT TIE STRAINS AT SIDE OF COLUMN IN UNIT 3 [DEMEC GAUGES]

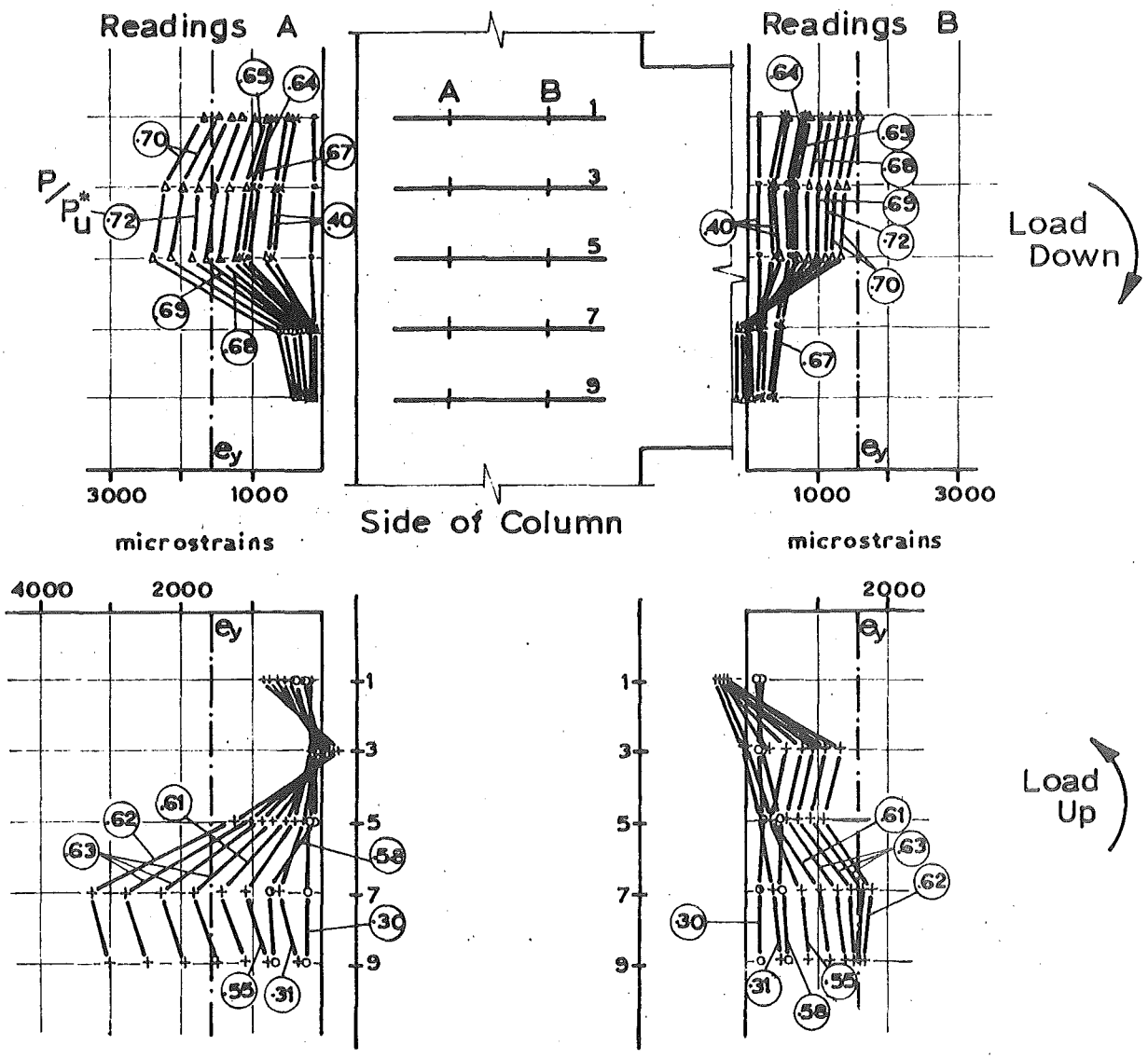

FIG. 6.8 (c) THE DISTRIBUTION OF JOINT TIE STRAINS AT SIDE OF COLUMN IN UNIT 3 [ELECTRIC RESISTANCE STRAIN GAUGES]

of the ties during the application of the five instrumented cycles.

Strain readings on the side of the joint ties from both sources are shown in Figs. 6.8 (b) and 6.8 (c) for comparison, and the distribution of strains in the ties generally bear little relationship to each other. The DEMEC readings are similar in many respects to previous results with the majority of the bowing seemingly occurring in the post-elastic ranges of Runs 4 and 5. It is apparent that the two sources show comparable distributions during Runs 1, 2 and 3, however the tensile strains become negligible once bowing of the ties occurs, and the DEMEC distributions subsequently give meaningless results.

As Fig. 6.8 (c) shows, on the downward load runs it is the top ties which are more highly stressed, with the lower ties being subjected to very little tensile stress. On the upward load cycles the situation is reversed.

The strain distributions on each tie are shown in Figs. 6.9 (a) and 6.9 (b) where the electric resistance strain gauge readings only have been recorded. The symmetrical nature of the stress at the back of the ties is contrasted with the distributions on the sides of the ties where the readings A are consistently greater than the readings B except for the tie 3, which lends credence to the belief that this electric resistance strain gauge failed after Run 4.

The load strain relationships for gauges on all four sides of the ties are shown in Figs. 6.10 (a), 6.10 (b), 6.10 (c) and 6.10 (d). These show how the stress is developed during each run and the full effect of the ties is not imposed until the latter part of each run. The effect that bowing of the ties has on the DEMEC readings is shown by not only resulting in higher readings but also a greater variation. The relationship shown in Fig. 6.10 (d) shows how the bursting effect of the column is present even at the inside of the column where the restraining effect of the beam would

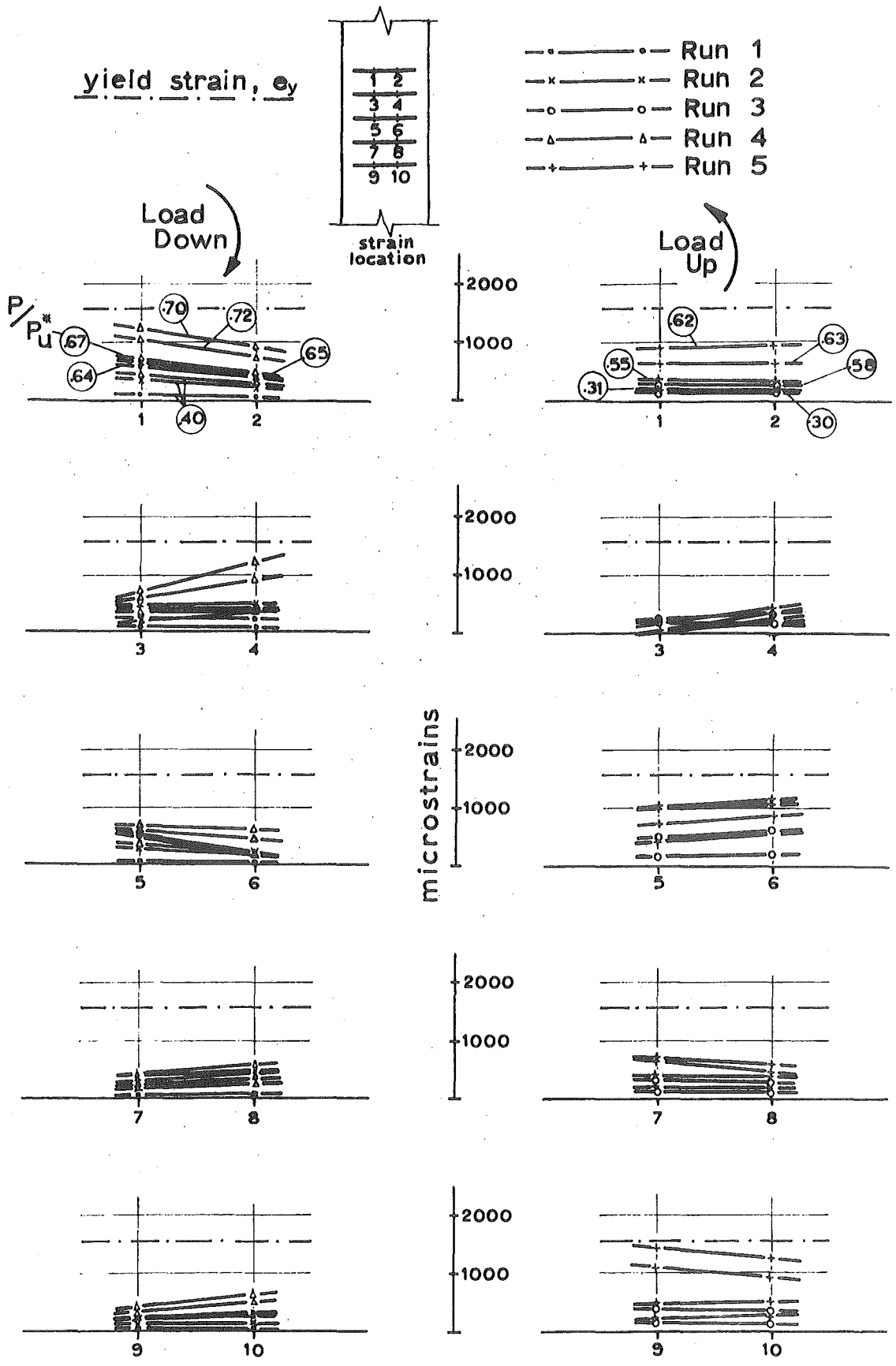

FIG. 6.9 (a) THE DISTRIBUTION OF STEEL STRAINS ON BACK OF JOINT TIES IN UNIT 3 [ELECTRIC RESISTANCE STRAIN GAUGES]

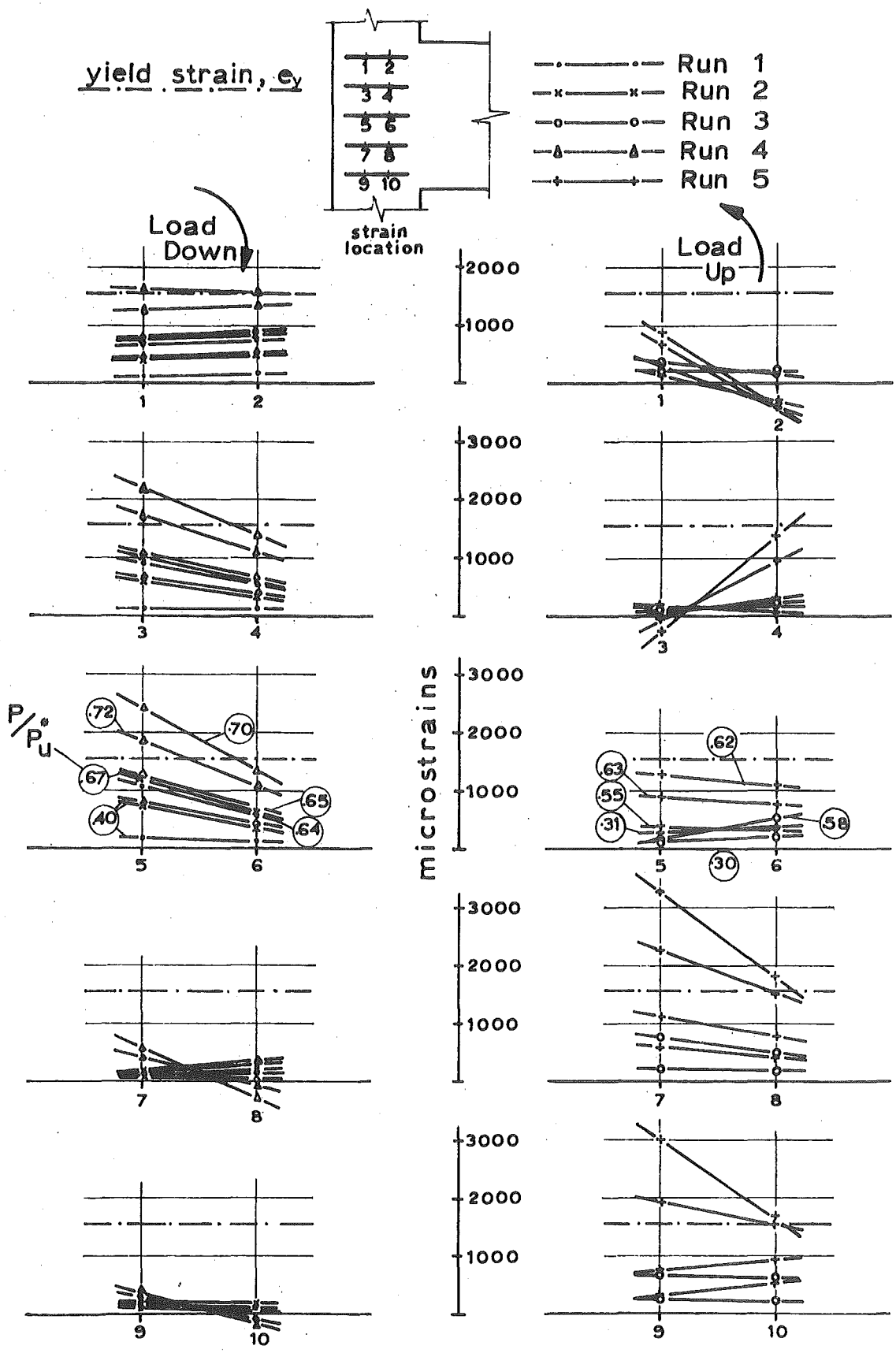

FIG. 6.9 (b) THE DISTRIBUTION OF STEEL STRAINS ON SIDE OF JOINT TIES IN UNIT 3 [ELECTRIC RESISTANCE STRAIN GAUGES]

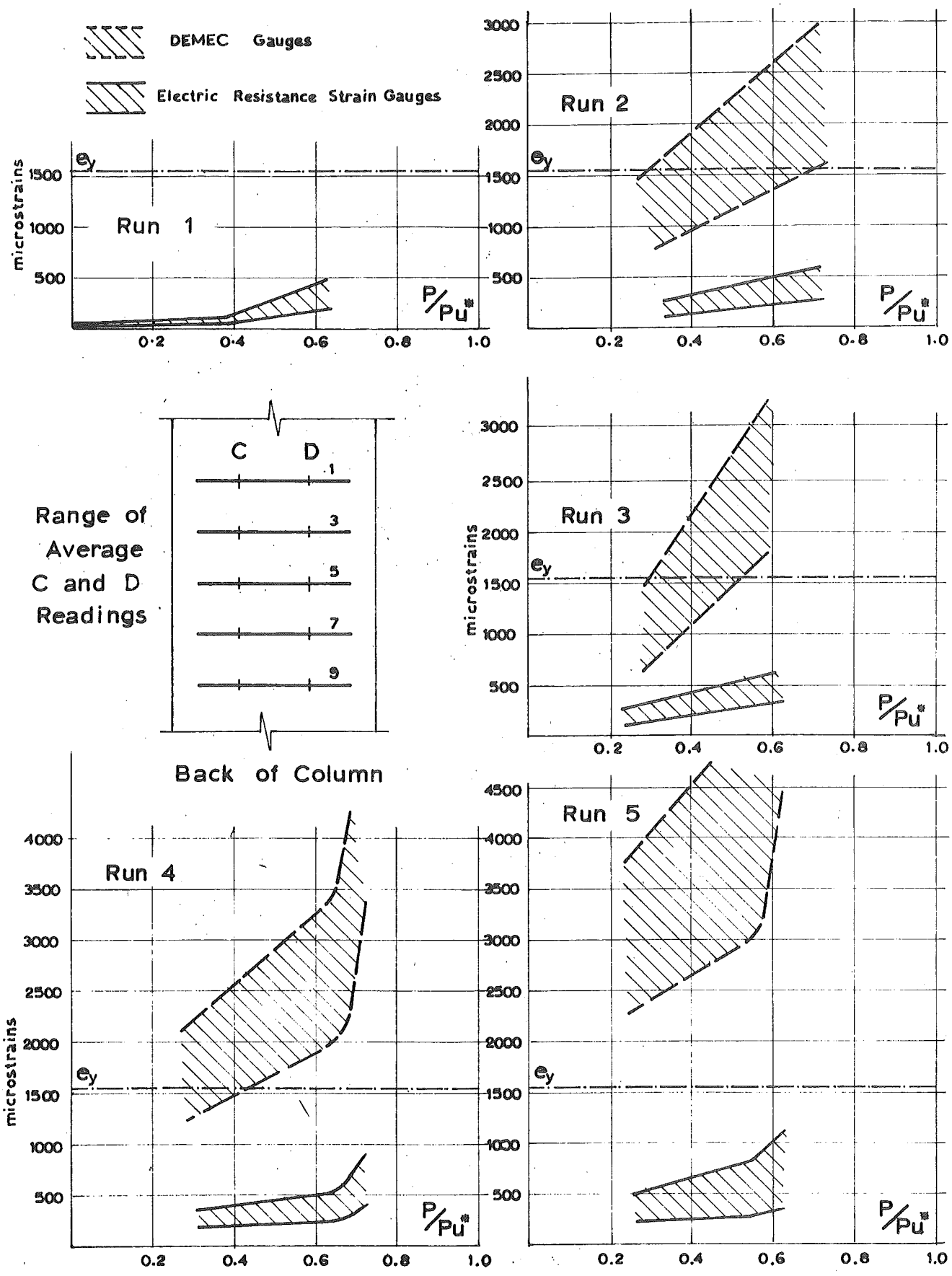

FIG. 6.10(a) THE LOAD-STRAIN RELATIONSHIP FOR JOINT TIES IN UNIT 3 AT BACK OF COLUMN

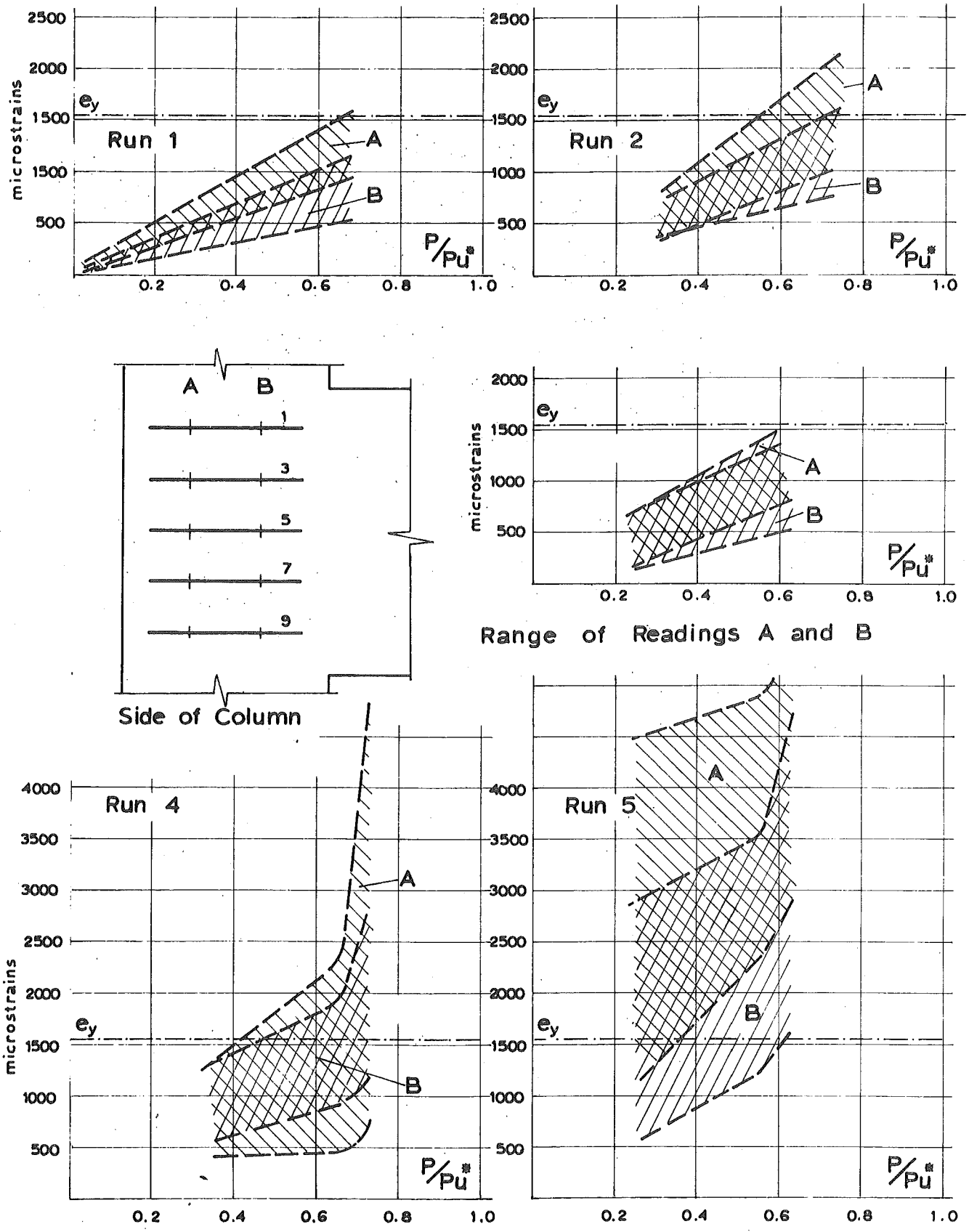

FIG. 6.10(b) THE LOAD-STRAIN RELATIONSHIP FOR JOINT TIES IN UNIT 3 AT SIDE OF COLUMN [DEMEC GAUGES]

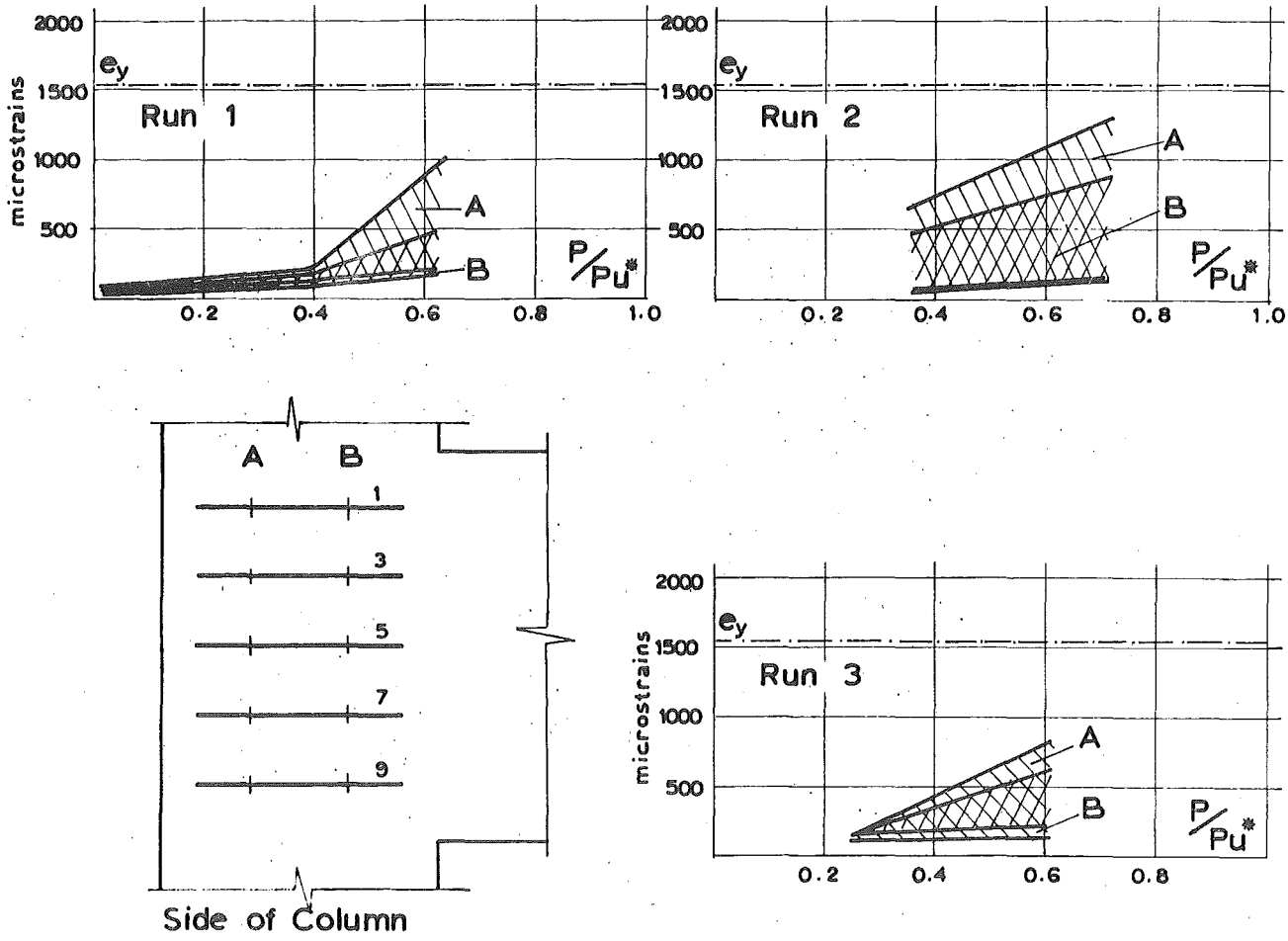

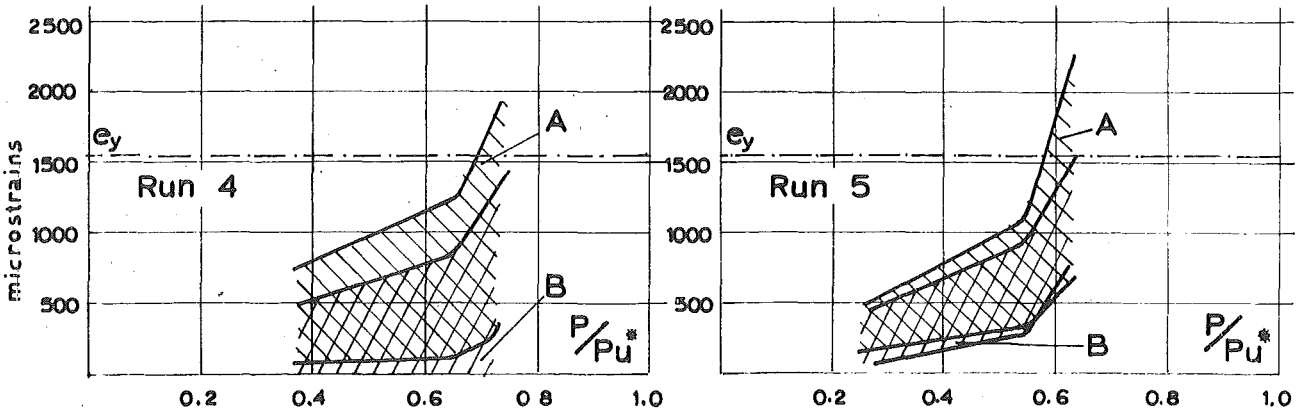

FIG. 6.10(c) THE LOAD-STRAIN RELATIONSHIP FOR JOINT TIES IN UNIT 3 AT SIDE OF COLUMN [ELECTRIC RESISTANCE STRAIN GAUGES]

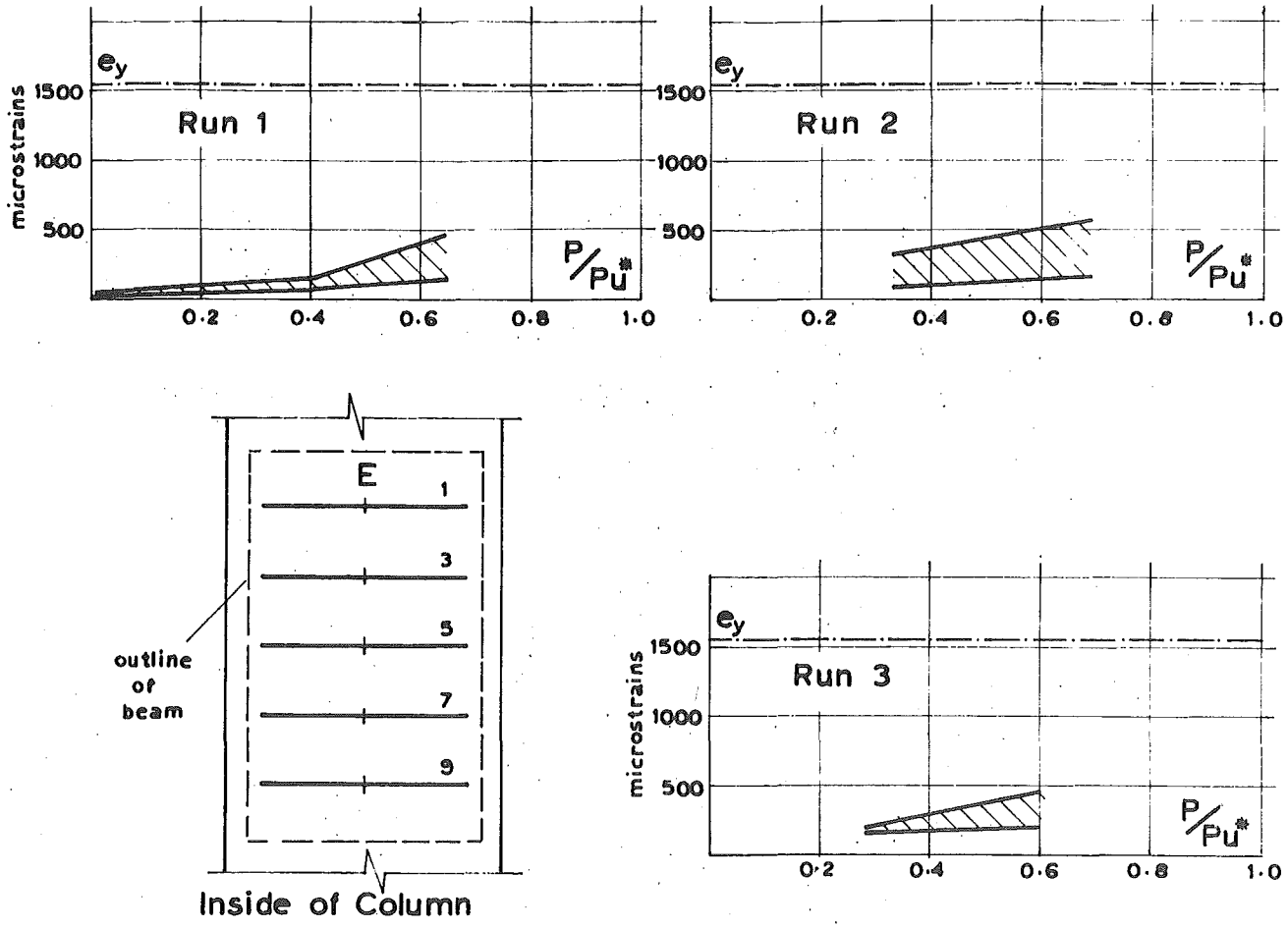

Range of Readings E

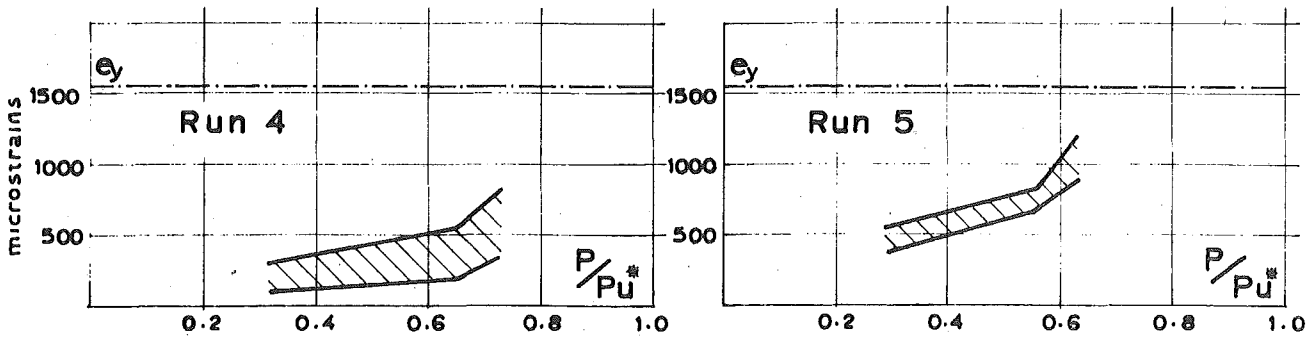

FIG. 6.10 (d) THE LOAD – STRAIN RELATIONSHIP FOR JOINT TIES IN UNIT 3 AT INSIDE OF COLUMN

seem to be considerable.

6.6 DEFORMATIONS:

6.6.1 Deflections:

The deflected shapes of the specimen at the peaks of Runs 1, 2 and 3 are shown in Fig. 6.11, and compared with the theoretically predicted shapes. The increased response of this specimen when subjected to similar loads to UNIT 2 indicates the effect that the concrete strength has on the deflection of the structure in the elastic range. The concrete strength has a considerable effect on the extent of flexural cracking and on distortion of the joint due to diagonal tension cracking, which results in the larger deflections.

6.6.2 Moment-Rotation Relationships:

The relationships, shown in Fig. 6.12, indicate that the column was not as stiff in this specimen as in UNIT 2, during the elastic cycles. This was probably due to the reduction in concrete strength, which enabled cracks to form at lower loads. The increased joint confinement causes cracks to be propagated from the joint into the column region, lowering the stiffness of the column, accounting for the sudden degradation in stiffness near the peak of Run 1. The permanent rotation of the sections of the column is demonstrated by the bias each curve gets to one side of the origin.

6.6.3 Load-Deflection Relationship:

The relationship is shown in Fig. 6.13. The loss of stiffness of the specimen after Runs 4 and 5 is shown by the response of the specimen during elastic Runs 6 and 7 when only 10% of the theoretical ultimate load

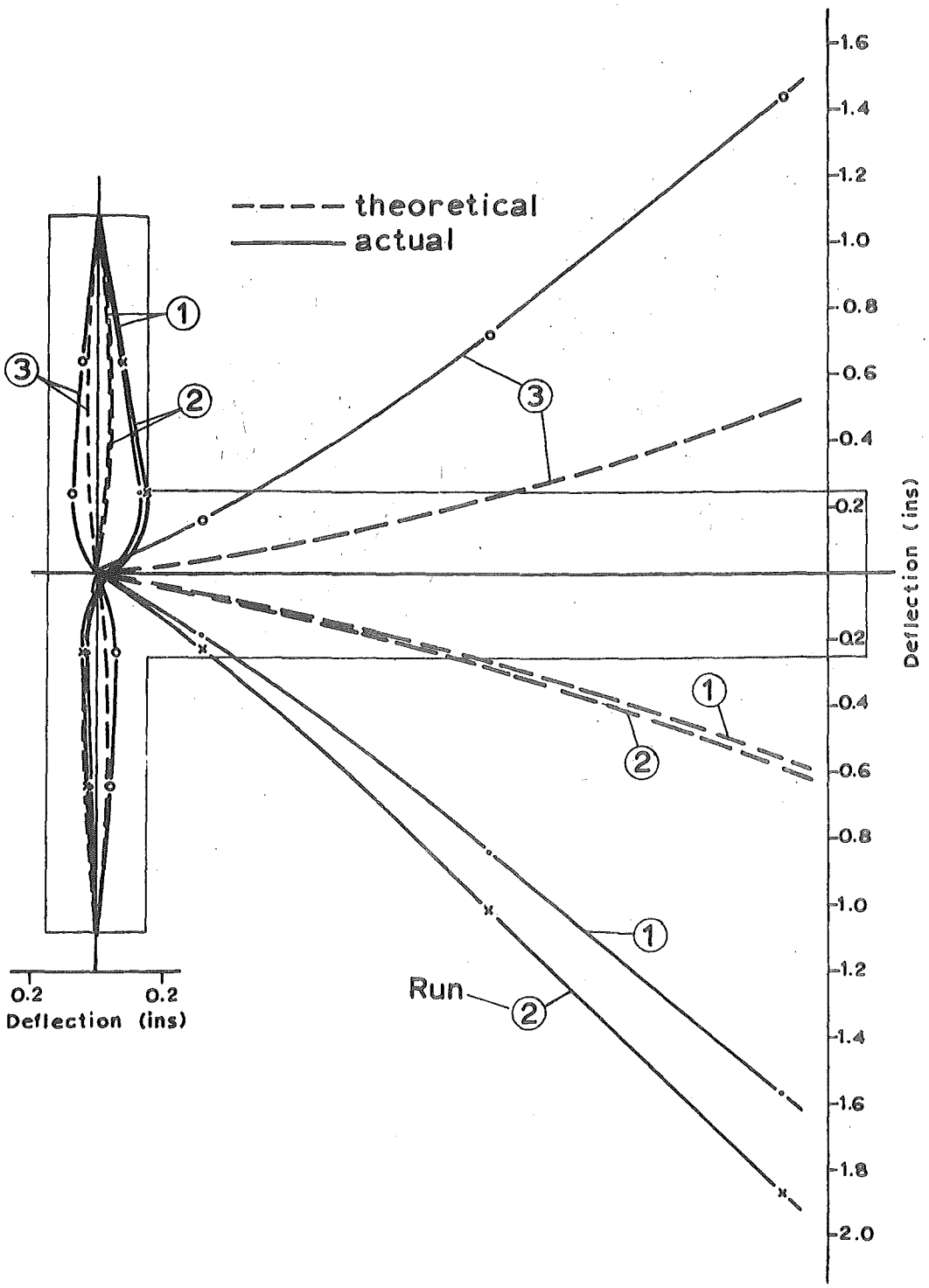

FIG. 6.11 DEFLECTED SHAPES OF UNIT 3 AT PEAKS OF ELASTIC LOAD RUNS

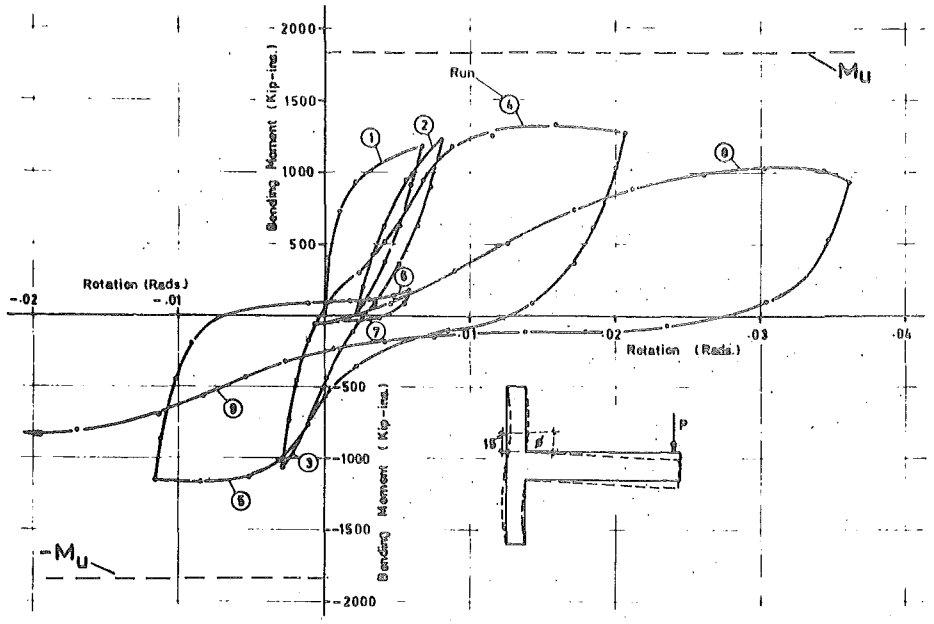

(a) COLUMN ABOVE THE JOINT

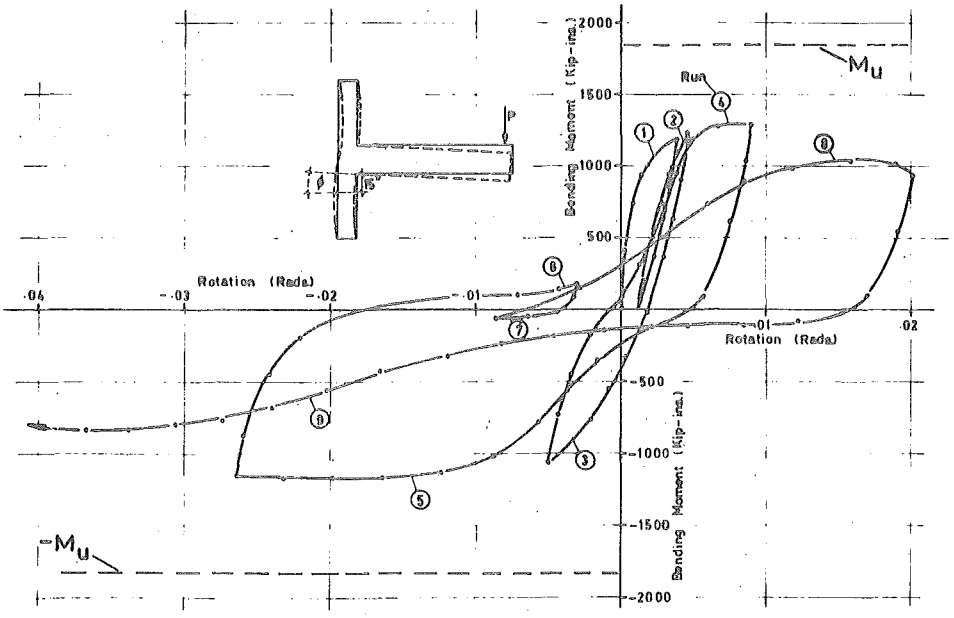

(b) COLUMN BELOW THE JOINT

FIG. 6.12 THE MOMENT - ROTATION RELATIONSHIPS FOR UNIT 3

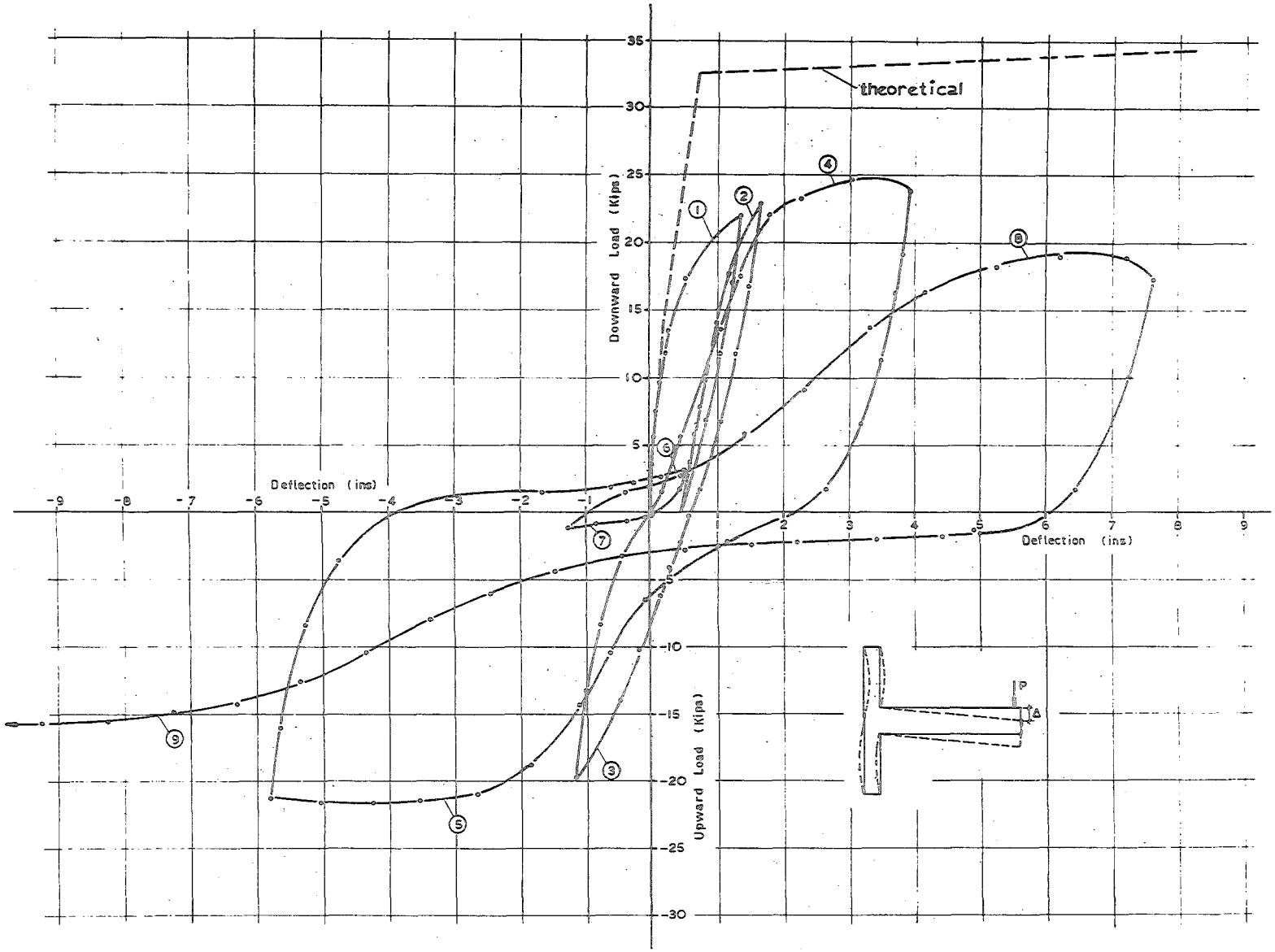

FIG. 6.13 THE LOAD DEFLECTION RELATIONSHIP FOR UNIT 3

is resisted at an equivalent deflection to the initial elastic cycles. The resilience of the specimen showed a slight improvement over UNIT 2, with the maximum load resisted during Run 8 being 22% less than that of Run 4.

Table 6.1 indicates the stiffness of the specimen and the ductility factors obtained during each load run.

TABLE 6.1 Performance of UNIT 3 During Load Cycling.

Run	Maximum Load P_{max} (kips)	$\frac{P_{max}}{P^*_u} \times 100$ (%)	Ductility Factor	Average % Stiffness †
1	22.0	64.4	-	42.4
2	22.9	67.0	-	50.9
3	19.7	57.6	-	29.3
4	24.7	72.2	5.2	32.4
5	21.6	63.2	8.9	11.3
6	3.2	9.4	-	3.2
7	1.2	3.5	-	2.3
8	19.0	55.6	11.3	7.6
9	15.6	45.6	17.1	2.9

† Expressed as % of the theoretical stiffness.

6.7 CRACKING:

The cracking showed a very similar pattern to the previous two specimens, with diagonal tension cracks being confined generally to the joint. Large bond stress and bond failure of the flexural bars was indicated by the cracks following the lines of both the column and beam flexural bars. Vertical cracks down the back of the column, Fig. 6.14, indicated column expansion as early as Run 1. The low concrete tensile strength could be the reason for the expansion of the column being initiated so early in the load sequence, and this could be an important factor when determining column bursting forces.

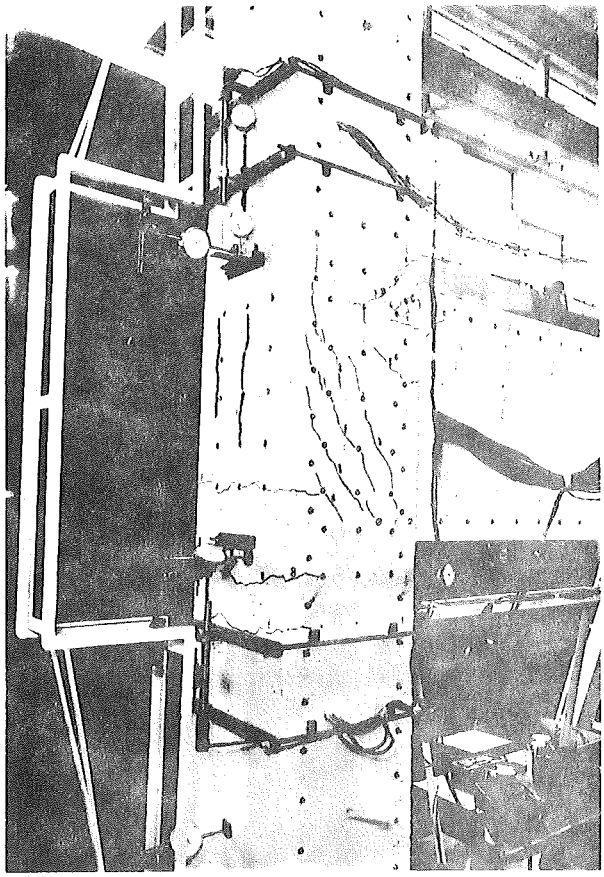

FIG. 6.14 UNIT 3 ON LOAD RUN 1

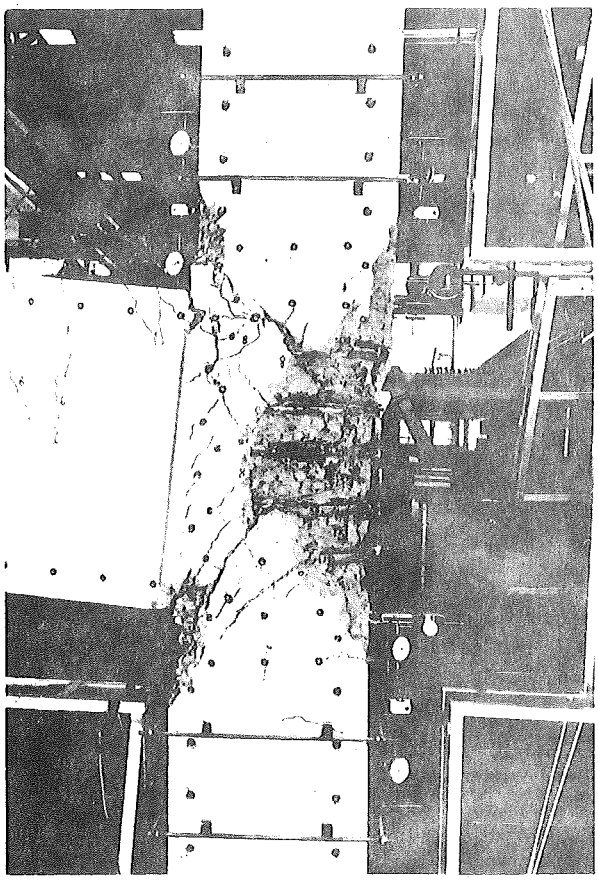

FIG. 6.15 UNIT 3 AT FAILURE

There was more evidence of concrete outside the joint region spalling in this specimen, due to crushing and cracking of the concrete, than had been observed in previous specimens.

6.8 THE FAILURE MECHANISM:

The loss of stiffness and subsequent deterioration of the joint due to diagonal tension cracking indicated the gradual approach of failure. The nine joint ties enabled the specimen to withstand the load cycling without the diagonal tension cracks widening sufficiently to cause shear failure in the joint. However, although the core was well confined the concrete in the core appeared to be crushed by the diagonal compression forces. This weakened the bond strength of the beam flexural bars which meant that the joint could not be maintained as an integral unit. The joint degradation caused by bond failure of the flexural bars lead to a failure similar to UNIT 2. Fig. 6.15 shows the specimen at failure.

CHAPTER SEVEN.

UNIT 4.

7.1 INTRODUCTION:

The change in the reinforcing detail and its effect on the behaviour of UNIT 4 are described in this chapter in an attempt to determine the reasons for the improvement in its performance compared with the previous specimens.

7.2 DETAIL OF REINFORCEMENT:

Since little improvement in load capacity had been achieved in the previous three specimens, it was apparent that a radical change of the joint detail was required. The inability of the flexural bars to develop the required bond strength was a fundamental cause of these premature failures and indicated the necessity for improved bond performance. This can be achieved either by ensuring more favourable bond conditions or by reducing the required bond stress. The first method has been attempted in UNITS 2 and 3 by increasing the confinement. To investigate the effect of the second method the continuous arrangement of beam flexural bars has been dispensed with in UNIT 4, the beam flexural steel consisting of separate top and bottom bars, thereby providing increased anchorage length in the column.

In order to determine the problems directly attributable to the continuous arrangement, the reinforcement detail, as shown in Fig. 7.1, was unchanged otherwise from UNIT 3.

7.3 GENERAL PERFORMANCE.

It was obvious from the behaviour of this specimen, even during the

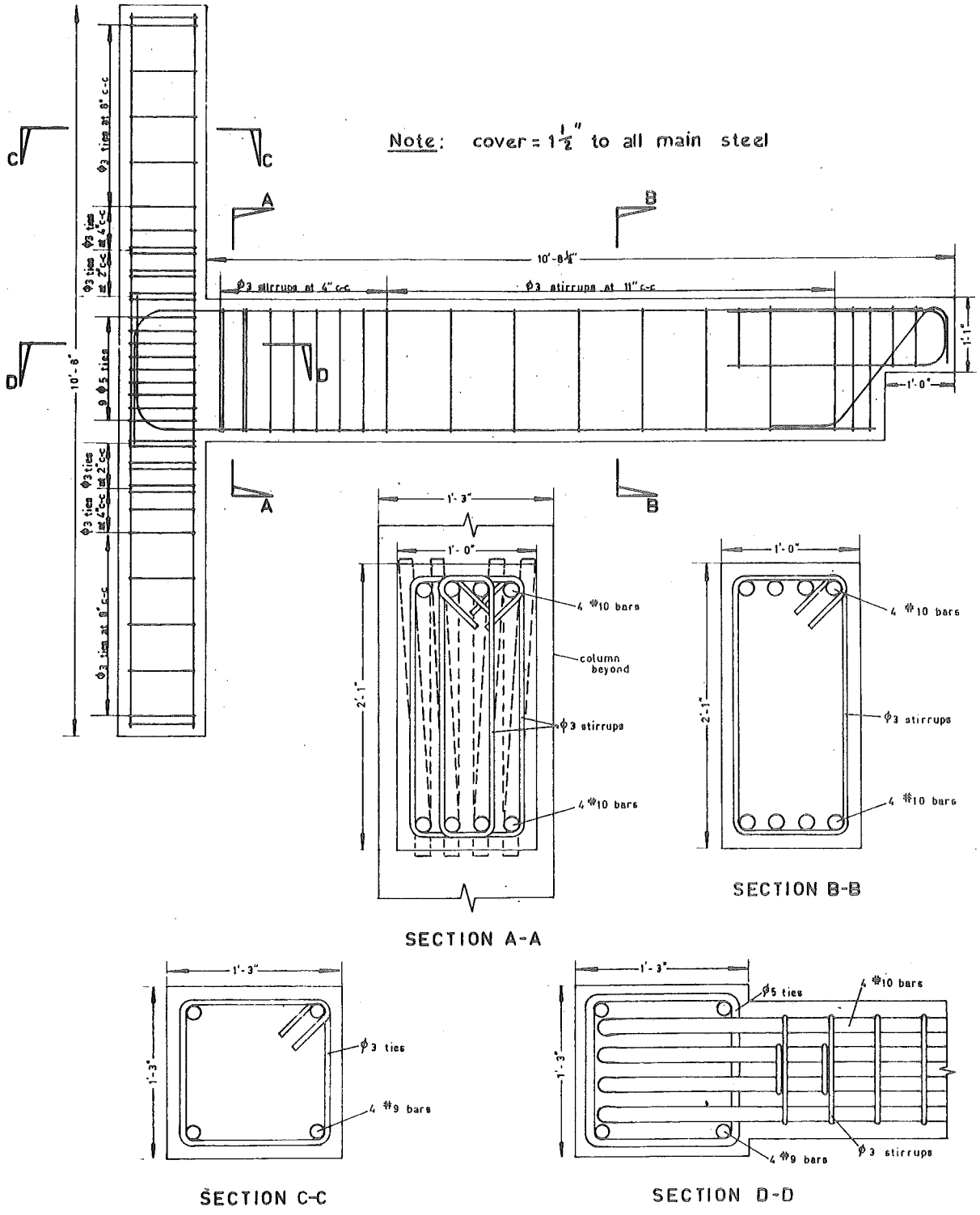

FIG. 7.1 REINFORCING DETAIL FOR UNIT 4

elastic cycles, that there was a vast improvement in performance over the previous specimens.

Although diagonal tension cracks formed during Runs 1, 2 and 3 they did not widen perceptibly and the joint was still intact, as shown in Fig. 7.2, prior to the application of the post-elastic cycles. The major diagonal tension cracks, running between opposite corners of the joint, opened during Runs 4 and 5, however, evidence of concrete crushing and tension cracks outside the joint region indicated flexural yielding of the steel in the column on both upward and downward runs.

The appearance of the specimen at the peak of Run 8, shown in Fig. 7.3, demonstrates how the cover concrete remained on the joint over a far greater proportion of the load sequence than it did for the previous specimens. The increased confinement in the joint reduced the tendency for bond failure of either column or beam flexural bars and substantially improved the resilience of the specimen.

However, the most interesting facet of the behaviour of UNIT 4 was that it resisted 90% of its theoretical ultimate capacity, substantially more than any of the previous three specimens.

7.4 BEHAVIOUR OF FLEXURAL REINFORCEMENT:

7.4.1 Column Bars:

The strain distributions shown in Fig. 7.4 (a) and 7.4 (b) show yielding which occurred in the column bars during both upward and downward load runs. The inner column bars are, as predicted for this situation, the only bars which yield since they are in tension in the critical region for both directions of loading.

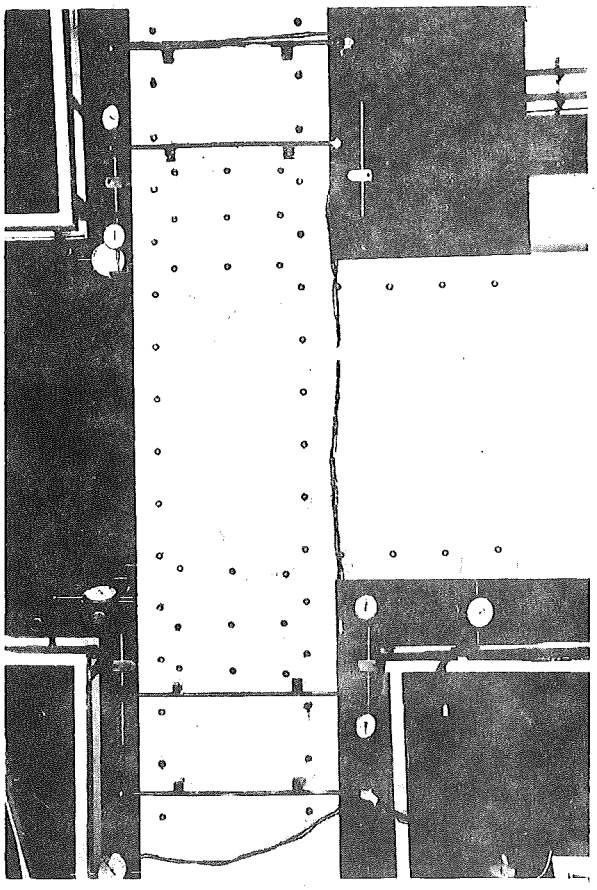

FIG. 7.2 UNIT 4 ON LOAD RUN 3

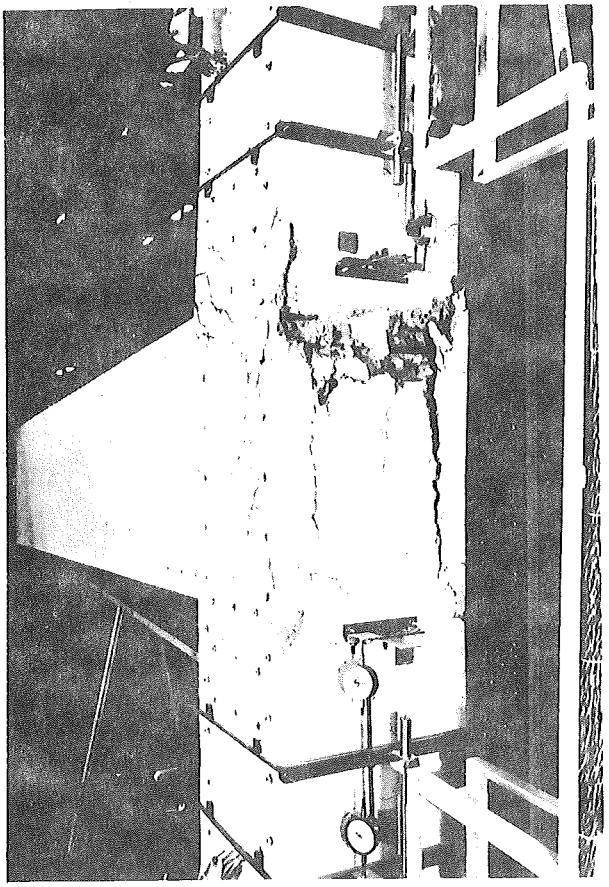

FIG. 7.3 UNIT 4 ON LOAD RUN 8

FIG. 7.6 END OF TOP BEAM FLEXURAL BAR LIFTED OFF BEARING SURFACE

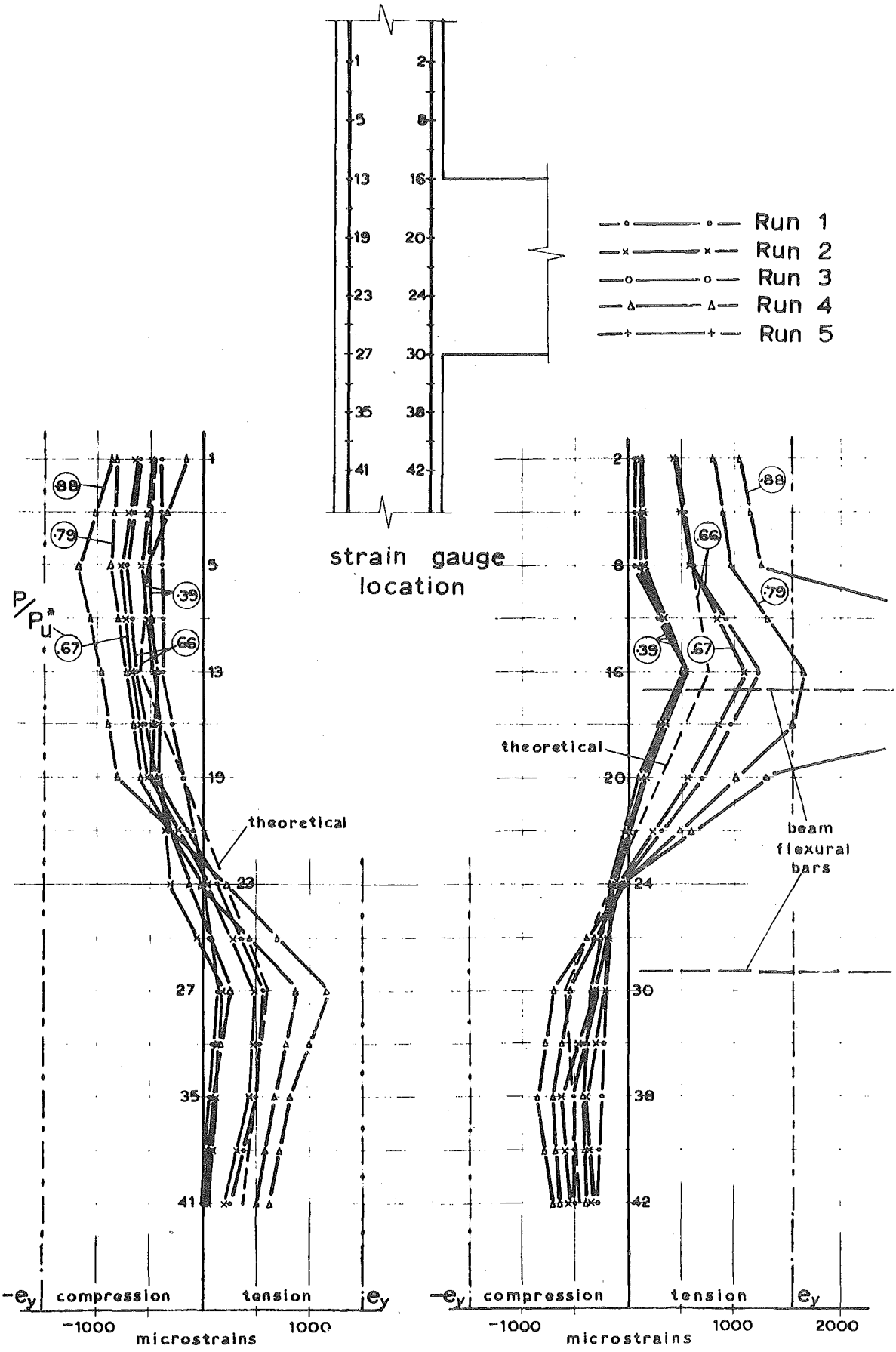

FIG. 7.4 (a) THE DISTRIBUTION OF STEEL STRAINS IN COLUMN FLEXURAL BARS IN UNIT 4 [FOR DOWNWARD LOAD RUNS]

For strain gauge locations see Fig. 7.4(a)

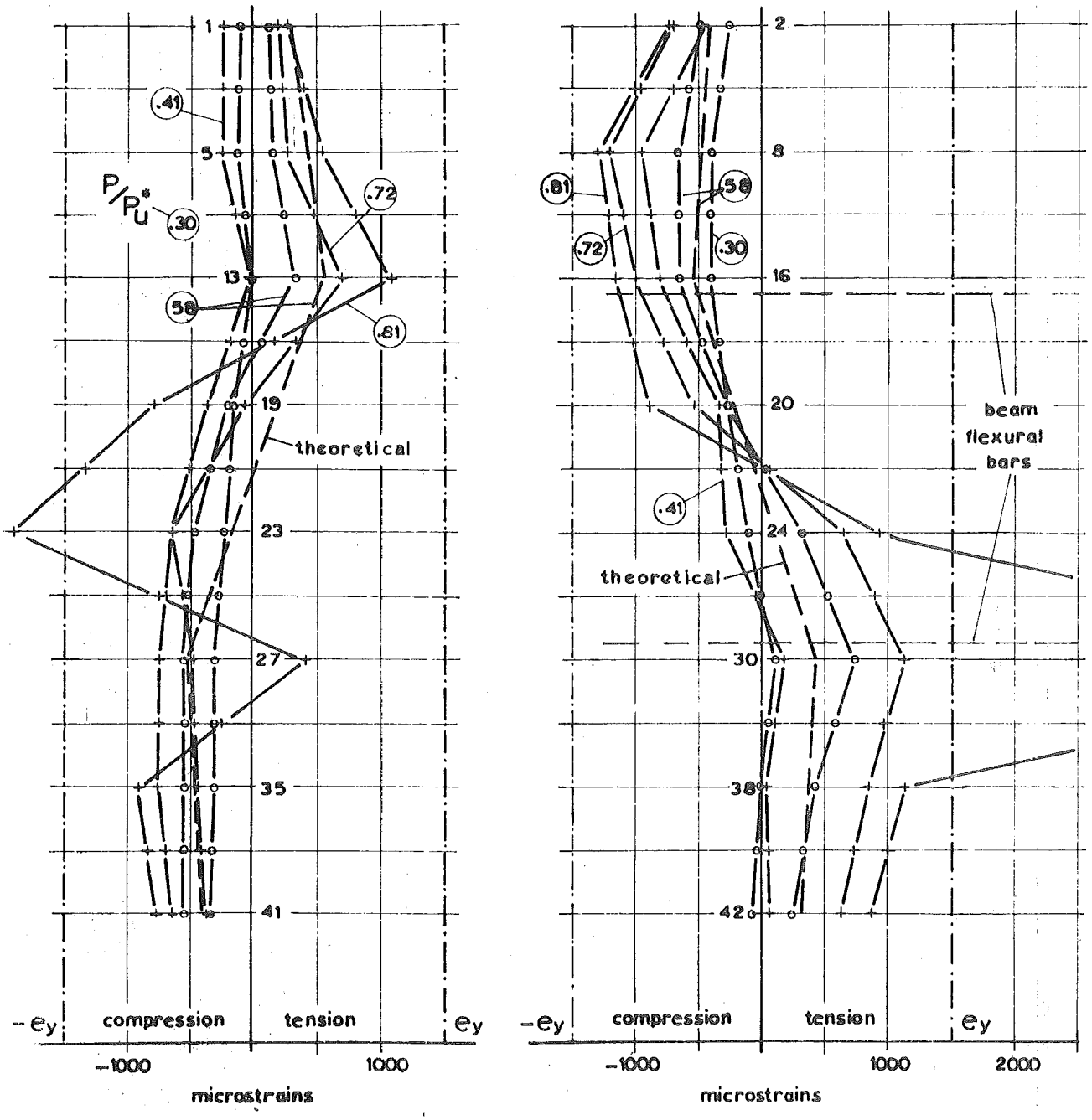

FIG. 7.4(b) THE DISTRIBUTION OF STEEL STRAINS IN COLUMN FLEXURAL BARS IN UNIT 4 [FOR UPWARD LOAD RUNS]

Some of the strain readings on the outer column bars during Run 5 indicate a distribution inconsistent with what would be expected. This is in the region where the top beam flexural bars terminate, and since, on upward load runs these bars are in compression the bearing stress at the ends of the bars could cause lateral bowing of the column bars thereby influencing the strain readings.

Even though the strain at different load increments indicates a higher stress than had been recorded for previous specimens, the absence of splitting cracks, Fig. 7.2, means that the efficiency of the bond must have been substantially improved.

7.4.2 Beam Bars:

From the strain distributions shown in Figs. 7.5 (a) and 7.5 (b) the anchorage length appears adequate for downward load during the elastic cycles, however subsequent deterioration in bond during the post-elastic cycles resulted in bond failure of the top bars, as indicated by the strain distribution shown in Fig. 7.5 (a) for Run 8. A similar pattern was evident for the bottom bars on upward load runs except that there appeared to be a residual stress at the end of the bars. However, the strain distribution, shown in Fig. 7.5 (b) suggests that there was an anomaly between the readings of gauges 7* and 8*.

The residual stress at the end of the bars, when they are subject to a compression stress, is due to the bearing pressure of the end of the bar on the concrete. The effect is shown in Fig. 7.6, which is a detail taken from the circled area of Fig. 7.16. where the beam flexural bar, now in tension, has lifted off the concrete bearing surface.

In many cases the stress in the tensile bars is greater inside the column than in the beam. Theoretically the maximum stress should be at the intersection of the inner column bars, since this is where the column tensile

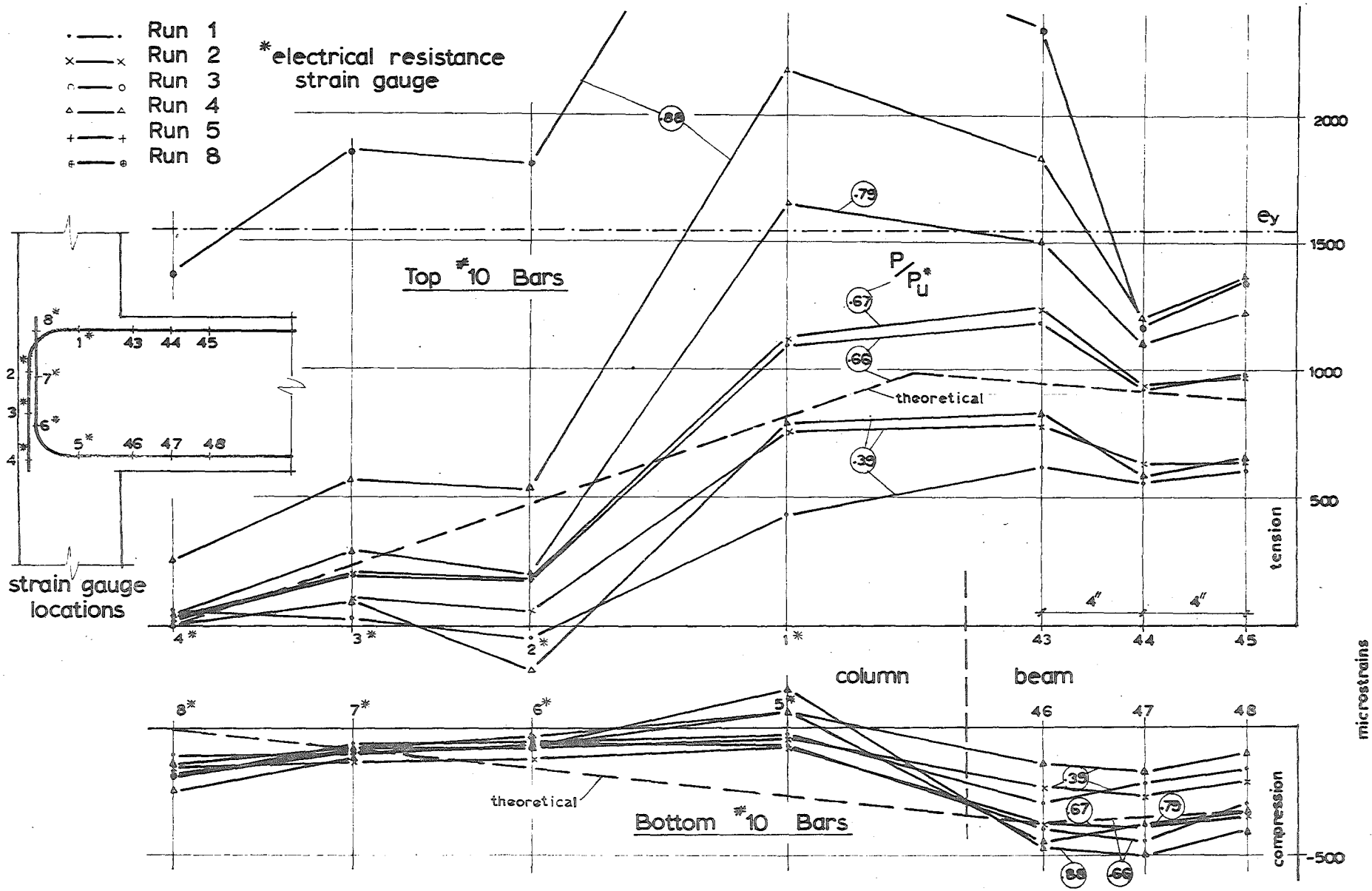

FIG. 7.5(a) THE DISTRIBUTION OF STEEL STRAINS IN BEAM FLEXURAL BARS IN UNIT 4 [FOR DOWNWARD LOAD RUNS]

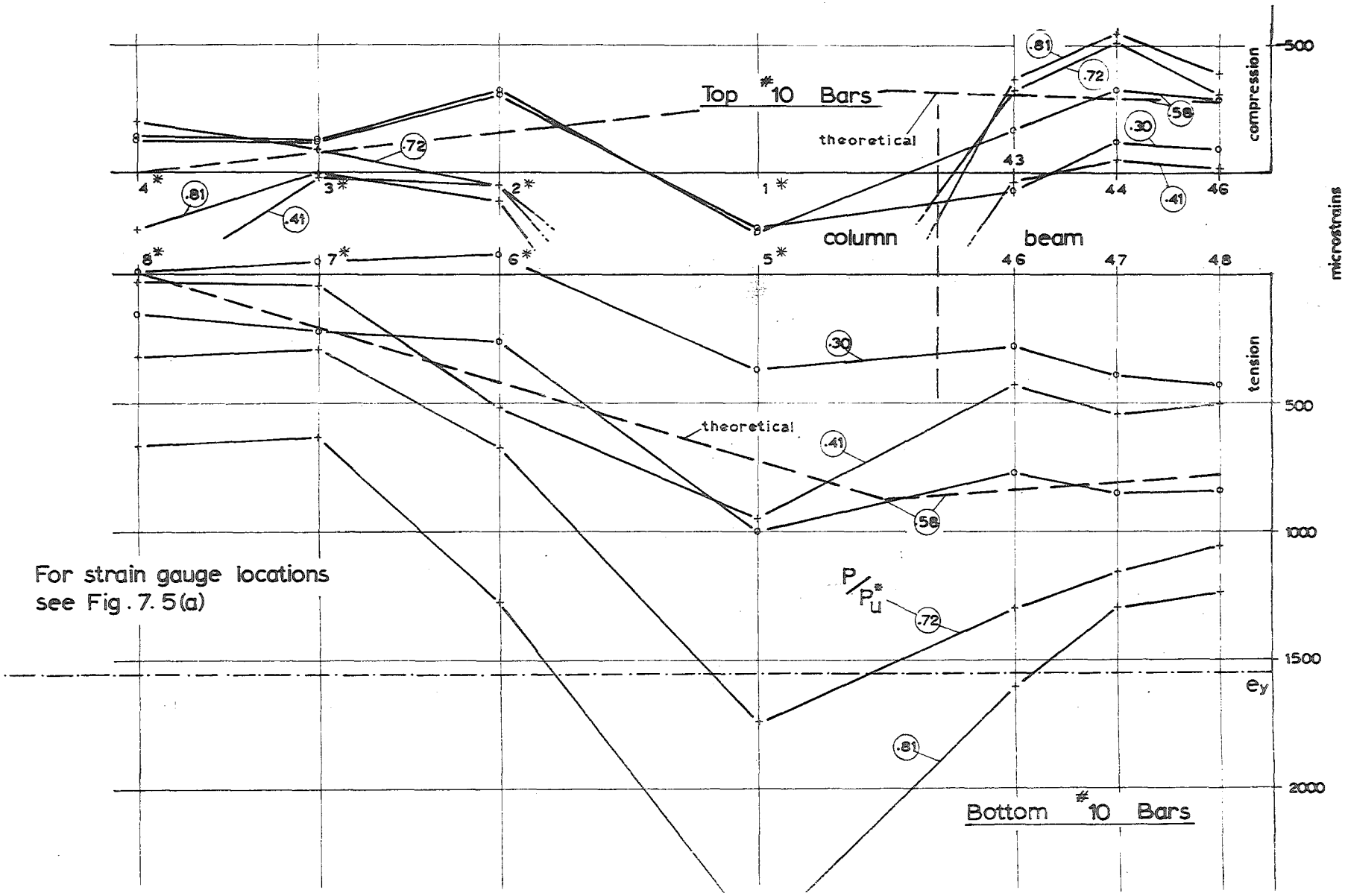

FIG. 7.5(b) THE DISTRIBUTION OF STEEL STRAINS IN BEAM FLEXURAL BARS IN UNIT 4 [FOR UPWARD LOAD RUNS]

force is introduced.

7.5 BEHAVIOUR OF TRANSVERSE REINFORCEMENT:

7.5.1 Column Ties:

The strain distributions on the column ties above and below the joint are shown in Fig. 7.7. These regions were subjected to greater rotations and more flexural cracking than in any of the previous specimens, however as can be seen from the strain distributions, it was still only the ties closest to the joint which were significantly affected. These are also most prone to bowing, being near the area of internal cracking, which casts doubt on the accuracy of the DEMEC readings. However, because of the failure being mainly confined to the joint region, the actual stress in the ties was considered secondary to their ability to prevent a brittle column failure.

7.5.2 Joint Ties:

This was the first specimen to be subjected to a post-elastic cycle without any of the joint ties yielding. The strain distributions are shown in Figs. 7.8 (a) and 7.8 (b).

The strain readings on the back of the joint ties show an apparently random distribution, with all the ties working effectively and being subjected to similar stresses.

The distribution of strain at the side of the ties, in comparison with the back, shows definite tendencies for the stress in a particular tie to be dependent on the direction of loading. For this specimen, the higher stress occurs in the lower ties during downward load runs and in the upper

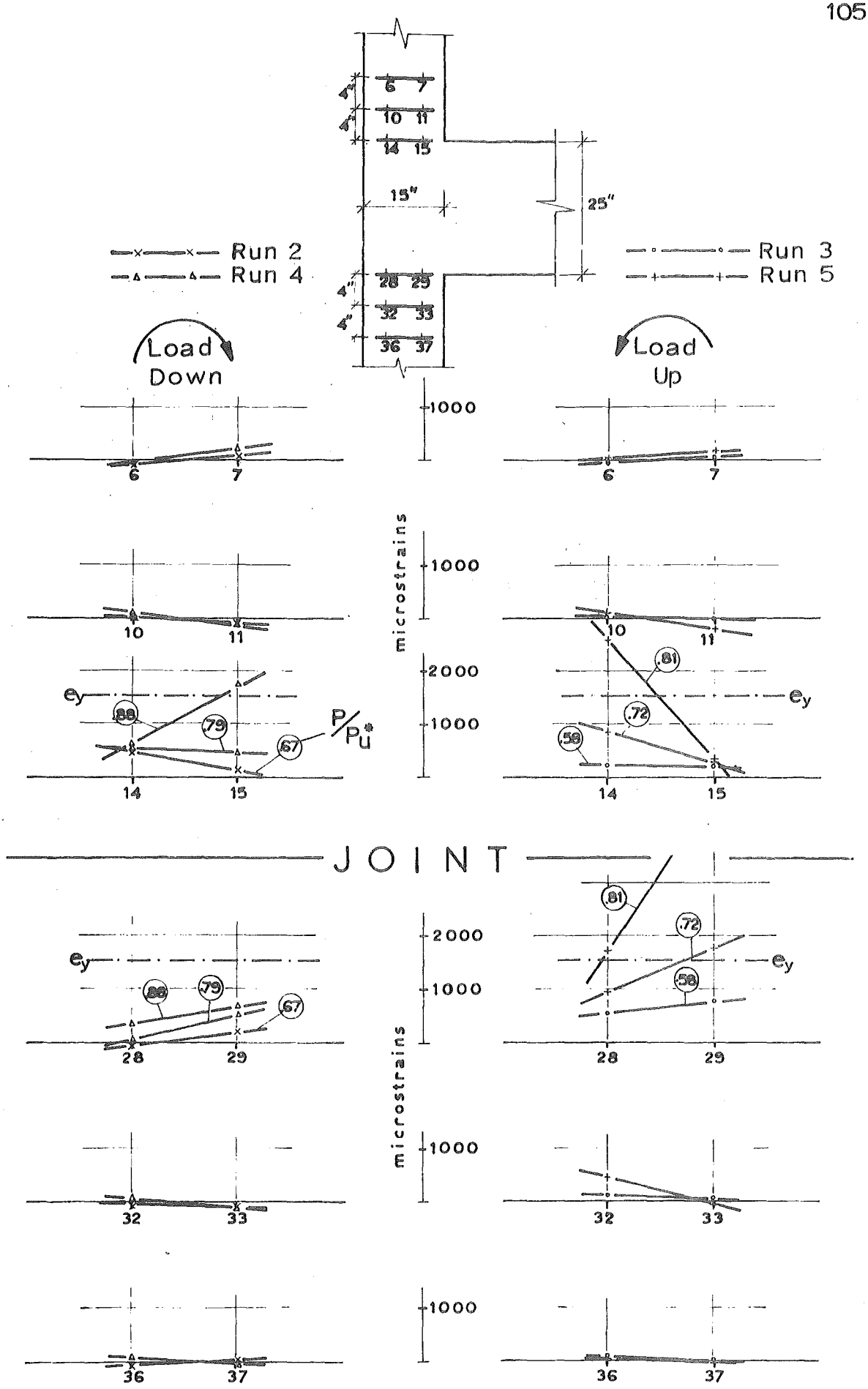

FIG. 7.7 THE DISTRIBUTION OF STEEL STRAINS IN THE COLUMN TIES OF UNIT 4

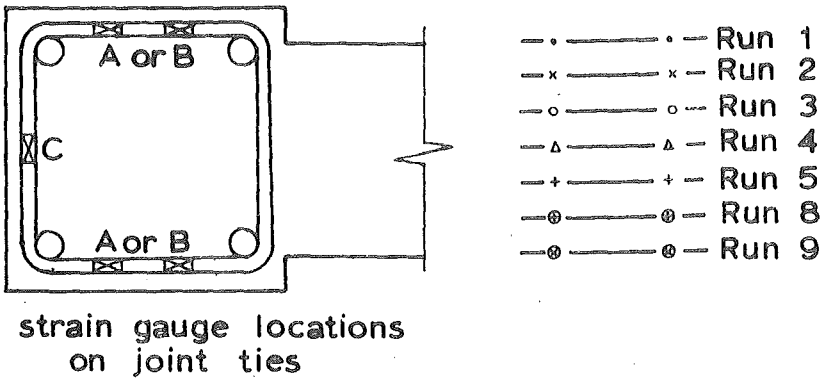

strain gauge locations
on joint ties

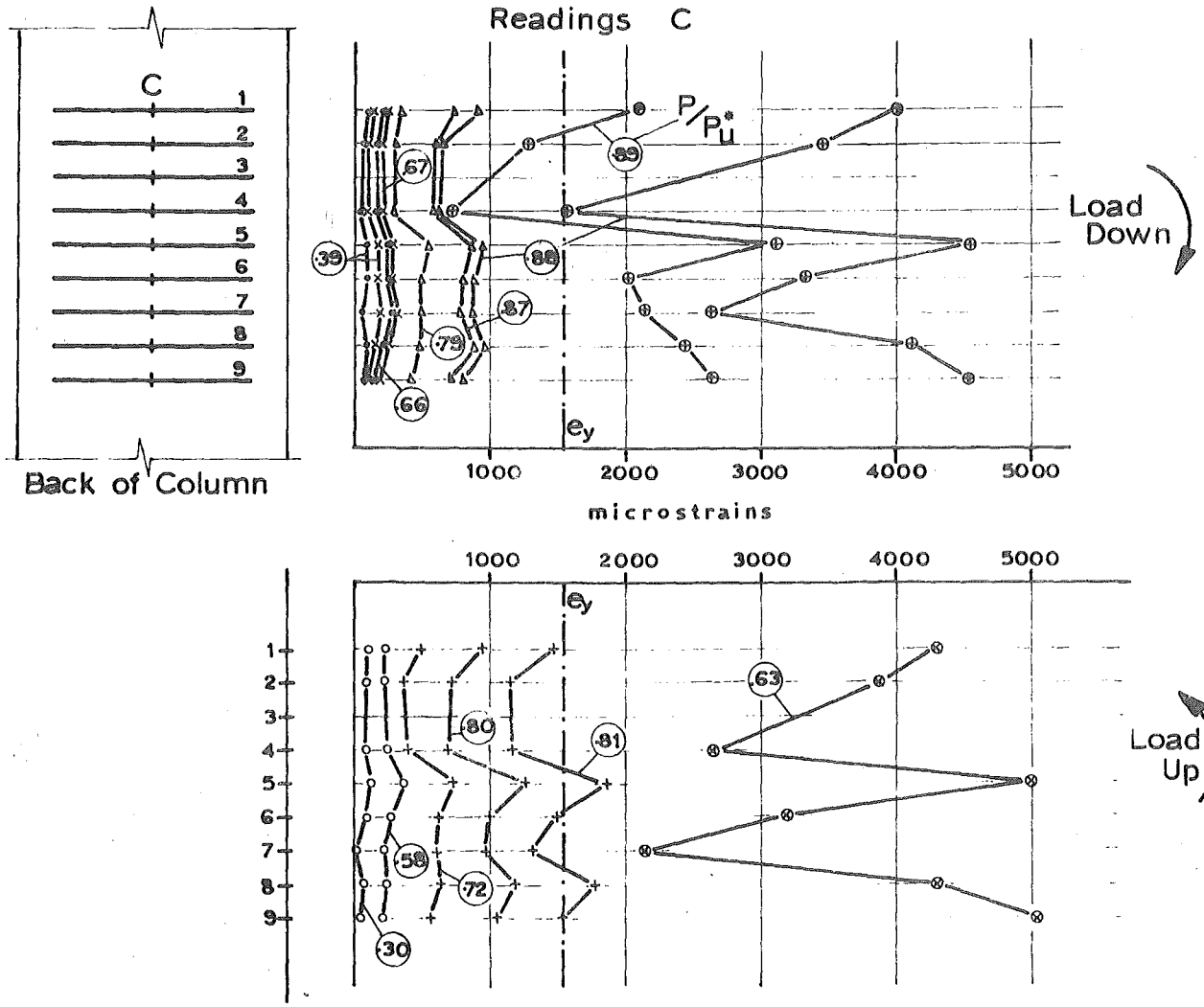

FIG. 7.8 (a) THE DISTRIBUTION OF JOINT TIE STRAINS AT BACK OF COLUMN IN UNIT 4

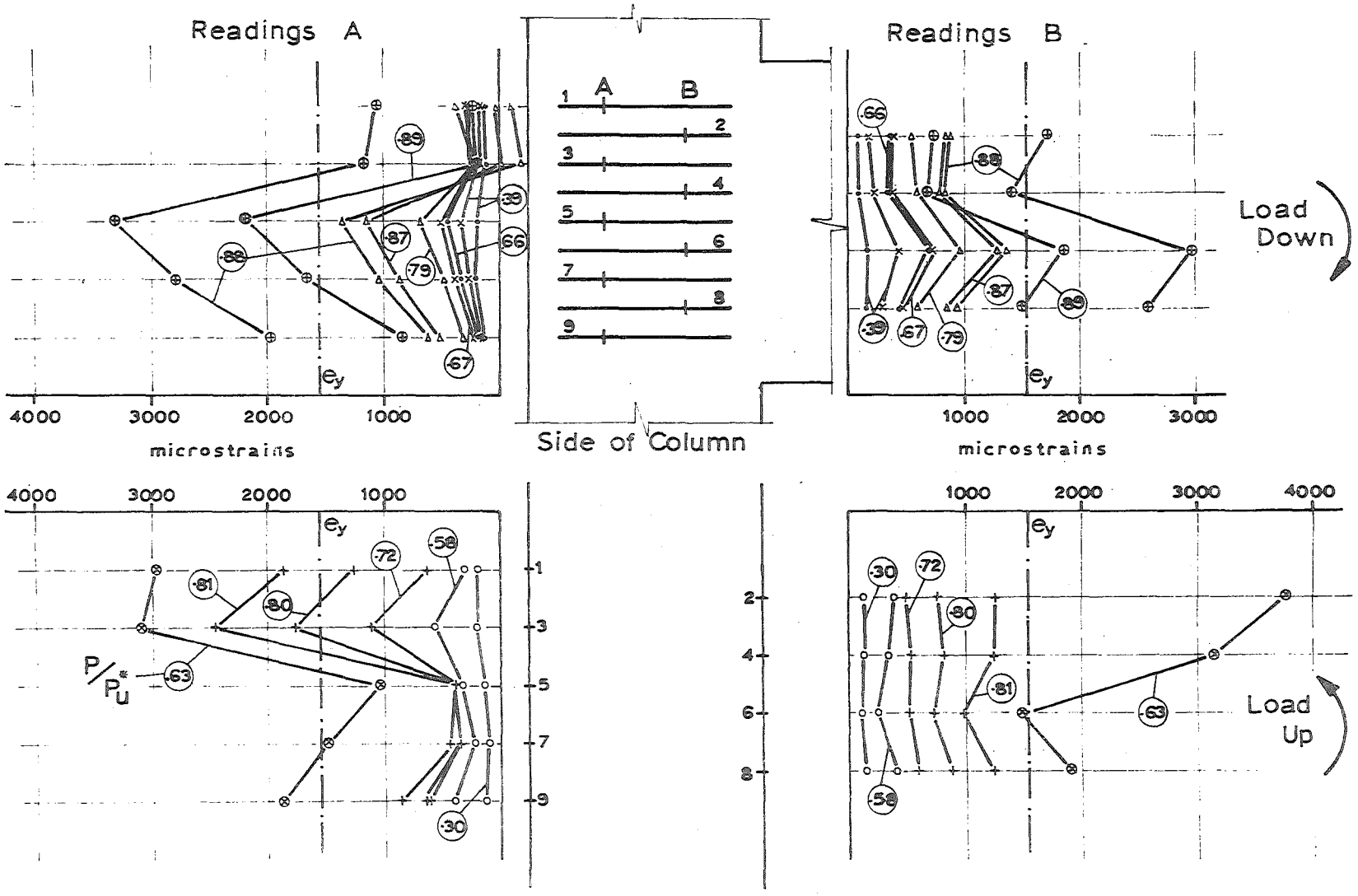

FIG. 7.8 (b) THE DISTRIBUTION OF JOINT TIE STRAINS AT SIDE OF COLUMN IN UNIT 4

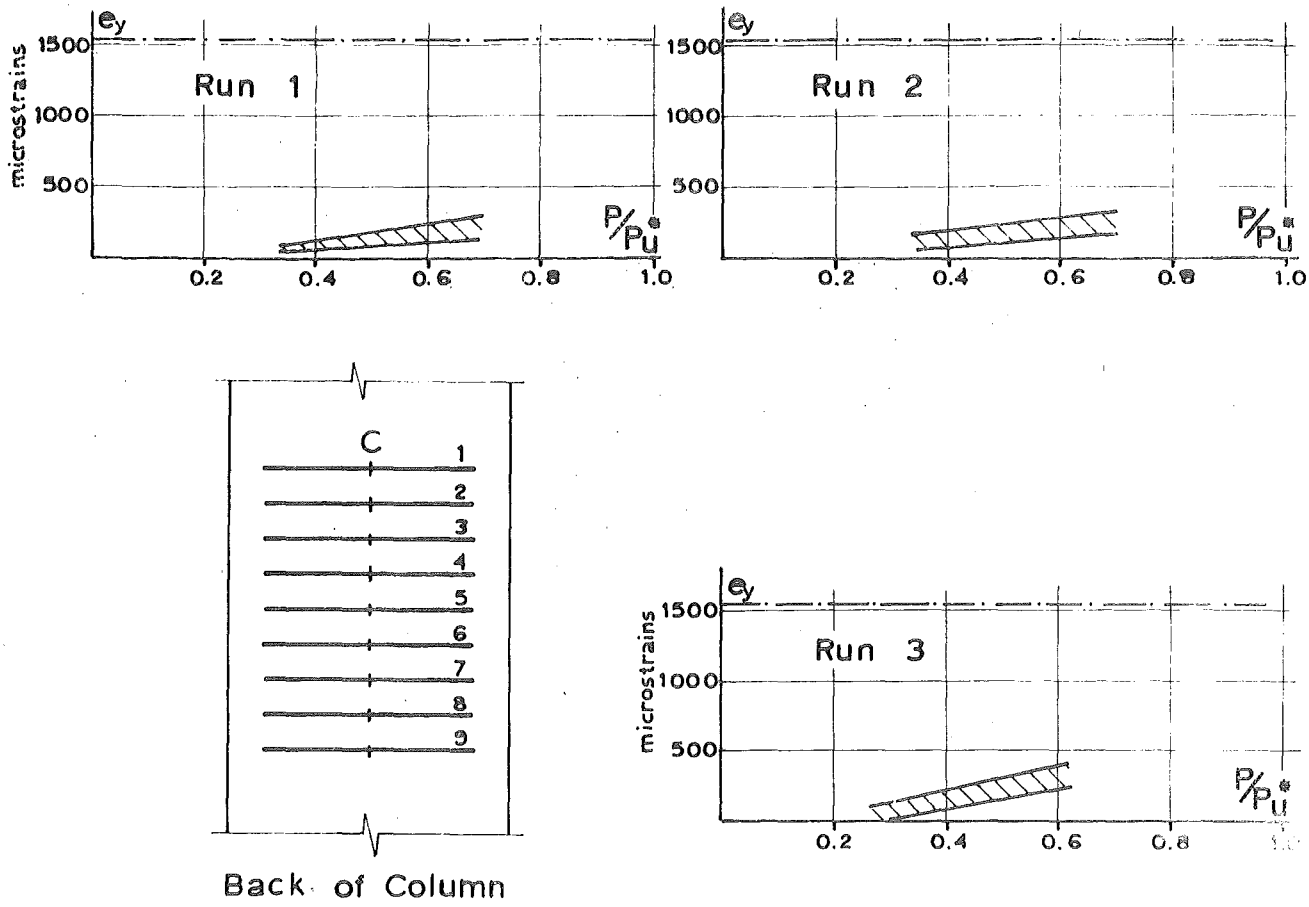

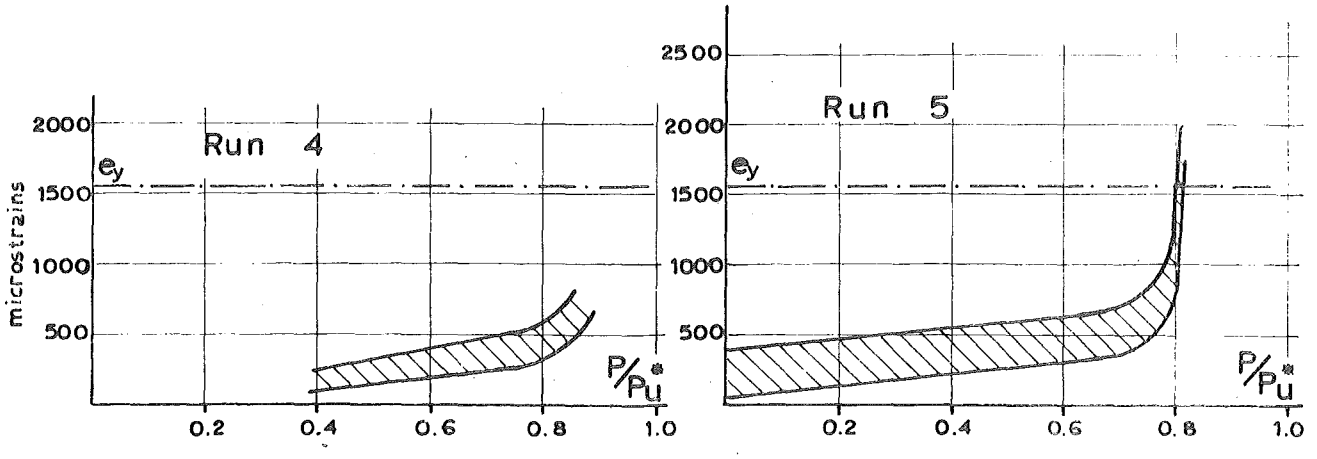

FIG. 7.9(a) THE LOAD-STRAIN RELATIONSHIP FOR JOINT TIES IN UNIT 4 AT BACK OF COLUMN

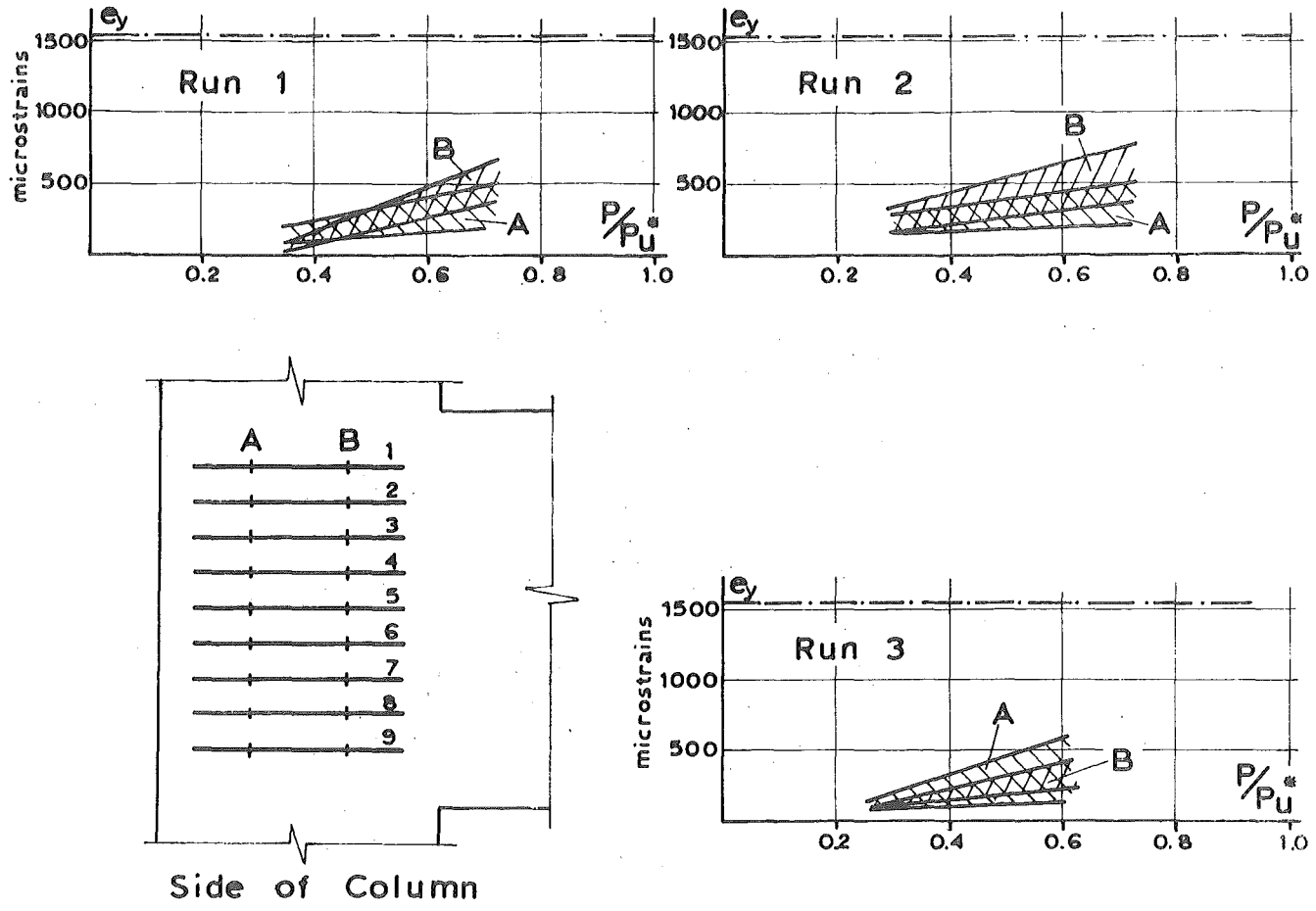

Range of Readings A and B

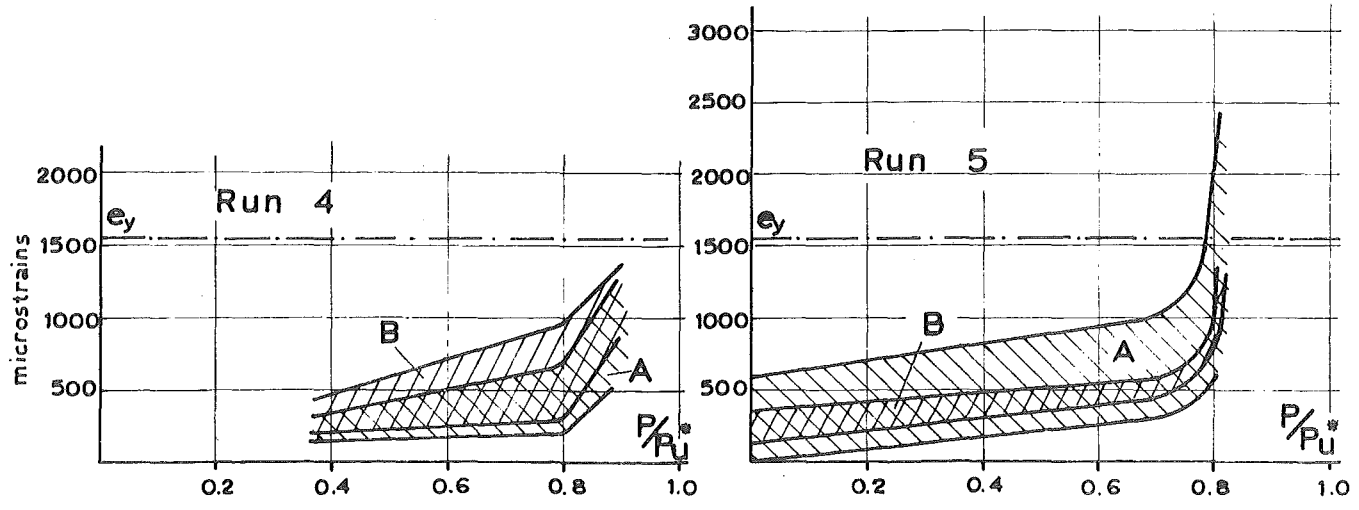

FIG. 7.9(b) THE LOAD-STRAIN RELATIONSHIP FOR JOINT TIES IN UNIT 4 AT SIDE OF COLUMN

ties on the upward load runs. This is the opposite effect to what was observed in the previous specimens and suggests that this joint has a completely different load resisting mechanism for this reinforcement detail. There is also a distinct similarity between the distribution of readings A and B on each tie, indicating that they are to some extent dependent on each other, the bond stress along the tie not being significant.

The development of strain in the ties is shown in Figs. 7.9 (a) and 7.9 (b). The inclusion of the nine ties in the joint ensures that the stresses are kept low during elastic cycles, when shear resistance appears to be the major function of the ties. However when bursting forces are exerted during post-elastic cycles the effect can be clearly seen from the load-strain relationships.

Although the ties were only fully effective for one post-elastic cycle before they yielded, from a practical point of view, nine ties would seem to be a maximum amount of transverse reinforcement for this particular joint.

7.6 DEFORMATIONS:

7.6.1 Deflections:

The deflected shapes of the specimen at the peaks of the elastic cycles are shown in Fig. 7.10 and compared with the theoretical shapes. The observed behaviour of the specimen acting more as an integral unit in the joint region would account for the better correlation between theoretical and actual deflected shapes for this specimen.

7.6.2 Moment-Rotation Relationships:

The relationships, shown in Fig. 7.11, emphasise the extent to which the rotation occurs in the region of lower axial load. The column was obviously much stiffer than for UNIT 3 which suggests that it is affected

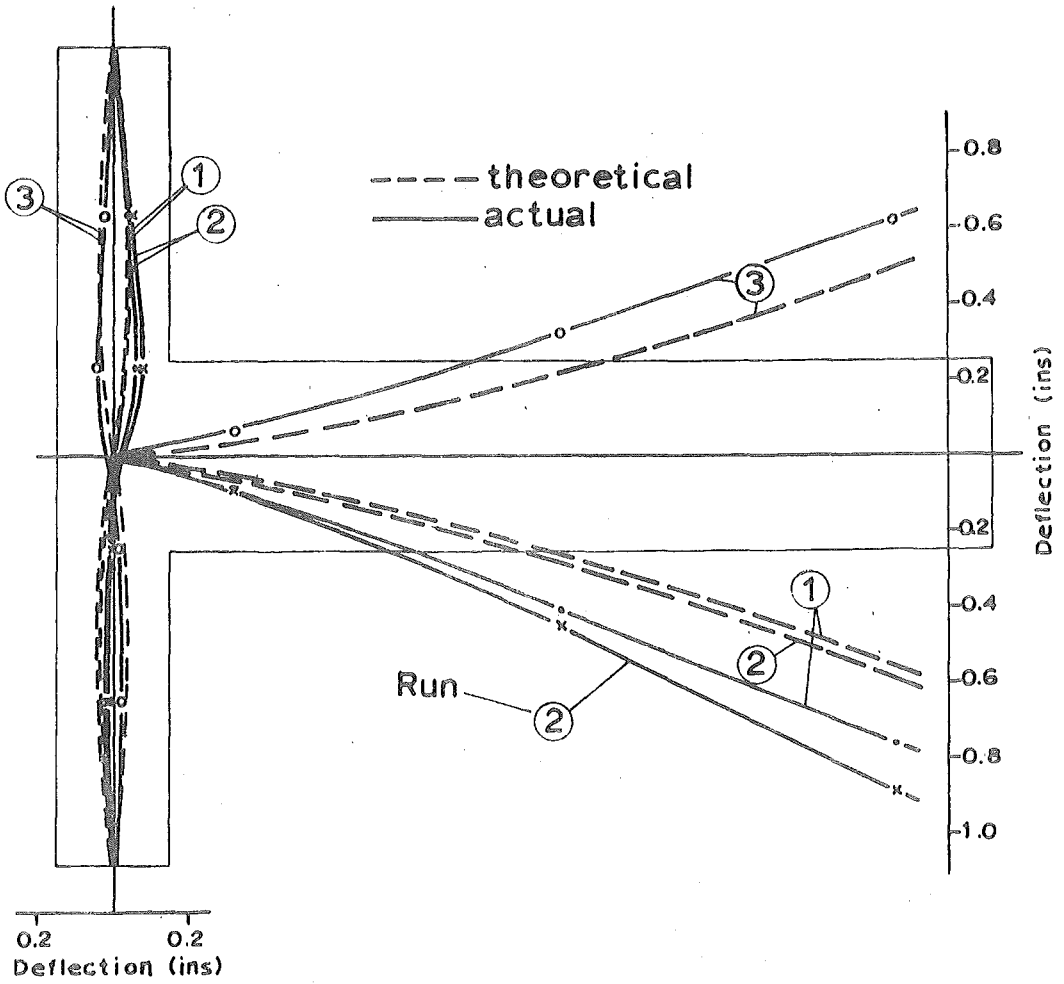

FIG. 7.10 DEFLECTED SHAPES OF UNIT 4 AT PEAKS OF ELASTIC LOAD RUNS

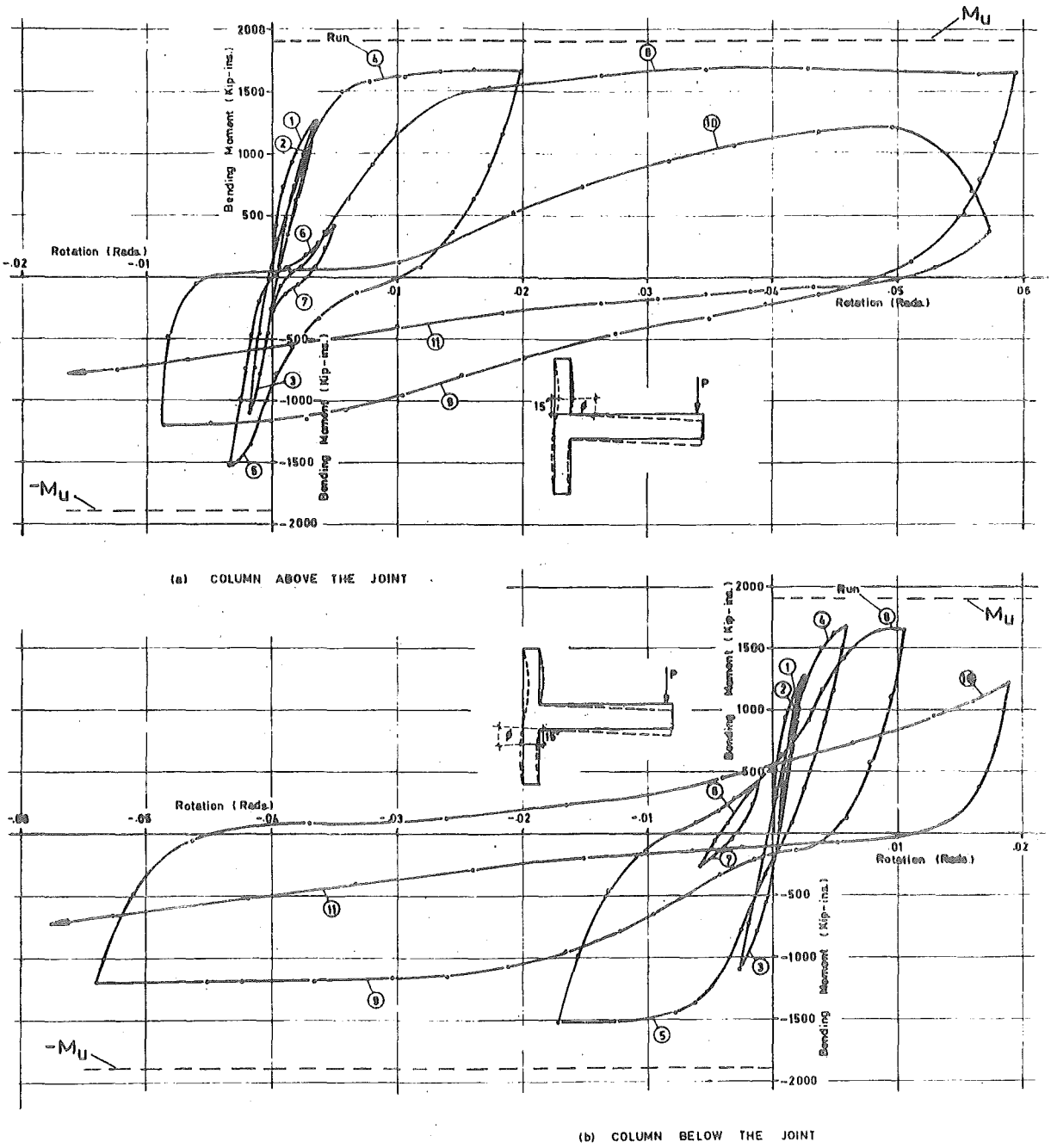

FIG. 7.11 THE MOMENT-ROTATION RELATIONSHIPS FOR UNIT 4

by the overall stiffness of the specimen rather than the extent of cracking in the column itself.

7.6.3 Load-Deflection Relationship:

The improved load resisting characteristics and resilience are amply demonstrated by the relationship shown in Fig. 7.12. Adequate stiffness of the specimen was sustained up to Run 8, after which the stiffness degradation and loss of load capacity became apparent, as shown in Table 7.1.

The increased resilience of the specimen over UNIT 3 is emphasised by the fact that the maximum load capacity of the specimen was acheived during Run 8.

TABLE 7.1 Performance of UNIT 4 During Load Cycling.

Run	Maximum Load P_{max} (kips)	$\frac{P_{max}}{P^*_u} \times 100$ (%)	Ductility Factor	Average % Stiffness †
1	23.2	66.3	-	76.2
2	23.6	67.4	-	92.0
3	20.3	58.0	-	81.7
4	31.0	88.7	4.0	53.7
5	28.4	81.1	4.6	33.7
6	7.9	22.6	-	17.0
7	4.9	14.0	-	18.2
8	31.3	89.6	10.7	18.0
9	22.2	63.5	16.0	6.5
10	22.6	64.6	21.8	3.6
11	13.8	39.4	19.0	2.2

† Expressed as % of the theoretical stiffness.

7.7 CRACKING:

The development of the diagonal tension cracks shown in Fig. 7.2 eventually lead to a major crack running between opposite corners of the

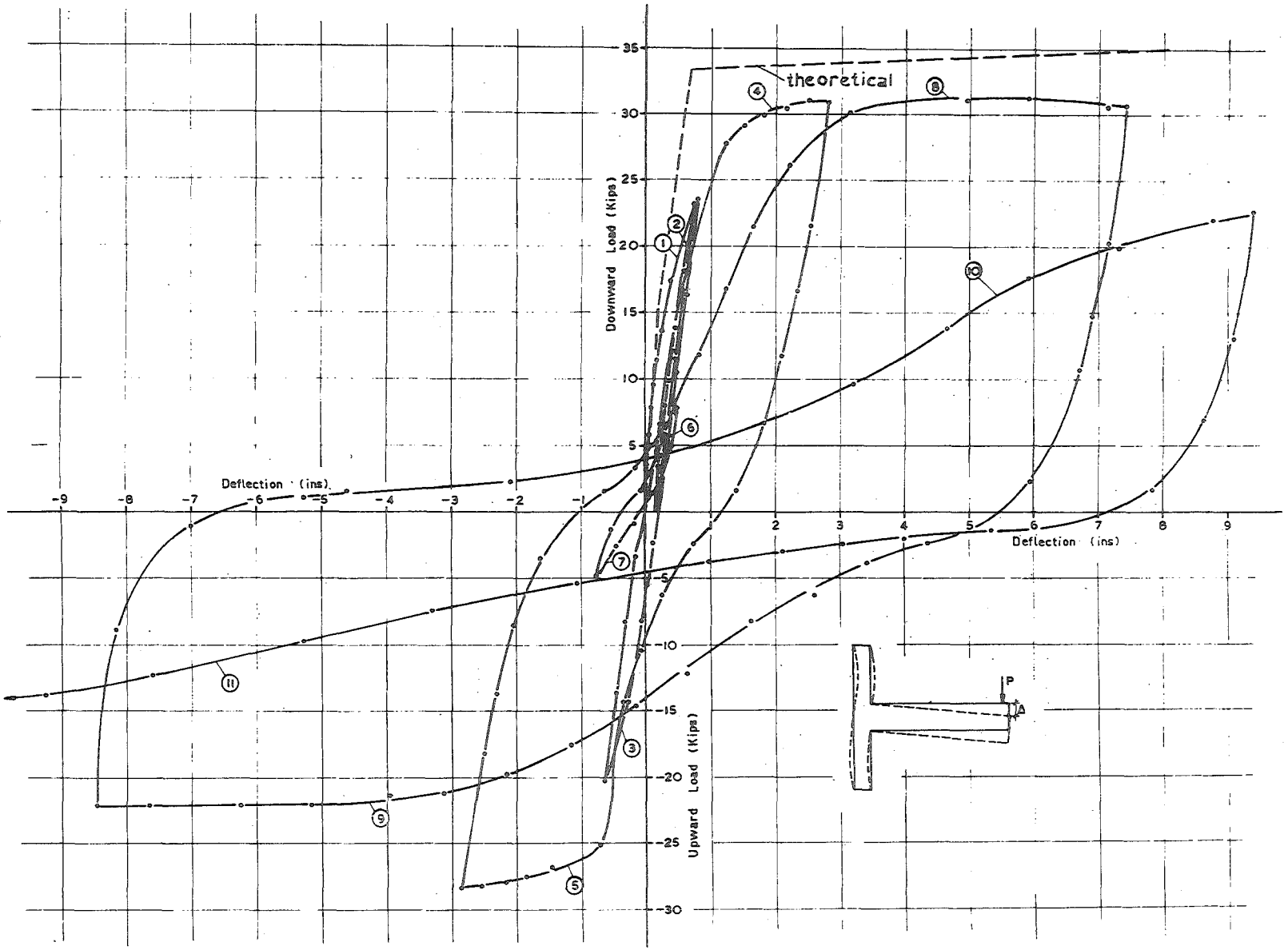

FIG. 7.12 THE LOAD DEFLECTION RELATIONSHIP FOR UNIT 4

joint. Figs. 7.13 and 7.14 show the specimen at the peaks of Runs 4 and 5 respectively where it is shown that not only the diagonal tension cracks were widening, but also flexural cracks at the junction of the beam and column. Fig. 7.15 shows the specimen at the peak of Run 8, when flexural yielding of both the beam and column bars has occurred and the cover concrete is being forced off the back and sides of the joint. The cover concrete was eventually completely removed from the joint, as shown by Fig. 7.16.

7.8 FAILURE MECHANISM:

The increase in load capacity of this specimen over the previous three was primarily attributable to the increase in anchorage length of the beam flexural bars.

At this stage it should be noted that the joint ties were more regularly spaced than they were for UNIT 3. However since this may have affected the confinement slightly it would be more likely to improve the resilience rather than the load capacity.

Because of the increased anchorage length of the beam flexural bars the tendency for bond failure was minimised, until the repetitive load cycling reduced the bond sufficiently to allow differential movement. Since the anchorage length was not enough to dissipate the tensile stress in the top beam bars during Run 4, the first post-elastic run, a further increase in the length of the bars would possibly enable the theoretical ultimate capacity of the specimen to be attained. The movement of the flexural steel in the joint is the prime cause of load capacity reduction and initiates the joint deterioration by breaking the cohesion within the joint.

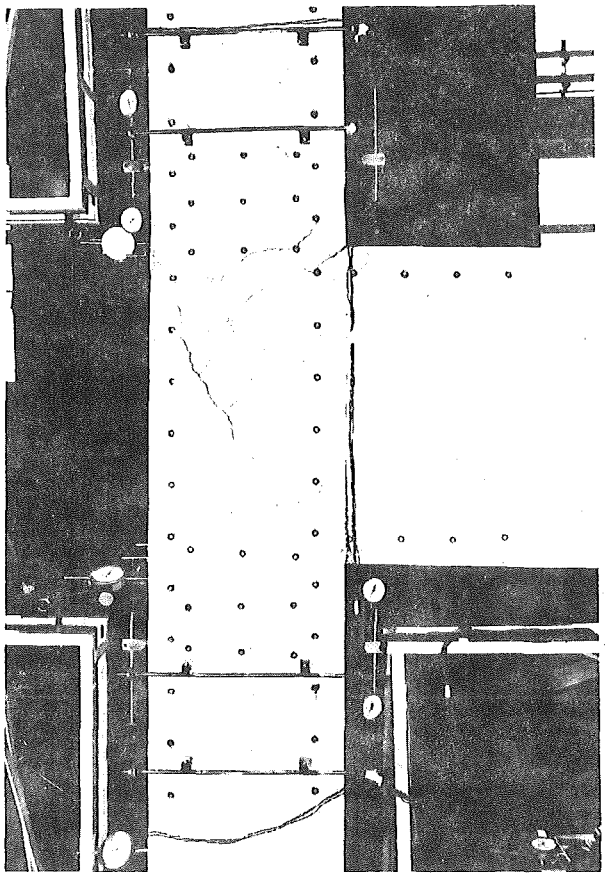

FIG. 7.13 UNIT 4 ON LOAD RUN 4

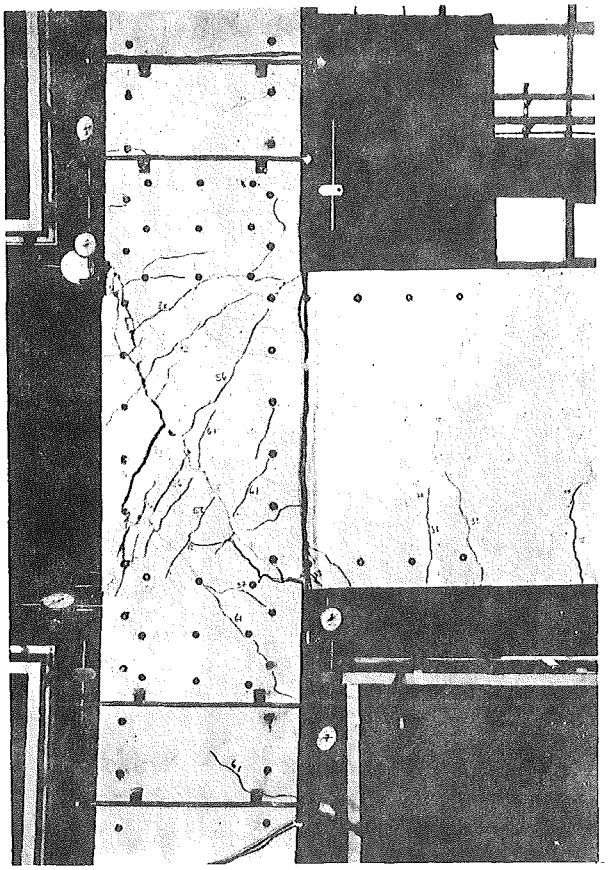

FIG. 7.14 UNIT 4 ON LOAD RUN 5

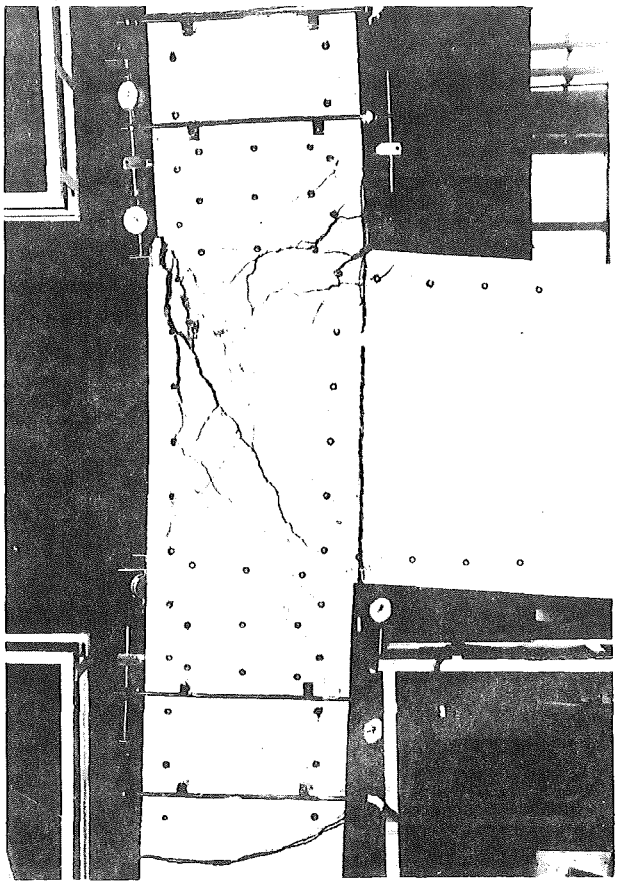

FIG. 7.15 UNIT 4 ON LOAD RUN 8

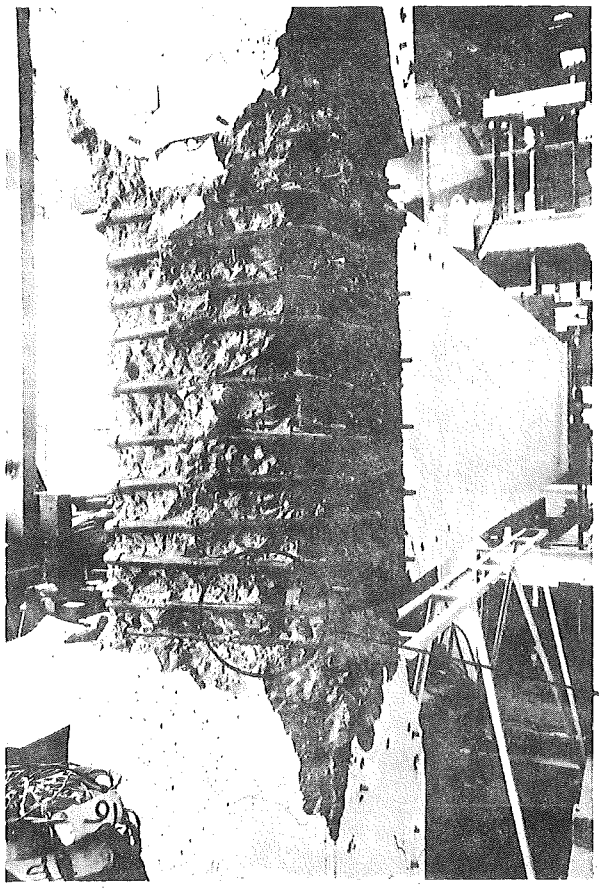

FIG. 7.16 UNIT 4
AT FAILURE

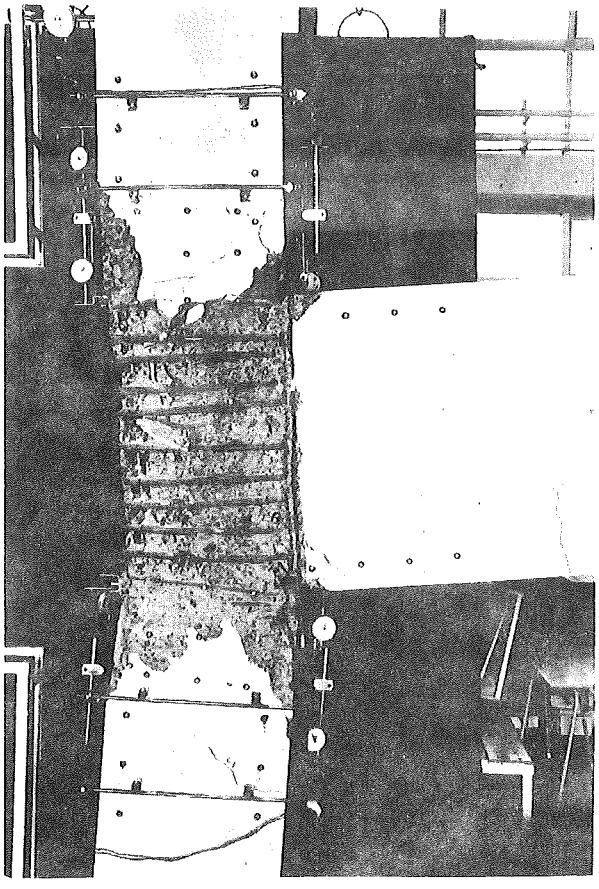

FIG. 7.17 UNIT 4
AT FAILURE

Although bond failure eventually dominated the stiffness degradation and overall performance of the specimen, yielding of the flexural steel did occur and would also have influenced the behaviour to some extent. Fig. 7.17 shows the specimen at the peak of cycle 11 where it is obvious that the joint is still well confined by the ties, and the majority of rotation is provided by the column outside the joint region.

CHAPTER EIGHT.

DISCUSSION AND CONCLUSIONS.

8.1 COMPARISON OF SPECIMENS:

The beam-column joint is generally considered to provide its load resistance by a type of truss mechanism, where the joint ties and the concrete provide the tension and compression struts respectively. Two alternative methods of distributing the forces on downward load runs are shown in Figs. 8.1 (a) and 8.1 (b). Each of these would have a characteristic crack pattern determined by the fact that compression cannot be carried across an open crack. Fig. 8.2 shows the forces imposed on the joint of UNIT 4 and the crack pattern at the peak of Run 1. Since the cracking does not correspond to either of the distributions shown in Fig. 8.1, it is probable that the actual mechanism is some combination of these distributions. However, to be effective both these systems require the joint to perform as an integral unit. Because of the tendency for bond failure of the flexural bars in the first three specimens, the force in the outer column bars could not be distributed, since they were virtually separated from the majority of the joint. Therefore the effectiveness of the truss mechanism was significantly reduced.

The initial elastic cycles served to break up the joint sufficiently so that the load capacity of the first three specimens was limited by the bond stress which could be developed between the beam flexural bars and the cracked concrete in the joint. Table 8.1 compares the bond stress

TABLE 8.1 Bond Stress Developed in Beam Flexural Bars.

Unit	$P_{max.}$ (kips)	$M_{max.}$ (kip-in)	f_s (ksi)	$f_s + f'_s$ (ksi)	$u_{max.}$ (psi)	$\frac{u_{max.}}{f'_c}$
1	24.3	2960	29.4	40.5	317	5.2
2	27.3	3330	33.0	44.6	350	4.7
3	24.8	3020	30.0	41.9	328	5.6
4	31.3	3820	37.9	-	377	5.8

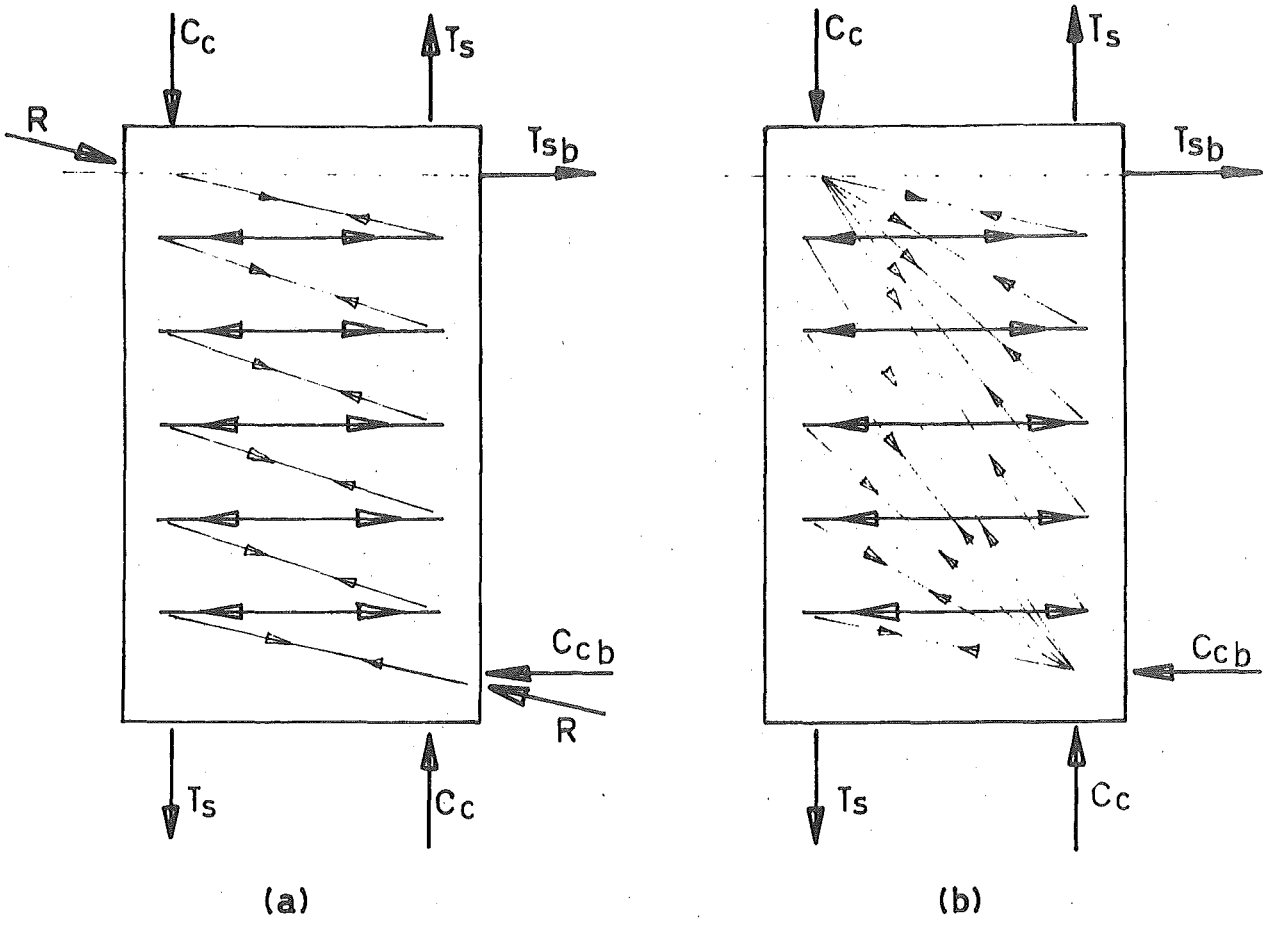

FIG. 8.1 DISTRIBUTION OF INTERNAL FORCES

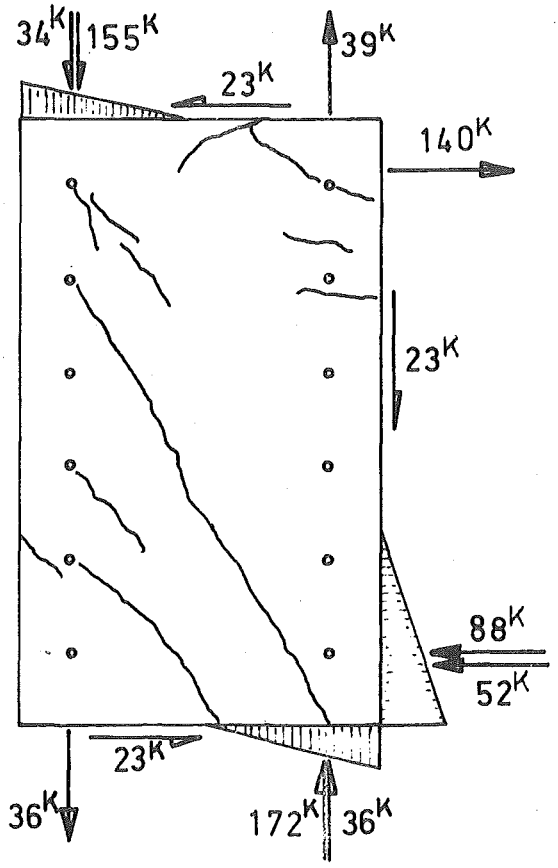

FIG. 8.2 FORCES ON JOINT OF UNIT 4 (RUN 1)

developed in the beam flexural bars for each of the specimens, although the value given for UNIT 4 does not represent the ultimate bond stress. The recommendation by ACI 318 - 63 is given as

$$u_u = \frac{9.5}{D} \sqrt{f'_c} = 7.6 \sqrt{f'_c}$$

However, from Table 8.1, no specimen attained this level. A more realistic figure for this situation would be that specified for top bars

$$u_u = \frac{6.7}{D} \sqrt{f'_c} = 5.3 \sqrt{f'_c}$$

which would represent the maximum obtainable bond stress unless the concrete is more adequately confined as in UNIT 4. The anchorage length required in UNIT 4 on the ACI 318 - 63 recommendation is

$$L = \frac{f_y A_s}{7.6 \sqrt{f'_c}\, \pi D} = \frac{45000 \times .5}{7.6 \times 63 \times 16}$$

$$= 28.5 \text{ in.}$$

In UNIT 4, 32 in. of anchorage was provided, which should therefore have been adequate to develop the required bond stress.

Since the failures were always concrete failures the maximum loads resisted by the specimens were largely dependent on the tensile and crushing strength of the concrete. This was shown to be the case particularly for the first three specimens. The maximum loads obtained and the theoretical ultimate and yield loads for each specimen are shown in Table 8.2 for comparison.

TABLE 8.2 Comparison of Theoretical and Actual Loads.

UNIT	f'_c (ksi)	theoretical yield load P^*_y (kips)	actual maximum load P_{max} (kips)	theoretical ultimate load P^*_u (kips)	$\frac{P_{max}}{P^*_u} \times 100$ %
1	3.73	32.7	24.3	34.3	71%
2	5.57	35.2	27.0	35.9	75%
3	3.44	32.3	24.7	34.2	72%
4	4.22	33.3	31.3	35.0	90%

The maximum column moment achieved in UNIT 4 was

$$M_c = 1690 \text{ kip-in.}$$

which is lower than the theoretical moment at first yield of the tension steel, for a column of this size. Therefore if the column had been behaving as a composite structural member the flexural steel would not have yielded. The fact that the steel did yield suggests that only the column core was the effective structural member. By neglecting the structural action of the cover concrete the ultimate moment capacity of the column core, of dimensions 13.5" x 13.5" is

$$M_{uc} = 1760 \text{ kip-in.}$$

However this moment capacity was not achieved due to the premature joint failure.

The difference in stiffness of the specimens was quite apparent during testing and Table 8.3 tabulates the deflection characteristics for comparison. The theoretical rotation of the column and beam have been determined for both uncracked and cracked sections and compared with the actual values obtained in Runs 1, 2 and 3.

The column rotation is predicted reasonably accurately in most cases by the theory of a cracked concrete section. However the deflection at the end of the beam is, in all cases, greater than theoretically predicted. This is due to joint distortion not being taken into account when computing the theoretical rotations and deflections. It can be seen from Table 8.3 that joint distortion can have a considerable effect on the deflection of the beam, expecially in UNIT 3 where the low concrete strength means that joint distortion accounts for more than 60% of the total deflection of the beam.

The extra rotation of the joint also affects the deflection of the column as shown by the figures of deflected shapes in each chapter.

TABLE 8.3 Comparison of Theoretical and Actual Rotations and Deflections.

UNIT	Run	Maximum Load $P_{max.}$ (kips)	theoretical uncracked		theoretical cracked		actual		$\frac{\Delta_{cr.}}{\Delta} \times 100$
			$\phi_{uncr.}$ rads x 10^{-2}	$\Delta_{uncr.}$ (in)	$\phi_{cr.}$ rads x 10^{-2}	$\Delta_{cr.}$ (in)	ϕ rads x 10^{-2}	Δ (in)	%
1	1	23.9	.13	.38	.22	.61	.30	1.28	48%
	2	24.3	.13	.39	.23	.62	.34	1.50	41%
	3	20.9	.11	.33	.20	.54	.26	1.15	47%
2	1	24.0	.11	.33	.20	.55	.18	0.80	69%
	2	26.3	.12	.36	.21	.61	.25	1.01	61%
	3	22.7	.12	.36	.21	.58	.16	0.83	70%
3	1	22.0	.12	.36	.21	.58	.33	1.37	42%
	2	22.9	.13	.37	.22	.60	.41	1.66	36%
	3	19.7	.11	.31	.19	.51	.25	1.18	43%
4	1	23.2	.12	.35	.21	.58	.17	.76	76%
	2	23.6	.12	.36	.21	.59	.18	.80	74%
	3	20.3	.11	.31	.18	.51	.13	.63	81%

A comparison can be made between the shear reinforcement provided in the joint of each specimen and the theoretical requirements.

Table 8.4 compares the amount of shear reinforcement by various different methods. Methods A and B are commonly used in design and are those recommended by the ACI[5]. Method C is the most conservative method, not allowing for any shear resistance from the concrete. The shear reinforcement for these three methods is provided on the basis of 45° cracking. Methods D,E,and F differ from these in the way in which shear reinforcement is computed. The basis behind the theory is that the major shear crack runs between opposite corners of the joint, and the ties are provided to prevent the joint from separating along this crack.

TABLE 8.4: Joint Shear Reinforcement.

UNIT	Number of Ties (m)	Ratio: shear reinforcement provided / required shear reinforcement					
		A	B	C	D	E	F
1	5	0.83	0.67	0.52	1.34	1.07	0.84
2	7	1.25	0.91	0.70	2.02	1.47	1.12
3	9	1.48	1.20	0.94	2.38	1.93	1.51
4	9	1.50	1.17	0.91	2.42	1.89	1.47

A: $V_c = 3.5\ bd\ \sqrt{f'_c\ (1 + 0.002\ {}^{N}/_{A_g})}$; $V_s = A_v f_y\ {}^{d}/_{s}$

B: $V_c = bd\ (1.9\sqrt{f'_c} + 2500 p_w \frac{V_u d}{M'})$; $V_s = A_v f_y\ {}^{d}/_{s}$

C: $V_c = 0$; $V_s = A_v f_y\ {}^{d}/_{s}$

D: V_c as for A; $V_s = m2a_v f_y$

E: V_c as for B; $V_s = m2a_v f_y$

F: $V_c = 0$; $V_s = m2a_v f_y$

8.2 CRITICISM OF THE DETAIL:

The 45° crack theory has been developed from shear tests on reinforced concrete flexural members. However when the member is subjected to a compressive stress, such as a column under axial load, the angle of cracking is affected. For example using the situation shown in Fig. 8.2, for any element within the joint:

$$\text{shear stress,} \qquad v = \frac{140}{15 \times 15} = 623 \text{ psi}$$

$$\text{compressive stress,} \qquad f = \frac{148}{15 \times 15} = 658 \text{ psi}$$

The direction of maximum diagonal tension is found from

$$\tan \alpha = \frac{2v}{f} = 1.89$$

$$\alpha = 31^\circ$$

The angle of the main crack shown in Fig. 8.2 is 33° to the vertical. Therefore it is apparent that the present recommendations for design of shear

reinforcement in joints is based on an invalid assumption.

The formula used to determine the amount of transverse confining steel required is based on maintaining the original strength of the column when the cover concrete has been removed, however it would seem more appropriate to provide this reinforcement on a basis of achieving adequate ductility. These tests have shown that cover concrete provides minimal structural resistance during post-elastic load cycles, and therefore it would seem desirable to consider the column core as the structural member. Then the A_g/A_c ratio is meaningless, and only serves to introduce a highly variable factor when considering different size columns. The bursting pressure should be more dependent on the N/A_c ratio and probably on the value of f'_c. The restraining effect of the hoops is dependent on f_y, A_{sh}, s and h'. However as shown in Fig. 8.3 the restraint provided by the hoops relies on the flexural resistance of one leg of the hoop between its two supports. Since the stress on the bar is dependent on $(h')^2$, more emphasis should be placed on reducing the value of h' as much as possible. Since only four column flexural bars were provided the legs of each tie were unrestrained over a distance of more than 12 in. This was shown to be particularly unfavourable for confinement but generally, with a greater number of bars in the column the problem is not as critical as it was here.

The major downfall of the detail was caused by the method of anchoring the beam bars in the column in the continuous form. As shown in Section 8.1 the bond stress required to attain theoretical ultimate load was greater than could be developed, due partly to the lack of confinement which meant that the only efficient bond was on the inside of the anchorage hooks. The dimensions of the joint meant that the horizontal length of anchorage before the hook, which provides the most efficient anchorage for the beam bars, was small enough to allow rotation of the beam bars within the column once the bond was weakened. UNIT 4 showed that adequate anchorage could be provided if detailed properly.

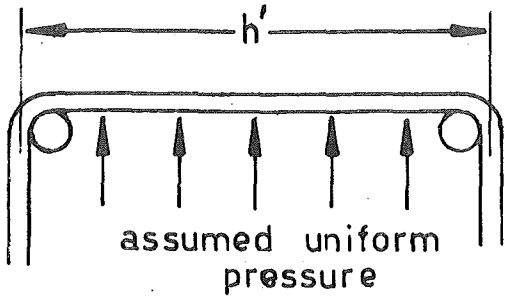

FIG. 8.3 PRESSURE ON ONE LEG OF TIE

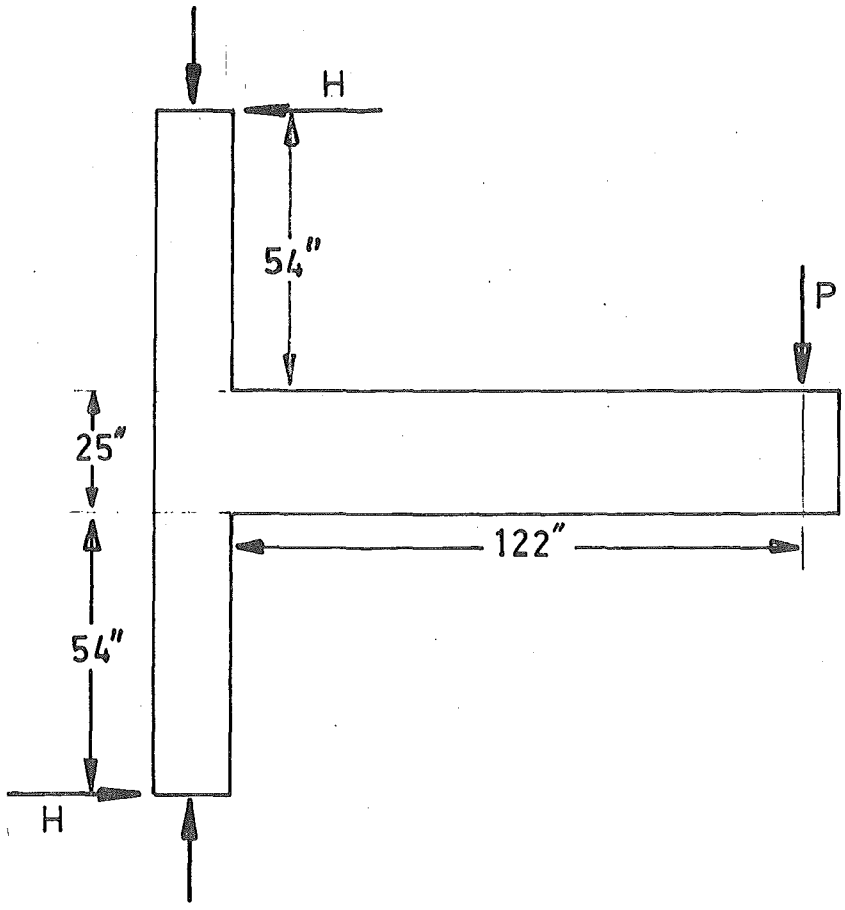

FIG. 8.4 DIMENSIONS OF SPECIMEN

The original analysis, based on centre-line dimensions indicated that the beam was 20% stronger than the column. However, if the analysis was done accounting for the actual size of members this was not the case. Fig. 8.4 shows the load situation. At theoretical ultimate of the column

$$M_{uc} = 1875 \text{ kip-in.}$$

$$M_b = 122\ P = 122 \times \frac{1875}{54} \quad \text{Since } P = H.$$

$$= 4230 \text{ kip-in.}$$

$$\frac{M_{ub}}{M_b} = \frac{4500}{4230} = 1.07$$

Due to this oversight the beam would actually be on the point of yielding which was not anticipated. However it did not affect the outcome of the results significantly since the theoretical ultimate load was not attained during testing.

8.3 RECOMMENDATIONS:

These recommendations apply only to isolated joints, since if beams frame in on any of the other three sides of the joint they would act as efficient confinement for the column core, and also keep the joint intact, providing more favourable bond and shear conditions. Special provisions also apply because of the cyclic load imposed. It was apparent during testing that many of the regions, which would have adequately withstood a direct load application, gradually deteriorated under the reversed loading, thereby reducing the load capacity. When designing for ductility it is obvious that code requirements must be adhered to, with particular emphasis being placed on the strength of the joint.

The anchorage lengths, particularly for the beam flexural bars, must at least comply with the requirements of ACI 318 - 71. The theory which was the basis of the continuous arrangement in UNITS 1, 2, and 3 is therefore

not applicable. In fact an anchorage length of 50 in. is required (see Appendix B), which would mean carrying the beam flexural bars through the joint, necessitating a stub at the back of the column. The separate anchorages appeared to give sufficient development length in UNIT 4. An increase in anchorage length would ensure the maximum load capacity was retained over a greater number of load cycles. Construction techniques require a construction joint in the column just below the level of the beam, and therefore, for ease of construction, the anchorage length of the top beam flexural bars should not protrude below this level. This is the reason for the popularity of the continuous arrangement. If necessary the size of the bars can be reduced and the number of bars increased in order to reduce the required development length.

The design of the joint reinforcement is a critical factor in determining the strength of the joint. From the results obtained the diagonal tension cracks run between opposite corners of the joint. Therefore, all the joint ties cross the major crack, although on each load run not all the ties work efficiently. It can be assumed that a certain percentage of the ties work to their full capacity on each load run, neglecting the remaining ties. For example, if 75% of the ties are effective, then for the joint design:

$$V_s = 0.75\ m\ 2a_v\ f_y$$

$V_c = 0$ $\qquad 171.3 = 0.75\ m\ 2 \times 0.31 \times 45$

number of ties, $m = 8.2$

Nine joint ties would be required. For this type of mechanism the shear resistance of the concrete should be neglected.

Tests could be carried out on joints of both narrow and wide columns to investigate the theory of corner-to-corner cracking and also to determine to what extent the configuration of the anchorage detail in the joint

affects the bond strength of the beam flexural bars.

In order to improve the confinement within the joint of these specimens, the reduction in the unrestrained length of the legs of the ties could only be achieved by cross-ties, laterally restraining the legs of each tie. The effect of reducing the unrestrained length needs to be investigated in greater detail. However it is obvious from the bowing of the ties in these tests that there should be an upper limit on the value of h'. This is particularly so when large shear forces are imposed, since it is apparent that once the steel has yielded its effectiveness as confining reinforcement is significantly reduced.

APPENDIX A.

A.1 MATERIALS.

The ready mixed concrete was brought to the laboratory by agitator truck from the plant. Concrete with a cement content of 390 lb/yd^3 and water: cement ratio of 0.701 was specified. This gave a certified crushing strength of 2,500 psi at 28 days and a 3 in. slump. Actual concrete crushing strengths at the time of testing were found from compression tests on standard cylinders, 12 in. high by 6in. diameter. Tests were also performed on 3" x 3" x 12" prisms to determine the tensile strength of the concrete. The average of four compressive tests and three tensile tests for each specimen are given in Table A.1.

TABLE A.1. Material Properties.

UNIT	Concrete		#10 beam flexural steel		#9 column flexural steel		∅5 joint ties		∅3 beam stirrups		column ties *	
	f'_c (psi)	f_t (psi)	f_y (ksi)	f_u (ksi)	f_y (ksi)	f_u (ksi)	f_y (ksi)	f_u (ksi)	f_y (ksi)	f_u (ksi)	f_y (ksi)	f_u (ksi)
1	3730	610	43.1	66.8	44.7	68.7	45.1	72.8	43.6	69.6	48.6	75.3
2	5570	770	42.2	66.6	45.3	69.6	46.7	72.6	44.1	69.9	48.2	73.2
3	3440	550	41.9	66.6	45.2	69.0	45.4	72.3	43.3	68.9	46.4	71.6
4	4220	640	43.7	68.1	45.4	69.7	45.4	72.3	43.5	69.3	46.8	71.6

* ∅2 ties in UNITS 1 and 2; ∅3 ties in UNITS 3 and 4.

The mild steel reinforcing bars used throughout the testing had a guaranteed minimum yield strength of 40,000 psi. Deformed bar was used as longitudinal steel and plain bars as transverse steel. The average yield and ultimate tensile strengths for all the bars are given in Table A.1.

A.2 FABRICATION OF SPECIMEN.

The reinforcing bars were cut to length and cold bent to form the components of the structure. Then the strain measuring devices, either demec studs or electric resistance strain gauges, were placed in position

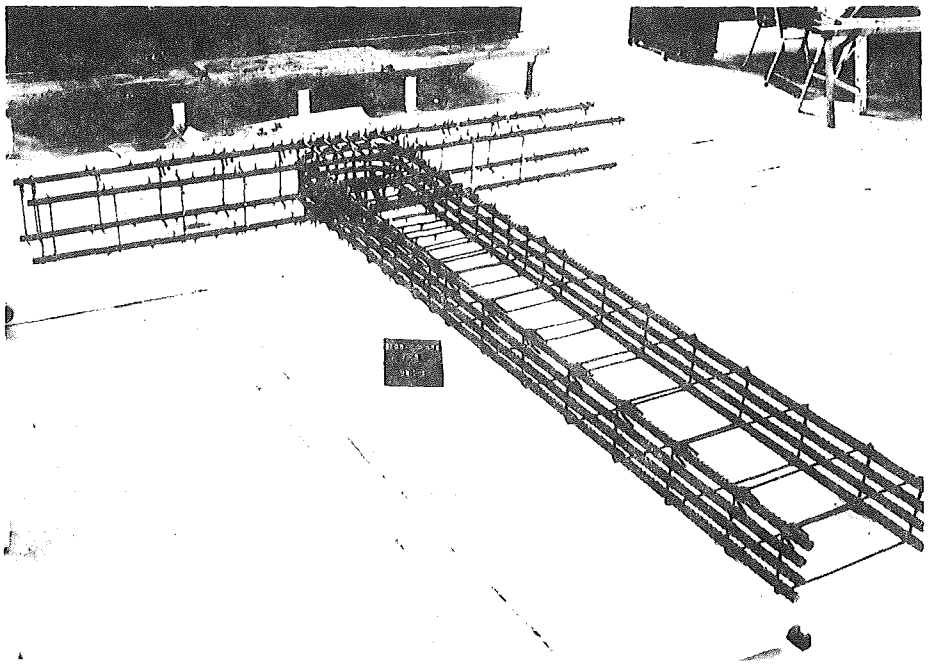

FIG. A.1
REINFORCING CAGE OF UNIT 1

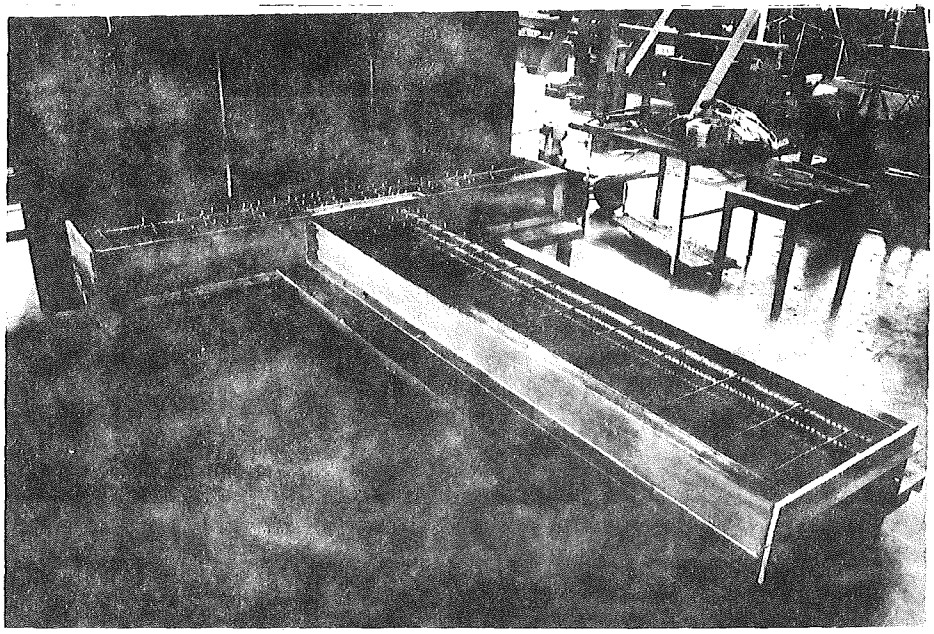

FIG. A.2
REINFORCING CAGE POSITIONED IN MOULD

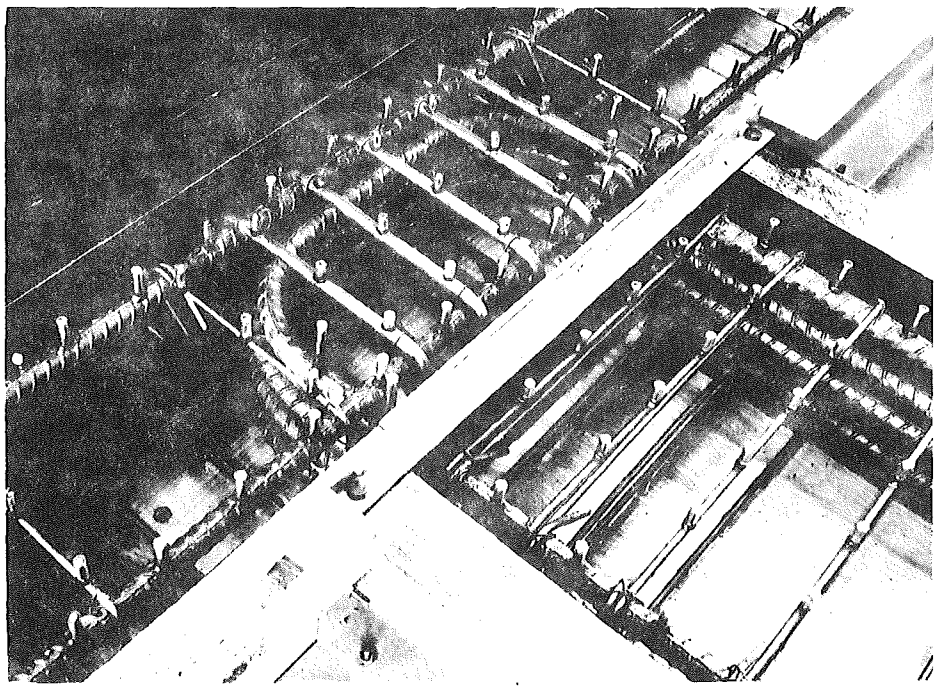

FIG. A.3
JOINT OF UNIT 1 SHOWING DEMEC STUDS

before the reinforcing cage was put together. The transverse and longitudinal bars were tied together with tie-wire to form the reinforcing cage, as shown in Fig. A.1, except at the extremities of the beam and column where the bars were tack welded in order to position them accurately. Then the cage was lowered into position in the beam-column mould, as shown in Figs. A.2 and A.3.

The mould itself, shown in Fig. A.2, consisted of coreboard sheets bolted to a steel framework. This rested on adjustable legs which could be raised or lowered to minimise deflection of the base. The sides of the mould were steel channel sections which ensured the dimensional accuracy of the members. These were bolted to the base of the mould and could be easily removed when stripping the specimen.

When the concrete arrived it was placed evenly over the reinforcing and vibrated with a spud vibrator. The concrete was then covered and moist cured for seven days before the mould was stripped and the specimen prepared for testing.

A.3 TEST RIG.

The test rig had been designed and used for testing prestressed concrete frames[12] and minor modifications to the capacity and the beam loading apparatus enabled it to be suitable for testing these reinforced concrete beam-column joints. The test rig and specimen are shown in Fig. A.4. The loading head above the hydraulic ram at the top of the column transfers the load to the laboratory floor by means of an A-frame arrangement in the plane perpendicular to the diagram. The rollers at the top and bottom of the column enable the column to rotate as hinged supports. The available deflections were 16" in the upward direction and 10" in the downward direction for UNITS 1 and 2. The "step" at the end of the beam in UNITS 3 and 4 shown in Figs. 6.1 and 7.1 enable the available downward deflection to be increased also to 16".

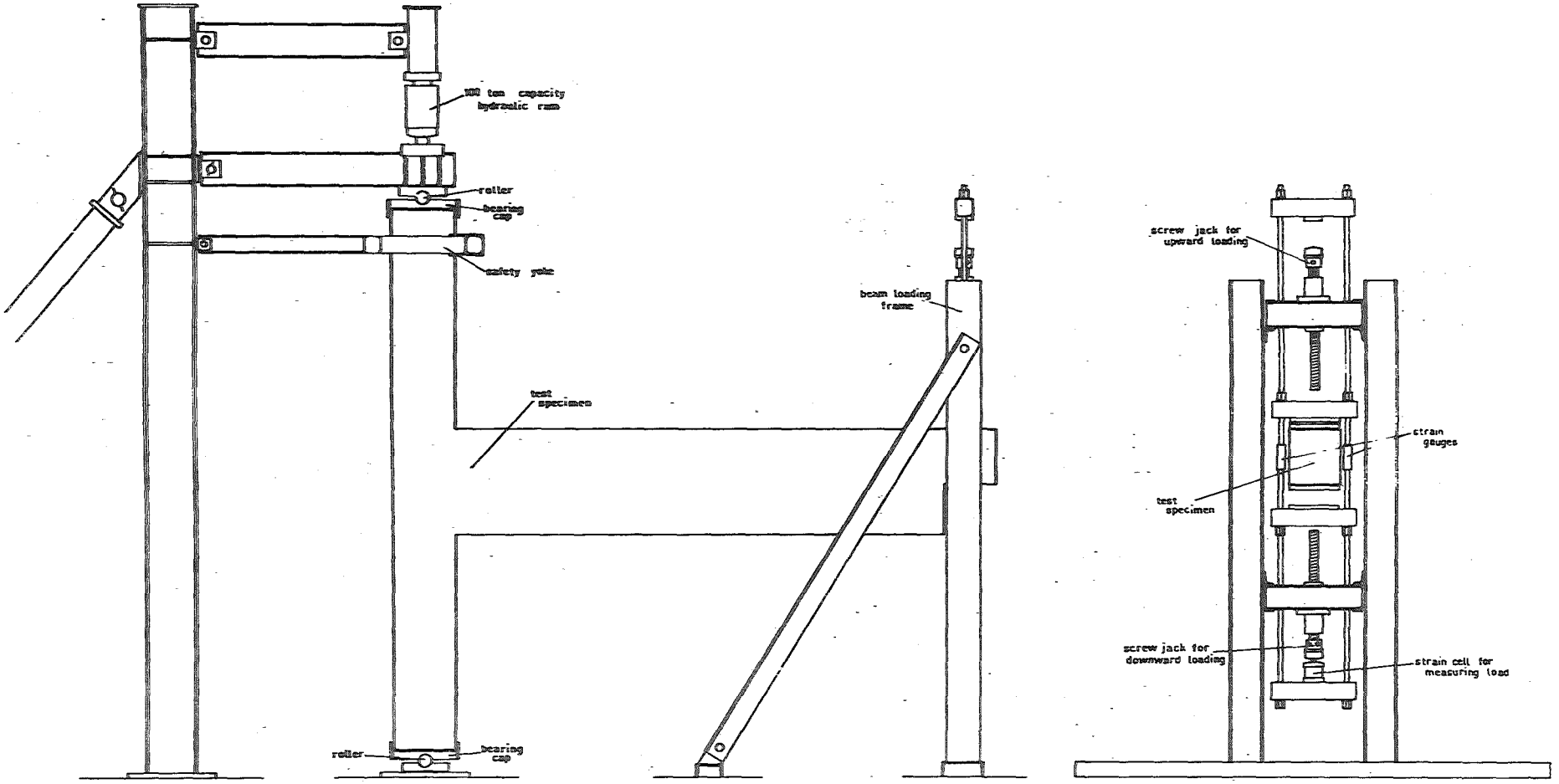

FIG. A.4 (a) TEST RIG AND SPECIMEN

(b) BEAM LOADING FRAME

A.4 APPLICATION OF LOAD.

The column load was applied by means of a 100 ton capacity hydraulic ram at the top of the column, readily adjustable by a hand pump. The minimum column load of 148 kips remained constant on downward load runs, however the load at the top of the column varied on upward load runs. Occasional adjustment of the load was necessary at times to allow for movement of the column.

The end beam load was applied by means of screw jacks as shown in Fig. A.4. The screw jacks allow for application of measured displacements which is desirable when loading into the post-elastic range. The position of the apparatus in Fig. A.4 is as it would be for a downward load run. On reversal of load the load cell is transferred to the upper screw jack and the load applied.

A.5 INSTRUMENTATION.

A.5.1 Load Measurement.

The hydraulic ram at the top of the column was connected in parallel with another 100 ton capacity hydraulic ram and 100 ton load cell which were braced against the loading head of a test machine. Since the hydraulic pressure in both hoses was the same, the load cell gave a measure of the load being applied at the top of the column.

The 20 ton load cell shown in Fig. A.4 was used to measure the load on the end of the beam.

Both of these load cells were calibrated on an Avery 250,000 lb Universal Testing Machine with a Budd Strain Bridge.

The electric resistance strain gauges on the 1 in. diameter high strength tension rods, shown in Fig. A.4 (b) gave an alternative measure-

ment of the beam load. Two active and two compensating gauges on each bar ensured that the results were accurate even if bending of the bars occurred.

These strain gauges were calibrated against the 20 ton load cell and recorded directly by the movement of the pens on the Y - axes of two X - Y plotters connected in series (see section A.5.2).

A.5.2 Rotations.

Frames were connected to the column above and below the joint at distances of $7\frac{1}{2}$ in. and 15 in. from the beam, as shown in Fig. A.5. Dial gauges were attached to the frames to record the column rotation over the 15 in. immediately adjacent to the joint. However the majority of the rotation occurred between the beam face and the first gauge frame, a distance of $7\frac{1}{2}$ in. This region, which represents a distance of t/2, generally provided greater than 80% of the total column rotation. Fig. A.6 shows the 1 in. capacity, 0.001 in. Mercer dial gauges attached to the frames above the joint at the back of the column.

Linear variable displacement transducers were also connected between the first frame and the beam as shown in Fig. A.6. These gave a measure of the column rotation as a movement of the pens on the X - axes of the X - Y plotters. One X - Y plotter recorded the column rotation above the joint, and the other recorded the column rotation below the joint. When combined with the load measurement as described in section A.5.1, the X - Y plotters gave a direct plot of the load-rotation relationships for each region during the test. The linear variable displacement transducers were calibrated against a micrometer which could be read directly to 0.001 in.

A.5.3 Deflections.

Dial gauges were positioned on the specimen to record the deflect-

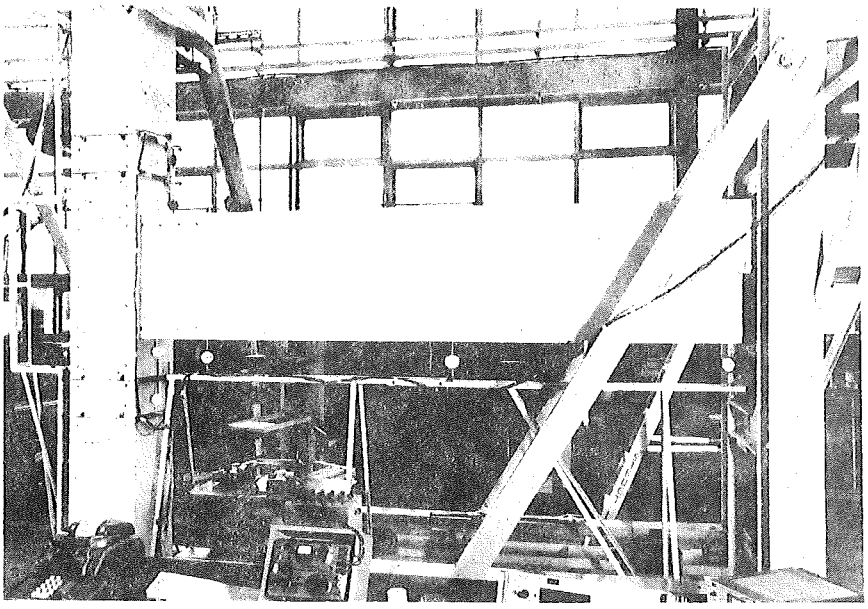

FIG. A.5 SPECIMEN PREPARED FOR TESTING

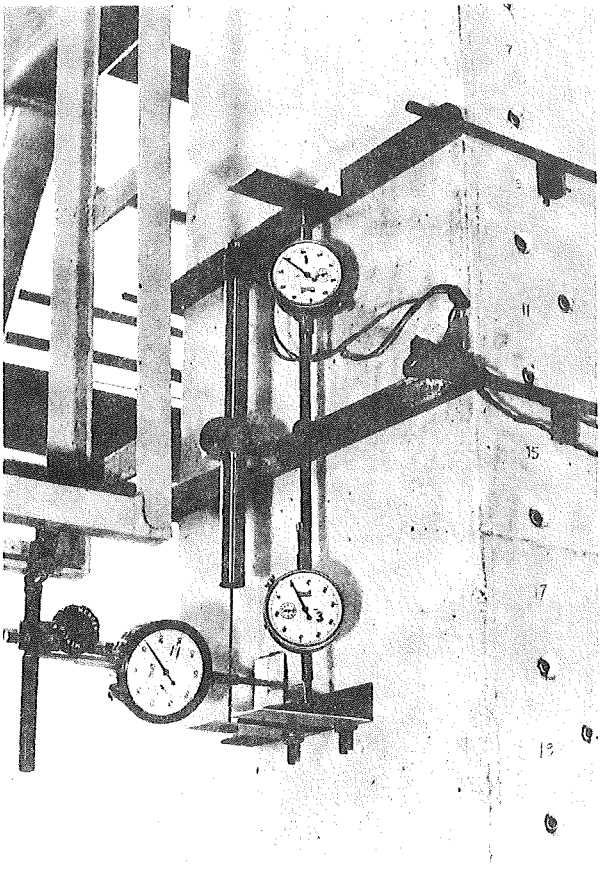

FIG. A.6 ROTATION AND DEFLECTION RECORDING APPARATUS

ions of the beam and column so that deflected shapes could be obtained. These were 2 in. capacity 0.001 in. Mercer dial gauges, one of which can be seen in Fig. A.6 recording the column deflection.

For deflections at the end of the beam a graduated scale was attached to the beam loading frame and a pointer on the beam gave deflection readings, once the dial gauge had exceeded the limit of its travel.

To record the movement of the test rig a steel rule was attached to the horizontal reaction frame at the top of the column which was read through a fixed theodolite. Adjustments were made to the deflection readings to compensate for this movement.

A.5.4 Strain Measurements.

A.5.4.1 DEMEC Gauges.

These were used to record the strain readings on all the reinforcing steel for UNITS 1 and 2. The advantage of this method is that the readings give a continuous distribution of strain along the reinforcing bar. Each reading, on the side of the specimen was duplicated with a reading on the opposite side. The mean of these readings was plotted in the strain distribution diagrams provided each reading did not vary by more than 10% from the mean. The demec studs on which the readings are taken can be seen clearly in Fig. A.3. The most apparent inaccuracy in these readings occurs when the reinforcing bar is bent, rather than being subjected to a direct tensile, or compressive strain. This was the case with the joint ties in these specimens when they bowed outwards due to the bursting pressure from the column core. From the recorded strain readings it is apparent that the ties bowed as shown in Fig. A.7, due to the configuration of the cracks. To determine the effect that bowing of the ties has on the strain readings,

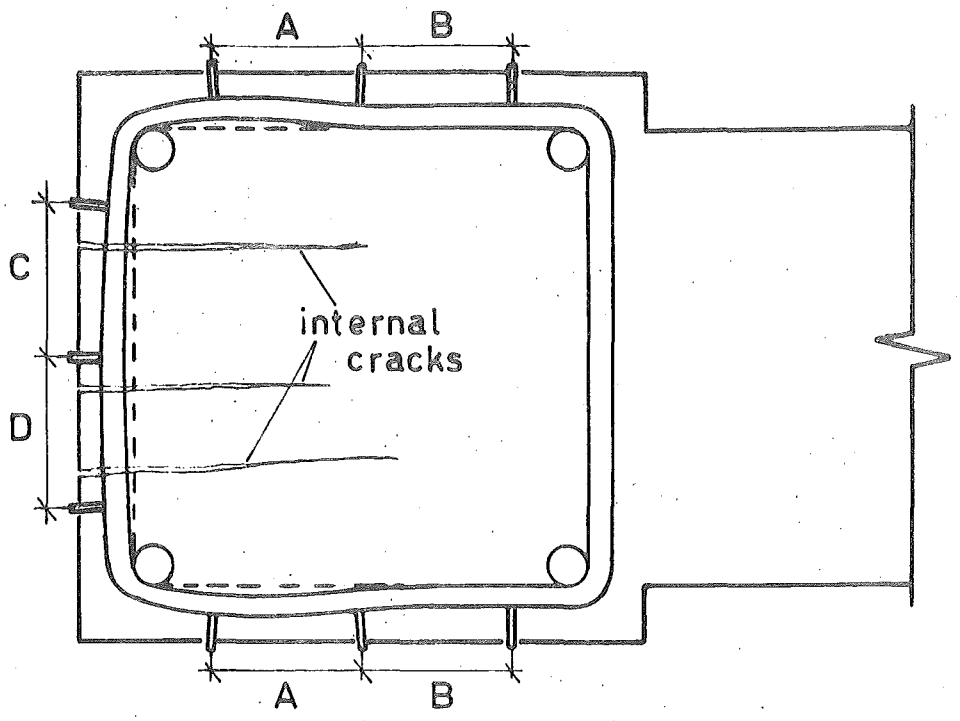

FIG. A.7 BOWING OF JOINT TIES DUE TO BURSTING PRESSURE OF COLUMN CORE

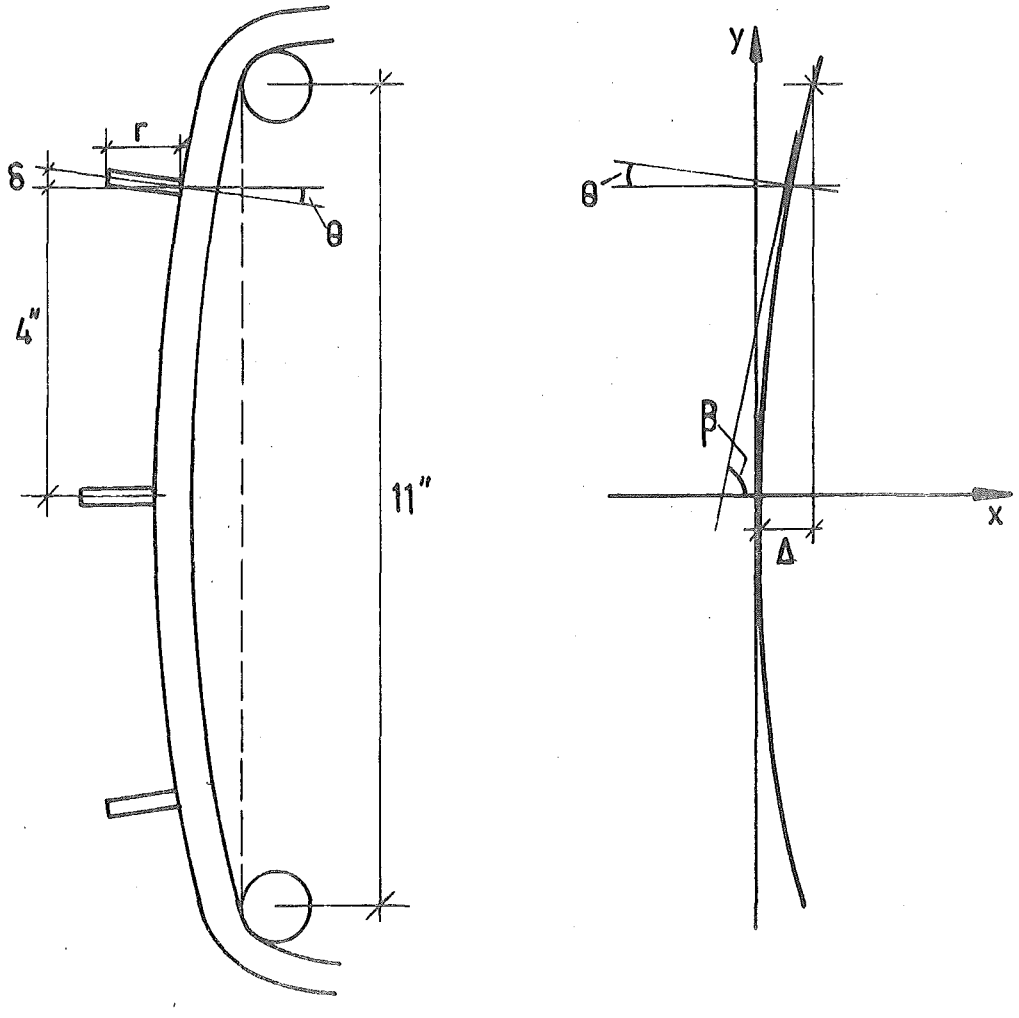

FIG. A.8 SHAPE OF BACK OF TIE DUE TO INTERNAL PRESSURE

assume as in Figs. A.8 (a) and (b) that the curve at the back of the column resembles a parabola.

Then

$$\delta = r\theta$$

where $r = \frac{1}{2}$ in. for $\frac{5}{8}$ in. diameter joint ties

$$\text{but } \delta = 4e^* \times 10^{-6} \text{ in.}$$

where e* is the difference between the DEMEC reading and the actual strain, in microstrains.

$$\theta = 8e^* \times 10^{-6} \text{ rads.} \qquad \text{(A.1).}$$

from Fig. A.8 (b)

$$y^2 = 4gx$$

$$(5.5)^2 = 4g\Delta$$

$$g = \frac{7.56}{\Delta}$$

at y = 4: $x = \frac{4}{g} = \frac{4\Delta}{7.56}$

$$\cot\theta = \tan\beta = \frac{4}{8\Delta} \times 7.56$$

$$\cot\theta = \frac{7.56}{2\Delta} \qquad \text{(A.2).}$$

A relationship can be established between equations (A.1) and (A.2) to determine the difference in strain readings.

For example, when $\Delta = 0.01$ in.

from Eqn. A.2 $\cot\theta = 378.$

i.e. $\theta = 0^\circ\ 9'$

$= 2.62 \times 10^{-3}$ rads.

from Eqn. A.1 $e^* = 330$ microstrains.

For low values of θ, this will be a linear relationship. From this it can be seen that the tie only has to bow outwards a very small amount to produce a substantial inaccuracy in the strain readings from the DEMEC gauge.

The column bars are also prone to local bending, producing the same

inaccuracies, when they are not adequately confined. This effect can be seen on the strain distribution diagrams in the region where the beam tensile bars enter the column.

To check on the theory of the joint ties bowing and giving false DEMEC strain readings, electric resistance strain gauges were placed between the demec studs on the joint ties of UNIT 3.

A.5.4.2 Electric Resistance Strain Gauges.

The gauges used were KYOWA type KF - 10 - C8 - 11 of length 10 mm. and 120 ohm resistance. These were attached to the reinforcing bars with Eastman 910 adhesive which, in preliminary calibration tests, gave satisfactory results right up to fracture of the test bar. The gauges used on the test specimens were waterproofed with sealing wax and waterproof Denso Tape. However this was inadequate, and in some cases was found to contribute to failure of the gauges. Fig. A.9 shows the electric resistance strain gauges positioned on the joint ties, covered with the waterproof tape.

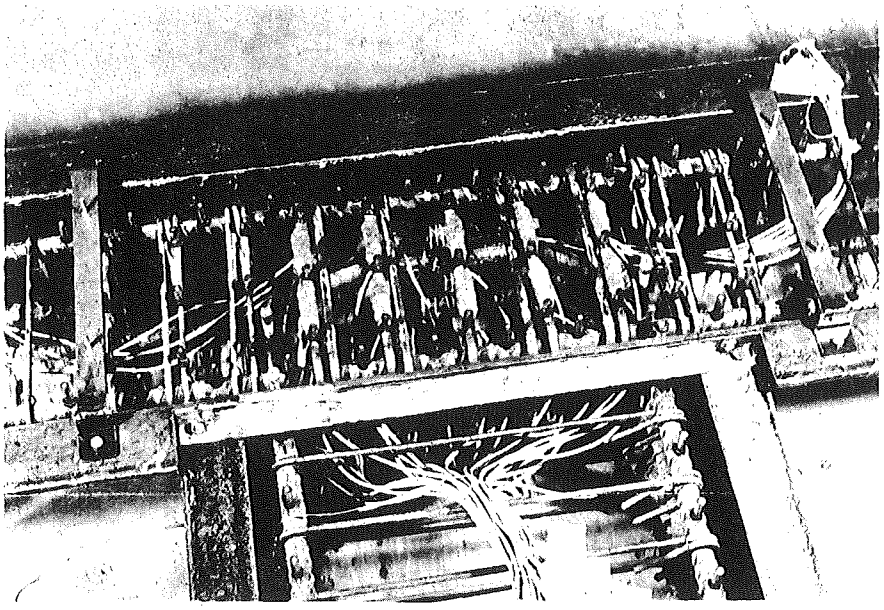

FIG. A.9 JOINT OF REINFORCING CAGE OF UNIT 3 POSITIONED IN MOULD

The strain gauge readings are shown for UNITS 3 and 4 in Chapters 6 and 7 and the distribution of strain in the joint ties verifies that the bowing of these ties affects the DEMEC readings to a marked degree. This means that the DEMEC readings on the joint ties of UNIT 1 and 2 are not representative of the tensile strain in the steel. However they give an indication of the bowing of the ties, and have been shown as dashed lines on the strain distribution diagrams.

APPENDIX B.

B.1 DESIGN CALCULATIONS.

B.1.1 Column Reinforcement:

$$A_{st} = 4 \text{ in}^2$$

$$bd = 15 \times 12.94 \text{ in}^2$$

$$p_t = \frac{A_{st}}{bd}$$

$$= \frac{4}{15 \times 12.94}$$

$$= 0.0206$$

B.1.2 Balanced Load of Column:

$$e_y = \frac{45000}{29 \times 10^6} = 0.00155$$

$$\frac{c_b}{d} = \frac{0.003}{0.003 + e_y}$$

$$c_b = \frac{0.003 \times 12.94}{0.00455}$$

$$= 8.55 \text{ in.}$$

$$a_b = 0.85 \times 8.55 = 7.26 \text{ in.}$$

$$(e'_s = 0.003 \times \frac{c_b - 2.1}{c_b} = 0.0023, \text{ compression steel is also yielding}).$$

$$N_b = 0.85 f'_c a_b b$$

$$= 0.85 \times 4000 \times 7.26 \times 15$$

$$= 370{,}000 \text{ lbs.}$$

B.1.3 Ultimate Moment Capacity of the Column.

at ultimate $a = \frac{N}{0.85 f'_c b}$

$$= \frac{148}{0.85 \times 4000 \times 15}$$

$$= 2.90 \text{ in.}$$

$$M_{uc} = 0.85 f'_c ab \left(\frac{t}{2} - \frac{a}{2}\right) + A_s f_y \left(d - \frac{t}{2}\right) + A'_s f_y \left(\frac{t}{2} - d'\right)$$

$$= 0.85 \times 4 \times 2.9 \times 15 \ (7.5 - 1.45) + 2 \times 90 \times 5.44$$

$$= 895 + 980$$

$$= 1875 \text{ kip-in.}$$

B.1.4 Beam Reinforcement:

$$A_s = A'_s = 4 \times 1.23 = 4.92 \text{ in}^2.$$

$$bd = 12 \times 22.9$$

$$p = p' = \frac{4.92}{12 \times 22.9}$$

$$= 0.018$$

B.1.5 Anchorage Requirements from A.C.I. 318 - 71.

$$L_d = 0.04 a_s \frac{f_y}{f'_c}$$

$$= 0.04 \times \frac{25}{64} \times \frac{45,000}{4000}$$

$$= 34.9 \text{ in.}$$

$(0.004 \ Df_y = 0.004 \times 1.25 \times 45,000 = 22 \text{ in}).$

from 12.5.1 (d)

reduction factor of $\frac{1.1 \ M_{uc}}{1.2 \ M_{uc}}$ is applied since $M_{uo} = 1.2 \ M_u$

$$L_d = 34.9 \times \frac{1.1}{1.2}$$

$$= 32.0 \text{ in.}$$

from 12.8 using a standard hook

$$90^\circ \text{ bend} + 12 \ D = 15".$$

$$f_h = 360 \sqrt{4000} = 22,800$$

increase of 30% is allowed for confinement

$$f_h = 22,800 \times 1.3$$

$$= 29,600 \text{ psi.}$$

$$L_e = 0.04 \times \frac{25}{64} \times \frac{29600}{4000}$$

$$= 23 \text{ in.}$$

Therefore 9 in. must be provided apart from the standard hook, measured from the column face.

B.1.6 Analysis of U-type Anchorage Detail.

Since the beam was expected to remain in the elastic range, when one set of bars is at maximum stress in tension the stress in the opposing bars can be found from equilibrium and strain compatibility.

$$k = \sqrt{n^2 (p' + p)^2 + 2n \left(p' \frac{d'}{d} + p\right)} - n (p' + p).$$

$$p = p' = 0.018$$

$$\frac{d'}{d} = \frac{2.1}{22.9} = 0.092$$

$$k = 0.628 - 0.286$$

$$= 0.342$$

$$kd = 7.8 \text{ in.}$$

$$f'_s = f_s \frac{kd - 2.1}{22.9 - kd}$$

$$= \frac{5.7}{15.1} f_s$$

$$= 0.378 f_s$$

From code requirements, the anchorage length of bars in compression is obtained from 12.6.1, ACI 318 - 71, where

$$L_d = \frac{0.02 f_y D}{\sqrt{f'_c}}$$

$$= \frac{0.02 \times 45000 \times 1.25}{\sqrt{4000}}$$

$$= 17.8 \text{ in.}$$

Total length of anchorage for the bars would be

$$L_d = 32 + 18.$$

$$= 50 \text{ in.}$$

However, this is assuming that the bars are stressed to their yield stress. When the bars are kept at a lower stress then, theoretically, they require less anchorage length. The anchorage length required in compression would be

$$L_d = 0.378 \times 17.8$$

$$= 6.7 \text{ in.}$$

Total length of anchorage required would then be

$$L_d = 32 + 7$$

$$= 39 \text{ in.}$$

The U-type of anchorage detail in this beam provides 40 in. of anchorage between column faces.

$$\text{bond strength } u = \frac{(f_s + f'_s)\, 4\pi D^2}{4\pi D \times L \times 4}$$

$$= \frac{(f_s + f'_s)\, D}{4L}$$

$$= \frac{1.378\, f_s\, D}{4L}$$

To determine the steel stress in the bars, f_s, at maximum load:

$$M_b = A_s f_s \left(d - \frac{kd}{3}\right) - A'_s f'_s \left(d' - \frac{kd}{3}\right)$$

$$= 4.92\, f_s\, (20.3) - 4.92 \times 0.378\, f_s\, (0.5).$$

$$= 101\, f_s$$

$$M_{bmax.} = 4230 \text{ kip-in (section 8.2).}$$

$$f_s = \frac{M_b}{101}$$

$$= 41{,}800 \text{ psi}$$

B.1.7 Joint Hoops for Confinement from A.C.I. 318 - 71.

from A.6.4.3 $A_{sh} = \frac{h' p'_s s}{2}$

where from 10.9.2: $p'_s = 0.45 (A_g/A_c - 1) \frac{f'_c}{f_y}$

using $\frac{5}{8}$ in. diameter hoops:

$$p'_s = 0.45 (0.28) \frac{4000}{45000}$$

$$= 0.126 \frac{f'_c}{f_y} > 0.12 \, f'_c/f_y$$

$$= 0.0112$$

$$s = \frac{2 A_{sh}}{h' p'_s}$$

$$= \frac{0.612}{12.625 \times 0.0112}$$

$$= 4.3 \text{ in.}$$

but the maximum allowable spacing is 4 in.

Therefore five hoops are required in the space of the joint.

B.1.8. Joint Ties for Shear:

maximum force expected for the design specimen.

$$T = 41.8 \times 4.92$$

$$= 206 \text{ kips.}$$

column shear = $H = \frac{1875}{54}$

$$= 34.7 \text{ kips.}$$

joint shear force $V_j = T - H.$

$$= 171.3 \text{ kips.}$$

from 11.4.3, ACI 318 - 71:

The method used for UNITS 1 and 2 was:-

$$V_c = v_c bd = 3.5 \, bd \sqrt{f'_c \, (1 + 0.002 \, N/A_g}$$

$$= 3.5 \times 15 \times 12.94 \sqrt{4000 \, (1 + 0.002 \times \frac{14[illegible]}{[illegible]})}$$

$$= 65.3 \text{ kips.}$$

$$V_s = V_j - V_c$$

$$= 171.3 - 65.3$$

$$= 106 \text{ kips.}$$

$$\text{from } a_v = \frac{V_s s}{2 f_y d}$$

$$ma_v = \frac{106 \times 20.8}{2 \times 45 \times 12.94}$$

for $\frac{5}{8}$ in. diameter ties:

$$a_v = 0.307 \text{ in}^2.$$

number of ties, $$m = \frac{106 \times 20.8}{2 \times 45 \times 12.94 \times 0.307}$$

$$= 6.1$$

Five joint ties were used in UNIT 1, and seven in UNIT 2.

The more conservative method from ACI 318 - 71, 11.4.3, gives

$$V_c = v_c bd = bd \left(1.9 \sqrt{f'_c} + 2500 p \frac{V_u d}{M'}\right)$$

$$M' = M_u - N_u \left(\frac{4t - d}{8}\right)$$

$$= 1875 - 148 \left(\frac{60 - 12.94}{8}\right)$$

$$= 1005 \text{ kip-in.}$$

$$V_c = 15 \times 12.94 \left(1.9 \sqrt{4000} + 2500 \times 0.0206 \times \frac{2220}{1005}\right)$$

$$= 44.3 \text{ kips.}$$

$$V_s = 171.3 - 44.3$$

$$= 127 \text{ kips.}$$

number of ties, $$m = \frac{127 \times 20.8}{2 \times 45 \times 12.94 \times 0.307}$$

$$= 7.4$$

Therefore the nine joint ties, used in both UNITS 3 and 4, more than satisifed code requirements.

In order to compare the use of the different methods shown in Table 8.4, actual material properties for each specimen were inserted in the above equations.

8.1.9 Column Ties for Shear.

$$V_c = 44.3 \text{ kips.}$$

$$V_u = \text{II} = 34.7 \text{ kips.}$$

nominal $\frac{1}{4}$ in. diameter ties only are required at the least spacing of:

$$16\ D = 16 \times 1\tfrac{1}{8} = 18 \text{ in.}$$

$$48\ D = 48 \times \tfrac{1}{4} = 12 \text{ in.}$$

$$\text{or } 15 \text{ in.}$$

Therefore column ties were $\frac{1}{4}$" diameter at 12 in. spacing, in UNITS 1 and 2.

B.1.10 Confinement of the Column:

using $\frac{3}{8}$ in. diameter ties:

$$A_c = 12.75" \times 12.75" = 162.5 \text{ in}^2.$$

$$p'_s = 0.45\ (0.385) \times \frac{4000}{45000}$$

$$= 0.0153$$

$$s = \frac{2 \times 0.11}{0.0153 \times 12.375}$$

$$= 1.2 \text{ in.}$$

Because of the unlikelihood of a failure outside the joint region the $\frac{3}{8}$ in. diameter ties were at 2 in. spacing, in the region immediately adjacent to the joint.

B.1.11 Shear in the Beam:

$$P_{max.} = 34.7 \text{ kips.}$$

$$V_c = v_c bd = 2\sqrt{f'_c}\ bd$$

$$= 2\sqrt{4000} \times 12 \times 22.9$$

$$= 35 \text{ kips.}$$

nominal stirrups only required in the beam.

B.2 THEORETICAL PREDICTIONS.

B.2.1 Cracking.

B.2.1.1 Beam:

When the beam is on the point of cracking.

$$f_c = f_t$$

from equilibrium and similar triangles

$$kd = 12.5 \text{ in.}$$

$$M = \tfrac{1}{2} f_c bkd \left(\tfrac{2}{3} \times 25\right) + f_s A_s (20.8).$$

$$f_s = f'_s = nf_t \times \frac{kd - 2.1}{kd}$$

$$= 0.83\, nf_t$$

$$M = \tfrac{1}{2} f_t \times 12 \times 12.5 \times \frac{50}{3} + 4.92 \times 20.8 \times 0.83\, nf_t$$

$$= (1250 + 85\, n)\, f_t$$

The loads at which cracking is predicted to occur in the beam are given in Table B.1.

TABLE B.1. Beam Cracking Loads.

UNIT	f'_c (psi)	n	f_t (psi)	$M_{cr.}$ (kip-in)	P_{cr} (kips)
1	3730	8.3	610	1190	9.8
2	5570	6.8	770	1410	11.6
3	3440	8.7	550	1090	8.9
4	4220	7.8	640	1220	10.0

Where

$$n = \frac{29 \times 10^6}{w^{1.5}\, 33\sqrt{f'_c}}$$

B.2.1.2 Column.

$$f = \frac{N}{A_n} + \frac{M\bar{y}}{I_c}$$

$$A_n = A_g + (n - 1)\, A_{st}$$

$$= 225 + 4\,(n - 1)$$

$$\bar{y} = 7.5 \text{ in.}$$

$$I_c = \frac{bt^3}{12} + A_{st}(n-1)\left(\frac{t}{2} - d'\right)^2$$

$$= \frac{15 \times (15)^3}{12} + 4(n-1)(5.44)^2$$

$$= 4220 + 118(n-1)$$

When the concrete is at its ultimate tensile strength in the tension fibre:

$$f_t = \frac{N}{A_n} \pm \frac{M_{cr}.\bar{y}}{I_c}$$

Table B.2 gives the predicted cracking loads for the column.

TABLE B.2 Column Cracking Loads.

UNIT	n-1	$\frac{N}{A_n}$ (psi)	f_t (psi)	I_c (in^4)	$M_{cr.}$ (kip-in)	$P_{cr.}$ (kips)
1	7.3	583	610	5081	809	15.0
2	5.8	597	770	4905	895	16.6
3	7.7	578	550	5129	771	14.3
4	6.8	587	640	5023	823	15.2

B.2.2 Yield Load:

At first yield of the column flexural steel:

$$f'_s = \frac{c - d'}{d - c} f_y$$

$$= \frac{a - 0.85d'}{0.85d - a} f_y$$

$$= \frac{a - 1.75}{11.0 - a} \times 45$$

and $N = 0.85 f'_c ab + A'_s f'_s - A_s f_y$

$$148 = 0.85 f'_c \times 15a + 2 \times \frac{a - 1.75}{11.0 - a} \times 45 - 2 \times 45$$

$$= 12.75 f'_c a + 90\left(\frac{2a - 12.75}{11.0 - a}\right)$$

$$a^2 - \left(\frac{25.7}{f'_c} + 11.0\right) a + \frac{217.5}{f'_c} = 0 \qquad \text{(B.1)}$$

from this equation and

$$M = 0.85\, f'_c ab \left(\frac{t}{2} - \frac{a}{2}\right) + A'_s f'_s \left(\frac{t}{2} - d'\right) + A_s f_y \left(d - \frac{t}{2}\right)$$

$$= 12.75\, f'_c a \left(7.5 - \frac{a}{2}\right) + 10.9 \left(f'_s + f_y\right)$$

the moment and therefore the load, at which first yield of the column flexural steel should theoretically occur, can be determined. These are given in Table B.3 for each specimen.

TABLE B.3 Theoretical Yield Loads.

UNIT	f'_c (ksi)	a (in)	f'_s (ksi)	M kip-in
1	3.73	4.28	16.9	1766
2	5.57	3.14	8.0	1900
3	3.44	4.55	19.5	1745
4	4.22	3.92	13.8	1808

B.2.3 Rotations.

The rotation of the column can be found by the moment-area method.

$$\phi = \frac{M}{E_c I_c} \times \frac{54}{2} \times \frac{54 \times 2}{3} \times \frac{1}{54}$$

and $M = 54\, P$

$$\phi = \frac{972P}{E_c I_c}$$

where $E_c = w^{1.5}\, 33 \sqrt{f'_c}$

TABLE B.4 Load-Rotation Relationships for the Column.

UNIT	E_c (psi x 10^{-6})	Uncracked Section		Cracked Section	
		I_c (in^4)	ϕ (rads x 10^8)	I_c (in^4)	ϕ (rads x 10^8)
1	3.48	5081	5.49 P	2966	9.42 P
2	4.25	4905	4.66 P	2806	8.15 P
3	3.34	5129	5.67 P	3020	9.64 P
4	3.70	5023	5.23 P	2909	9.04 P

The load rotation relationship is given in Table B.4 for the column in the uncracked and cracked conditions.

When the column is cracked, the extent of cracking depends on the magnitude of P. However this was found to have a negligible effect on the value of I_c, for the range considered.

$$I_c = \frac{b(kd)^3}{12} + bkd\left(\frac{t}{2} - \frac{kd}{2}\right)^2 + A_s (n-1)\left(d - \frac{t}{2}\right)^2 + A'_s (n-1)\left(\frac{t}{2} - d'\right)^2$$

$$= \frac{b(kd)^3}{12} + bkd\left(\frac{t}{2} - \frac{kd}{2}\right)^2 + A_{st} (n-1)(5.44)^2$$

$$= 1.25 (kd)^3 + 15\, kd\left(7.5 - \frac{kd}{2}\right)^2 + 118 (n-1)$$

The value of kd is found from the relationship derived in section B.2.7.

B.2.4 Deflections:

The deflections caused by column rotation and bending of the beam are derived and shown in Table B.5. The effect of joint distortion on the overall deflection for each specimen can be obtained from Table 8.3.

$$\Delta_{v1} = 129\, \phi$$

where ϕ is obtained in section B.2.3.

$$\Delta_{v2} = \frac{P (129)^3}{3 E_c I_b}$$

before cracking:

$$I_b = \frac{bt^3}{12} + A_s (n-1)\left(d - \frac{t}{2}\right)^2 + A'_s (n-1)\left(\frac{t}{2} - d'\right)^2$$

$$= \frac{bt^3}{12} + A_s (n-1)(10.4)^2$$

$$= 15625 + 1063 (n-1)$$

after cracking:

$$I_b = \frac{b(kd)^3}{12} + bkd\left(\frac{t}{2} - \frac{kd}{2}\right)^2 + 2 A_s (n-1)(10.4)^2$$

$$= (kd)^3 + 12\, kd\left(12.5 - \frac{kd}{2}\right)^2 + 1063 (n-1)$$

The derivation of kd for each specimen is given in section B.2.7.

TABLE B.5 Load-Deflection Relationships for the Beam.

UNIT	E_c (psi x 10^{-6})	Uncracked Section				Cracked Section			
		Δ_{v1} (in x 10^6)	I_b (in^4)	Δ_{v2} (in x 10^6)	$\Delta_v = \Delta_{v1} + \Delta_{v2}$	Δ_{v1} (in x 10^6)	I_b (in^4)	Δ_{v_2} (in x 10^6)	$\Delta_v = \Delta_{v1} + \Delta_{v2}$
1	3.48	7.08 P	23,390	8.81 P	15.9 P	12.15 P	15170	13.58 P	25.7 P
2	4.25	6.01 P	21,800	7.73 P	13.7 P	10.51 P	13480	12.51 P	23.0 P
3	3.34	7.32 P	23,800	9.02 P	16.3 P	12.44 P	15620	13.73 P	26.2 P
4	3.70	6.75 P	22,860	8.47 P	15.2 P	11.65 P	14590	13.28 P	24.9 P

B.2.5 Ultimate Moment of the Column.

From the formulae.

$$N = 0.85\, f'_c ab$$

$$\text{and } M_u = 0.85\, f'_c ab \left(\frac{t}{2} - \frac{a}{2}\right) + A_s f_y \left(d - \frac{t}{2}\right) + A'_s f_y \left(\frac{t}{2} - d'\right)$$

the theoretical ultimate loads are found and are given in Table B.6.

$$a = \frac{N}{0.85\, f'_c b}$$

$$= \frac{148}{0.85 \times f'_c \times 15}$$

$$= \frac{11.6}{f'_c}$$

$$M_{uc} = 0.85\, f'_c ab \left(\frac{t}{2} - \frac{a}{2}\right) + 2\, A_s f_y\, (5.44).$$

$$= 148\, (7.5 - \tfrac{a}{2}) + 10.88\, f_y$$

TABLE B.6 Theoretical Ultimate Moments for the Column.

UNIT	f'_c (ksi)	a (in)	f_y (ksi)	M_{uc} (kip-in)
1	3.73	3.11	44.7	1851
2	5.57	2.08	45.3	1940
3	3.44	3.36	45.2	1843
4	4.22	2.75	45.4	1892

B.2.6 Rotational Ductility:

This theory does not apply to these tests since no specimen actually attained its theoretical ultimate load. However the theoretical rotational ductility available in the design specimen is given by

ϕ_u/ϕ_y, where

$$\phi_u = \frac{e_{cu}}{c} \text{ at ultimate.}$$

$$\phi_y = \frac{e_c}{c} \text{ at first yield of the flexural steel.}$$

at first yield: as given by Equation B.1 in Section B.2.2.

$$a^2 - \left(\frac{25.7}{f'_c} + 11\right) a + \frac{217.5}{f'_c} = 0.$$

for the design specimen f'_c = 4 ksi.

$$a^2 - 17.42\, a + 5.44 = 0.$$

$$a = 4.06 \text{ in.}$$

$$c = 4.77 \text{ in.}$$

$$e_c = \frac{c}{d - c} \times \frac{f_y}{E_s}$$

$$\phi_y = \frac{f_y}{(d - c)\, E_s}$$

$$= \frac{45000}{8.17 \times 29 \times 10^6}$$

$$= 1.90 \times 10^{-4} \text{ rads.}$$

at ultimate: as given in section B.2.5.

$$a = \frac{11.6}{f'_c}$$

$$= 2.90 \text{ in.}$$

$$c = 3.41 \text{ in.}$$

$$\phi_u = \frac{0.01}{3.41}$$

$$= 2.93 \times 10^{-3} \text{ rads.}$$

$$\phi_u/\phi_y = \frac{2.93 \times 10^{-3}}{1.90 \times 10^{-4}}$$

$$= 15.4$$

B.2.7 Theoretical Steel Strains:

B.2.7.1 Beam Steel.

By assuming that the beam remains in the elastic range, the steel stress can be related directly to the applied moment as shown below.

The relationships are given in Table B.7.

$$k = \sqrt{n^2 (p' + p)^2 + 2n \left(p' \frac{d'}{d} + p\right)} - n (p' + p)$$

$$f'_s = f_s \frac{kd - 2.1}{22.9 - kd}$$

$$M = A_s f_s \left(d - \frac{kd}{3}\right) - A'_s f'_s \left(d' - \frac{kd}{3}\right)$$

TABLE B.7 Moment-Stress Relationships for Beam Steel.

UNIT	n	k	kd (in)	f'_s	M/f_s (in^3)
1	8.3	0.343	7.85	0.378 f_s	100.6
2	6.8	0.326	7.46	0.350 f_s	100.9
3	8.7	0.348	7.97	0.396 f_s	100.5
4	7.8	0.337	7.72	0.368 f_s	100.7

B.2.7.2 Column Steel.

In the column, the steel stresses must be computed individually for each value of applied moment. The steel strains are calculated for the peaks of load runs 1 and 3 for each specimen. Table B.8 tabulates the steel stress. The different values of column load refer to the fact that the load at the top and bottom of the column differs on any particular increment. The larger load has been approximated to 170 kips for convenience.

$$f'_s = n f_c \frac{kd - 2.1}{kd} \qquad \text{(B.2)}$$

$$f_s = n f_c \frac{12.9 - kd}{kd}$$

$$N = C + C_s - T$$

$$= \tfrac{1}{2} f_c bkd + A'_s f'_s$$

$$= 7.5 f_c kd + 2 (f'_s - f_s) \qquad \text{(B.3)}$$

$$M = C \left(\frac{t}{2} - \frac{kd}{3}\right) + 5.44 (C_s + T) \qquad \text{(B.4)}$$

from (B.4) $M = 7.5 f_c kd \left(7.5 - \frac{kd}{3}\right) + 5.44 \times 2 \times f_c \times \frac{10.8}{kd}$

$$f_c = \frac{M\ kd}{56.25(kd)^2 - 2.5\ (kd)^3 + 943}$$

the assumption that n = 8 has a negligible effect on the results and simplifies the calculations.

$$N = (7.5\ kd + 2n\ \frac{2kd - 15}{kd})\ f_c$$

$$= (7.5\ kd + 2n\ \frac{2kd - 15}{kd})\ \frac{M\ kd}{56.25\ (kd)^2 - 2.5\ (kd)^3 + 943}$$

when N = 148 kips.

$$(kd)^3 - (kd)^2\ (22.5 - 0.0203\ M) + 0.0865\ Mkd - 0.649\ M - 377 = 0.$$

when N = 170 kips:

$$(kd)^3 - (kd)^2\ (22.5 - 0.0176\ M) + 0.0754\ Mkd - 0.565\ M - 377 = 0.$$

TABLE B.8 Stress in Column Bars.

UNIT	RUN	Column Load = 148 kips				Column Load = 170 kips			
		kd (in)	f_c (psi)	f'_s (psi)	f_s (psi)	kd (in)	f_c (psi)	f'_s (psi)	f_s (psi)
1	1	6.69	3185	18130	24540	7.26	3180	18750	20500
	3	7.27	2765	19670	21400	7.99	2750	16820	14020
2	1	6.68	3200	14920	20240	7.24	3190	15390	16940
	3	7.05	2900	13840	16360	7.75	2890	14320	13060
3	1	7.00	2920	17780	21400	7.70	2910	18400	17100
	3	7.51	2630	16490	16410	8.28	2610	16930	12630
4	1	6.80	3090	16660	21620	7.40	3080	17200	17840
	3	7.39	2690	15020	15660	8.22	2680	15580	11910

The stresses are then converted to strains from

$$e_s = f_s/E_s$$

and plotted on the strain diagrams.

The stress in the bars due to axial load only is found from:

$$N = f_c (A_n + n A_{st})$$

$$= f_c (221 + 32).$$

$$= 253 f_c$$

when N = 148 kips:

$$f_c = \frac{148,000}{253} = 585 \text{ psi}$$

when N = 170 kips:

$$f_c = \frac{170000}{253} = 633 \text{ psi}$$

Strain in the column bars is obtained from:

$$e_s = \frac{nf_c}{E_s}$$

These values are plotted at the top and bottom of the column bars on the strain distributions.

B.2.8 Ultimate Moment Capacity of the Column Core of UNIT 4.

The dimensions of the column core, out-to-out of the $\frac{3}{8}$ in. diameter column ties are $13\frac{1}{2}$" x $13\frac{1}{2}$".

$$a = \frac{148}{0.85 \times 4.22 \times 13.5} = 3.05 \text{ in.}$$

$$M_{uc} = 148 (6.75 - 1.52) + 2 \times 90.8 \times 5.44.$$

$$= 1760 \text{ kip-in.}$$

B.2.9 Bond Stress Developed in Beam Flexural Bars.

The stress can be determined from section B.2.7.1. Then for UNITS 1, 2 and 3:

$$u = \frac{A_s f_s + A'_s f'_s}{4\pi DL}$$

$$= \frac{4.92\ (f_s + f'_s)}{\pi \times 5 \times 40}$$

$$= 0.0784\ (f_s + f'_s)$$

for UNIT 4:

$$u = \frac{A_s f_s}{4\pi DL}$$

$$= \frac{4.92\ f_s}{\pi \times 5 \times 32.0.}$$

$$= 0.0979\ f_s$$

A comparison of the maximum bond stress developed by the bars is given in Table 8.1.

APPENDIX C.

BIBLIOGRAPHY.

1. BLUME J.A., NEWMARK N.M., and CORNING L.H., "Design of Multi-story Reinforced Concrete Buildings for Earthquake Motions", Portland Cement Association, Stokie, Illinois, 1961.

2. WEIGEL R.L. et. al. (1970) "Earthquake Engineering " Prentice-Hall, Inc., New Jersey.

3. SEISMOLOGY COMMITTEE OF THE STRUCTURAL ENGINEERS ASSOCIATION OF CALIFORNIA (1968). "Recommended Lateral Force Requirements", San Francisco.

4. PARK, R. (1968) "Ductility of Reinforced Concrete Frames Under Seismic Loading" New Zealand Engineering, Vol. 23, No. 11, pp 427 - 35.

5. ACI COMMITTEE 318 (1970) "Proposed Revision of ACI 318 - 63: Building Code Requirements for Reinforced Concrete" Journal of the ACI., Vol. 67, No. 2, pp 77 - 186.

6. McKENZIE G.H.F. (1969) "A Critical Look at the Design of Reinforced Concrete for Ductility". Bull. N.Z. Soc. Earthquake Eng. Vol. 2 No. 3, pp 295 - 307.

7. HOGNESTAD E., (1951) "A Study of Combined Bending and Axial Load in Reinforced Concrete Members" University of Illinois Engineering Experimental Station Bulletin No. 399.

8. CORLEY G., and HANSON N.W., (1969) "Design of Beam-Column Joints for Seismic Resistant Reinforced Concrete Frames". Proc. 4th World Conference on Earthquake Engineering, Santiago.

9. HANSON N.W., and CONNOR H.W., (1967) "Seismic Resistance of Reinforced Concrete Beam-Column Joints". Proc. A.S.C.E. 93, ST5 (October) pp 533 - 560.

10. HANSON N.W., (1971) "Seismic Resistance of Concrete Frames with Grade 60 Reinforcement". Proc. A.S.C.E. 97, ST6 (June) pp 1685 - 1700.

11. MEGGET, L.M. (1971): "Anchorage of Beam Reinforcement in Seismic Resistant Reinforced Concrete Frames". Unpublished M.E. Report University of Canterbury, New Zealand.

12. BLAKELEY R.W.G., (1971) "Ductility of Prestressed Concrete Frames Under Seismic Loading". Ph.D. Thesis in Civil Engineering University of Canterbury, New Zealand.

13. AMERICAN CONCRETE INSTITUTE (1963): "ACI 318 - 63 Building Code Requirements for Reinforced Concrete", Detroit.

14. PARK R., and PAULAY T., (1970) "Ultimate Strength Design of Reinforced Concrete Structures". Printed for a Seminar Arranged by Departments of Civil Engineering and Extension Studies, University of Canterbury, Vol. 1.

15. BENNETT W.B., PARME A.L., HANSON N.W., SBAROUNIS J.A., (1965) "Laboratory Investigation of Reinforced Concrete Beam-Column

Connections Under Lateral Loads". Proc. 34th Annual Convention S.E.A.O.C., Coronado.

16. ATCHLEY W.L., and FURR H.L., (1967) "Strength and Energy Absorption Capabilities of Plain Concrete Under Dynamic and Static Loadings". Journal of the ACI, Vol. 64, No. 11 pp 745 - 56.

17. TAKEDA T., SOZEN M.A., and NEILSON N.N., (1970) "Reinforced Concrete Response to Simulated Earthquakes" Proc. A.S.C.E. 96 ST 12 (December) pp 2557 - 2573.

18. ———————— (1964) "An Investigation of the Bond of Deformed Steel Bars with Concrete". Translation No. 112, Cement and Concrete Association.